Structural, electronic and magnetic properties of metal phthalocyanines

A thesis submitted for the degree of

Doctor of Philosophy

University of Warwick

Luke Rochford

Supervised by **Prof.Tim S. Jones**

Department of Chemistry

University of Warwick, Coventry, U.K.

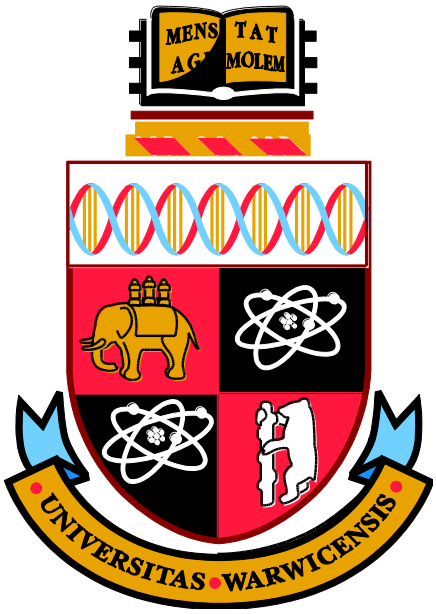

September 2013

Abstract

Metal phthalocyanines (MPcs) prepared as single crystals, polycrystalline powders and thin films have been analysed using a combination of surface science techniques, diffraction based structural characterisation and magnetic characterisation.

Vanadium oxide phthalocyanine (VOPc) prepared as thin films on the (111) surface of gold, silver and copper is analysed by (STM) low energy electron diffraction (LEED) and ultraviolet photoemission spectroscopy (UPS). Similar surface and electronic structure is observed on gold and silver, but profoundly different assembly and electronic properties were observed on copper.

The effect of increasing the substrate temperature during growth on the structure and morphology of iron phthalocyanine (FePc) and manganese phthalocyanine (MnPc) is investigated using atomic force microscopy (AFM), scanning electron microscopy (SEM) and X-ray diffraction (XRD). An evaporated copper iodide (CuI) structural template layer is also used to alter the arrangement of FePc molecules in thin films.

The single crystal structure of fluorinated copper phthalocyanine (F_{16}CuPc) is re-determined using synchrotron X-ray diffraction. Thin films of F_{16}CuPc grown on graphene oxide supports are analysed using X-ray diffraction (XRD), transmission electron microscopy (TEM) and selected area electron diffraction (SAED). This allows assignment of both crystal structure and texture in polycrystalline thin films of a variety of thicknesses.

F_{16}CuPc is also analysed using superconducting quantum interference (SQUID) magnetometry in both powder and thin film morphologies. 3, 4, 9, 10-perylenetetracarboxylic dianhydride (PTCDA) structural template layers are used to alter the orientation of crystallites and the effect of this on the magnetic properties are analysed.

Table of contents

Declaration

The experimental work presented here was conducted by me between July 2009 and July 2013 with the exception of the experiments details below. Single crystal XRD experiments were performed at the Diamond synchrotron at the Harwell science and innovation campus with help from Dr.Dean Keeble (Warwick Physics). TEM images and diffraction patterns were collected with help from Priyanka Pandey (Warwick Physics) and Dr. Richard Beanland (Warwick Physics). SQUID measurements were performed in collaboration with Imperial College London and theoretical support for the experimental work was provided by Dr. Wei Wu (Imperial College London) and Dr. A. J. Fischer (University College London).

None of the work contained in this thesis has previously been submitted for a higher degree

Acknowledgements

Firstly I would like to thank Professor Tim Jones for the opportunity to work in his research group at the University of Warwick. The equipment and resources he made available to me enabled research and made it a pleasure to undertake, thanks for everything Tim!

I am grateful to the Engineering and Physical Sciences Research Council (EPSRC) for project funding and the department of Chemistry for excellently maintained infrastructure.

The Jones' group (past and present members!) have taken what could easily have been a torturous four years and made every day a pleasure. To Ian, Dawn, Tom, Nicola, Paul, Nat, Edd, Jay, Gavin, Chloe, Stefan, Raff, Junliang, Virendra, Tomasz and Mark, I say a huge 'thank you' and I look forward to working with you in the future. Thank you also to collaborators from Warwick Physics including Gavin, Neil, Richard, Priyanka and Dean – your time put aside for discussions and collaborative experiments has been hugely helpful. I would also like to thank everyone from Imperial, UCL and the LCN including Zhenlin, Solveig, Wei, Sandrine, Gabe, Nick and Andy for making such a large consortium feel so friendly!

Without the unquestioning support of my family I would never have attempted the huge undertaking of studying towards my PhD, and for this I am eternally grateful. My siblings Adrian, David and Sophie are a constant source of support and pride to me; thanks all of you for being so patient when I talk about atoms, molecules and point groups!

Finally to my parents I say the biggest thank you of all, I could not have wished for a more supportive team behind me for the entirety of my life. Your gentle encouragement and unequivocal love have made every point in my education and scientific career a joy to experience.

List of publications

1 *- Utilising n-type vanadium oxide films as hole-extracting layers for small molecule organic photovoltaics*

I. Hancox, **L. A. Rochford**, D. Clare, P. Sullivan, and T. S. Jones, *Applied Physics Letters*, **2011**, 99, 013304

2 *- The effect of a MoO_x hole-extracting layer on the performance of organic photovoltaic cells based on small molecule planar heterojunctions*

I. Hancox, P. Sullivan, K.V. Chauhan, N. Beaumont, **L.A. Rochford**, R.A. Hatton and T.S. Jones**,** *Organic Electronics*, **2010**, 11, 2019-2025

3 - *Resolving the Nanoscale Morphology and Crystallographic Structure of Molecular Thin Films: F16CuPc on Graphene Oxide*

P. A. Pandey, **L. A. Rochford**, D. S. Keeble, J. P. Rourke, T. S. Jones, R. Beanland, and N. l. R. Wilson, *Chemistry of Materials*, **2012**, 24, 1365-1370

4 - *Understanding the Multiple Orientations of Isolated Superellipsoidal Hematite Particles at the Oil-Water Interface*

A. R. Morgan, N. Ballard, **L. A. Rochford**, G. Nurumbetov, T. S. Skelhon, and S. A. F. Bon, *Soft Matter*, **2013**, 9, 487-491

5 - *Optimisation of a High Work Function Solution Processed Vanadium Oxide Hole-Extracting Layer for Small Molecule and Polymer Organic Photovoltaic Cells*

I. Hancox, **L. A. Rochford**, D. Clare, M. Walker, J. J. Mudd, P. Sullivan, S. Schumann, C. F. McConville, and T. S. Jones, *J Phys Chem C,* **2013**, 117, 49-57

6 - *Magnetic properties of copper hexadecafluoro-phthalocyanine thin films and powders*

W. Wu, **L. A. Rochford**, S. Felton, Z. Wu, J. L. Yang, S. Heutz, G. Aeppli, T. S. Jones, N. M. Harrison, and A. J. Fisher, *J. Appl. Phys.* **2013**, 113, 013914

7 *– Investigating multiple orientations within vanadium oxide phthalocyanine monolayers on Au(111)*

L. A. Rochford, I. Hancox, T.S.Jones, *Surface Science* Submitted **2014**

List of abbreviations

AFM	Atomic force microscopy
BCC	Body-centred cubic
C_{60}	Buckminsterfullerene
CB	Conduction band
CuI	Copper iodide
CuPc	Copper phthalocyanine
DFT	Density functional theory
F_{16}CuPc	Perfluorinated copper phthalocyanine
FCC	Face-centred cubic
FePc	Iron phthalocyanine
H_2Pc	Metal free (dihydrogen) phthalocyanine
HOMO	Highest occupied molecular orbital
HOPG	Highly oriented pyrolytic graphite
HRTEM	High-resolution transmission electron microscopy
IBA	Ion bombardment and annealing
IPES	Inverse photoemission spectroscopy
K-cell	Knudsen cell
LDOS	Local density of states
LEED	Low energy electron diffraction
LUMO	Lowest unoccupied molecular orbital
MBE	Molecular beam epitaxy
ML	Monolayer
MnPc	Manganese phthalocyanine
MPc	Metallo-phthalocyanine

OMBD	Organic molecular beam deposition
Pc	Phthalocyanine (ligand)
PES	Photoelectron / photoemission spectroscopy
PTCDA	Perylene-3,4,9,10-tetracarboxylic dianhydride
QCM	Quartz crystal microbalance
RHEED	Reflection high energy electron diffraction
R_q	Route mean square roughness
SAED	Selected area electron diffraction
SEM	Scanning electron microscopy
STM	Scanning tunnelling microscopy
UHV	Ultra-high vacuum
UPS	Ultraviolet photoemission spectroscopy
UV	Ultraviolet
VB	Valence band
VOPc	Vanadyl phthalocyanine
XPS	X-ray photoemission spectroscopy
XRD	X-ray diffraction
ZnPc	Zinc phthalocyanine

Chapter One

Introduction

1.1 – Introduction

Small molecular semiconducting materials have attracted significant interest in the last three decades due to their potential applications in a variety of organic electronic devices[1]. This chapter will summarise the state of the art of each of the analysis techniques used to study phthalocyanine semiconductors. All materials and substrates selected for study will also be introduced and selected previous work will be discussed.

Organic semiconductors (OSCs) possess some important advantages over the inorganic materials which currently dominate commercial devices in electronics[2] and photovoltaics[3]. Chief among these is the ability to use chemical modification to select desirable characteristics in materials used to fabricate devices[4]. Such routes allow a unique approach to materials design where a variety of theoretical and experimental organic and physical chemistry can be applied. Similar modification is not possible with inorganic materials as the irreducible building block of any device structure is atomic, whether a single atom (in the case of silicon) or a collection of atomic species for binary or ternary materials. As such adding functional groups or chemical moieties changes the composition of the material rather than simply modifying its behaviour. While adding dopants to crystalline materials is an effective method of property control[2], this is a markedly different approach to chemical modification and similar doping studies have been conducted with organic

materials[5]. Design of molecular systems through chemical synthesis offers precise control over frontier orbital energy levels, crystal structure and physical properties[6].

The ability to make these changes to materials systems presents a new set of problems, as intentionally changing one aspect of a molecule's behaviour can have unforeseen implications. For example, adding fluorine atoms as electron withdrawing substituents around a phthalocyanine ring to alter the position of highest occupied molecular orbital (HOMO) or lowest unoccupied molecular orbital (LUMO) states can drastically alter its self-assembly on surfaces[7,8]. Changes in axial substituents in large aromatic molecules made to affect crystal structure can affect charge transport and performance in devices such as transistors. As such each material system must be understood from a chemical, electronic and structural perspective before chemical or physical changes are made and evaluated. To this end a wealth of research has demonstrated the effective application of multi-technique characterisation to films prepared and maintained in ultrahigh vacuum[9]. As with inorganic semiconductors in previous decades, the understanding of OSCs is approaching the point of maturity where measurements on model systems can provide insight into and allow further development of electronic devices[10].

Vacuum processing is widely used industrially to fabricate commercial electronic devices so using preparation and characterisation methods based in vacuum is highly complementary. Combination of real space and reciprocal space structure determination and photoemission spectroscopy with versatile in-vacuo preparation methods can provide in depth understanding of new or established materials systems[11,12].

In order to gain an understanding comparable with that present in inorganic semiconductors many of the same or similar techniques have been used over the past few decades to probe the properties of organic semiconductor materials. Understanding electro- or optically active organic materials can be split into two broad and overlapping fields, techniques which aim to understand the bulk properties of materials and those designed to probe surfaces. Bulk measurements are usually conducted with materials deliberately prepared as large single crystals or as purified powders composed of smaller crystals[13]. Crystal structure and transport properties of organic materials are routinely conducted to understand their intrinsic behaviour[14]. Single crystals allow removal of the problems associated with grain boundaries that are known to complicate structural measurements and scatter charge carriers in electrical measurements[15]. Structural measurements are of particular significance and in a single crystal sample all lattice planes are present with scattering intensities large enough to map atomic positions within unit cells. Without this information indexing and understanding the more limited data routinely collected from thin film samples is extremely difficult.

A huge variety of materials have been demonstrated in device architectures and some devices nearing commercial maturity have emerged in the last few years[16]. Despite this a huge disparity exists between the amount of device characterisation and basic structural and spectroscopic characterisation of the materials applied therein.

Archetypal materials including acenes[17,18], phthalocyanines[19,20] and perylenes[21,22] have been widely characterised on a variety of substrates by real space and reciprocal space structural analysis techniques and an assortment of spectroscopies. As a complete literature

these studies emphasise the sensitivity of small molecule semiconductors to substrate, preparation conditions and even characterisation method[23]. Without a definitive knowledge of each material and substrate or preparation method combination application of these materials in commercial devices or technological platforms is fraught with difficulty. As phthalocyanines are most widely used in this work they will be the only molecules discussed at significant length.

1.2 - Materials

1.2.1. Phthalocyanines

Phthalocyanines (Pcs) are a class of organic semiconductors based on the 'parent' dihydrogen phthalocyanine which was first synthesised in 1907[24]. Phthalocyanines all contain the fourfold isoindole-centred phthalocyanato ligand and a complexed chemical species within the central cavity (Fig. 1.1). The phthalocyanato ligand is capable of accommodating a variety of atoms, and a wide variety of phthalocyanines have been synthesised[25]. The first metal centred phthalocyanine to be synthesised was in 1927[26] and since then MPc molecules have been demonstrated in a huge variety of applications in electronic and optoelectronic devices[27].

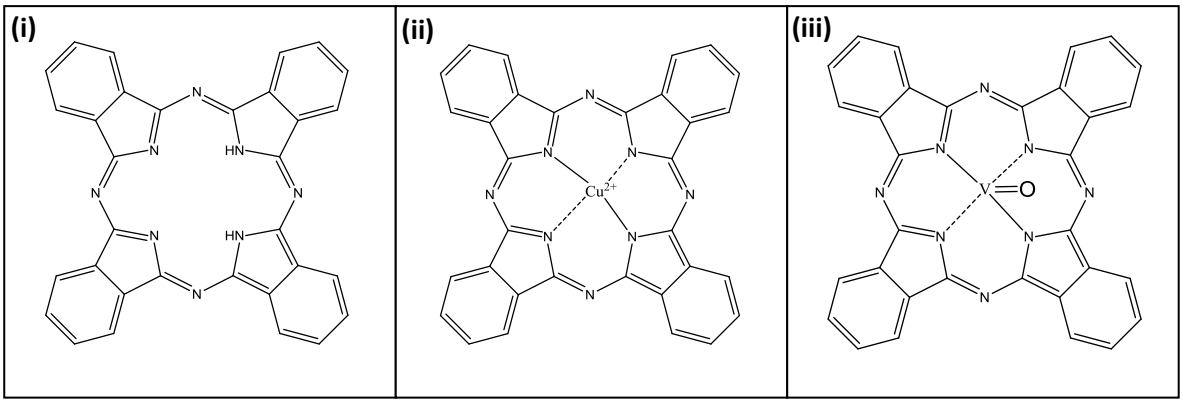

Figure 1.1 – The chemical structures of (i) the 'parent' dihydrogen phthalocyanine, (ii) Cu(II) phthalocyanine and (iii) vanadium xxide (vanadyl) phthalocyanine

1.2.1.1. Surface studies of Phthalocyanines

Phthalocyanine thin films have been prepared using most available film preparation techniques, both by solution processed routes[28] and vacuum deposition[29]. Active layers are often in the tens of nanometre range and can present properties significantly different from bulk crystalline samples of the same material[30,31], so careful analysis is necessary to fully understand their nature and properties. As the surface area is so large in films with these dimensions, understanding the surface structure of organic semiconductors and establishing surface to property relationships is crucial.

A huge variety of phthalocyanine-surface combinations have been studied using surface science methodologies. Techniques typically used to study OSC interfaces include scanning tunnelling microscopy (STM)[32], atomic force microscopy (AFM)[30], low energy electron diffraction (LEED)[33] and ultraviolet photoemission spectroscopy (UPS)[34]. Identical samples are commonly analysed by each technique in turn without exposure to air when films of evaporable materials are prepared *in vacuo*.

1.2.1.1.1 Scanning Tunnelling microscopy

With the increase in availability of user friendly commercial scanned probe surface imaging systems in the last decade years it is hardly surprising that scanned probe microscopy has become hugely popular in the study of organic semiconductors. Recent developments in sample and tip preparation in atomic force and scanning tunnelling microscopy conducted in ultrahigh vacuum have allowed unprecedented resolution of molecules and even individual bonds[35].

The scanning tunnelling microscope has proved an indispensable tool for the exploration of two dimensional structures and local density of states in isolated molecules and thin films of phthalocyanines. Routinely resolving sub-molecular structure, self-assembly and molecular packing allows a deep understanding of the surfaces of phthalocyanine thin films.

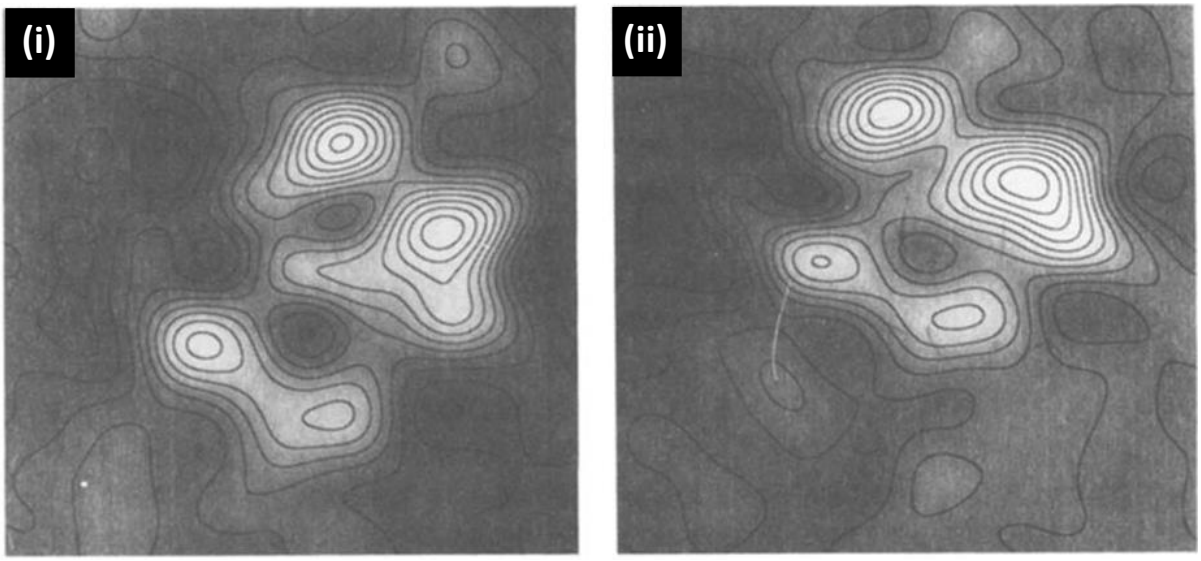

Figure 1.2 – STM contour map before (i) and after (ii) correction for piezo drift of a single CuPc molecule (reproduced from [36]).

The first molecular resolution images of phthalocyanines were published by Gimzewski et al.[36] from results obtained at IBM research labs in Zurich (Fig. 1.2). While other molecular systems such as lipid bilayers and DNA[37] had been imaged with STM, this work is the first example of using evaporation in UHV to prepare and directly image the surface structure of a technologically useful molecule at an interface. In this case the interface was between CuPc molecules and a polycrystalline silver surface which had also been evaporated in UHV conditions.

While advances in data acquisition and STM instrumentation have produced higher resolution images from which more information can be extracted, important questions that are still relevant to the field today were raised in this early work. The complex nature of the tunnelling process is both recognised and discussed, along with the nature of the molecule-substrate interaction in the adsorption process. Unlike inorganic surfaces the orbitals involved in the process of tunnelling and therefore the images produced are not immediately obvious as molecular orbitals in small molecules are often complex.

Observations including the narrow range of appropriate voltage biases for imaging, the presence of molecular surface diffusion at low coverage and, most importantly, that high electric fields applied to the tunnel junction can change the surface topology due to the delicate nature of the surface-molecule interaction were made.

Over the next decade numerous other works explored the possibilities of using STM to image phthalocyanine molecules and films prepared on surfaces by evaporation in UHV. Theoretical approximations to molecular density of states[38] and even direct simulation of STM images[39] were approached with a variety of computational methods. It became clear that comparison of sub molecular resolution images with simulations of the orbitals involved in the tunnelling process could provide insight into the electronic structure of MPc molecules on surfaces. The first group to successfully use the approach of STM imaging on MPc films to explore an issue of chemical enquiry was that of Hipps[40] at Washington state University.

The motivation for Hipps' research was the lack of understanding of the interaction between metal phthalocyanines and supporting substrates, despite a variety of publications in which MPc molecules were successfully imaged at surfaces[41,42,43]. With the postulate that the electronic charge distribution and adsorption geometry reflects the nature of the MPc-substrate interaction, STM was employed to explore monolayers of CoPc and CuPc on the Au (111) surface. Significant theoretical work existed in which STM images of phthalocyanines were simulated using local density of states approximations. Calculations predicted a 'hole' in the centre of the CuPc molecule when imaged by the STM tip, rationalised by the occupied and unoccupied orbitals centred on the copper atom being

much further (approx. 1eV) from the Fermi energy than that of the LUMO of the phthalocyanine ligand. Tunnelling into the ligand was therefore energetically favoured producing large tunnelling currents and a peak in the constant current height profile. As the tip travelled across the Cu atom the less favourable tunnelling conditions required the tip to move closer to the sample to maintain the tunnelling current and as such produce a dip in the height profile. It follows then that exchanging the central metal atom of the MPc species would change the height profile of the centre of the molecule by affecting the local electron density.

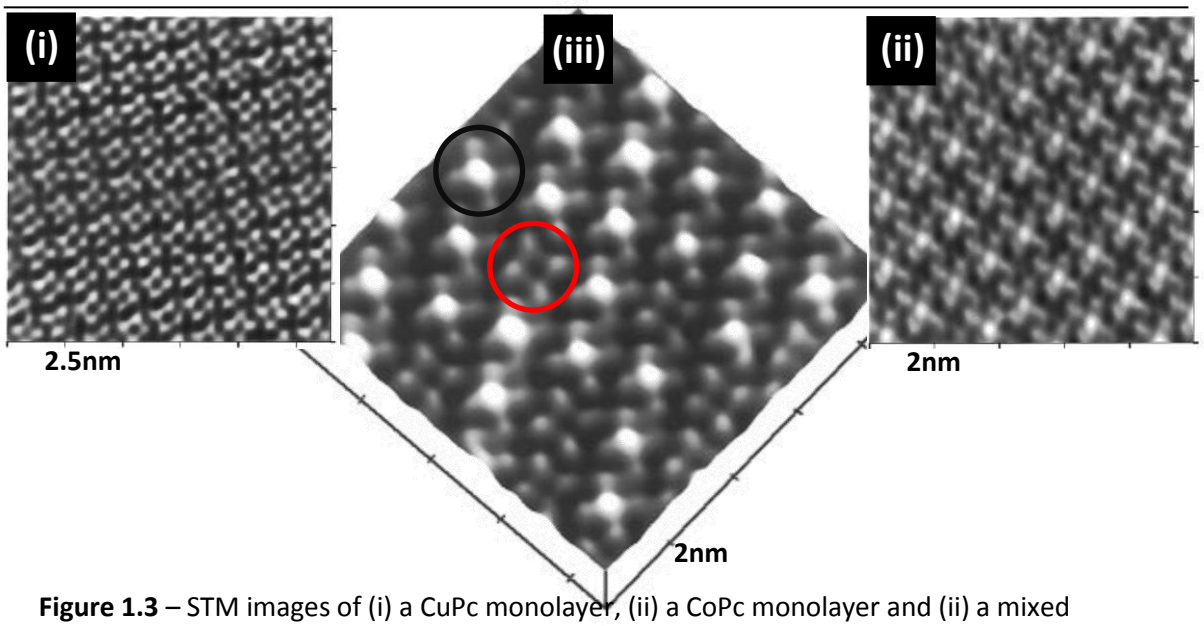

Figure 1.3 – STM images of (i) a CuPc monolayer, (ii) a CoPc monolayer and (ii) a mixed monolayer. The red circle marks a CuPc molecule and the black circle a CoPc molecule (reproduced from [40])

CoPc and CuPc molecules were used to demonstrate this phenomenon, evaporated firstly into single component thin films and finally co-deposited into a mixed monolayer structure. Profound differences were observed in the visualisation of CoPc and CuPc by the STM (Fig. 1.3) which could be rationalised by electron density differences in the metal at the centre of the molecule. For CuPc the cross like shape of the ligand system was clearly

resolved with a depression in the centre leading to the assumption that the Cu is not participating in the tunnelling process. However for CoPc the same ligand visualisation is present but instead of a hole in the centre of the molecule a protrusion is evident. When a mixed layer of molecules was prepared the individual species could be discerned by the presence of a depression for CuPc or a peak for CoPc, confirming the observed differences as the same tip and conditions could be used to image both species.

The apparent height of features in STM does, however, depend on a variety of parameters and with this in mind the authors discussed both a simplified model for the tunnelling process and three possible tunnelling mechanisms. In the simplest terms the Cu(II) species is considered to be acting as an insulator while the Co(II) acts as a conductor, and as STM images are composed of contours of constant current the dip and rise of the tip to maintain constant tunnelling conditions gives rise to these features.

Three tunnelling mechanisms are also suggested, first among which is that the tunnelling electrons are mediated mainly through the molecular LUMO. The bright central point could then be assigned to the empty 3_{dz2} orbital of the Co (II) centre. Secondly, a situation where the HOMO is the dominant tunnelling pathway and therefore the d_z^2 or (d_{xz} ,d_{yz}) pair provide the observed contrast. These orbitals do show significant projection out of the plane of the molecule but are located 2eV below the unbound ligand HOMO in CuPc and CoPc making such a tunnelling transition unlikely. Mediation by d-orbitals or coherent coupling of the molecular orbitals with the substrate and tip are also suggested. Finally, an incoherent process similar to orbital mediated tunnelling seen in MPc tunnel diodes is

considered, but this offers no information about the tunnelling process or the recorded image.

This work was the first to demonstrate the ability to solve a chemical problem, in this case the effect of changing the metal centre on the molecular density of states, by using STM and the phthalocyanine family of molecules. Contrary to previous reports and theoretical expectation this confirmed that the central metal atom (and its orbital configuration) as well as the ligand system needs to be considered to fully understand STM imaging of phthalocyanines.

More recent data present in literature have focused on understanding the structural and electronic aspects of the earliest stages of film formation. To overcome the problems of surface mobility at much less than one monolayer cryogenic temperatures are employed to kinetically freeze molecules at their adsorption sites, supressing thermal diffusion to allow low coverage imaging.

Countless examples of cryogenic STM studies of MPc molecules from isolated molecules up to monolayer coverage can be identified from literature in the last decade. However many studies are not carried out systematically and many gaps exist in the understanding of the MPc-substrate interaction. Iron phthalocyanine (FePc) has attracted significant attention due to its interesting magnetic properties and unusual behaviour in ultrathin layers. Cheng et al.[44] observed the very early stages of crystallisation of FePc on the (111) surface of gold, selecting 0.1, 0.3, 0.6 and 1 ML in order to observe coverage dependant behaviour (Fig. 1.4).

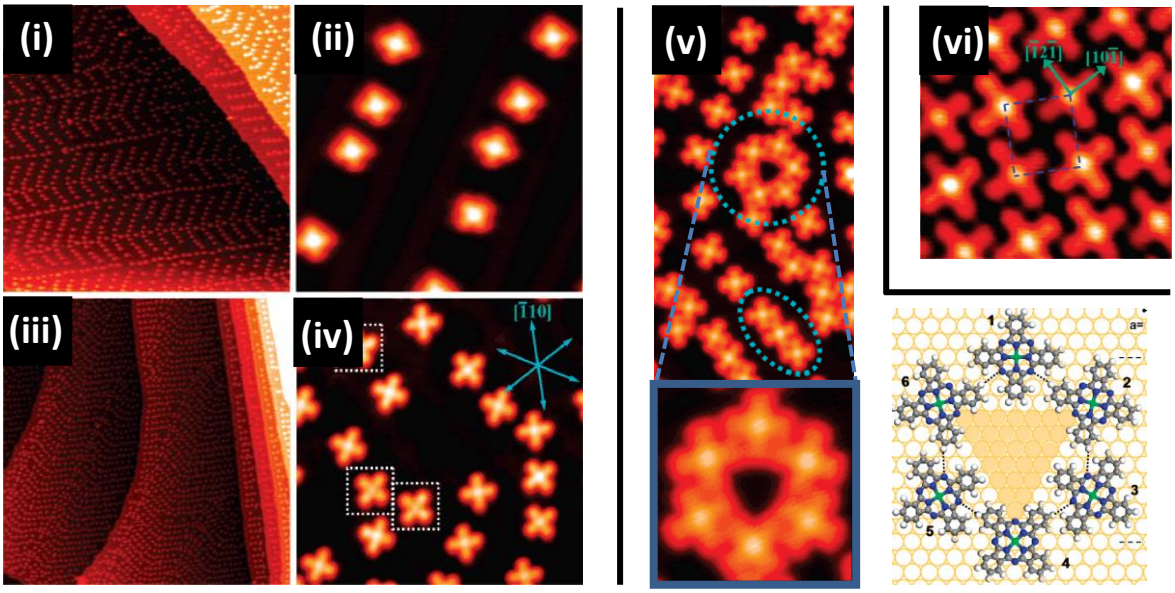

Figure 1.4 – STM images of FePc at (i,ii) 0.1ML (iii,iv) 0.3ML (v) 0.6ML and (vi) 1ML. A digitally enhanced section of (v) is included along with a model for the packing motif (reproduced from [44]).

At 0.1 and 0.3 ML the surface reconstruction of the gold produces an inhomogeneous distribution of molecules due to the preference for adsorption on face centred cubic (fcc) sites rather than body centred cubic (bcc) sites. In both cases molecules are dispersed across the surface rather than forming aggregates or ordered structures, suggesting intermolecular interactions are not causing self-assembly or directing the surface structure. As more molecules are added to the surface self-assembled structures begin to emerge, the most striking of which is a circular hexamer of molecules with a triangular vacancy at the centre.

The formation of this open framework structure is explained by considering adsorption configurations determined by the MPc-substrate interaction and the effect of elbow sites in the herringbone reconstruction. As a monolayer is reached a completely ordered structure is observed and no unusual assembly or orientation is present, only the most stable molecular orientation in a closely packed layer.

Emergent in the field of cryo-STM of MPc systems is the ability to use the STM to directly observe properties of isolated molecules. The interesting magnetic properties of FePc have made it a prime candidate for this kind of research. Tsukahara et al.[45] showed in a 2009 paper that the magnetic characteristics of FePc on both clean and oxidised copper surfaces is highly sensitive to the adsorption architecture of the molecule. Two geometrically different adsorption geometries were identified, both of which correspond to the molecule adsorbing 'flat' with respect to the substrate with the ligand π system orthogonal to the substrate plane. The difference between the two, labelled alpha and beta, is the angle created by an imaginary line passing through opposite lobes of the phthalocyanine and the (001) direction of the substrate. While this difference is only 15° the effect on the properties of the molecule, in this case the zero field splitting and magnetic anisotropy as measured by inelastic electron tunnelling spectroscopy, is profound. On the clean Cu (110) (2x1) oxygen reconstructed surface the response to an applied magnetic field of each adsorption motif is different due to the different magnitudes of the zero field splitting present.

By monitoring and understanding very subtle changes in the structures of MPc thin films a much better understanding of their properties can be achieved. STM studies allow the morphological and electronic surface structure of films to be studied and correlated with other physical properties.

1.2.1.1.2 Low Energy Electron Diffraction (LEED)

Low energy electron diffraction has become an increasingly neglected technique since the wide adoption of high-resolution real space scanning probe techniques. Other electron diffraction and imaging techniques such as scanning electron microscopy (SEM), transmission electron microscopy (TEM) and selected area electron diffraction (SAED) are useful to study phthalocyanine films, but are limited in resolution or experimental suitability. For example, TEM and SAED have been applied to a variety of phthalocyanine crystals[46] and thin films[47], but samples are extremely sensitive to electron beams. While using low-dose electron optics and cryogenic sample stages can alleviate some of these problems[48] they remain limited in scope experimentally and most often exposure to air is necessary before characterisation. SEM is also routinely employed to characterise the structure and composition of phthalocyanine thin films. SEM allows high resolution of surface structures but lacks the ability to resolve individual molecules and only gives limited depth of field information.

Application of LEED can be hugely complementary to scanned probe imaging and electronic structure measurements as it provides insight into the surface structure of crystalline samples. LEED optics employing a nano-amp primary beam current have been shown to cause no damage to samples at the beam energies required to collect diffraction patterns[49].

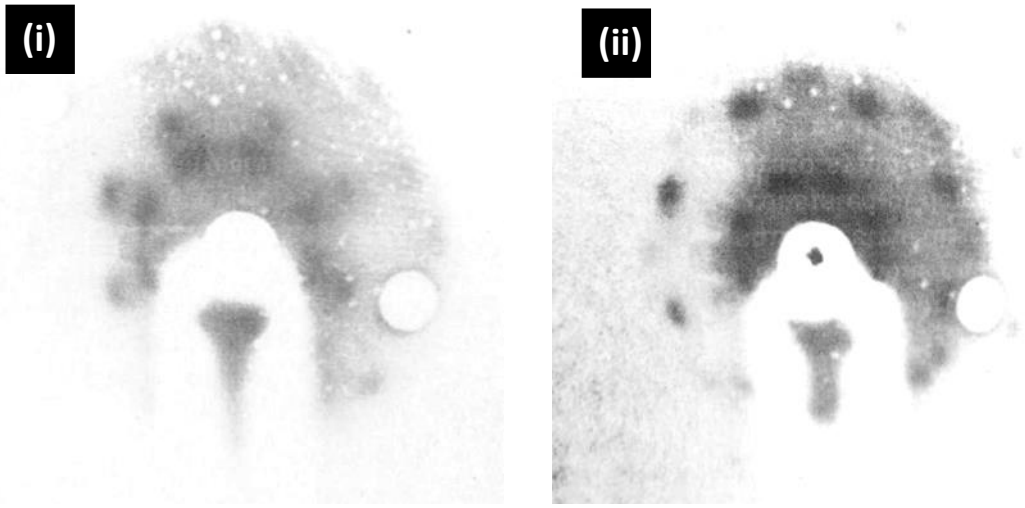

Figure 1.5 – LEED patterns of (i) monolayer and (ii) multilayer films of CuPc on the Cu(100) surface. Beam energies are 15eV in each case (reproduced from [50], inverted for clarity)

Buchholz et al.[50] were among the first to observe LEED patterns (Fig.1. 5) for ordered layers of MPc molecules, publishing patterns from CuPc and FePc as well as metal free phthalocyanine on copper single crystal surfaces in 1976. This work long predates the invention of scanned probe techniques for real space surface imaging and was one of the first to suggest surface crystal structures for thin MPc films. Monolayer films were grown onto Cu (111) and Cu (100) surfaces held at room temperature and patterns were recorded which were dependant on the substrate and the molecule present. The most significant observation of all was that the surface structures observed did not match any of the crystallographic planes present in single crystals of the materials used. Two possible explanations of this behaviour are that a reconstruction or reorganisation of the surface is present, or that a completely new crystal structure is present in the MPc over-layer due to constraints imposed by the substrate. This provides even more evidence that the MPc-substrate interaction is of huge importance as in this case the crystal structure and growth is different from that observed in bulk samples of the same material.

Examples exist of both planar and non-planar phthalocyanines deposited on semiconducting[51] and insulating substrates as well as a variety of metal surfaces[52]. Papers using LEED as the lone analysis technique often include quantum mechanical or thermodynamic simulations to provide insight into the epitaxial relationships in MPc thin films.

More recently LEED has been demonstrated in combination with other surface analysis techniques to either confirm observations from other methods or provide more information about complex MPc systems. Gopakumar et al.[53] used both LEED and STM to investigate PdPc on HOPG in the same multi technique UHV system. LEED patterns displayed far more spots than expected from the quadratic unit cell of perfectly ordered MPcs adsorbed with π systems orthogonal to the substrate. Indexing of the patterns was possible if the over-layer symmetry was considered to be 10° mismatched with one of the graphite lattice directions, and as such six rotationally inequivalent domains were present (Fig 1.6).

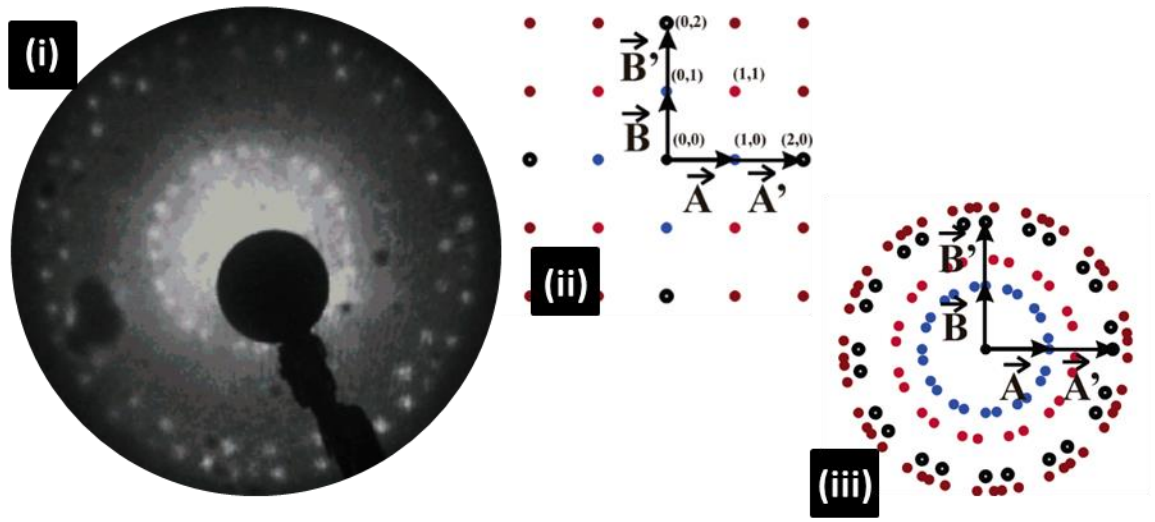

Figure 1.6 – LEED pattern of (i) monolayer coverage of PdPc on graphite (beam energy 15eV). The proposed lattice for the PbPc layer is shown in (ii) and (iii) shows a rotational superposition of multiple patterns (reproduced from X).

While high resolution images were produced large scale imaging in such quantity to be able to statistically predict the number of rotationally unique domains present would be onerous. In LEED experiments an average representation of the surface crystallography within the probed area is produced so the consequences of polycrystallinity in thin films such as these are obvious from a single pattern.

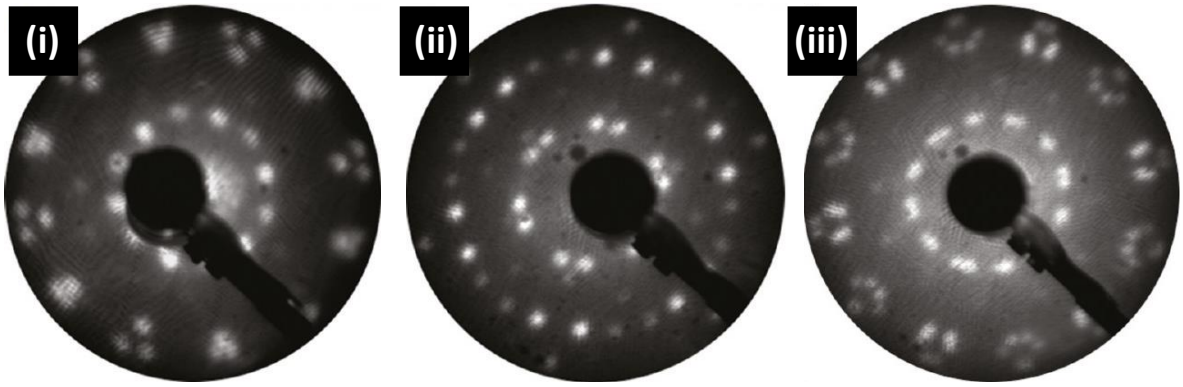

Figure 1.7 – LEED patterns of FePc on Ag (111) with increasing coverage. Patterns correspond to (i,ii) commensurate submonolayers and (iii) incommensurate structure at one monolayer (reproduced from [54]).

While STM can be effective in imaging films at various stages of growth it is often not feasible to use the STM as a real time monitoring tool in the growth of MPc films. LEED can, however, be applied in real time during deposition as no instrumental components or probes must be exposed to the flux of molecular beams. Bobaru et al.[54] investigated FePc from submonolayer to monolayer coverage using a combination of STM and LEED on the (111) surface of silver. So called 'live-LEED' experiments tracked the evolution of the LEED pattern of the film during deposition and the intensity profile of the (10) substrate spot was used to monitor order in the film. Three significant patterns (Fig. 1.7) are highlighted at 180, 240 and 330 seconds during growth at 0.22 ML/min. Firstly a diffuse ring pattern attributed

to a two dimensional gas phase being formed on the surface is observed followed by a commensurate overlayer and finally an incommensurate phase. STM was used to probe these three points on repeated growth runs and produced very similar molecular resolution images for both spot patterns observed. Without using LEED to probe the surface crystallography it would be hard or impossible to discern any of the subtle differences in the two structures.

1.2.1.1.3. Ultraviolet Photoemission Spectroscopy

Since the electronic properties of organic semiconductor films depend strongly upon the nature of the interface between the organic material and substrate[55], it should be expected that work is currently being undertaken to characterise films and interfaces. While core level X-ray photoelectron spectroscopy (XPS) is of huge importance to understand the higher binding energy portions of the electronic structure of molecules it will not be discussed here as none was undertaken during this work.

Ultraviolet photoemission spectroscopy (UPS) allows determination of the low binding energy region of the electronic structure of molecules which ultimately governs their charge transport behaviour. UPS is widely used to measure the work function and highest occupied molecular orbital (HOMO) position of organic materials evaporated in thin films. As the UPS spectrum of a molecular system is an approximation to its density of states, theoretical calculations can enhance the amount of information extracted from the technique[56]. Huge insights can be gained into the energy level alignments at interfaces

whether these interfaces are applied in electronic devices or purely studied from a surface science perspective.

One of the first systematic UPS studies of solid state organic semiconductors was undertaken by Sato et al.[57] in 1981 in order to investigate polarisation energies in molecular solids. Comparison of gas phase UPS spectra and their solid state counterparts was used to evaluate the magnitude of polarisation energies in a total of 44 materials. Polycyclic aromatic hydrocarbons were shown to share a common polarisation (P_+) value of 1.7eV regardless of differences in molecular size and crystal structure. A few compounds did exhibit values significant higher or lower than this common value, with these observations attributed to large molecular polarisabilities and structural complexity respectively. The authors make an important conclusion; polarisation energy in a molecular solid is dependent upon the intrinsic molecular polarisability and molecular packing in crystalline solids.

This understanding of the difference in behaviour from gas to condensed phase and the impact of such changes upon electronic structure are hugely important in interpreting UPS data in the solid state. In a more recent article the topic was revisited by Hill et al.[58] from the perspective of investigating charge separation in organic semiconductors. When we consider applying organic materials in electronic or optoelectronic devices we are really considering their method of and ability to transport electrons and holes.

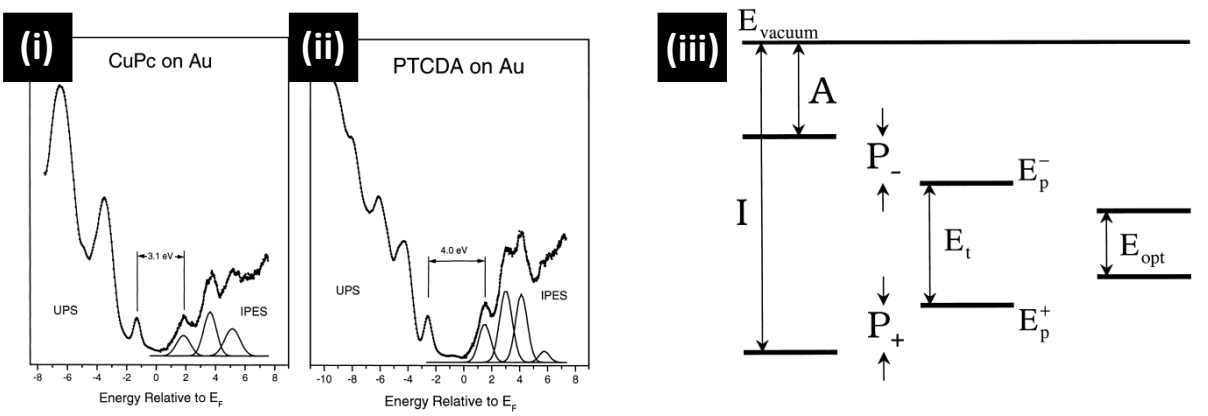

Figure 1.8 – Combination UPS/IPES spectra for (i) CuPc and (ii) PTCDA along with (iii) a schematic of the impact of polarisation energies upon band structure (reproduced from [58]).

In contrast to covalently bound inorganic semiconductors localisation and polarisation effects dominate excitation and transport dynamics in organic materials which are held together by relatively long range forces. Particularly for organic photovoltaic (OPV) applications the exciton binding energy, or charge separation energy, is of huge importance and values are significantly larger than those found in inorganics[59]. The authors used a combination of UPS to observe the occupied states at low binding energy (HOMO) and inverse photoemission spectroscopy (IPES) to observe low lying unoccupied states (LUMO) in five organic materials including CuPc (Fig. 1.8). This allowed the transport gap (E_t), (the energy required to create a free electron and hole pair) to be calculated and compared to the optical gap (E_{opt}) which is calculated from the onset of optical absorption. Values for the transport gap were significantly larger than those for the optical gap suggesting a strong electron-hole correlation in organic semiconductors.

Although approached from a more fundamental standpoint than most experimental work relating to device structures, work such as that of Hill et al. provides an understanding of the electronic structure and transport phenomena in organic semiconductors which is

indispensable. Hill and Kahn presented another particularly significant contribution to the field by discussing the nature and importance of energy level alignment at organic/organic interfaces in semiconductor heterostructures[60]. The authors suggest that predicting the energetic position of the HOMO and LUMO of materials present at an organic/organic interface (like those found in organic light emitting diode (OLED) or OPV structures) is the most important energetic concern. However the assumption that a common vacuum level is present across the organic/organic interface and the requirement of Fermi level alignment at thermal equilibrium complicates matters.

A variety of work had already shown that the assumption of vacuum level alignment at organic/metal interfaces did not hold, partly due to the presence of interface dipoles. Hill and Kahn approached organic/organic interfaces with a similar question in mind; are vacuum level shifts evident in interfaces between two organic semiconductors? In order to address this question, organic layers were deposited onto gold supporting films and another organic layer was sequentially added and UPS spectra recorded. These measurements showed that unlike organic/metal interfaces, in organic/organic interfaces vacuum level alignment can be applied to understand energy level alignment. This is rationalised by highlighting the differences between organic/metal and organic/organic interfaces, namely the lack of chemical changes in the organic/organic case which may be present at metal/organic interfaces. Phenomena such as charge transfer or large interface dipoles may be present in the latter which can create states within the band gap of the OSC. Understanding transport behaviour in such architectures is clearly high dependant on our

understanding of the nature of the interaction between organic molecules and other species, whether an organic molecule or a part of an inorganic surface.

In the last decade a wide variety of both fundamental and device architecture experiments have been conducted using UPS. While many have tended to combine electronic surface probes like XPS and UPS with scanned probe or diffraction methods, the UPS component of such work provides the most robust electronic structure determination. UPS has been used to great effect to evaluate both Fermi level pinning[61] and electron transfer at organic/metal interfaces[62] and to understand the dominant electronic effects when such an interface is formed.

Niederhausen et al.[63] demonstrated both the importance of Fermi level pinning in understanding molecular heterointerfaces and the role it plays in the final electronic structure observed. The approach employed was to examine the interaction of a C_{60} sub monolayer which had been physically separated from a supporting Ag(111) surface by an evaporated interlayer of alpha-sexithiophene molecules. By preventing direct contact between the molecule and the surface electronic coupling is not possible and any direct interaction with a surface state or charge 'spilling out' of the surface is prevented.

The possibility of pinning the Fermi level of the C_{60} using a sexithiophene (6T)/Ag(111) structure which has a workfunction lower than the molecule's electron affinity is also introduced. Monitoring the change in the valence density of states by UPS allows a tentative explanation of the observed behaviour of this relatively complex heterostructure (Fig. 1.9).

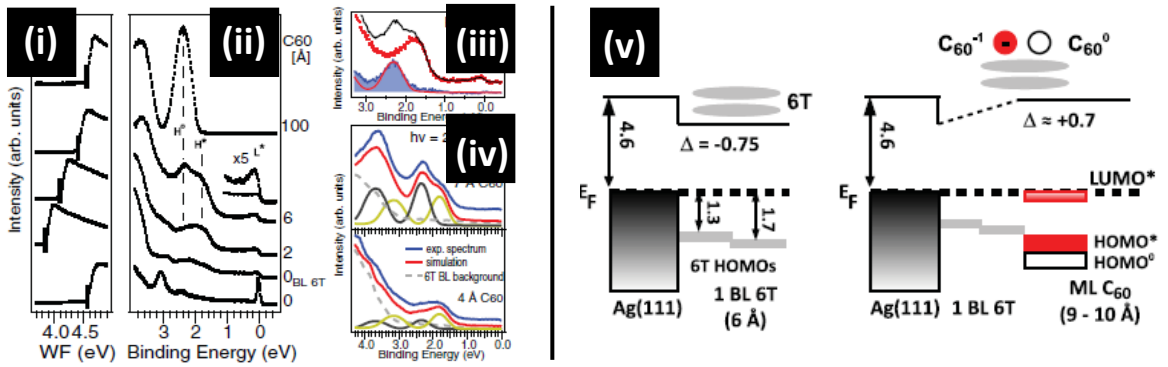

Figure 1.9 – UPS spectra for (i-iv) for C_{60}/6-T/Au(111) hetero-structures along with (v) a band structure schematic with induced charge transfer indicated (reproduced from [63]).

Initially the C_{60} LUMO sits below the Fermi level of the 6T/Ag(111) structure which has a workfunction of 3.85 eV while the electron affinity of the C_{60} is approximately 4eV. An energetically favourable electron transfer occurs and a dipole is formed between the negatively charge C_{60} molecule and the residual metal hole. Dipole-dipole repulsion essentially limits the possible density of charged molecules and experimental observations confirm that both charged and neutral C_{60} molecules are present on the surface. These negative C_{60} dipoles can screen the energy levels of other nearby C_{60} molecules and lift their LUMO levels above the Fermi level of the underlying layer therefore allowing them to remain unchanged. This suggestion rationalised the coexistence of both charged and neutral molecules and creates a 'doped' two dimensional C_{60} array physically separated from the substrate.

Experiments such as these shed even more light on the rich and complex nature of surface interactions and charge transport in organic semiconducting materials. As the field of organic electronics matures predicting the electronic properties of both materials and structures created from them will be of utmost importance. Examples of trends in electronic structure that can be used to predict properties of new molecules and unusual examples

that do not fall in line with expectations are prevalent in the literature. As such a keen experimental understanding and a robust approach to experimental design and data analysis are vital when techniques such as UPS are applied to organic molecules.

1.2.1.2. Crystal Structure of Phthalocyanines

Crystal structure determination of phthalocyanine materials is a widely studied, complex and often inconsistent field of research. Some of this is due to inherent difficulties with the crystallography of large molecules which are highly sensitive to preparation conditions and exhibit multiple subtle variations on similar crystal structures[25]. Unlike inorganic semiconductors sample preparation for single crystal XRD and TEM measurements can either drastically change the structure of a sample or destroy it completely[64]. As such knowledge of phthalocyanine crystal structures is a mixture of full structures from single crystals, unit cells without atomic positions from powder diffraction experiments and inference from comparison to molecules that are assumed to be iso-structural due to chemical similarities[13].

Although the phthalocyanine molecule was synthesised and structurally characterised in 1934 only chemical methods were initially used for structural analysis[65]. While molecular structure is vital in understanding a material for use in organic electronics, the solid state ordering of molecules in a crystal or film are of equal importance where phenomena such as charge transport are concerned. The first crystal structures were solved from single crystals of metal free, nickel, copper and platinum phthalocyanines in work by

Robertson et al.[66] from crystals prepared by sublimation (at low pressure in a flow of carbon dioxide). While atomic positions were not generated due to the relative simplicity of the available equipment and analysis methods, unit cell parameters could be determined in each case. Transition metal centred phthalocyanines have since been extensively studied by X-ray diffraction but due to the difficulties in preparing large single crystal samples methodology and results have varied considerably.

1.2.1.2.1. Single Crystals

One of the most commonly studied phthalocyanines, and one of the most widely studied small molecule semiconductors, is copper(II) phthalocyanine. From the original experiments by Robertson CuPc was found to be monoclinic with $P2_1/a$ symmetry and a tendency to elongate along the b axis (corresponding to the face-to-face molecular packing direction) in crystals to form high aspect ratio needles[66]. The unit cell was found to contain two flat molecules with square symmetry with an intrinsic tilt angle with respect to each other to create a 'herringbone' packing arrangement when viewed along the molecular axis (Fig. 1.10). In 1968 Brown et al. published a structural refinement based on single crystals which enabled atomic positions to be calculated[67]. Once again the tendency for the growth habit to elongate the crystal along the b axis was noted, and a two molecule unit cell with a tilted herringbone structure was observed. While only two significant studies had reached publication at this point they agreed on the volume and dimensions of the unit cell for the particular polymorph in question. They also concurred upon the herringbone arrangement of molecular planes within the unit cell.

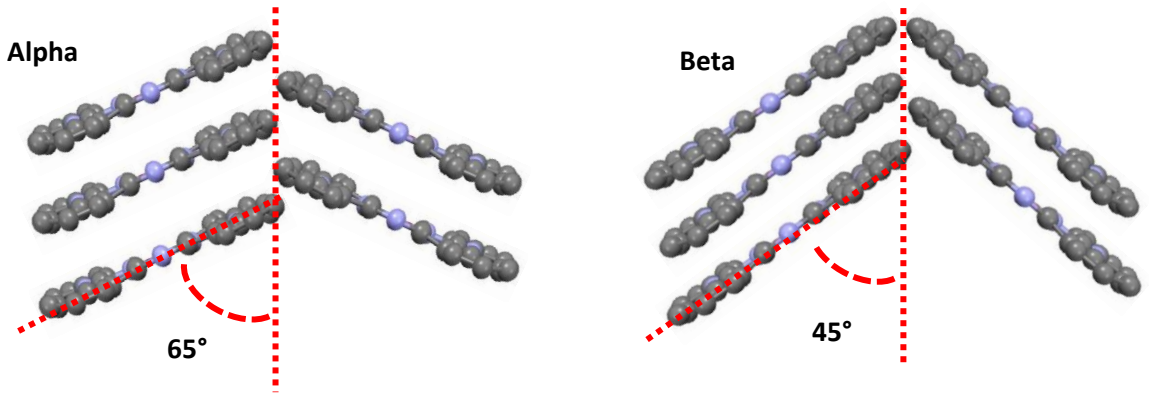

Figure 1.10 – Schematic of molecular packing in the reported alpha and beta modifications of the reported[66] CuPc crystal structure (viewed along the molecular plane).

Despite this, controversy surrounds the analysis of molecular packing within crystals of phthalocyanine molecules. This is partly due to the existence of multiple similar polymorphs of a single molecular species such as the archetypal alpha and beta modifications of the CuPc crystal structure[68]. Such subtle changes in structure are often difficult to observe making interpretation protracted and dependant on experimental and analytical accuracy. These difficulties are compounded by instances of structural inference, assuming that chemically similar compounds are isostructural, for example PtPc and CuPc. This has led to accepted terminology which is at best misleading and at worst scientifically incorrect. More detailed analysis of crystal structures can disprove such assumptions, which was shown by Hoshino at al. in the case of CuPc[69].

A wide variety of proposed structures and nomenclature for MPc crystal structures had been presented in the literature up to 2003 with a variety of packing motifs, intermolecular spacings and orbital overlaps. In CuPc the beta modification, as mentioned above, had been fully characterised by XRD experiments on single crystals. The alpha polymorph had been partially analysed by TEM of thick films grown on alkali-halide substrates with the assumption that PtPc and CuPc shared the same structure. Hoshino's

SAED patterns suggested that rather than the herringbone arrangement, the molecules were instead arranged in slipped parallel stacks (Fig. 1.11).

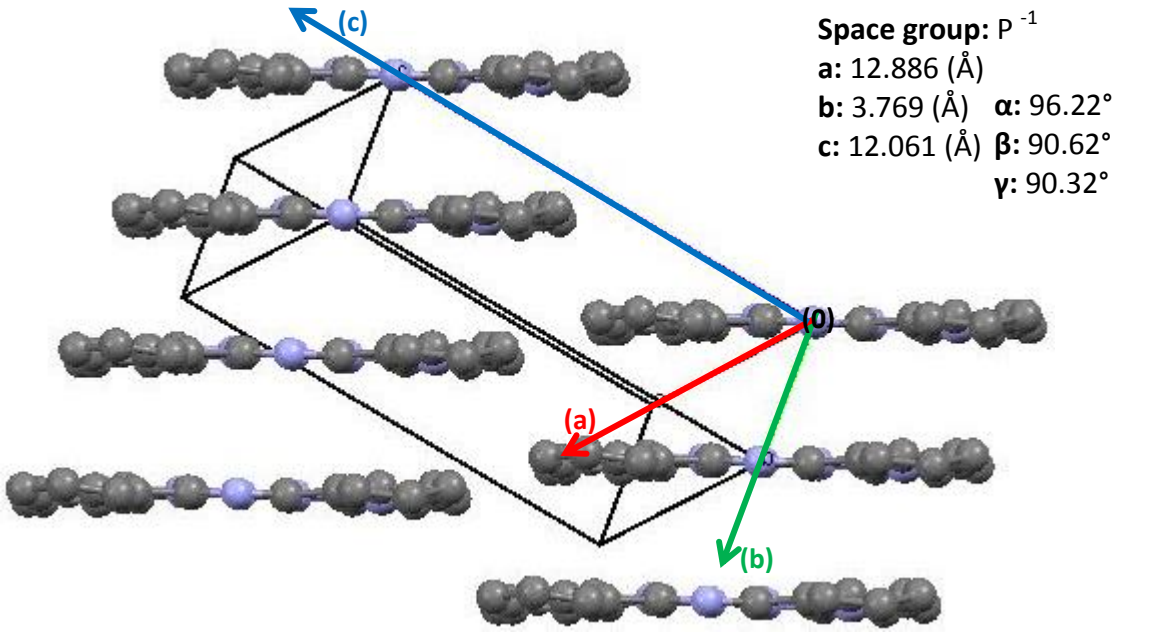

Figure 1.11 – Visualisation of the revised CuPc crystal structure (created with data from[69])

Lattice constants suggested that a single molecule was present in each unit cell, so each molecule must have the same relative orientation within the crystal. With this in mind four unique packing motifs could be identified, in contrast to those already suggested in the literature, which could be broadly applied to planar phthalocyanine molecules. Many more recent papers do not, however, recognise this deduction and refer to the original alpha and beta labels in films and crystals. This is one example of how convoluted and confusing the crystallography of phthalocyanines has become; a variety of proposed crystal structures and an assortment of labels for polymorphs applied to either the same or similar structures. This complicates analysis of phthalocyanine materials when they are applied in devices,

especially as charge transport and related phenomena are so dependent on crystal structure.

Many phthalocyanines that contain a non-planar central moiety such as vanadium oxide, titanium oxide or aluminium chloride exhibit more complex crystal structures than planar varieties. This is often attributed to the highly anisotropic intermolecular interactions in these molecules which contain large electronic or magnetic dipoles in their central species[70]. Structural analysis of non-planar phthalocyanines has received far less attention as a field than that of planar equivalents. Metal centred phthalocyanines with either oxygen species or counter ionic halides have been widely applied in electronic devices (for example titanium oxide[71], aluminium chloride[72] and vanadium oxide[73] phthalocyanines). Despite this complete structural characterisation of single crystals has not been undertaken for many of these compounds. Inference from similar molecules or characterisation of single structures within a polymorphic system has been used to gain an understanding of the molecular ordering present.

1.2.1.2.2. Thin Films

Crystallographic measurements on thin films of MPcs bring with them another set of intrinsic difficulties. The thicknesses of most technological interest are in the nanometre range, for example the tens or hundreds of nanometres used in OPV and organic thin film transistor (OTFT) devices, respectively[74]. The highest electron density atom in an MPc molecule is the metal in the central cavity, and as such it interacts with X-rays most strongly. Miller planes within the structure containing most metal atoms represent the highest

electron density planes through a crystal. In planar phthalocyanines the (100) plane exemplifies this and is observed most often and most easily in diffraction experiments[75]. Order in other directions may be hidden by these intense diffraction maxima or at such low intensity in laboratory X-ray diffractometers that they cannot be observed. Concomitant with this is the large degree of preferred orientation and the nano-crystalline nature of MPc thin films[76]. These factors lead both to a broadening of the diffraction peaks and can create unexpected intensity differences that may not be indicative of the true texture of the film.

To address these problems the intensity of the X-ray light can be increased by using a diffraction end station at a synchrotron light source where high intensity grazing incidence diffraction experiments have produced impressive results. Experimental time at synchrotrons is, however, limited and as such representative sets of samples are often measured rather than a full set of all possible preparations. Design of experiments is also difficult as experimental provision for evaporation monitoring and characterisation varies with synchrotron, beam line and end station. Laboratory X-ray diffractometers are much more commonly employed for crystal structure measurements due to cost, availability and ease of access. Modern diffractometers can be specified with highly flexible optics and geometries allowing a variety of experiments to be undertaken with organic thin films of sufficient crystallinity.

With the limitations discussed above in mind alternative methods of structure determination are used, and electron diffraction methods have been employed with some success. As previously discussed LEED is a powerful tool in the determination of surface crystal structure, but severe limitations are imposed by the MPc layers under investigation.

The extensive polycrystallinity observed in active layer films makes coherent scattering from surface features impossible. Most substrates used as electrodes in organic electronic devices are not flat and crystalline on the scale required for LEED experiments. The structural information provided by LEED can also only be applied to the surface of the substrates so the underlying structure cannot be interrogated. LEED is therefore not an appropriate technique for overall determination of crystal structures of phthalocyanine films thicker than a few monolayers.

Selected area electron diffraction (SAED) used in transmission electron microscopes has been successfully employed as a crystallographic tool for phthalocyanine materials. Once more many restrictions and limitations exist, the first of which is the choice of substrate or support. For use as a TEM support substrates must be thin enough for electrons to be transmitted through them and the film under study. This often requires bespoke grids or meshes which bear no resemblance to the substrates used for surface science studies[77]. Sample preparation is also problematic, as crystalline samples cannot easily be cut and polished as inorganic materials are, and molecular crystals are prone to damage from the transmitted electron beam. Despite such problems examples exist in the literature of in depth structural analysis of MPcs using both TEM imaging and selected area electron diffraction.

Kobayashi et al. published impressive molecular resolution images of ZnPc films on vacuum deposited carbon films as early as 1981[48]. By using a minimum exposure method and specially designed low dose electron optics crystalline domains of the polycrystalline film were resolved. Interpretation of images of weakly crystalline films of organic materials

(where the mechanism responsible for contrast is not clear) is fraught with difficulty. No electron diffraction patterns were published in this work, and structures are calculated from imaging alone (Fig. 1.12).

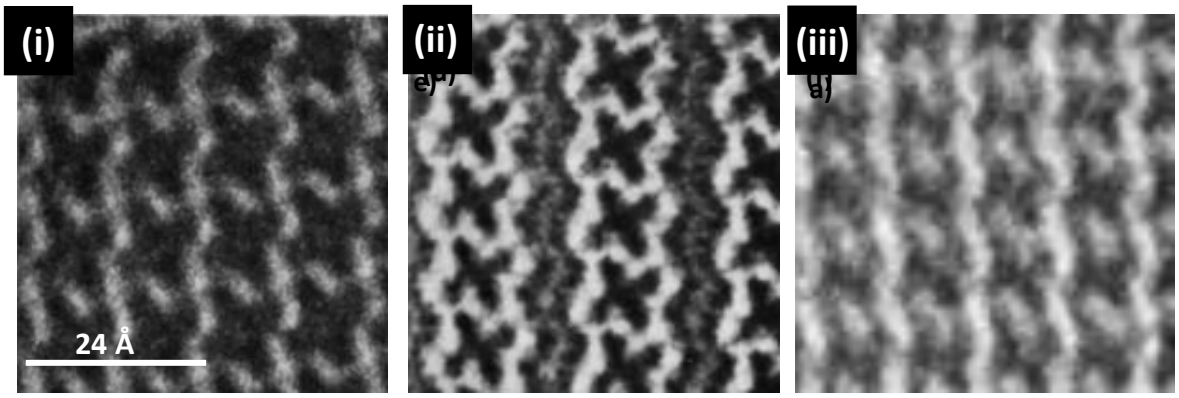

Figure 1.12 – TEM images of three proposed structural phases of ZnPc; (i) α-1 (ii) α-2 and (iii) α-3. Each image is on the same scale (reproduced from [48])

Rather than concentrating on the unit cell structure conclusions presented by the author, it is important to address the general view large scale images present of phthalocyanine thin films (Fig. 1.13). Small domains with a variety of lateral orientations and clear interference effects from stacking faults and small changes in angle are in evidence (Fig. 1.13, red circle). As the image is a cross sectional view through the out-of-substrate-plane structure of the film this agrees with many other observations of highly polycrystalline thin films.

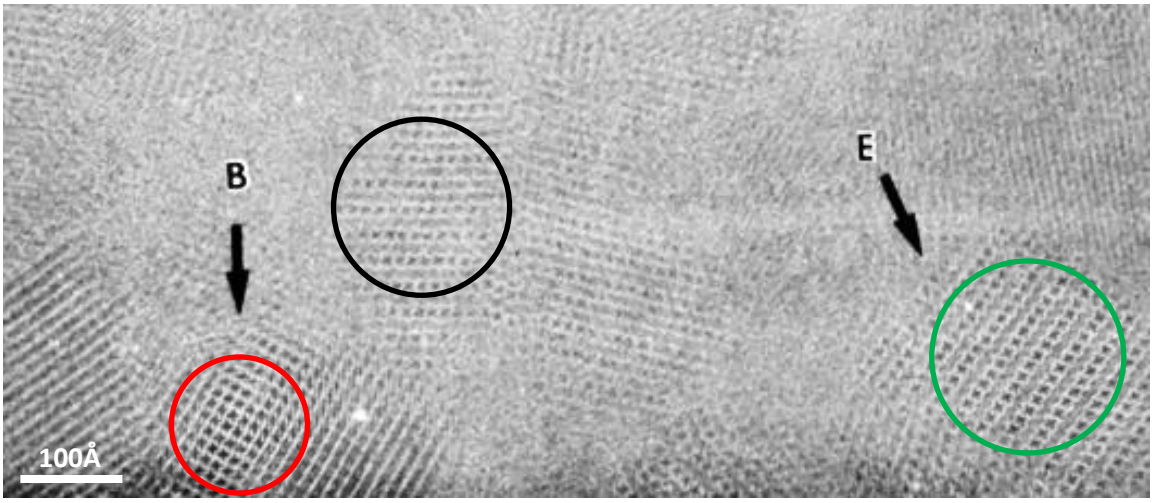

Figure 1.13 – TEM image of a ZnPc film; single domains are highlighted with coloured circles (reproduced from [48])

Diffraction patterns of planar phthalocyanines have been reported widely in the literature and structural assignments as well as epitaxial correlations have been made. In many cases films must undergo preparation before SAED experiments can begin; a supporting film is commonly evaporated on to the top of the film of interest. The substrate is then removed by flotation and the thin film is inverted onto the specimen grid. The problems presented by this are two-fold; firstly the new supporting film which is evaporated may either cause damage epitaxial strain or small changes in the crystal structure of the film. Secondly immersion in floatation media such as hydrofluoric acid can produce significant chemical or physical changes, and acid treatment can in fact induce phase transitions in phthalocyanines[78] (while sharp diffraction patterns are produced and discussions of structure are made the guarantee that no changes have been induced by sample preparation cannot).

Non-planar phthalocyanines have also been analysed by SAED, with structures indexed from diffraction patterns and compared to simulated structures or single crystal

reports. A recent paper by Pan et al.[79] investigated the effect of a thin under-layer upon the crystal structure of VOPc in layers then used for OTFT devices. Diffraction patterns were indexed to the only fully characterised phase of VOPc, despite the existence of multiple polymorphs in the literature which have not been solved. The same support film flotation technique was also used, and an assignment of the VOPc layer with respect to the underlying molecular templating layer is made (Fig. 1.14).

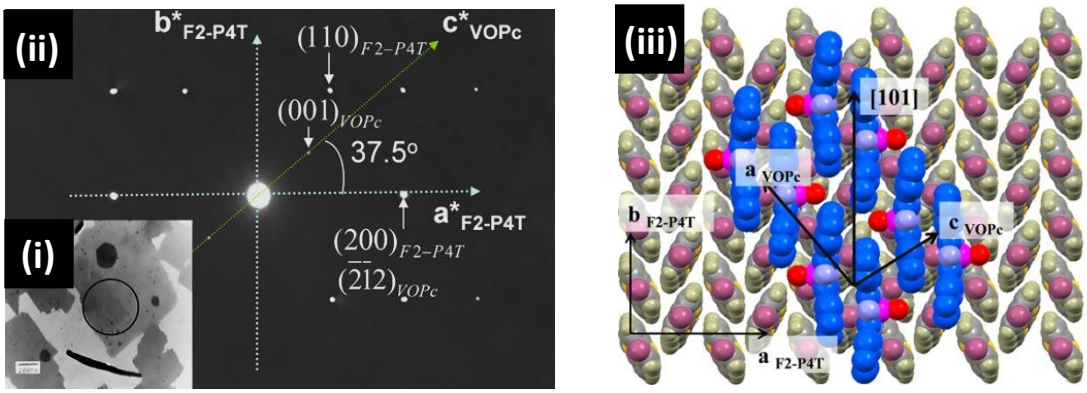

Figure 1.14 – (i) TEM image (ii) SAED pattern and (iii) proposed epitaxial structure of VOPc/F2-P4T multilayer structure (reproduced from [79]).

After the substrate is removed assignment of the relative direction of the incident beam with the axis of the crystalline film does not necessarily have any bearing to the original substrate/film relationship. While diffraction patterns do suggest a highly crystalline film over a large area the structure and relationship with the substrate are not robustly solved. Many other examples of useful but partial structural information of organic thin films from SAED exist in literature[80], but problems of sample preparation and the lack of thorough material structure investigation limit their scope.

Understanding the crystal structure of crystals and films of MPc molecules is a difficult task for both practical experimental reasons and due to the lack of a robust

catalogue of structural data in the literature. Single crystal structures are vital in understanding the solid state ordering crucial to charge transport and physical properties, while creating and analysing appropriate crystals is very difficult. Once processed into thin films laboratory diffraction techniques are useful in understanding their crystal structure but ultimately rely on indexing or comparison to a completely solved unit cell.

1.2.1.3. Magnetic properties of phthalocyanines

While phthalocyanines are established as useful organic semiconductors other aspects of their physical properties are attractive for technological applications, such as their magnetic characteristics. Characterisation of the magnetic properties of d-metal centred phthalocyanines has attracted significant interest and produced a variety of publications using an assortment of techniques. Research has centred mainly on two specific examples, phthalocyanines with central moieties of manganese and iron atoms. While other molecules have been investigated including CrPc[81], CoPc[82], NiPc[83], CuPc[82] and even briefly VOPc[81] the main discussion will be centred upon the two molecules on which most research has been based.

Systematic investigations into the magnetic properties of MPcs date back at least 48 years to the work of Lever et al.[81]. While measurements had been undertaken before this point no systematic study considering both experimental measurements and theoretical treatment of planar MPc systems had been conducted. MPc molecules were of interest mostly as a chance to study transition metal ions in a stable square planar geometry rather than as a useful material class for organic electronics. This work demonstrated that radically

different behaviour could be observed when the central species of the MPc was changed, and ground state configurations were suggested for all materials studied.

Of particular note in terms of magnetic properties is the Manganese centred planar metallo-phthalocyanine. MnPc is the most widely characterised MPc with respect to magnetism with experimental observations dating back to 1940[84] and detailed studies as early as 1965[81]. A variety of magnetically sensitive techniques have been used to characterise MnPc single crystals, powders and thin films at various temperatures and magnetic field strengths. Rather than focus on similarities and differences between methodologies and results, some clear trends and observations can be extracted from the literature as a whole. The most profound of these observations is a clear reliance of magnetic properties on crystal structure, rationalised by a change in through space intermolecular interactions[85]. In short MnPc in alpha and beta structural polymorphs is differentiated by a ca. 0.2 nm intermolecular spacing difference. This change is proposed to convert an antiferromagnetic one dimensional molecular chain structure (along the pi-stacking directions of the MnPc molecules) into a strongly ferromagnetic one. Once again the delicate balance of long range interactions in crystalline organic semiconductors is responsible for powerful property changes. While other MPc systems (including FePc, VOPc, CrPc and CoPc) have attracted some attention for magnetism studies such drastic behaviour changes have not been observed.

More recent work has attempted to reconcile structural changes with modifications in the exchange potentials which govern the observed magnetic characteristics in MPc thin films. If such changes could be firstly understood theoretically and finally controlled

experimentally stable materials with tuneable magnetic properties could be realised. Heutz et al.[86] achieved this in a publication of 2007 concerning the magnetic properties of MnPc and the widely used and closely related CuPc molecule. The polymorphism of planar MPc films is exploited here to produce changes in magnetic response and an under layer of another molecular system is used to alter the structure of the semiconductor in question to further alter the observed magnetic response. Alpha phase films were produced by evaporation onto ambient temperature substrates, beta phase by post growth annealing and a final 'new' phase utilising a PTCDA interlayer (Fig. 1.15).

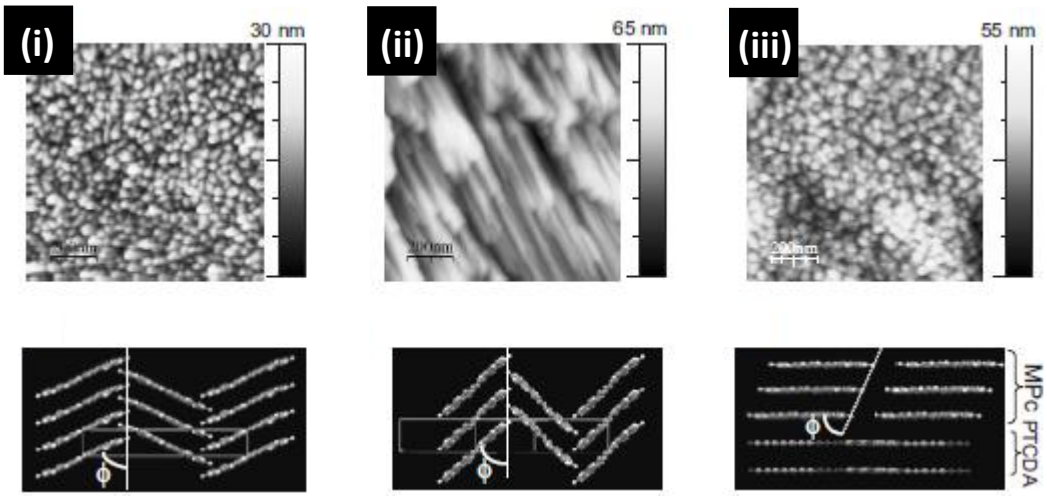

Figure 1.15 – AFM images of CuPc thin film structures: (i) CuPc/Kapton (ii) CuPc/Kapton (annealed) and (iii) CuPc/PTCDA/Kapton structure. Each structure has a crystal structure diagram below (reproduced from [86]).

The previously reported antiferro- to ferro- magnetic transition in MnPc was confirmed and the behaviour of CuPc through an analogous structure transition was contrasted to it. In CuPc initially antiferromagnetic character was converted to paramagnetism in the thermally modified beta phase film. The suggestion, therefore, was that by thermally converting between a metastable phase and global energy minimum magnetic interactions in a material approximated by one dimensional chains could be modified. While annealing produced an irreversible change in structure, if a reversible route to structural (and therefore magnetic) modification could be achieved a significant route to technological application of organic semiconductors with switchable spin states could be realised. In contrast to previous work AFM and XRD were used to characterise the films and ab initio calculations were employed to understand experimental observations.

1.3. Other Materials

A small selection of other materials (outside of MPc systems) has been employed during the course of the experimental work presented in this thesis and as such they are briefly summarised below.

1.3.1 PTCDA

3,4,9,10-perylene-tetracarboxylic-dianhydride (PTCDA) is a planar semiconducting small molecule which has been studied extensively both from a surface science perspective and in electronic devices[87]. This has been motivated partly by the ease with which high quality thin and ultrathin (approx. 1-2ML) films can be prepared in UHV conditions; usually attributed to the flat-lying geometry (molecular plane with respect to substrate plane) it adopts (Fig. 1.16). PTCDA was also demonstrated as a useful material[88] in organic-inorganic junction devices early in the lifecycle of organic electronics research.

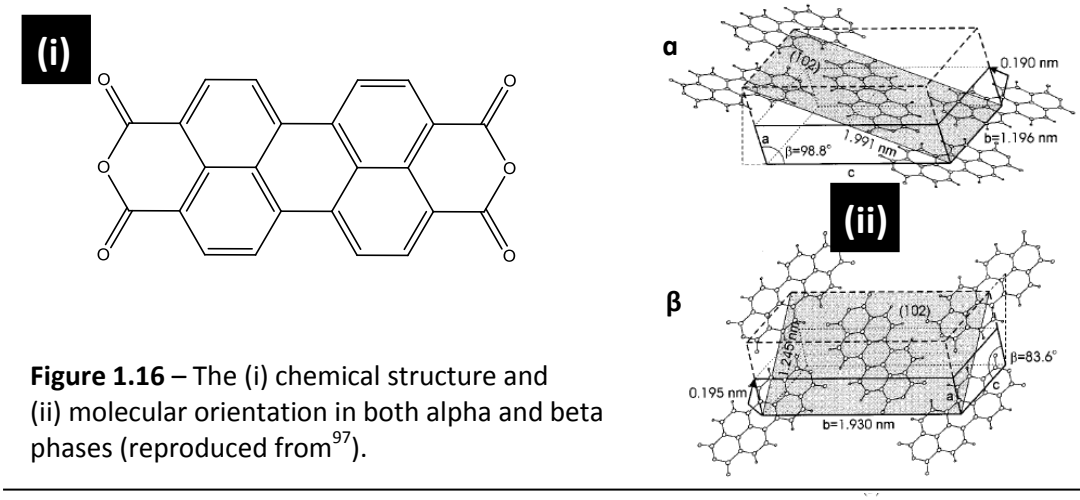

Figure 1.16 – The (i) chemical structure and (ii) molecular orientation in both alpha and beta phases (reproduced from[97]).

While PTCDA exhibits useful characteristics and complex behaviour on surfaces, in this work the reason for its use is the structural templating effects it can impose upon other organic materials. Heutz et al.[89] demonstrated the ability of thin layers of PTCDA deposited onto glass substrates to control the crystal structure observed by XRD in an overlayer of the dihydrogen phthalocyanine derivative. Later work demonstrated that this effect could be exploited to improve the performance of OPV devices incorporating MPc films as active layers[90]. While this behaviour might be initially surprising, considering the weak and long range nature of the interactions present in organic

crystals, introduction of a periodic 'template' layer could easily disrupt preferred adsorption geometries.

1.3.2 Copper Iodide

Copper (I) iodide is a binary metal halide which has been applied in this work as another vacuum evaporable structural templating layer. Other uses in industrial and research chemistry are widespread, but CuI has been shown to affect a change in crystal structure in organic semiconductors in recent literature. Copper iodide is considered to be a large band gap (approx. 3 eV) p-type semiconductor which can be prepared as thin films by evaporation in vacuum[91].

Copper iodide exists in three polymorphs in the solid state, a low temperature zinc blende intermediate beta phase wurtzite structure and a final high temperature rock salt alpha phase[92]. Each of these shows different electrochemical and semiconducting properties as can be expected from polymorphs of a semiconducting metal halide. Structural and topographical characterisation of evaporated thin films is not present in literature up to this point.

Layers of copper iodide have been shown to affect the crystallisation mechanism of MPc layers in a similar way to PTCDA. Cheng et al. demonstrated the efficacy of CuI 'buffer' layers in modifying the relative orientation of crystallites in a CuPc thin film employed as an active layer in an OPV device[93]. XRD analysis indicated that the overall out-of-plane orientation of the MPc layer changed on the addition of the CuI layer, suggesting switching from the pi-stacking MPc along the substrate plane to being out of plane. This is based on the indexing of the observed diffraction peaks in XRD traces, and agrees qualitatively with the previous work on controlling the orientation of MPc layers.

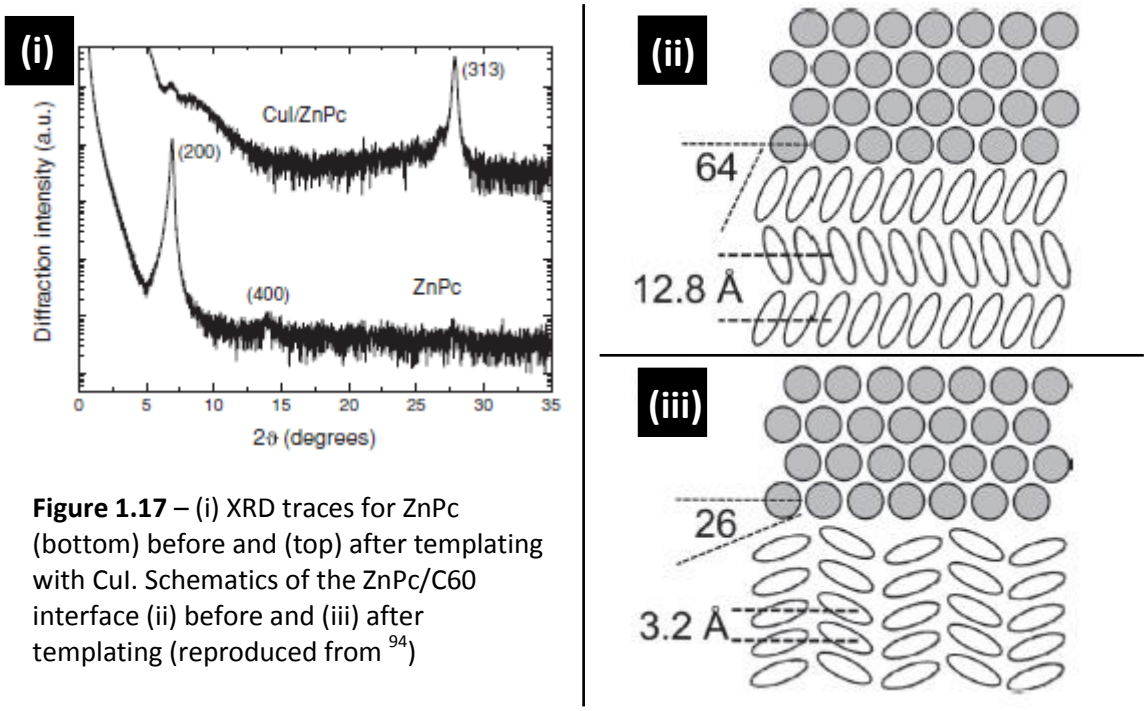

Figure 1.17 – (i) XRD traces for ZnPc (bottom) before and (top) after templating with CuI. Schematics of the ZnPc/C60 interface (ii) before and (iii) after templating (reproduced from [94])

More recently Rand et al.[94] further developed the understanding of this effect by applying CuI as a templating layer in ZnPc/C_{60} OPV devices. Structural changes induced by the thin CuI layer were observed (fig. 1.17) but the authors stress the importance of considering the interface between the ZnPc and C_{60} rather than the ZnPc/CuI interface alone. By modelling charge transfer processes it was suggested that charge transfer far from the templating interface is improved, and the change in structure of the ZnPc active layer is significant at both interfaces.

1.4. Substrates

The selection of substrates for the study of organic molecules is a difficult task, since if the intrinsic properties of materials are to be studied any influence of substrate chemistry or structure would ideally be removed. Restrictions are also imposed by the techniques involved, the two most stringent of which are for LEED and STM studies. In the case of LEED the surface should be both flat and highly ordered over large regions (approx. 100 nm) for patterns to be routinely recorded and indexed. For STM the surface must be conductive to allow the tunnelling of electrons between the sample and the tip, and for high resolution imaging should be as flat as possible over large (approx. 100 nm^2) areas.

To satisfy these restrictions metal single crystals were chosen as they provide robust, reusable, chemically inert and well characterised platforms for the study of organic molecules while being commercially available and simple to prepare in UHV.

1.4.1. Metal Single Crystal Surfaces

Noble metal single crystal surfaces (silver, gold and copper) were selected as they fulfilled the requirements described above. In order to produce measurements of wide applicability and relevance crystal surfaces that represent those used as electrodes in commercial applications were chosen. As evaporation is widespread as a method for metal electrode creation and evaporated metal films tend to a (111) orientation on most substrates, the (111) face of the three coinage metals was chosen.

1.4.1.1. The (111) surface

The only single crystal surfaces used as substrates for UHV surface science were aligned to the (111) Miller plane, so it is the only one that will be described here. The (111) plane of a face centred cubic (FCC) unit cell (Fig 1.18) represents a high density hexagonally packed array of atoms, and each of the metals used crystallise in this manner.

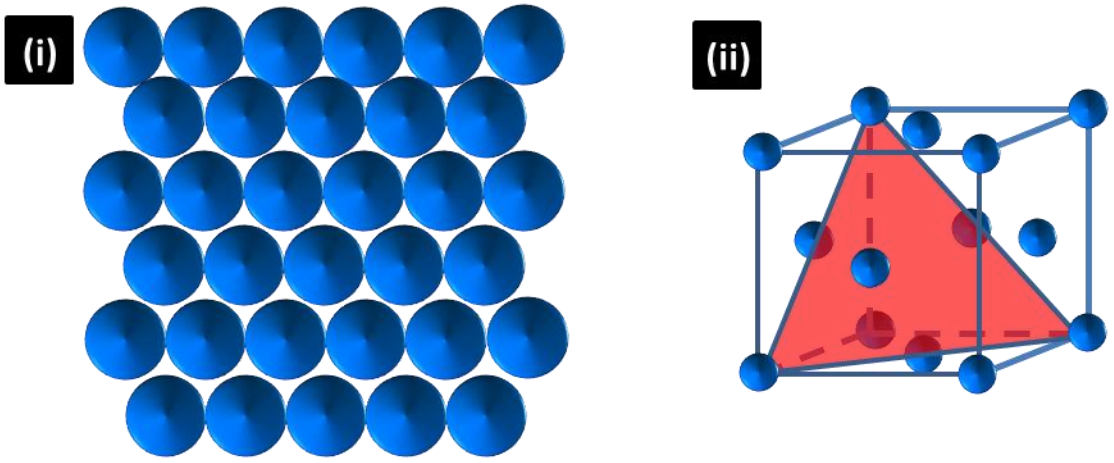

Figure 1.18 – The (i) plan view structure of a (111) surface and (ii) the (111) plane in an FCC unit cell

1.4.1.1.1 Au (111) surface reconstruction

Au (111) is the only face centred cubic metal surface which exhibits a surface reconstruction without adsorbates. This reconstruction is a long range transition between face centred cubic and hexagonal close packing, and the strain-induced buckling of the surface is visualised as bright lines running along the surface in a 'herringbone' pattern[95] (Fig. 1.19). The nature and structure of the 22x√3 reconstruction is well characterised and understood, and is only mentioned here to highlight the difference between reconstructed and unreconstructed metal surfaces.

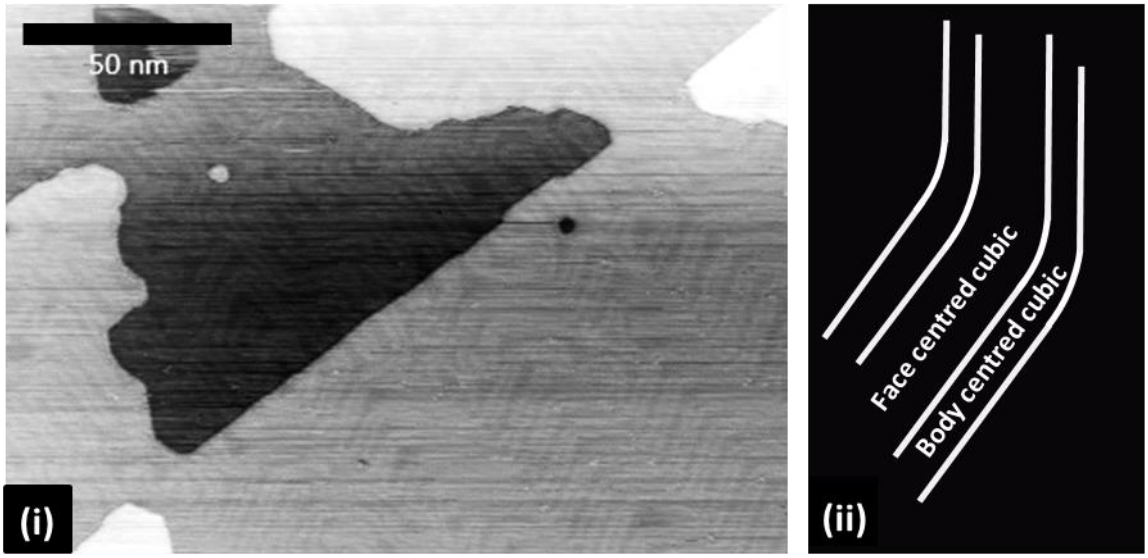

Figure 1.19 – STM image of (i) reconstructed Au(111) and (ii) a schematic of the surface reconstruction.

In the case of Au (111) a non-uniform energetic landscape is presented to an impinging molecule where local energy minima are found in the 'elbow' sites of the 120° turns in the reconstruction lines. This behaviour is not observed in the case of the unreconstructed surfaces of Ag (111) and Cu (111) and can have dramatic impacts on the adsorption architecture of molecular species[96].

1.5 – Thin film growth modes

The morphological and structural changes observed during the growth of thin films are an expression of the interplay between substrate-adsorbate and adsorbate-adsorbate interactions. In the growth of thin films this behaviour is conventionally be split into three dominant modes of growth[98]. While organic and inorganic systems show pronounced differences in growth characteristics due to the different interactions present in their solid state structures[99, 100] these three modes are useful models in both cases.

The first (and simplest) growth mode is layer by layer (Frank-van der Merwe, **Fig 1.20**) growth wherein each monolayer is completed before the next begins to grow. In general this behaviour is observed where the interaction between adsorbates (atoms of molecules) and the substrate is the stronger or more favourable than that between adsorbates. This kind of behaviour is commonly observed when epitaxial relationships are present between the overlayer and the substrate.

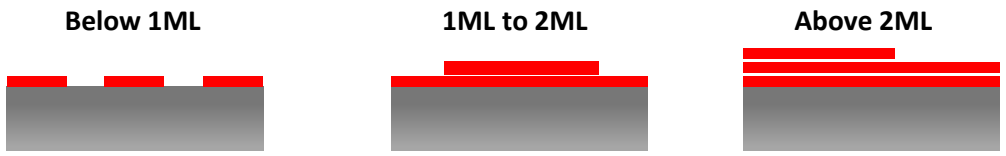

Figure 1.20 – Frank-van der Merwe (Layer-by-layer) film growth schematic

In the second case a 'wetting layer' can form on the substrate followed by the three dimension island (Stranski-Krastanov, **Fig 1.21**) growth out of the substrate plane. This modification of morphology after the first layer is attributed to factors including disparity in lattice parameters or surface energies between the growing layer and substrate. The wetting layer can be composed of

more than a single atomic or molecular layer but this type of growth usually features a critical thickness at which the growth is modified from layer-by-layer. Deposition past the critical thickness will result in larger 3D islands or nucleate more but will not produce two dimensional layers.

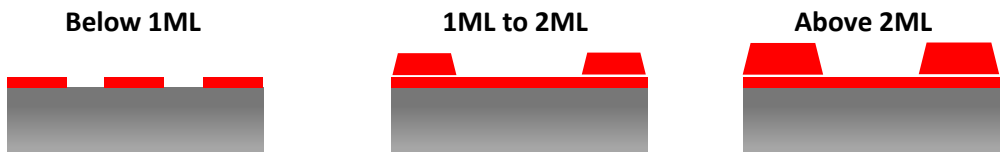

Figure 1.21 – Stranski-Krastanov (wetting layer plus island) film growth schematic

The final mode considered in classical growth models is that of island growth from the earliest stages of film formation (Volmer-Weber, **Fig 1.22**). In this regime the interactions between impinging atoms or molecules are stronger than with the substrate. Islands are formed to minimise the contact area of the film with the substrate and successive deposition leads to larger islands.

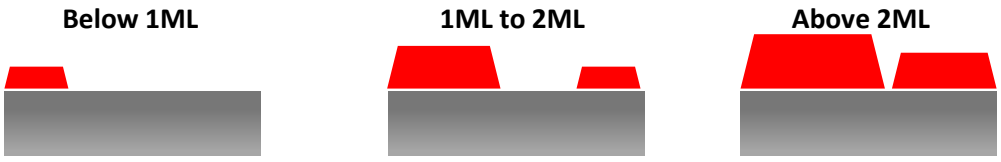

Figure 1.22 – Volmer-Weber (three dimensional island) film growth schematic

These islands can grow until they coalesce and completely cover the substrate but this will be at a much greater thickness than either of the other growth modes considered here. Archetypal systems for this kind of growth are metals such as gold on flat insulating substrates such including mica or alkali halide single crystals.

In each of these growth modes the thermodynamics of film formation are governed by the relative surface energies of the two materials (starting surface and film), γ_A and γ_B ($\gamma_A<\gamma_B$) and the interfacial energy of the growth interface, γ^*. This final term is the excess energy present at the surface when compared to the bulk of the material due to the disruption of the equilibrium bonding arrangement. If material A with the higher surface energy is deposited onto a surface of material B, $\gamma_A+ \gamma^*< \gamma_B$ and layer by layer growth is usually observed. In a situation where the lower surface energy material is deposited onto a surface of the other $\gamma_B+ \gamma^*> \gamma_A$ island growth minimising the overall area of the interface is preferred. Factors including crystallographic strain and thickness dependant structure can alter each of the surface energies which can complicate the growth modes. For this reason growth is often considered using combinations of these simplistic models.

1.6 – Motivation and aims

1.6.1. - Motivation

The fundamental motivation for the research undertaken here is the understanding of the relationship between the structure and morphology of thin phthalocyanine films and their physical properties. Properties of phthalocyanine films including; absorption of visible light, transport of electron or holes and response to magnetic or electric fields can be exploited to create useful electronic devices. Changes in the structure or morphology of phthalocyanine thin films have been demonstrated to strongly alter their physical properties, for example changes in crystal structure altering peak adsorption wavelengths in non-planar varieties. Phthalocyanines are also very sensitive to preparation conditions: factors such as choice of substrate along with rate and temperature of deposition can strongly affect structure and therefore physical properties. Fundamental understanding of structure-property relationships and accurate measurement of physical properties in phthalocyanine systems will inform the design and creation of more efficient and well understood devices.

The methods for phthalocyanine film preparation in vacuum for use in devices are relatively mature, allowing the creation of efficient devices with complex multi-layered structures. Most of the vacuum systems used do not include in-situ characterisation and complete devices are fabricated for testing. Probing structure or properties at points before the end of growth can therefore only realistically be undertaken by preparing single-component films of a variety of thicknesses. This process can be onerous, especially if the end goal of the growth process is a complete device from which a single figure of merit will be extracted. For this reason many fundamental investigations of structure-property relationships have not been undertaken and there is a lack of high quality data in

the literature. This dearth of understanding is compounded by the experimental impossibility to use a single characterisation method or instrument to monitor changes in structure or properties during growth. For example, monolayers of phthalocyanines create highly ordered structures but the X-ray intensity available in laboratory diffractometers makes measuring their periodicity impossible. While surface sensitive diffraction techniques (such as LEED) can be used to negate this problem the ultrahigh vacuum conditions required are not achieved in growth systems used for device fabrication. While thicker films can be analysed using laboratory X-ray diffractometers, any changes in structure below the critical thickness at which a signal is observed will be hidden. Despite this, a few examples of thickness dependant structure and properties are present in the literature and make the importance of probing multiple thicknesses apparent.

Three film thickness regimes have been chosen; the first monolayer, intermediate layers of 10-50 nm thickness and 'thick' films between 100-200 nm. Ideally the same characterisation methodology would be used to continuously monitor growing films; experimental limitations and the hugely polycrystalline nature of phthalocyanine films prevent this. Also, not all characterisation methods can be successfully applied in all thickness regimes due to the sensitivity limits of the available equipment. For example, XRD can only be used to probe crystal structure above thicknesses of approximately 30 nm in phthalocyanines but at this point film surfaces become too rough for meaningful STM imaging. These two factors necessitate the separation (to a certain extent) of property and structure measurements but it is the intention in this work that information gained in each regime can improve the understanding in the others.

The earliest stages of formation of phthalocyanine films are hugely important in determining the properties of the final film. In order to understand and control the surface and electronic structure of these interfaces model systems are commonly used to produce high quality surface characterisation data. Metal single crystals are used due to their commercial availability, relative

ease of preparation in vacuum and similarities to electrodes used in commercial electronic devices. Differences may, however, be expected in the surface and electronic structure produced by the same molecule on the (111) faces of different metals. This complicates the choice of metal crystal for a single molecular system and this is compounded when comparisons between molecules are desired. Using the same experimental equipment to probe each surface will make differences in the self-assembly and electronic structure immediately evident. These data can then be used to compare the behaviour on multiple metals and inform the choice of both model substrate and possibly even electrode system in commercial devices.

Another issue in using phthalocyanine molecules in electro- or optically active devices is the lack of control of surface morphology in active layers between 10 and 50 nm (commonly used in OPV and OTFT devices). Although structural and morphological control of phthalocyanine layers using evaporated organic and inorganic layers has been demonstrated the nature of the interaction and underlying causes are not known. With this in mind copper iodide (which has previously been used as a structural template for phthalocyanines) was to be prepared and characterised and subsequent controlled growth of phthalocyanine layers will be undertaken. Surface characterisation of this system will allow a deeper understanding of the underlying cause of the structural modification which has previously been reported.

Chemical modification of phthalocyanines has been used to alter their optical and electronic properties in recent years but the effect of the modification on their magnetic properties has been largely ignored. This is surprising as phthalocyanines, especially transition metal centred versions, have shown unique and promising magnetic behaviour in thin films and powders. The copper phthalocyanine and fluorinated copper phthalocyanine pair of molecules can be used to test this behaviour. In both cases the molecule is commercially available and can be purified and processed into thin films using evaporation in vacuum. It is hoped that magnetic measurements of the

fluorinated system will increase our understanding of the impact of the modification of the electronic structure of the molecule upon its magnetic properties.

1.6.2 – Aims

- To compare and contrast the growth of monolayers of phthalocyanines on the (111) surfaces of gold, copper and silver. Vanadium oxide phthalocyanine will be used as the central oxovanadium moiety creates a non-planar structure and much less previous characterisation has been carried out on this class of phthalocyanine.
    - Surface structure will be probed using STM and LEED while electronic structure measurements will rely on UPS

- To grow copper iodide thin films by evaporation in vacuum followed by characterisation of their surface and crystal structure. Substrate growth temperature will be used in an attempt to control the morphology before these films are used as molecular templates for the growth of a planar phthalocyanine film.
    - XRD will be used to measure the crystal structure of both the template layer and phthalocyanine film and a combination of (SEM) and AFM will be used to monitor changes in morphology and growth behaviour.

- To establish the magnetic characteristics of fully fluorinated copper phthalocyanine and compare this behaviour to the previously measured hydrogenated equivalent
    - Thin films and powders will be subjected to the same magnetic characterisation, and the effect of an organic templating layer (PTCDA) on this system will be investigated

References:

(1) Forrest, S. R. The path to ubiquitous and low-cost organic electronic appliances on plastic. *Nature* **2004**, *428*, 911–8.

(2) Pierret, R. F. *Semiconductor device fundamentals*; Addison Wesley, 1996.

(3) Nelson, J. *The Physics of Solar Cells*; Imperial College Press, 2003.

(4) Anthony, J. E. Functionalized acenes and heteroacenes for organic electronics. *Chemical reviews* **2006**, *106*, 5028–48.

(5) Cahen, D.; Kahn, A. Electron Energetics at Surfaces and Interfaces: Concepts and Experiments. *Advanced Materials* **2003**, *15*, 271–277.

(6) Anthony, J. E.; Brooks, J. S.; Eaton, D. L.; Parkin, S. R. Functionalized Pentacene: Improved Electronic Properties from Control of Solid-State Order. *Journal of the American Chemical Society* **2001**, *123*, 9482–9483.

(7) De Oteyza, D. G.; El-Sayed, A.; Garcia-Lastra, J. M.; Goiri, E.; Krauss, T. N.; Turak, A.; Barrena, E.; Dosch, H.; Zegenhagen, J.; Rubio, A.; Wakayama, Y.; Ortega, J. E. Copper-phthalocyanine based metal-organic interfaces: the effect of fluorination, the substrate, and its symmetry. *The Journal of Chemical Physics* **2010**, *133*, 214703.

(8) Koudia, M.; Abel, M.; Maurel, C.; Bliek, A.; Catalin, D.; Mossoyan, M.; Mossoyan, J.-C.; Porte, L. Influence of chlorine substitution on the self-assembly of zinc phthalocyanine. *The Journal of Physical Chemistry. B* **2006**, *110*, 10058–62.

(9) Wang, Y.; Wu, K.; Kröger, J.; Berndt, R. Review Article: Structures of phthalocyanine molecules on surfaces studied by STM. *AIP Advances* **2012**, *2*, 041402.

(10) Koch, N.; Kahn, A.; Ghijsen, J.; Pireaux, J.-J.; Schwartz, J.; Johnson, R. L.; Elschner, A. Conjugated organic molecules on metal versus polymer electrodes: Demonstration of a key energy level alignment mechanism. *Applied Physics Letters* **2003**, *82*, 70.

(11) Klappenberger, F.; Weber-Bargioni, a; Auwärter, W.; Marschall, M.; Schiffrin, A.; Barth, J. V Temperature dependence of conformation, chemical state, and metal-directed assembly of tetrapyridyl-porphyrin on Cu(111). *The Journal of Chemical Physics* **2008**, *129*, 214702.

(12) Nicoara, N.; Román, E.; Gómez-Rodríguez, J. M.; Martín-Gago, J. a.; Méndez, J. Scanning tunneling and photoemission spectroscopies at the PTCDA/Au(111) interface. *Organic Electronics* **2006**, *7*, 287–294.

(13) Engel, M. K. M. M. K.; Complexes, P. Single crystal and solid state molecular structures of phthalocyanine complexes. *Kawamura Rikagaku Kenkyusho Hokoku* **1997**, *D*, 11–54.

(14) Horowitz, G. Organic Field-Effect Transistors. *Advanced Materials* **1998**, *10*, 365–377.

(15) De Boer, R. W. I.; Gershenson, M. E.; Morpurgo, A. F.; Podzorov, V. Organic single-crystal field-effect transistors, *Physica Status Solidi (a)* **2004**, *201*, 1302–1331.

(16) Leo, K. Organic light-emitting diodes: Efficient and flexible solution. *Nature Photonics* **2011**, *5*, 716–718.

(17) Wang, Y.; Ji, W.; Shi, D.; Du, S.; Seidel, C.; Ma, Y.; Gao, H.-J.; Chi, L.; Fuchs, H. Structural evolution of pentacene on a Ag(110) surface. *Physical Review B* **2004**, *69*, 075408.

(18) Chen, Q.; McDowall, A. J.; Richardson, N. V. Ordered Structures of Tetracene and Pentacene on Cu(110) Surfaces. *Langmuir* **2003**, *19*, 10164–10171.

(19) Yim, S.; Jones, T. S. Structure of phthalocyanine overlayers on the surfaces of InSb and InAs. *Surface Science* **2002**, *521*, 151–159.

(20) Bayliss, S. Thin film properties and surface morphology of metal free phthalocyanine films grown by organic molecular beam deposition. *Physical Chemistry Chemical Physics* **1999**, *1*, 3673–3676.

(21) Ludwig, C.; Gompf, B.; Glatz, W.; Petersen, J.; Eisenmenger, W.; Mobus, M.; Zimmermann, U.; Karl, N. Video-STM, LEED and X-ray diffraction investigations of PTCDA on graphite. *Zeitschrift fur Physik B Condensed Matter* **1992**, *86*, 397–404.

(22) Chen, Q.; McDowall, A. J.; Richardson, N. V. Growth and Evolution of Perylene Thin Films on Cu(110). *Chemistry of Materials* **2003**, *15*, 4113–4117.

(23) Schlaf, R.; Merritt, C. D.; Crisafulli, L. A.; Kafafi, Z. H. Organic semiconductor interfaces: Discrimination between charging and band bending related shifts in frontier orbital line-up measurements with photoemission spectroscopy. *Journal of Applied Physics* **1999**, *86*, 5678.

(24) Braun, A.; Tcherniac, J. Über die Produkte der Einwirkung von Acetanhydrid auf Phthalamid. *Berichte der deutschen chemischen Gesellschaft* **1907**, *40*, 2709–2714.

(25) Leznoff, C.C. Lever, A. B. P. *Phthalocyanines : Properties and Applications*; VCH (New York), 1989.

(26) De Diesbach, H.; Von der Weid, E. Quelques sels complexes des o-dinitriles avec le cuivre et la pyridine. *Helvetica Chimica Acta* **1927**, *10*, 886–888.

(27) Peumans, P.; Yakimov, A.; Forrest, S. R. Small molecular weight organic thin-film photodetectors and solar cells. *Journal of Applied Physics* **2003**, *93*, 3693.

(28) Bao, Z.; Rogers, J. A.; Katz, H. E. Printable organic and polymeric semiconducting materials and devices. *Journal of Materials Chemistry* **1999**, *9*, 1895–1904.

(29) Forrest, S. R. Ultrathin Organic Films Grown by Organic Molecular Beam Deposition and Related Techniques. *Chemical Reviews* **1997**, *97*, 1793–1896.

(30) Ottaviano, L.; Di Nardo, S.; Lozzi, L.; Passacantando, M.; Picozzi, P.; Santucci, S. Thin and ultra-thin films of nickel phthalocyanine grown on highly oriented pyrolitic graphite: an XPS, UHV-AFM and air tapping-mode AFM study. *Surface Science* **1997**, *373*, 318–332.

(31) De Oteyza, D. G.; Barrena, E.; Ossó, J. O.; Sellner, S.; Dosch, H. Thickness-dependent structural transitions in fluorinated copper-phthalocyanine (F16CuPc) films. *Journal of the American Chemical Society* **2006**, *128*, 15052–3.

(32) Lippel, P.; Wilson, R.; Miller, M.; Wöll, C.; Chiang, S. High-Resolution Imaging of Copper-Phthalocyanine by Scanning-Tunneling Microscopy. *Physical Review Letters* **1989**, *62*, 171–174.

(33) Chizhov, I.; Scoles, G.; Kahn, A. The Influence of Steps on the Orientation of Copper Phthalocyanine Monolayers on Au(111). *Langmuir* **2000**, *16*, 4358–4361.

(34) Hill, I. G.; Kahn, A. Combined photoemission/in vacuo transport study of the indium tin oxide/copper phthalocyanine/N,N[sup ']-diphenyl-N,N[sup ']-bis(l-naphthyl)-1,1[sup ']biphenyl-4,4[sup ''']diamine molecular organic semiconductor system. *Journal of Applied Physics* **1999**, *86*, 2116.

(35) Repp, J.; Meyer, G.; Paavilainen, S.; Olsson, F. E.; Persson, M. Imaging bond formation between a gold atom and pentacene on an insulating surface. *Science (New York, N.Y.)* **2006**, *312*, 1196–9.

(36) Gimzewski, J.; Stoll, E.; Schlittler, R. Scanning tunneling microscopy of individual molecules of copper phthalocyanine adsorbed on polycrystalline silver surfaces. *Surface Science* **1987**, *181*, 267–277.

(37) Baró, A. M.; Miranda, R.; Alamán, J.; García, N.; Binnig, G.; Rohrer, H.; Gerber, C.; Carrascosa, J. L. Determination of surface topography of biological specimens at high resolution by scanning tunnelling microscopy. *Nature* **1985**, *315*, 253–254.

(38) Tersoff, J.; Hamann, D. R. Theory and Application for the Scanning Tunneling Microscope. *Physical Review Letters* **1983**, *50*, 1998–2001.

(39) Tsukada, M.; Kobayashi, K.; Isshiki, N.; Kageshima, H. First-principles theory of scanning tunneling microscopy. *Surface Science Reports* **1991**, *13*, 267–304.

(40) Lu, X.; Hipps, K. W.; Wang, X. D.; Mazur, U. Scanning Tunneling Microscopy of Metal Phthalocyanines: d 7 and d 9 Cases. *Journal of the American Chemical Society* **1996**, *118*, 7197–7202.

(41) Pomerantz, M.; Aviram, A.; McCorkle, R. A.; Li, L.; Schrott, A. G. Rectification of STM Current to Graphite Covered with Phthalocyanine Molecules. *Science (New York, N.Y.)* **1992**, *255*, 1115–8.

(42) Manivannan, A.; Nagahara, L. A.; Yanagi, H.; Kouzeki, T.; Ashida, M.; Maruyama, Y.; Hashimoto, K.; Fujishima, A. Scanning tunneling microscopy observations of zincnaphthalocyanine on MoS_2. *Thin Solid Films* **1993**, *226*, 6–8.

(43) Rochet, F.; Dufour, G.; Roulet, H.; Motta, N.; Sgarlata, A.; Piancastelli, M. N.; De Crescenzi, M. Copper phthalocyanine on Si(111)-7 × 7 and Si(001)-2 × 1: an XPS/AES and STM study. *Surface Science* **1994**, *319*, 10–20.

(44) Cheng, Z. H.; Gao, L.; Deng, Z. T.; Jiang, N.; Liu, Q.; Shi, D. X.; Du, S. X.; Guo, H. M.; Gao, H.-J. Adsorption Behavior of Iron Phthalocyanine on Au(111) Surface at Submonolayer Coverage. *Journal of Physical Chemistry C* **2007**, *111*, 9240–9244.

(45) Tsukahara, N.; Noto, K.; Ohara, M.; Shiraki, S.; Takagi, N.; Shin, S.; Kawai, M. Adsorption-Induced Switching of Magnetic Anisotropy in a Single Iron(II) Phthalocyanine Molecule on an Oxidized Cu(110) Surface. *Physical Review Letters* **2009**, *102*, 167203.

(46) Tang, Q.; Li, H.; Liu, Y.; Hu, W. High-performance air-stable n-type transistors with an asymmetrical device configuration based on organic single-crystalline submicrometer/nanometer ribbons. *Journal of the American Chemical Society* **2006**, *128*, 14634–9.

(47) Hooks, D. E.; Fritz, T.; Ward, M. D. Epitaxy and Molecular Organization on Solid Substrates. *Advanced Materials* **2001**, *13*, 227–241.

(48) Kobayashi, T.; Fujiyoshi, Y.; Iwatsu, F.; Uyeda, N. High-resolution TEM images of zinc phthalocyanine polymorphs in thin films. *Acta Crystallographica Section A* **1981**, *37*, 692–697.

(49) Kamiya Okudaira, K.; Hasegawa, S.; Ishii, H.; Seki, K.; Harada, Y.; Ueno, N. Structure of copper- and H[sub 2]-phthalocyanine thin films on MoS[sub 2] studied by angle-resolved ultraviolet photoelectron spectroscopy and low energy electron diffraction. *Journal of Applied Physics* **1999**, *85*, 6453.

(50) Buchholz, J. C.; Somorjai, G. A. The surface structures of phthalocyanine monolayers and vapor-grown films: A low-energy electron diffraction study. *The Journal of Chemical Physics* **1977**, *66*, 573.

(51) Cox, J. J.; Bayliss, S. M.; Jones, T. S. Ordered copper phthalocyanine overlayers on InAs and InSb (100) surfaces. *Surface Science* **1999**, *433-435*, 152–156.

(52) Stadler, C.; Hansen, S.; Kröger, I.; Kumpf, C.; Umbach, E. Tuning intermolecular interaction in long-range-ordered submonolayer organic films. *Nature Physics* **2009**, *5*, 153–158.

(53) Gopakumar, T. G.; Lackinger, M.; Hackert, M.; Müller, F.; Hietschold, M. Adsorption of Palladium Phthalocyanine on Graphite: STM and LEED Study. *The Journal of Physical Chemistry B* **2004**, *108*, 7839–7843.

(54) Bobaru, S. C.; Salomon, E.; Layet, J.-M.; Angot, T. Structural Properties of Iron Phtalocyanines on Ag(111): From the Submonolayer to Monolayer Range. *The Journal of Physical Chemistry C* **2011**, *115*, 5875–5879.

(55) Hill, I. G.; Rajagopal, A.; Kahn, A.; Hu, Y. Molecular level alignment at organic semiconductor-metal interfaces. *Applied Physics Letters* **1998**, *73*, 662.

(56) Baldo, M.; Forrest, S. Interface-limited injection in amorphous organic semiconductors. *Physical Review B* **2001**, *64*, 085201.

(57) Sato, N.; Seki, K.; Inokuchi, H. Polarization energies of organic solids determined by ultraviolet photoelectron spectroscopy. *Journal of the Chemical Society, Faraday Transactions 2* **1981**, *77*, 1621.

(58) Hill, I.; Kahn, A.; Soos, Z.; Pascal, Jr, R. A. Charge-separation energy in films of π-conjugated organic molecules. *Chemical Physics Letters* **2000**, *327*, 181–188.

(59) Bansal, N.; Reynolds, L. X.; MacLachlan, A.; Lutz, T.; Ashraf, R. S.; Zhang, W.; Nielsen, C. B.; McCulloch, I.; Rebois, D. G.; Kirchartz, T.; Hill, M. S.; Molloy, K. C.; Nelson, J.; Haque, S. A Influence of crystallinity and energetics on charge separation in polymer-inorganic nanocomposite films for solar cells. *Scientific reports* **2013**, *3*, 1531.

(60) Hill, I. G.; Kahn, A. Energy level alignment at interfaces of organic semiconductor heterostructures. *Journal of Applied Physics* **1998**, *84*, 5583.

(61) Cho, S. W.; DeMasi, A.; Preston, A. R. H.; Smith, K. E.; Piper, L. F. J.; Chauhan, K. V.; Jones, T. S. Probing the effect of relative molecular orientation on the photovoltaic device performance of an organic bilayer heterojunction using soft X-ray spectroscopies. *Applied Physics Letters* **2012**, *100*, 263302.

(62) Krull, C.; Robles, R.; Mugarza, A.; Gambardella, P. Site- and orbital-dependent charge donation and spin manipulation in electron-doped metal phthalocyanines. *Nature Materials* **2013**, *12*, 337–43.

(63) Niederhausen, J.; Amsalem, P.; Wilke, A.; Schlesinger, R.; Winkler, S.; Vollmer, A.; Rabe, J. P.; Koch, N. Doping of C_{60} (sub)monolayers by Fermi-level pinning induced electron transfer. *Physical Review B* **2012**, *86*, 081411.

(64) Hayashida, M.; Kawasaki, T.; Kimura, Y.; Takai, Y. Estimation of suitable condition for observing copper–phthalocyanine crystalline film by transmission electron microscopy. *Nuclear Instruments and Methods in Physics Research Section B: Beam Interactions with Materials and Atoms* **2006**, *248*, 273–278.

(65) Dent, C. E.; Linstead, R. P.; Lowe, A. R. Phthalocyanines. Part VI. The structure of the phthalocyanines. *Journal of the Chemical Society (Resumed)* **1934**, 1033.

(66) Robertson, J. M. An X-ray study of the structure of the phthalocyanines. Part I. The metal-free, nickel, copper, and platinum compounds. *Journal of the Chemical Society (Resumed)* **1935**, 615.

(67) Brown, C. J. Crystal structure of Beta-copper phthalocyanine. *Journal of the Chemical Society A: Inorganic, Physical, Theoretical* **1968**, 2488.

(68) Gould, R. Structure and electrical conduction properties of phthalocyanine thin films. *Coordination Chemistry Reviews* **1996**, *156*, 237–274.

(69) Hoshino, A.; Takenaka, Y.; Miyaji, H. Redetermination of the crystal structure of α-copper phthalocyanine grown on KCl. *Acta Crystallographica Section B Structural Science* **2003**, *59*, 393–403.

(70) Griffiths, C. H.; Walker, M. S.; Goldstein, P. Polymorphism in Vanadyl Phthalocyanine. *Molecular Crystals and Liquid Crystals* **1976**, *33*, 149–170.

(71) Brumbach, M.; Placencia, D.; Armstrong, N. R. Titanyl Phthalocyanine/C_{60} Heterojunctions: Band-Edge Offsets and Photovoltaic Device Performance. *Journal of Physical Chemistry C* **2008**, *112*, 3142–3151.

(72) Kim, D. Y.; So, F.; Gao, Y. Aluminum phthalocyanine chloride/C_{60} organic photovoltaic cells with high open-circuit voltages. *Solar Energy Materials and Solar Cells* **2009**, *93*, 1688–1691.

(73) Wang, L.; Liu, G.; Wang, H.; Song, D.; Yu, B.; Yan, D. Switch-on transient behavior of vanadium phthalocyanine based organic transistors. *Applied Physics Letters* **2007**, *91*, 063511.

(74) Hancox, I.; Sullivan, P.; Chauhan, K. V.; Beaumont, N.; Rochford, L. A.; Hatton, R. A.; Jones, T. S. The effect of a MoOx hole-extracting layer on the performance of organic photovoltaic cells based on small molecule planar heterojunctions. *Organic Electronics* **2010**, *11*, 2019–2025.

(75) Schünemann, C.; Elschner, C.; Levin, A. ; Levichkova, M.; Leo, K.; Riede, M. Zinc phthalocyanine — Influence of substrate temperature, film thickness, and kind of substrate on the morphology. *Thin Solid Films* **2011**, *519*, 3939–3945.

(76) Bayliss, S. M.; Heutz, S.; Rumbles, G.; Jones, T. S. Thin film properties and surface morphology of metal free phthalocyanine films grown by organic molecular beam deposition. *Physical Chemistry Chemical Physics* **1999**, *1*, 3673–3676.

(77) Brinkmann, M.; Wittmann, J.-C.; Barthel, M.; Hanack, M.; Chaumont, C. Highly Ordered Titanyl Phthalocyanine Films Grown by Directional Crystallization on Oriented Poly(Tetrafluoroethylene) Substrate. *Chemistry of Materials* **2002**, *14*, 904–914.

(78) Berger, O.; Fischer, W.; Adolphi, B. Studies on phase transformations of Cu-phthalocyanine thin films. *Journal of Materials Chemistry* **2000**, *11*, 331–346.

(79) Pan, F.; Tian, H.; Qian, X.; Huang, L.; Geng, Y.; Yan, D. High performance vanadyl phthalocyanine thin-film transistors based on fluorobenzene end-capped quaterthiophene as the inducing layer. *Organic Electronics* **2011**, *12*, 1358–1363.

(80) Tong, W. Y.; Djurisić, a B.; Xie, M. H.; Ng, a C. M.; Cheung, K. Y.; Chan, W. K.; Leung, Y. H.; Lin, H. W.; Gwo, S. Metal phthalocyanine nanoribbons and nanowires. *The Journal of Physical Chemistry. B* **2006**, *110*, 17406–13.

(81) Lever, A. B. P. 336. The magnetic behaviour of transition-metal phathalocyanines. *Journal of the Chemical Society (Resumed)* **1965**, 1821.

(82) Miyoshi, H. The Magnetic Properties of Manganese(II) Phthalocyanine. II. *Bulletin of the Chemical Society of Japan* **1974**, *47*, 561–565.

(83) Senff, H.; Klemm, W. Magnetochemische Untersuchungen, XXXV. Schwermetallkomplexe des Phthalocyanins. *Journal fur Praktische Chemie* **1939**, *154*, 73–81.

(84) Ishikawa, N. *Functional Phthalocyanine Molecular Materials*; Jiang, J., Ed.; Springer Berlin Heidelberg: Berlin, Heidelberg, 2010; Vol. 135, pp. 211–228.

(85) Wu, W.; Kerridge, A.; Harker, A.; Fisher, A. Structure-dependent exchange in the organic magnets Cu(II)Pc and Mn(II)Pc. *Physical Review B* **2008**, *77*, 184403.

(86) Heutz, S.; Mitra, C.; Wu, W.; Fisher, A. J.; Kerridge, A.; Stoneham, M.; Harker, a. H.; Gardener, J.; Tseng, H.-H.; Jones, T. S.; Renner, C.; Aeppli, G. Molecular Thin Films: A New Type of Magnetic Switch. *Advanced Materials* **2007**, *19*, 3618–3622.

(87) Tautz, F. S. Structure and bonding of large aromatic molecules on noble metal surfaces: The example of PTCDA. *Progress in Surface Science* **2007**, *82*, 479–520.

(88) Forrest, S. R. Organic-on-inorganic semiconductor contact barrier devices. *Applied Physics Letters* **1982**, *41*, 90.

(89) Heutz, S.; Cloots, R.; Jones, T. S. Structural templating effects in molecular heterostructures grown by organic molecular-beam deposition. *Applied Physics Letters* **2000**, *77*, 3938.

(90) Sullivan, P.; Jones, T. S.; Ferguson, A. J.; Heutz, S. Structural templating as a route to improved photovoltaic performance in copper phthalocyanine/fullerene (C_{60}) heterojunctions. *Applied Physics Letters* **2007**, *91*, 233114.

(91) Bührer, W.; Hälg, W. Crystal structure of high-temperature cuprous iodide and cuprous bromide. *Electrochimica Acta* **1977**, *22*, 701–704.

(92) Yashima, M.; Xu, Q.; Yoshiasa, A.; Wada, S. Crystal structure, electron density and diffusion path of the fast-ion conductor copper iodide CuI. *Journal of Materials Chemistry* **2006**, *16*, 4393.

(93) Cheng, C. H.; Wang, J.; Du, G. T.; Shi, S. H.; Du, Z. J.; Fan, Z. Q.; Bian, J. M.; Wang, M. S. Organic solar cells with remarkable enhanced efficiency by using a CuI buffer to control the molecular orientation and modify the anode. *Applied Physics Letters* **2010**, *97*, 083305.

(94) Rand, B. P.; Cheyns, D.; Vasseur, K.; Giebink, N. C.; Mothy, S.; Yi, Y.; Coropceanu, V.; Beljonne, D.; Cornil, J.; Brédas, J.-L.; Genoe, J. The Impact of Molecular Orientation on the Photovoltaic Properties of a Phthalocyanine/Fullerene Heterojunction. *Advanced Functional Materials* **2012**, *22*, 2987–2995.

(95) Barth, J.; Brune, H.; Ertl, G.; Behm, R. Scanning tunneling microscopy observations on the reconstructed Au(111) surface: Atomic structure, long-range superstructure, rotational domains, and surface defects. *Physical review. B, Condensed matter* **1990**, *42*, 9307–9318.

(96) Barth, J. V Molecular architectonic on metal surfaces. *Annual Review of Physical Chemistry* **2007**, *58*, 375–407.

(97) Ogawa, T.; Kuwamoto, K.; Isoda, S.; Kobayashi, T.; Karl, N. 3,4:9,10-Perylenetetracarboxylic dianhydride (PTCDA) by electron crystallography. *Acta Crystallographica Section B Structural Science* **1999**, *55*, 123–130.

(98) D. A. King and P.D. Woodruff (eds.) Growth and properties of Ultrathin Epitaxial Layers. Elsevier (**1997**) Chapter 1

(99) Forrest, S.R. and Burrows, P.E. Growth modes of organic semiconductor thin films using molecular beam deposition: epitaxy, van der Waals epitaxy and quasi-epitaxy. *Supramol. Sci.* **1997**, 4, 127-139

(100) Forrest, S.R. Ultrathin organic films grown by organic molecular beam deposition and related techniques. *Chem. Rev* **1997**, 97,1793-1896

Chapter Two

Experimental

The experimental techniques used in this work can be split into those housed in a homebuilt multi-chamber UHV system and those under ambient conditions and as such ex situ to the creation of samples. The UHV system will be described first followed by the techniques housed within along with brief theoretical aspects key to their operation and interpretation. Ex-situ techniques will then be described in the same manner.

2.1 – The UHV system

The processes of substrate preparation, film growth and a variety of analysis techniques were undertaken in a custom built multi chamber UHV system (Fig. 2.1). Vacuum was maintained by a combination of oil free scroll pumps which provided backing pressures for turbo-molecular pumps and finally ion getter pumps for the highest vacuum. The system is made up of four chambers; the fast entry chamber (FEC), the transfer chamber housing the STM (STM/TRANS), the film growth chamber (GROWTH), and finally the analysis chamber (ANALYSIS). Each chamber is separated from the others by gate valves and each chamber (excluding the STM/TRANS) can be individually vented to atmospheric pressures of nitrogen and pumped to UHV. The FEC facilitates fast sample introduction and removal without venting any other chamber, and the base pressure of the system is in the low 10^{-10} mbar region after bakeout.

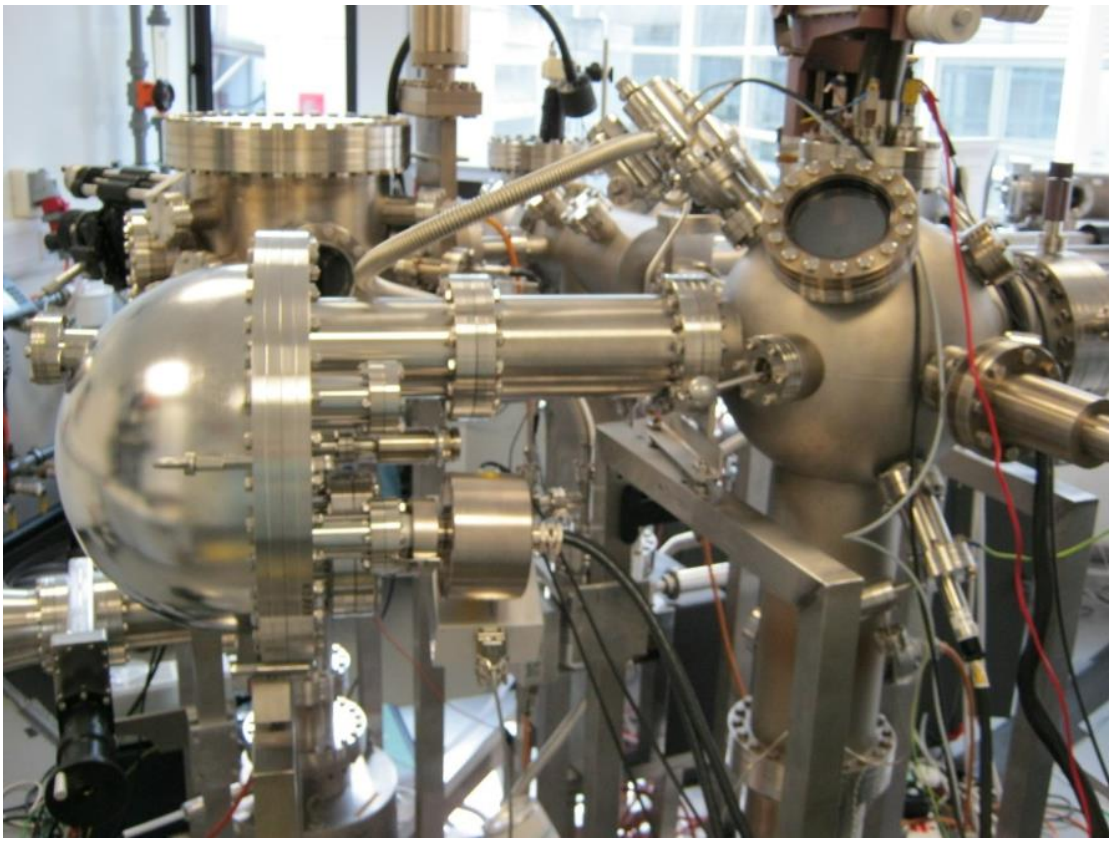

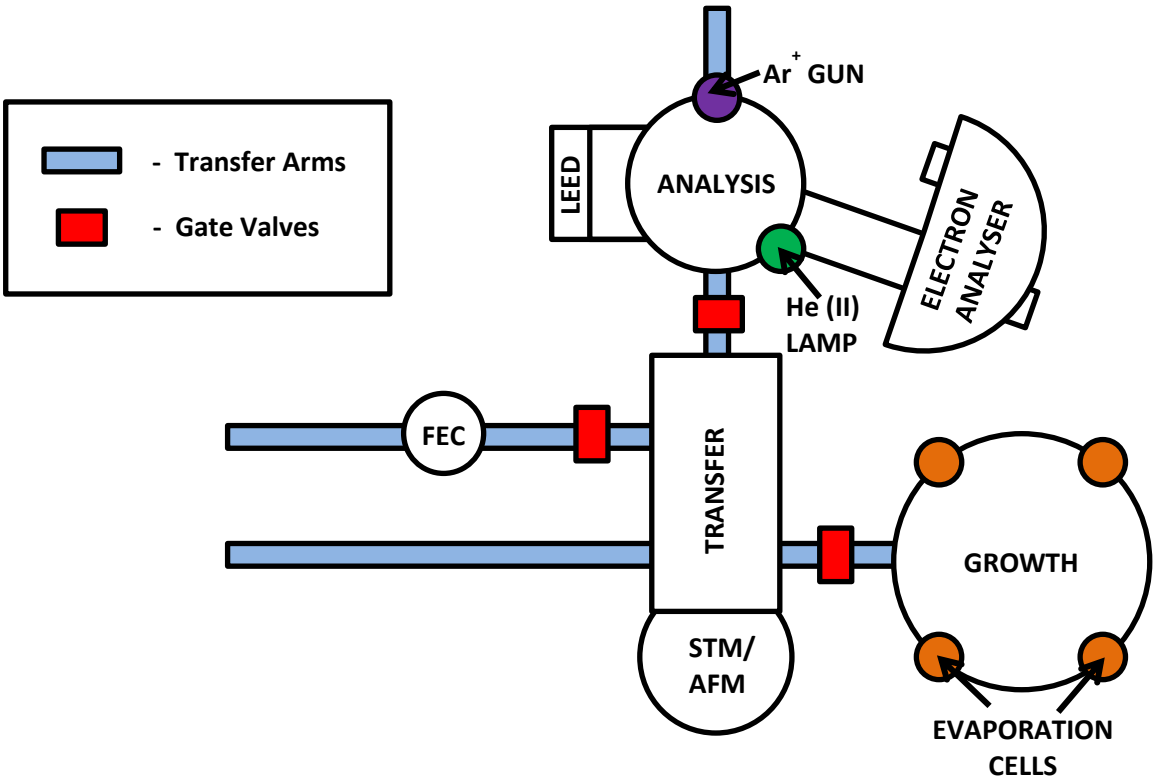

Figure 2.1 – Photograph and schematic of the UHV system

2.2 - UHV techniques

2.2.1 - Substrate Preparation

Each of the metal surfaces used as a substrate was prepared in vacuum by a combination of Ar+ bombardment and high temperature annealing. A PSP Vacuum ISIS3000© sample cleaning source was used to produce an energetically well-defined beam of Ar^+ ions. The energy of the impinging ions used was between 0.5 and 2 keV and the current at the sample due to bombardment could be measured with a Keithley© sourcemeter.

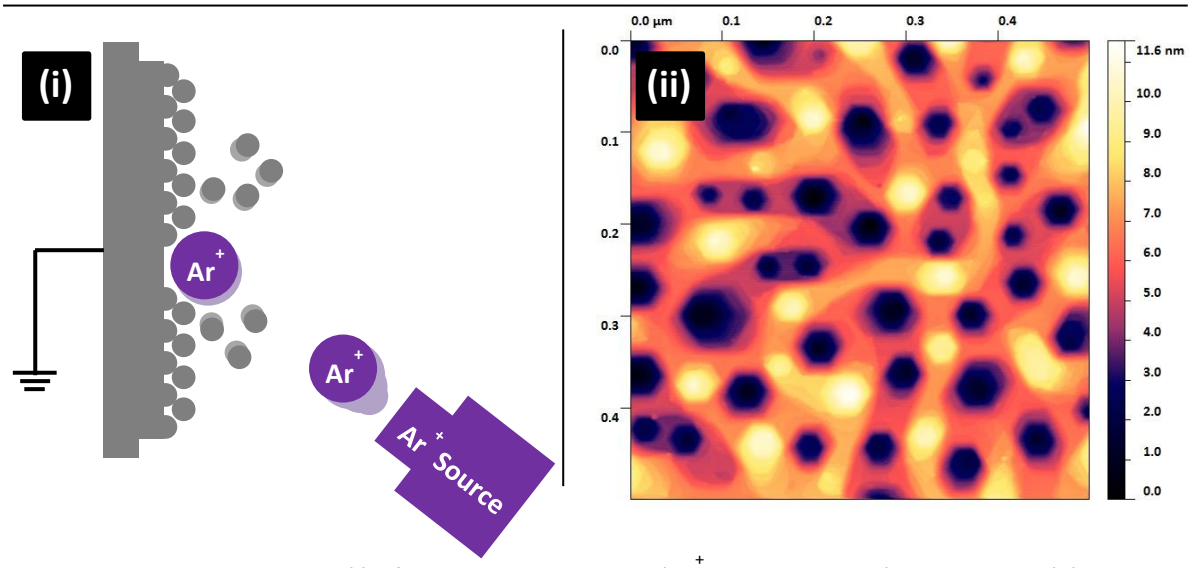

Figure 2.2 – A schematic (i) of the argon sputtering (Ar^+ bombardment) process and (ii) an STM image of sputter damage to an Ag (111) surface

Argon ion bombardment cleans the surface of metals by creating controlled sputter damage in the topmost atomic layers (Fig. 2.2). The relatively large size of the argon ion means that its kinetic energy is transferred to multiple smaller metal atoms, which are ejected from the surface. This creates holes in the surface which, on single crystal surfaces, often reflect the symmetry of the surface. Impurities such as oxide layers, atmospheric contaminants carried in to vacuum, or organic molecules can be removed by this procedure

as they are more volatile than metal atoms. As such they will not readily condense back on to the surface and are usually removed by the pumping in the UHV system.

A high temperature annealing step is then used to smooth the sputter damage and create large flat terraces which are desirable for the deposition of organic molecules. Increasing the temperature of the surface increases the mobility of adatoms and as such the holes left by sputtering can be filled in. In the UHV system used in this work a resistively heated tantalum filament is used to heat the plates upon which the metal surfaces are mounted. A thermocouple mounted in the head of the manipulator is used to measure the temperature produced which has a maximum of approx. 700°C. Cleanliness of substrates was checked with a combination of STM, UPS and LEED.

2.2.2 – Organic Molecular Beam Deposition (OMBD) of thin films

Thin films were grown by evaporation from solid powder using standard commercially available evaporation cells, while growth rates and thicknesses were monitored using a calibrated Quartz Crystal Microbalance apparatus.

All materials were commercially available and purchased as powders, details of the supplier will be given when each material is discussed later. Before use all materials were purified using thermal gradient sublimation[1] in a custom built high vacuum purification system (Fig. 2.3). Thermal gradient sublimation allows the separation of the desired majority molecular weight fraction of the sample from more and less volatile impurities. This is achieved by evaporation along a temperature gradient which exploits the difference in mean free path with molecular weight to fractionally separate impurities. Depending on the material between one and three cycles of purification were used to ensure no volatile impurities remained. After purification the materials were loaded into quartz or graphite

crucibles inside the evaporation cells and thoroughly degassed for at least 24 hours before use. When not in use the cells were maintained just below each materials evaporation temperature to avoid condensation of impurities.

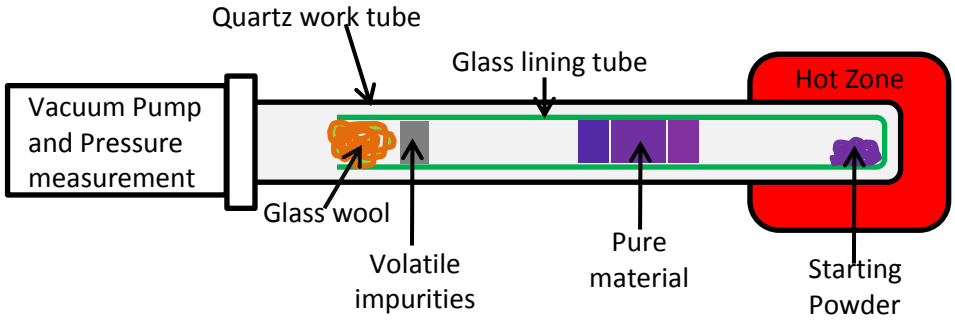

Figure 2.3 – Thermal gradient sublimation diagram

During growth substrates were held at ambient temperature, heated or annealed after growth without exposure to air. The manipulator used during growth has a dual k-type thermocouple assembly to monitor the temperature and a resistively heated tantalum element for high temperature growth and annealing.

2.2.3 – Low Energy Electron Diffraction (LEED)

LEED is a powerful technique for probing the long range two-dimensional order of the surfaces of crystalline samples[2]. In this work an Omicron SPECTALEED rear-view micro channel plate LEED optics was used to probe the structure of molecule-metal interfaces (Fig. 2.4). The system consists of an electron gun which creates an electron beam which is scattered by the sample through optics designed to eliminate inelastic scattering and finally illuminate a fluorescent screen (observed through a viewport in the UHV system). Patterns were captured using a commercially available CCD camera or a digital still camera. Energies in the region of 15 eV were necessary to observe the large lattices of the MPc molecules studied here.

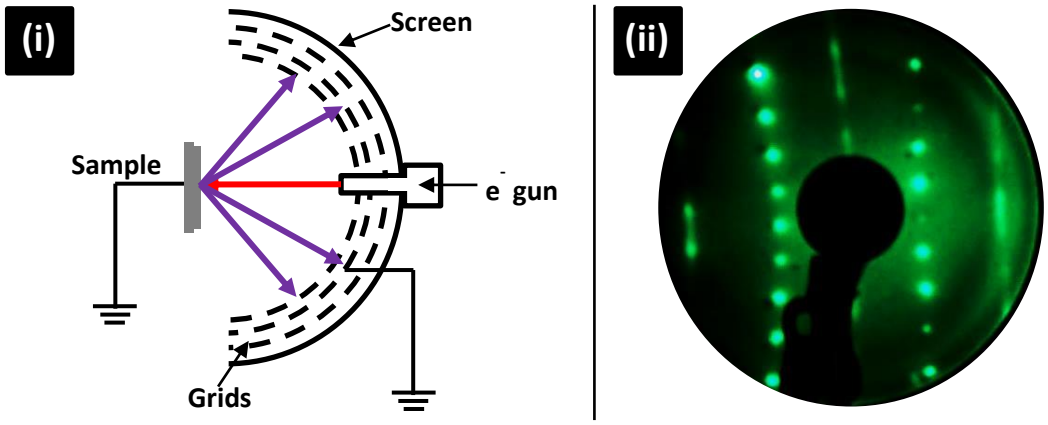

Figure 2.4 – (i) rear view LEED optics diagram and (ii) pattern from an InAs (001) (4x2) surface

2.2.3.1 – Surface Structure Notation

Classification of surface structures from LEED is often approached using Wood's notation, expressing the relationship between surface lattice vectors ($\mathbf{a_1}$ and $\mathbf{a_2}$) and adsorbate lattice vectors ($\mathbf{b_1}$ and $\mathbf{b_2}$). Structures are described as the ratios of the lengths of these vectors ($|\mathbf{b_1}|/|\mathbf{a_1}|$) and ($|\mathbf{b_2}|/|\mathbf{a_2}|$) and any rotational angle between them, θ. Surface lattices can be either primitive or centred like three dimensional unit cells. Wood's notation is extremely useful and simple for the description of commensurate structures with common periodicity (Fig. 2.5).

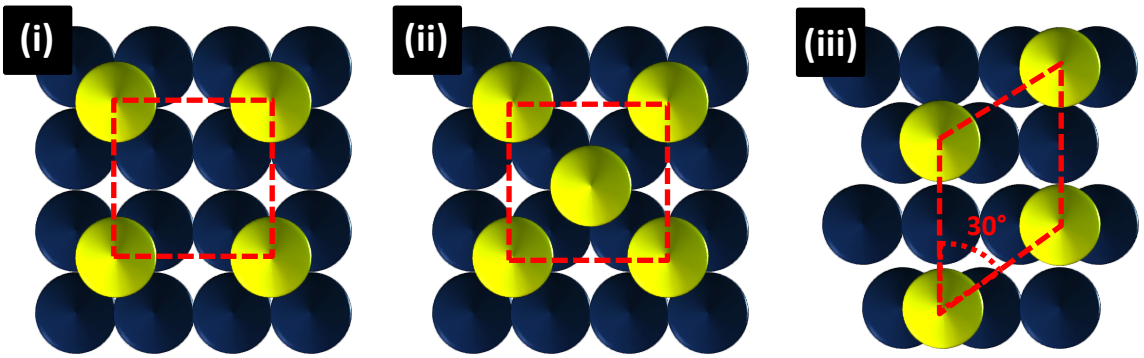

Figure 2.5 – Three related overlayer structures (i) 2x2 (ii) c(2x2) (iii) (√3 x √3)R30°

Wood's notation cannot be used in situations without commensurate epitaxial relationships and for these situations matrix notation more completely describes the surface structure. Matrix notation is demonstrated below where **a** and **b** are the same basis vectors as above.

$$\begin{pmatrix} \boldsymbol{b_1} \\ \boldsymbol{b_2} \end{pmatrix} = \begin{bmatrix} * & * \\ * & * \end{bmatrix} \begin{pmatrix} \boldsymbol{a_1} \\ \boldsymbol{a_2} \end{pmatrix}$$

If we consider a 2x2 structure on an FCC (100) surface we can construct a simple matrix to describe the vector relationship.

$$\boldsymbol{b_1} = 2\,.\,\boldsymbol{a_1} + 0\,.\,\boldsymbol{a_2}$$

$$\boldsymbol{b_2} = 0\,.\,\boldsymbol{a_1} + 2\,.\,\boldsymbol{a_2}$$

Therefore:

$$\begin{bmatrix} \mathbf{2} & \mathbf{0} \\ \mathbf{0} & \mathbf{2} \end{bmatrix}$$

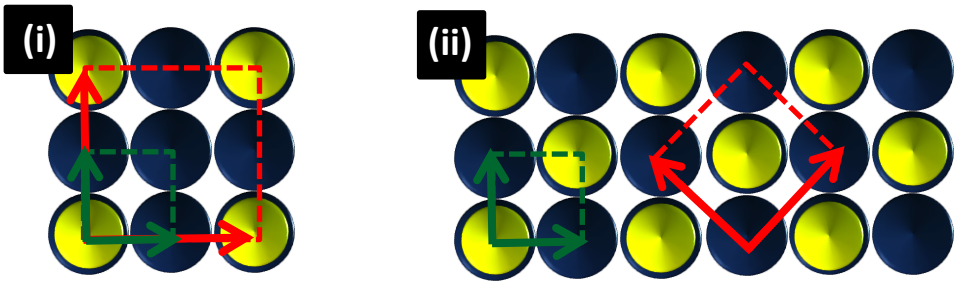

Figure 2.6 – Vector notation of surface structures (i) 2x2 and (ii) c(2x2).

And in the case of a c(2x2) structure the vector notation is as follows:

$$\boldsymbol{b_1} = 1\,.\,\boldsymbol{a_1} + 1\,.\,\boldsymbol{a_2}$$

$$\boldsymbol{b_2} = -1\,.\,\boldsymbol{a_1} + 1\,.\,\boldsymbol{a_2}$$

Therefore:

$$\begin{bmatrix} \mathbf{1} & \mathbf{1} \\ \mathbf{-1} & \mathbf{1} \end{bmatrix}$$

In contrast to Wood's notation matrix notation describes each basis vector as a linear combination of the overlayer vectors (Fig. 2.6). Wood's notation is simpler but more limited as substrate basis vectors are described as multiples of overlayer vectors and the angle of rotation between them is defined (when this is not zero).

2.2.4 – Scanning Tunnelling Microscopy (STM)

The scanning tunnelling microscope (STM) was developed by Binning and Rohrer and demonstrated practically for the first time in 1982[3], which led to the award of the Nobel Prize for Physics in 1986. Surface science was significantly enriched by the invention of STM, and after commercialisation the routine real space analysis of surfaces down to the atomic scale truly revolutionised the field.

Experimentally the STM is simple (Fig 2.7), an atomically sharp and well defined tip is positioned close to a conductive surface to facilitate electron tunnelling from one to the other. This tunnelling creates a small but measureable current in an external control circuit and the tip is scanned across the surface by piezoelectric positioners while this current is monitored. Variations in tunnelling current relate to changes in the local density of states (LDOS) at the surface and as such a three dimensional approximation to the electronic

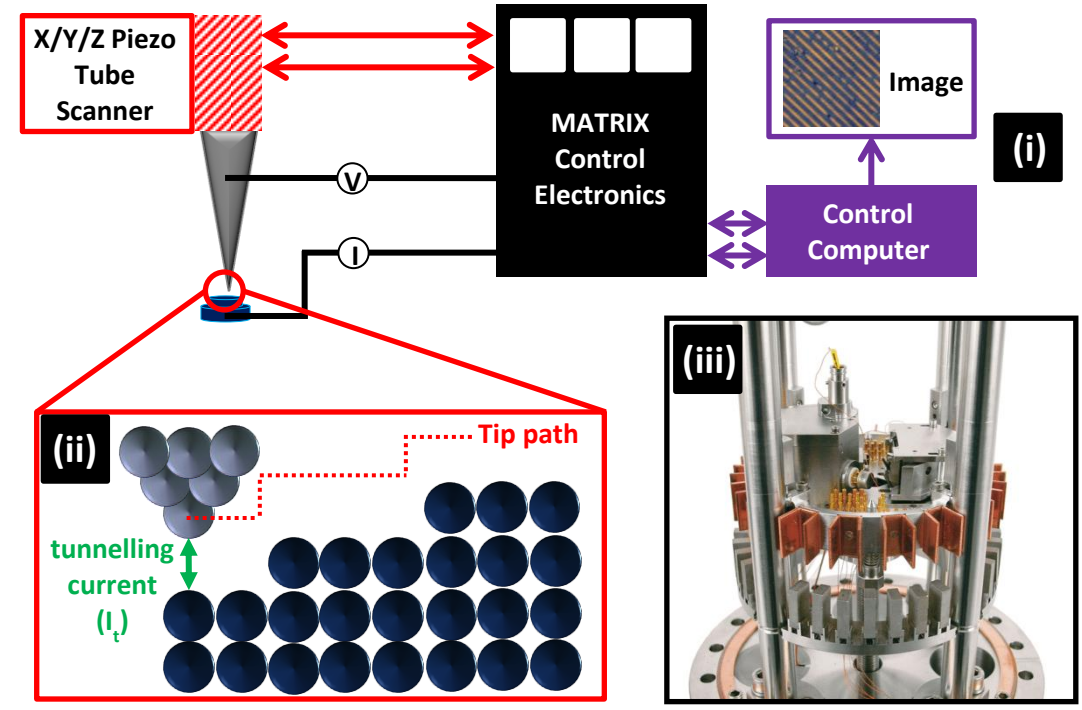

Figure 2.7 – (i) Schematic of the STM used in this work (ii) tip-sample relationship in constant current mode (iii) the OMICRON AFM/STM

topography of the surface is produced. Two modes of operation are used in STM, either a constant current is maintained by the control circuitry and the tip (and therefore the piezo positioners controlling tip motion) responds to corrugations in the LDOS or the tip height is maintained at an approximate constant and changes in tunnelling current are directly constructed into an image. In either case the LDOS of the surface is used to create an intrinsically three dimensional map of its topography. On clean flat surfaces this can produce images with atomic resolution and at interfaces with organic molecules sub-molecular resolution can routinely be realised. All images in this work have been recorded at room temperature in constant current mode using an Omicron AFM/STM, so only the constant current mode will be discussed.

The theoretical aspects of STM have been well described in a variety of research papers[4] and books[5,6] and as such only the most important theoretical aspects of operation will be considered here. The simplest treatment of a tip-surface tunnel junction is that of a one dimensional barrier model to represent the vacuum barrier between the two (in this work UHV is the only imaging environment). When separated we can consider the tip and sample to share a common vacuum level but have non-equivalent Fermi levels the position of which is defined by their work functions. At the surface of both the tip and the sample electron wave functions from the lattice decay exponentially into the vacuum (equation). This is constructed from the solution of the Schrödinger equation for a simplified square barrier to tunnelling.

$$\Psi = A.\exp(-\boldsymbol{k}Z)$$

Where $$\boldsymbol{k} = \frac{2\sqrt{(2m(\phi - E)}}{\hbar}$$

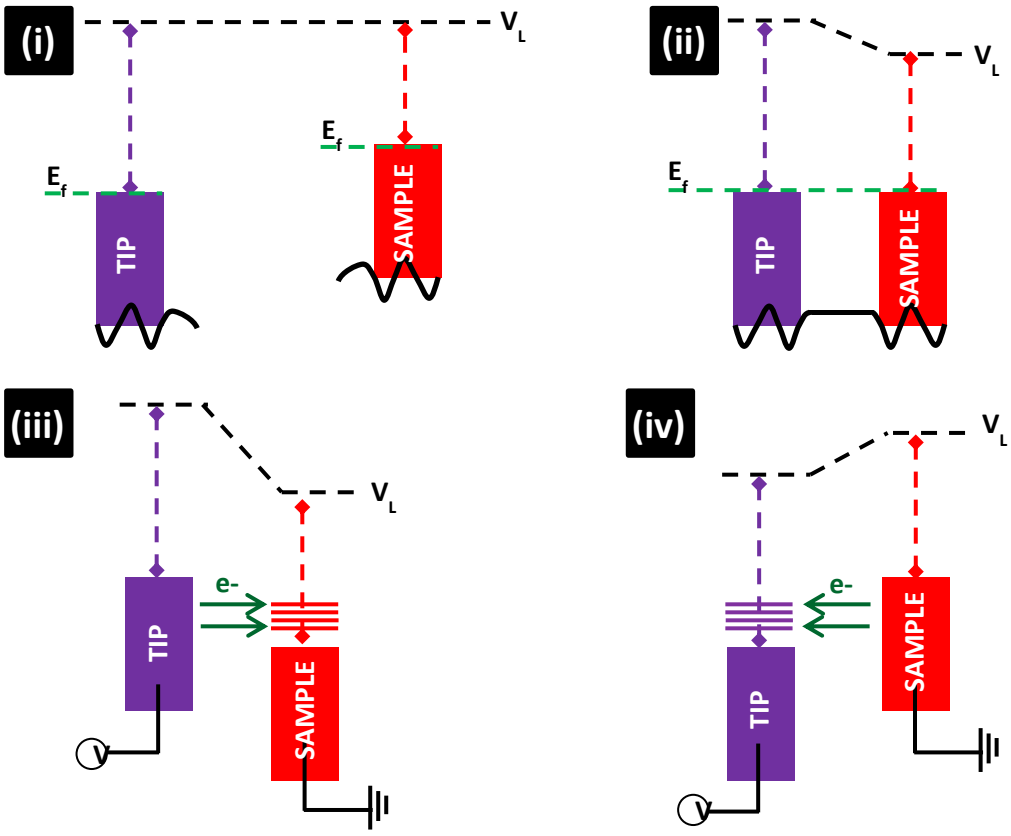

Figure 2.8 – Energetic considerations in STM for (i) isolated tip and sample (ii) tip and sample in tunnelling condition and the effects of a (iii) positive and (iv) negative applied bias

If the tip and sample are brought to a critical separation (typically 5-10 Å) and begin to interact they must reach thermodynamic equilibrium causing their Fermi levels to align (in effect a vacuum level shift) (Fig. 2.8). Transferring an electron between sample and tip in either direction would take place across an energetic barrier in the order of the work function of the sample or tip. While tunnelling can occur in this scenario applying a voltage bias across this junction shifts the energy levels in question up or down with the sign of the bias. This makes tunnelling into and out of states more accessible energetically and allows the selection of certain energy levels or orbitals as the contrast mechanism with careful choice of voltage. Depending on the direction (tip-sample or sample-tip) and sign of the

voltage bias applied filled or empty states in the LDOS of the sample can be selected for imaging.

The situation is complicated in the case of organic molecules at surfaces due to complexity of the LDOS due to molecular hybrid orbitals and the substrate-molecule interaction. Geometric protrusions and physical corrugation impact the path of the tip across contours of constant current, so STM topographs represent both the electronic and geometric properties of the surface.

When we consider imaging organic molecules with STM the states which tunnelling is occurring into or out of (from the tip) are closely related the HOMO and LUMO of the isolated molecule (**Fig 2.9**).

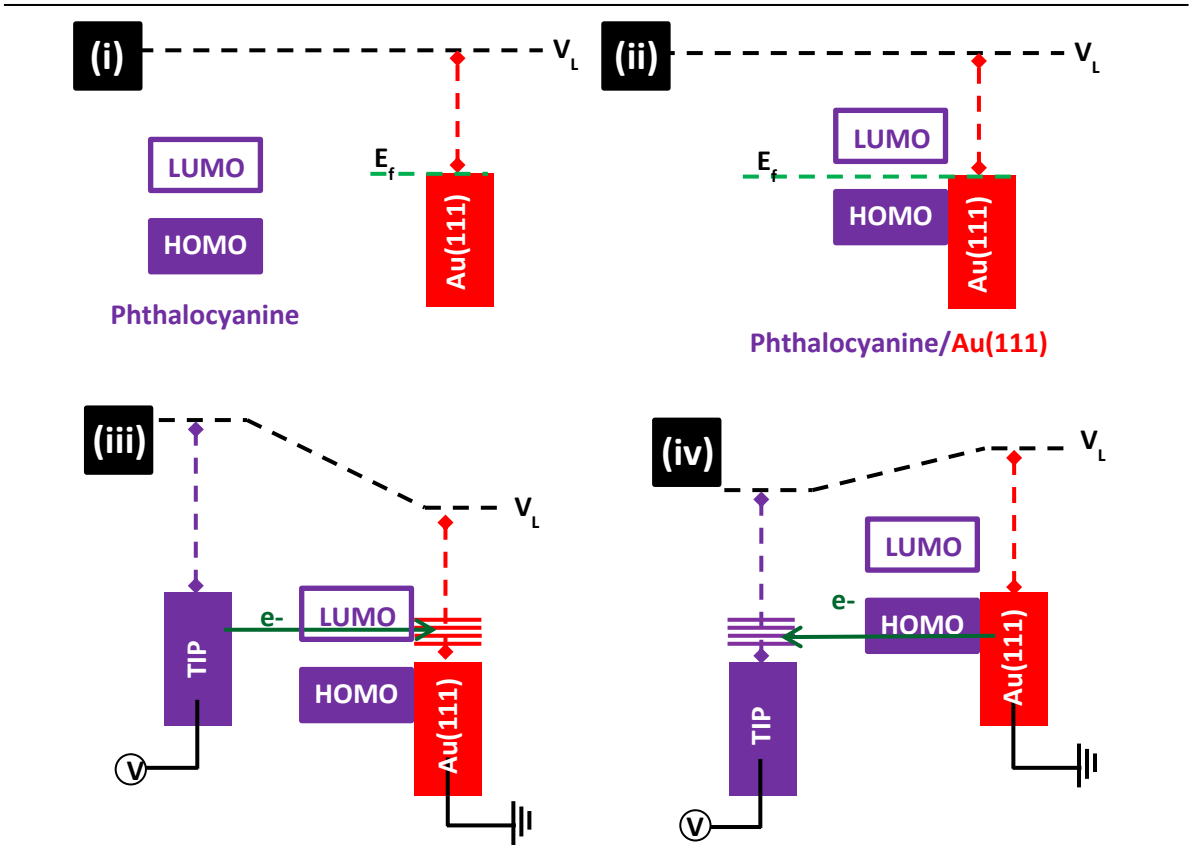

Figure 2.9 – Molecular orbitals in STM; (i) isolated phthalocyanine/substrate (ii) phthalocyanine molecule/substrate interface and the tunnelling mechanisms at (iii) positive and (iv) negative bias

On the surface of a metal the filled (HOMO) states of a phthalocyanine molecule will be positioned at higher binding energy than the Fermi level of the metal and unoccupied (LUMO) states above. It follows that empty states (positive bias) images will be representative of the LUMO of the adsorbed molecule and filled states will be representative of the HOMO. If all tunnelling is assumed to be purely elastic and only involving the LUMO and HOMO derived states into and from the tip the surface topography produced can be directly related to the LDOS of the molecular HOMO and LUMO.

Although the electronic structure of the free molecule can be heavily modified by adsorption onto metallic surfaces phthalocyanine molecules tend to retain a band gap and therefore have HOMO and LUMO derived levels. This suggests that differences in the images produced at positive and negative biases should be observed due to tunnelling into LUMO and HOMO states respectively.

The STM used in this work is an unmodified OMICRON UHV AFM/STM operated in STM constant current mode at ambient temperature. Tips were produced by electrochemical etching of polycrystalline tungsten wire in sodium hydroxide solution before rinsing in nitric acid and isopropanol. Once loaded into UHV voltage pulses and controlled indentation into single crystal metal surfaces were used to produce tips capable of atomic resolution if ex situ preparation was insufficient.

2.2.5 – Ultraviolet Photoemission Spectroscopy (UPS)

UPS is a valence band photoemission spectroscopy (PES) technique used here to probe the low binding energy portion of the electronic structure of organic thin films (Fig. 2.9). In principle when a solid is irradiated by photons with sufficient kinetic energy absorption of these photons leads to ejection of electrons due to the photoelectric effect. The kinetic energy of the emitted electrons is related to the binding energy of the state they were emitted from and the energy of the impinging photon (Fig 2.9).

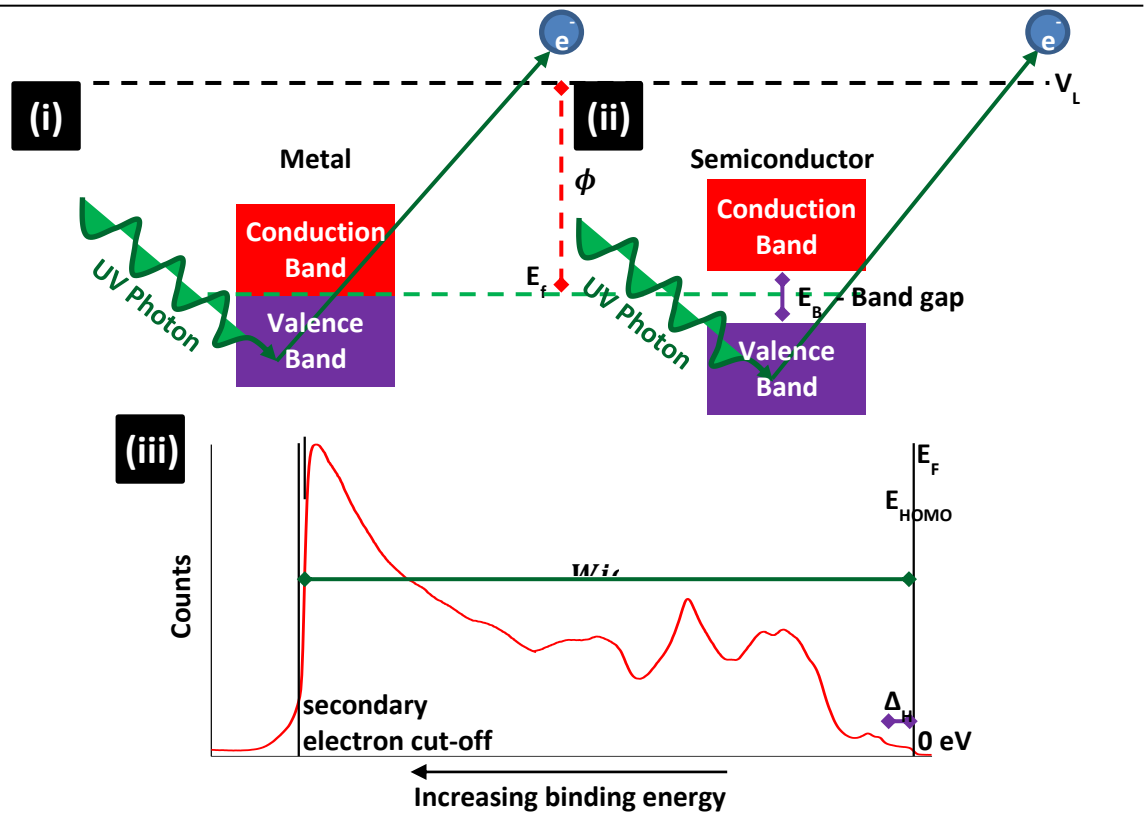

Figure 2.9 – Valence band photoemission in (i) metals and (b) semiconductors and an example of (iii) an organic/metal interface UPS spectrum

For an electron emitted from an occupied state below the Fermi level:

$$E_K = hv - E_B - \phi_S$$

Where $\boldsymbol{E_K}$ is the kinetic energy of the electron, $\boldsymbol{hv}$ is the incident photon energy, $\boldsymbol{E_B}$ is binding energy and $\boldsymbol{\phi_S}$ is the work function of the sample.

We can therefore express the energy of the electron ejected from the solid as either kinetic energy or binding energy, and in this work all spectra will use the binding energy scale. A typical UPS spectrum is shown in Fig 2.9 and each of the important features of the spectrum used to compute relevant values are labelled. The position of the low binding energy edge of the HOMO peak is indicated (E_{HOMO}) near to the Fermi edge (E_F) which corresponds to the closest measurable point to zero kinetic energy for metal surfaces. By taking the width of the spectrum (from the Fermi edge to the secondary electron cut-off) and subtracting this from the energy of the impinging photons the work function of the sample can be calculated (equation).

$$\phi_S = hv - Width/Secondary\ electron\ cut-off\ energy$$

As the system is calibrated to zero binding energy using the Fermi edge of a clean metal the position of the secondary electron cut-off is identical to the width of the valance band. Ionisation potential measurements are made by considering the work function of the substrate in combination with the barrier to hole injection (Δ_H).

$$I_P = \phi_S + \Delta_H$$

The UPS system used in this work was made up of a SPECS UVS 10/35 Helium I/II source (operating to produce He(I) plasma with ultraviolet photons of 21.21eV) and a SPECS PHOIBOS 100 hemispherical electron analyser. Energy scales in all spectra were referenced to the Fermi edge of argon sputter cleaned polycrystalline silver or single crystal substrates used for deposition. The analyser has a workfunction of around 4 eV and for this reason a negative 10 Volt bias was applied when collecting electron cut-off spectra. This allows low energy electrons to be measured as their energies would normally not allow them to overcome the work function difference between the sample and analyser.

2.3 – Ex-situ techniques

The operating principles of the ex-situ characterisation techniques used in this work will be briefly outlined and discussed in this chapter.

2.3.1 – Atomic Force Microscopy (AFM)

Atomic force microscopy (AFM) is a scanned probe microscopy technique allowing high resolution imaging of surfaces[7] (Fig. 2.10). Modern AFM instrumentation has shown routine resolution down to the atomic scale in UHV liquid environments and ambient conditions. AFM was developed by Binnig and Rohrer to extend the capabilities of STM to samples that are too insulating or rough for investigations requiring electron tunnelling.

All AFM images in this thesis were recorded using tapping mode (rather than contact mode) so only this mode will be described. The AFM operates by oscillating the tip close to its resonant frequency with amplitude $\mathbf{A_0}$. The piezo positioners are used to approach the tip towards the surface and a feedback loop senses changes in frequency due to damping of the oscillations as the tip begins to interact with the surface.

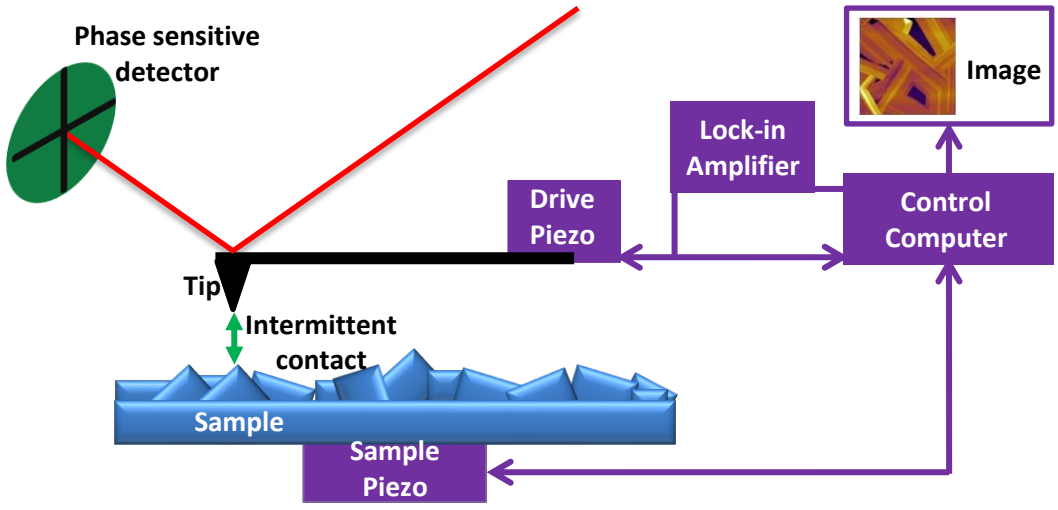

Figure 2.10 – Schematic of an AFM instrument operating in tapping mode

The sample is then scanned in the x and y directions by piezo pads to produce motion relative to the tip. As the force set-point is maintained by the feedback loop a constant separation from surface features is achieved. A laser beam is reflected from the back of the tip onto a four quadrant photo detector which allows the position of the tip to be tracked. Movement of the tip towards or away from the sample produces a change in the position of the laser spot on the detector and a corresponding voltage is produced. In this way three dimensional surface topographs can be recorded of soft or sensitive samples as the tapping mode of the tip does not exert large amounts of force on the sample surface. The frequency to which the tip is tuned and the set point chosen for imaging can be selected to provide a harder or softer tapping motion.

An MFP-3D AFM (Asylum Research, Santa Barbara, USA) operated in AC mode was used to record all AFM images presented in this work, using AC240TS (Olympus) tips.

2.3.2 – X-ray Diffraction (XRD)

X-ray diffraction (XRD) allows characterisation of crystalline structures by monitoring the diffraction angles of X-rays projected into the sample (Fig 2.11). Diffraction phenomena

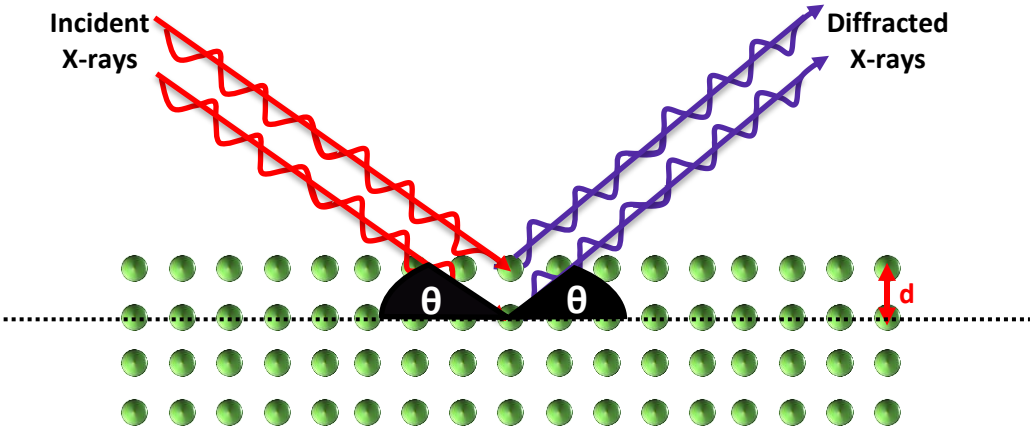

Figure 2.11 – Schematic of the process of X-ray diffraction

are observed when a path difference is introduced to the propagating X-ray wave front, in this case by atomic species arranged in an ordered structure. X-rays are scattered from the electron density of the crystal. Scattering by periodic arrays with interatomic spacings similar to the wavelength of the incident X-rays can produce coherent diffraction. A Cu K_α X-ray source with a wavelength of 1.5418 Å (a weighted average of the $K_{\alpha1}$ and $K_{\alpha2}$ lines) was used in this work and is widely used in laboratory thin film diffractometers. Interplanar spacings ($\mathbf{d_{hkl}}$) in crystals are in the same order of magnitude as the wavelength of the probe X-rays so diffraction can be observed. These spacing correspond to the perpendicular distances between Miller planes, imaginary planes passing through the unit cell of the crystal defined by three integer values (*h*, *k* and *l*) known as Miller indices. These indices are defined as the reciprocal of the fractional intercept of the crystal *a*, *b* and *c* unit cell edges.

Upon being scattered, X-rays can constructively interfere if they are in phase, and the angle at which this constructive interference occurs is determined by the Bragg equation:

$$\mathbf{n\lambda=2d\sin\theta}$$

where **λ** is the wavelength of the X-rays, **d** is the spacing responsible for the diffraction and **θ** is the diffraction angle.

This equation describes the condition for constructive interference: when the path difference between scattered X-rays is an integer number of X-ray wavelengths. As a simple model we can consider a set of lattice points (Figure 2.12) and two impinging X-rays, one of which is scattered elastically from a lattice point and another which is transmitted through to scatter from a second lattice plane.

If their angular path changes by the same amount there will be a path difference between the two scattered X-rays. Both rays can reach a point in space after diffraction and undergo constructive interference only if the path difference is equal to an integer value of the incident X-ray.

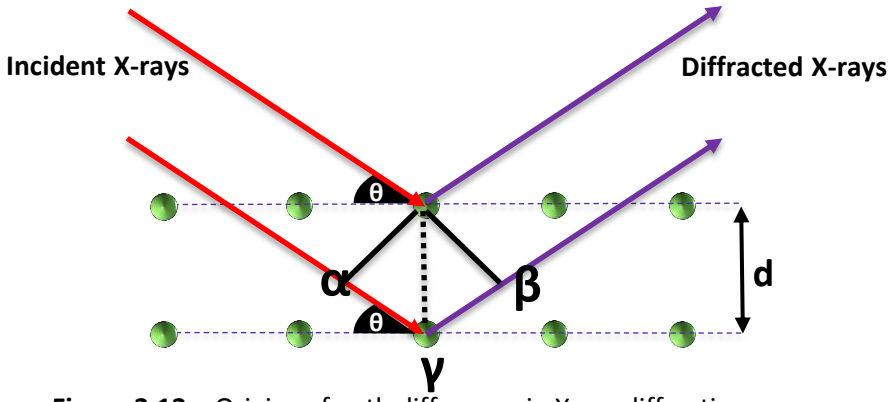

Figure 2.12 – Origins of path difference in X-ray diffraction

The path difference created is therefore **αγ + γβ** which must be equal to an integer number of wavelengths of the X-ray beam, **nλ,** to satisfy the Bragg condition and to observe constructive interference. This can be expressed as:

$$n\lambda = \alpha\gamma + \gamma\beta$$

and as $\sin\theta = \alpha\gamma/d$

$$\alpha\gamma = d\sin\theta$$

and $\alpha\gamma = \gamma\beta$

$$2d\sin\theta = n\lambda$$

also expressed as:

$$n\lambda = 2d\sin\theta$$

Therefore by using a monochromatic source of X-rays and observing the angles at which diffraction maxima are observed the size of the spacing responsible for the peak can be ascertained. Due to the geometry employed in the Bragg-Brentano experiments performed in this work, **2θ** is usually recorded and reported along with an arbitrary unit of intensity. In the configuration used in this work the sample is angularly scanned through **θ**

with respect to the X-ray tube and detector moves through **2θ**. This is useful for powder samples which may spill if tilted through large angles during scanning.

Peaks of diffraction intensity can be indexed directly to lattice planes if the lattice parameters (unit vectors and angles separating them) are known, as was the case in this work. Single crystal diffraction experiments are often used for OSC systems to measure the unit cell and atomic positions and peaks from thin films are indexed by comparison to previously solved single crystal structures.

In single crystal diffraction experiments all possible intensity maxima are present (although systematic absences and weak reflections may be observed) and no preferred orientation is observed. The crystalline sample is placed in a multi-axis goniometer stage allowing rotation of the crystal during collection. In each orientation a CCD detector is commonly used to collect all of the diffracted beams at once rather than scanning the detector through space as in powder type scans. Experimental requirements are more stringent for full structural characterisation; crystal quality and size are key factors in obtaining accurate crystal structures.

In this work all thin film XRD data were obtained using an X'Pert PRO (PANalytical) instrument with Cu K_α radiation ($\lambda \approx 1.5418$ Å); the mode and geometry will be presented with each data set. Single crystal measurements were undertaken at end-station I19 of Diamond light source at Harwell Science and Innovation Campus in Oxfordshire. Synchrotron radiation with $\lambda = 0.68890$ Å was used in single crystal diffraction experiments.

2.3.3 – Scanning Electron Microscopy (SEM)

Scanning electron microscopy (SEM) is an electron microscopy technique which uses the interaction of a beam of electrons with a surface to produce high resolution images constructed from backscattering interactions[8] (Fig. 2.12). SEM probes the surface and near surface features of a sample using a beam of approximately 1-30 kV electrons which are focused onto an area in the tens of nanometre range at the sample. Scan coils further down the optics of the instrument raster the electron beam across the surface and the secondary electrons generated within the interaction volume of the primary beam are used to create an image.

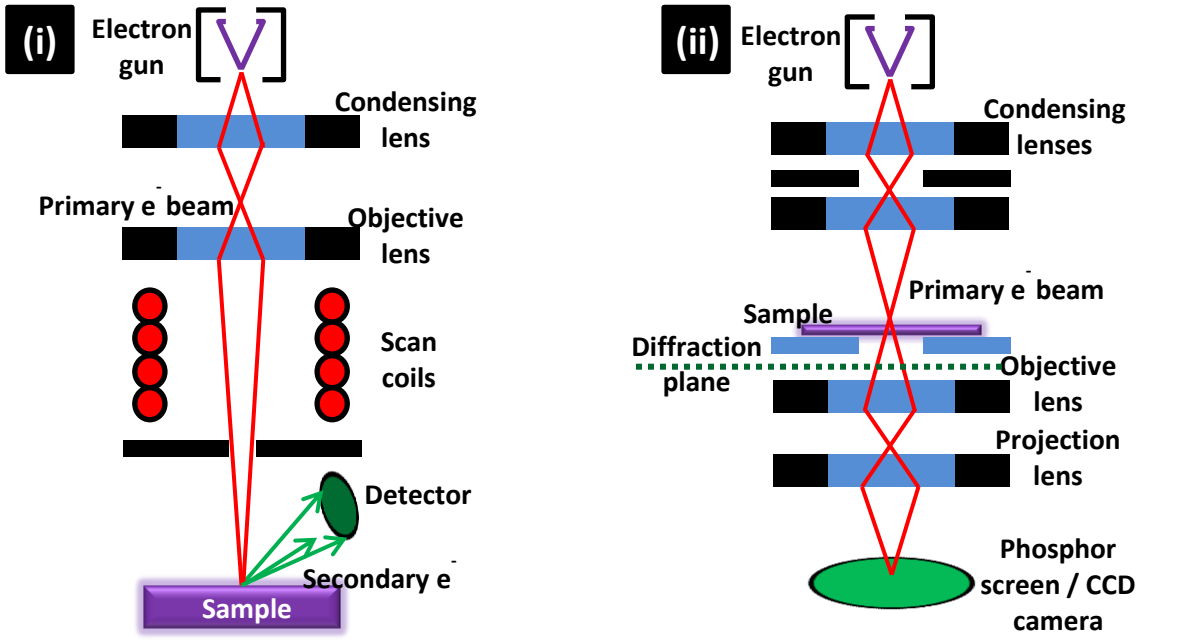

Figure 2.12 – Schematic diagrams of (i) the SEM (ii) the TEM

The primary beam is of relatively high energy but due to the interactions within the solid (and losses due to the generation of heat, X-rays and other mechanisms) secondary electrons are ejected with much lower energy. Accelerating voltages are therefore applied in the detection instrumentation where the detector is within the electron focusing optics (in-lens) or oriented to detect only secondary electrons (se-detector). The nature of the imaging mechanism in an SEM limits the resolution to the nanometre range and the contrast mechanism is dominated by differences in electron density.

In this work a SUPRA 55-VP (ZEISS) FEG-SEM was used to produce electron micrographs of solid samples. Samples were exposed to air after growth and before imaging, in some cases (to avoid charging) samples were coated with an amorphous thin film of carbon by evaporation.

2.3.4 – Transmission Electron Microscopy (TEM) and Selected Area Electron Diffraction (SAED)

Transmission electron microscopy (TEM) uses a high energy electron beam (80-200 kV) transmitted orthogonal to the substrate plane to image thin samples of solid materials (Fig 2.12). Electron focussing optics are used to control both spot size and the intensity profile being transmitted through the sample. As the electrons pass through the sample electrons both interact with and are scattered and can be imaged in the near-field diffraction plane or focused into an image further down the optics. When viewed in the diffraction plane spot and ring patterns are observed (which can be explained using very similar methods to those described above for XRD) for crystalline and semi crystalline materials. While calibration and orientation effects make crystallography complicated

selected area electron diffraction patterns can be extremely powerful in elucidating the crystal structures of samples.

If the imaging plane is selected bright field modes are most commonly used to create images. In this mode the interaction of the electron beam with the sample produces mass-thickness contrast in the imaging plane. By increasing the thickness of the sample (which reaches a maximum for transmission at a few hundred nanometres) or by introducing higher atomic number species (i.e. higher electron density) more scattering is present so a lower electron yield is present at the image plane.

In this work a 200FX (JEOL) TEM with a Gatan Orius CCD camera was used to produce electron micrographs and selected area diffraction patterns from solid samples. Samples were exposed to air after growth but no ex situ preparation or coating was undertaken.

References:

(1) McGhie, A. R.; Garito, A. F.; Heeger, A. J. A gradient sublimer for purification and crystal growth of organic donor and acceptor molecules. *Journal of Crystal Growth* **1974**, *22*, 295–297.

(2) Woodruff, D. P. ; Delchar, T. A. *Modern Techniques of Surface Science (Cambridge Solid State Science Series)*; Cambridge University Press, **1994** (2nd Edition).

(3) Binnig, G.; Rohrer, H.; Gerber, C.; Weibel, E. Surface studies by scanning tunneling microscopy. *Physical review letters* **1982**, *49*, 57–61.

(4) Behm, R.J.; Ertl, G.; Brune, H.; Barth, J. V.; Scanning tunnelling microscopy observations on the reconstructed Au (111) surface, *Physical Review B* **1990**, 42, 9307-9318

(5) Davies, P. R.; Bowker M. (eds.) Scanning tunnelling microscopy in surface science, nanoscience and catalysis, Wiley-VCH **2010** (1st Edition)

(6) Chen, C.J.; Introduction to scanning tunnelling microscopy, Oxford University Press **2008** (2nd Edition)

(7) Binnig, G.; Quate, C. F. Atomic Force Microscope. *Physical Review Letters* **1986**, *56*, 930–933.

(8) McMullan, D. Scanning electron microscopy 1928-1965. *Scanning* **2006**, *17*, 175–185.

Chapter 3

Surface and electronic structure of VOPc

Understanding the relationship between molecular self-assembly, surface structure and electronic properties at the earliest stages of film formation is critical if MPc molecules are intended for use in electronic devices[1]. The use of surface probes for analysis of thin MPc films in UHV has been established as the state of the art for evaporable systems over the last few decades. By combining scanning probe microscopy (AFM and STM) surface sensitive diffraction techniques (LEED and other ion or electron diffraction methods) and electronic structure measurements (UPS, XPS, Kelvin Probe) a comprehensive knowledge of MPc molecules at solid surfaces can be built up.

In this chapter the non-planar phthalocyanine VOPc is prepared in thin film morphology on the (111) surfaces of three noble metal single crystals (Au, Cu and Ag) by molecular beam deposition. The morphology of thin films is investigated using STM and LEED while UPS is used to measure their electronic properties.

LEED measurements indicate a multi-domain structure in which molecules adopt one of three symmetrically unique azimuthal orientations with respect to the surface on Au (111) and Ag (111). STM imaging allows the observation of each of these molecular environments simultaneously and 2-D Fourier analysis is used to relate LEED patterns and STM images.

A markedly different surface structure is observed on the Cu (111) surface by both LEED and STM, and UPS measurements are used to probe the underlying electronic interaction causing the change in molecular assembly compared to Au (111) and Ag (111).

3.1 – VOPc / Au (111)

At very low coverage (less than 0.2 ML) the VOPc/Au (111) surface is difficult to image with STM at room temperature (coverage was estimated from LEED spot intensities and calibrated quartz crystal microbalance measurements). This suggests that the VOPc molecules are highly surface mobile, similar to literature examples of other MPc molecules[2,3]. Most images consisted purely of lateral noise with some visible substrate step edges, but a few contained discernible features. The region shown in Fig 3.1 (approximately 0.1 ML) shows a low density of VOPc molecules adsorbed along the elbow sites of the herringbone reconstruction of the Au (111) surface. Molecular structure could not be discerned and only dark roughly circular depressions of around 2 nm in lateral size were observed.

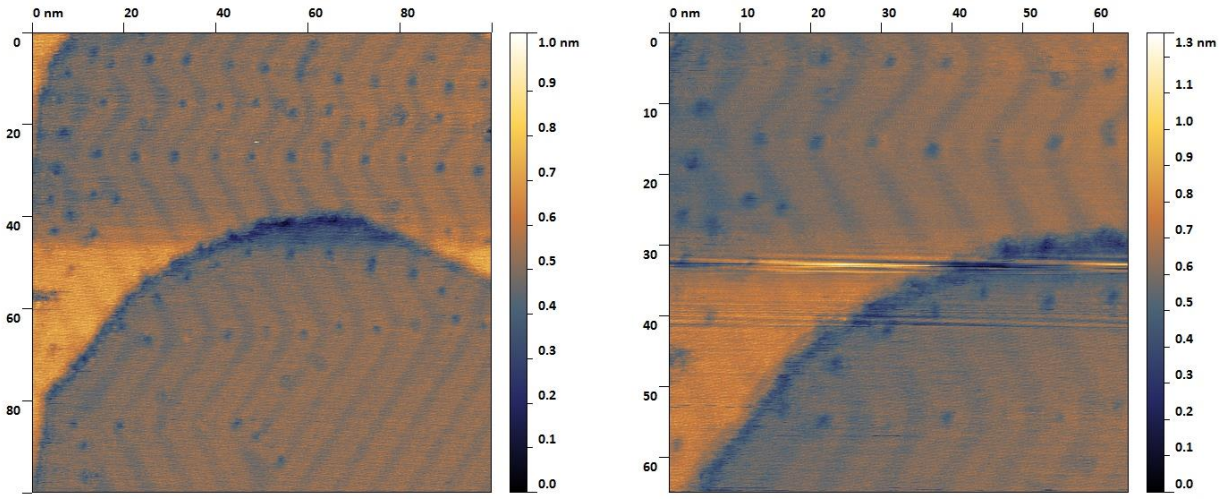

Figure 3.1 – STM of VOPc/Au (111) at approximately 0.1ML, V_s = -1.5 V, I = 65 pA

This kind of assembly is common in MPc films on Au (111)[4] as the elbow sites represent the lowest surface energy sites on the surface, although the influence of the tip cannot be disregarded. The tip may be dragging mobile molecules around the surface which then 'stick' at the elbow sites. Further analysis was not possible with the resolution obtained, and no further images could be recorded due to the instability of the surface.

On increasing the VOPc coverage (to approximately 0.2 ML) a higher density of features, assumed to be individual VOPc molecules, was observed. The 'herringbone' reconstruction of the Au surface is not observed and the features are harder to discern. This may be due to the surface mobility of molecules or adsorption of weakly bound molecules from the surface onto the STM tip.

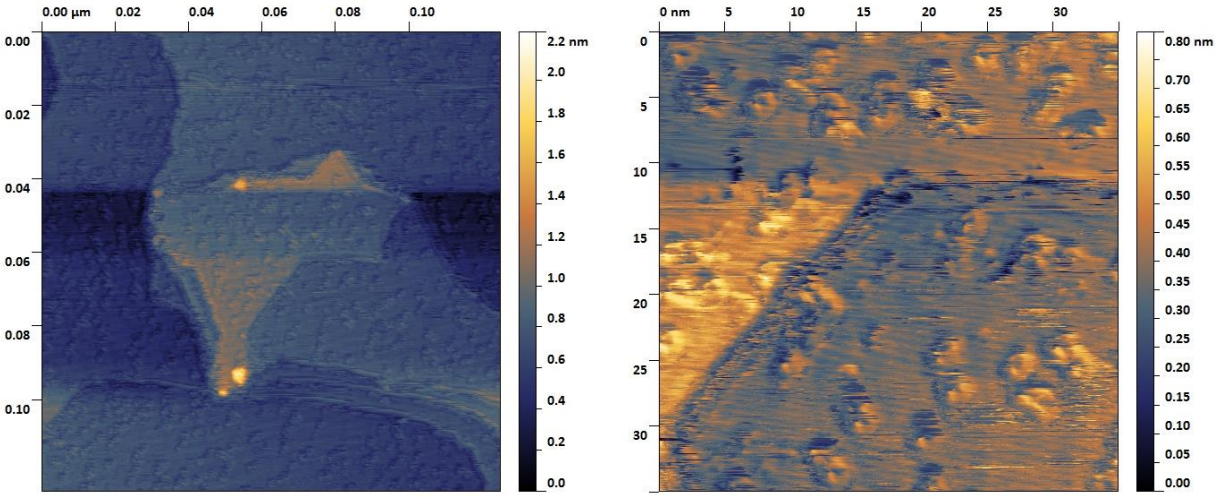

Figure 3.2 – STM of VOPc/Au (111) at approximately 0.2ML, V_s = -1.5 V, I = 65 pA

Further deposition (to approximately 0.3 ML) leads to an increase in the density of features observed and lines which can be observed between them (which may be a modified version of the herringbone reconstruction of the Au (111) substrate[5]) appear.

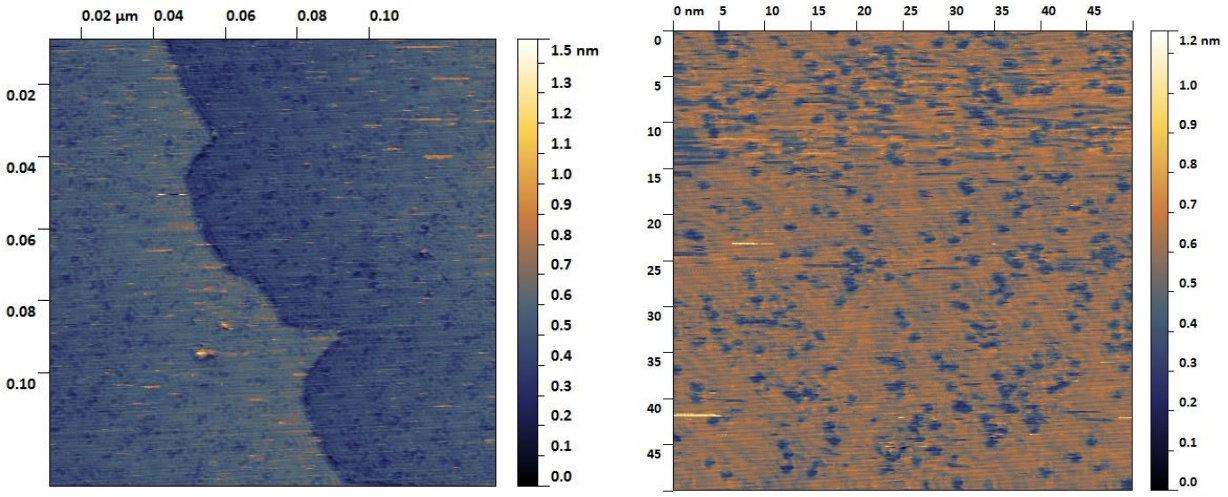

Figure 3.3 – STM of VOPc/Au (111) at approximately 0.3ML, V_s = -1.5 V, I = 65 pA

Due to the poor resolution of the topographs further comment on these features and structures impossible, and more images could not be recorded due to the instability of the tip and surface.

As the coverage is increased (to approximately 0.5ML), some areas of the substrate that appear to be self-assembled VOPc islands are observed (Fig. 3.4). These domains are small (approx. 20 x 20 nm) and are separated by areas in which no features can be discerned. High resolution imaging was not possible and the edges of self-assembled regions seem diffuse, suggesting that the surface structures are mobile and unstable at room temperature.

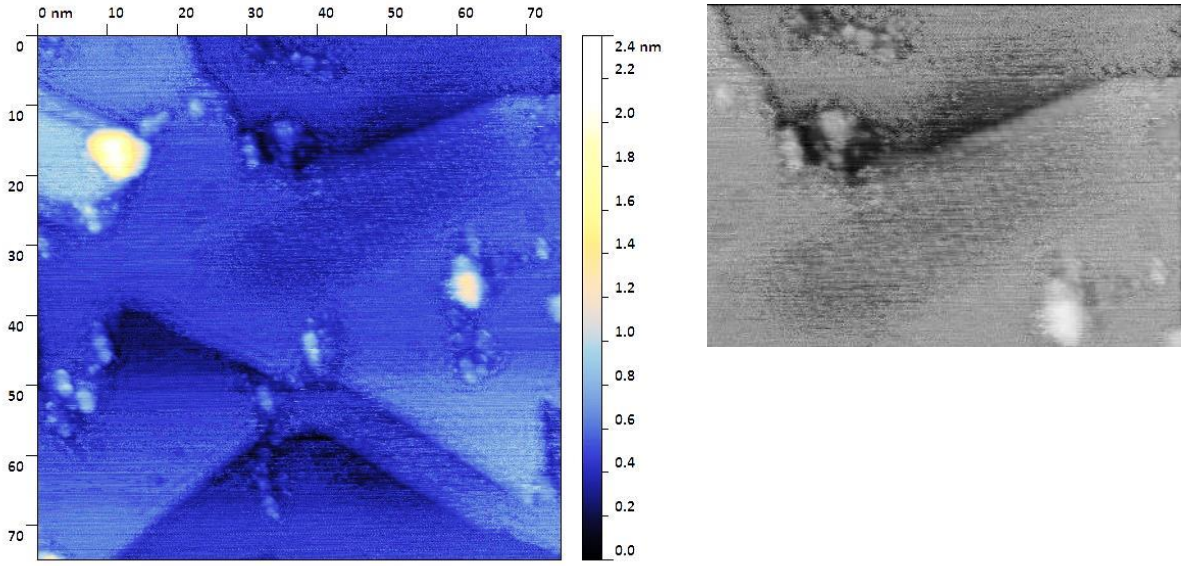

Figure 3.4 – STM of VOPc/Au (111) at approximately 0.5ML V_s = -1.5 V, I = 65 pA

Clear LEED patterns were not observed up to this point, a ring close to the specular beam was observed but focusing this feature for capture was not possible due to technical limitations.

When close to one monolayer (to approx. 0.9 ML) was present the film was stable enough to be imaged with molecular resolution at room temperature (Fig. 3.5). Single crystalline domains of approximately 10 x 10 nm^2 up to 50 x 50 nm^2 are observed, composed of molecules which are visualised similarly to those in the work of Barlow et al.[6]. As such they are assumed to be lying with their ligand Pi system orthogonal to the plane of the surface and the oxygen atom facing outward.

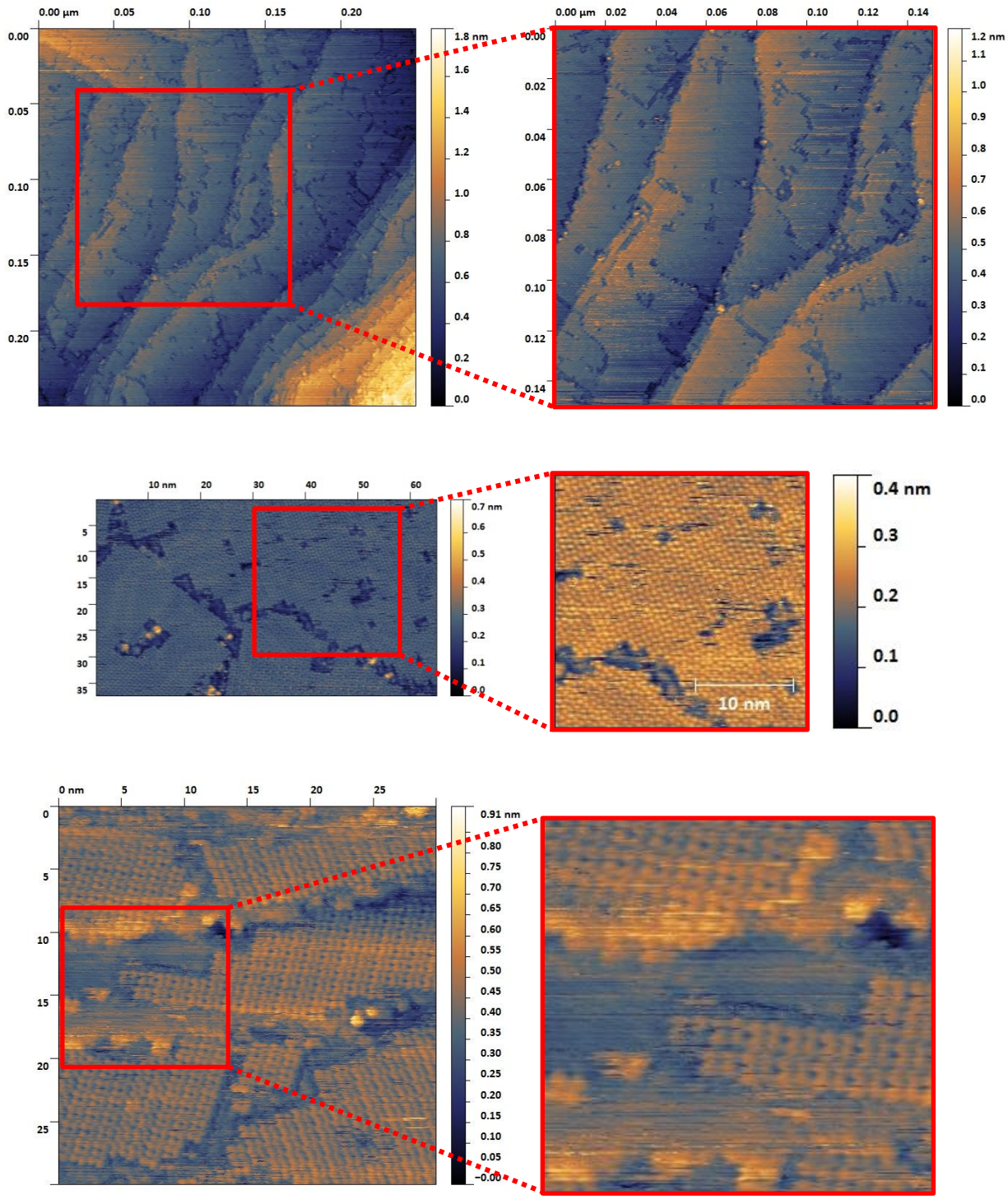

Figure 3.5– STM of VOPc/Au (111) at approximately 0.9ML, V_s = -1V, I = 85 pA

Single- and multi-molecule vacancies, missing rows and small (approx. 5 x 5 nm) areas of bare substrate (Fig. 3.6) can be observed within domains. Without changing imaging parameters frequent changes in contrast and resolution along with molecular visualisation were observed. This may be symptomatic of the adsorption and desorption of weakly bound molecules from the tip or surface.

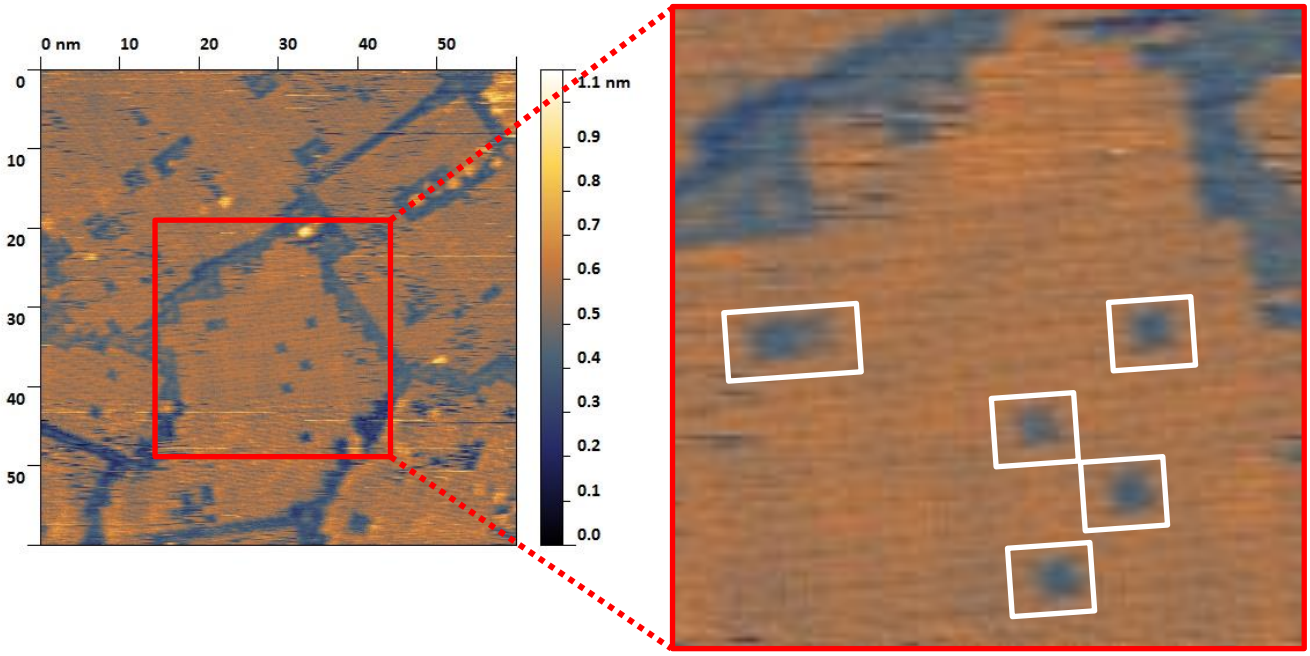

Figure 3.6 – STM of VOPc/Au (111) at approximately 0.9ML, V_s = -1V, I = 100 pA. White boxes show single and multi-molecule vacancies

The density of these defects is relatively high, to the extent that the largest regions observable without such imperfections is only 10 x 10 nm^2. While some of this may be due to the 'unfinished' nature of the surface the presence of ad-molecules and high polycrystallinity suggest a lack of layer-by layer growth. Areas with single isolated molecules (those not incorporated into islands) adsorbed on top of the monolayer are found on the surface. Figure 3.7 shows one such area, where a single VOPc molecule is positioned on top of a 15 nm wide section of VOPc monolayer.

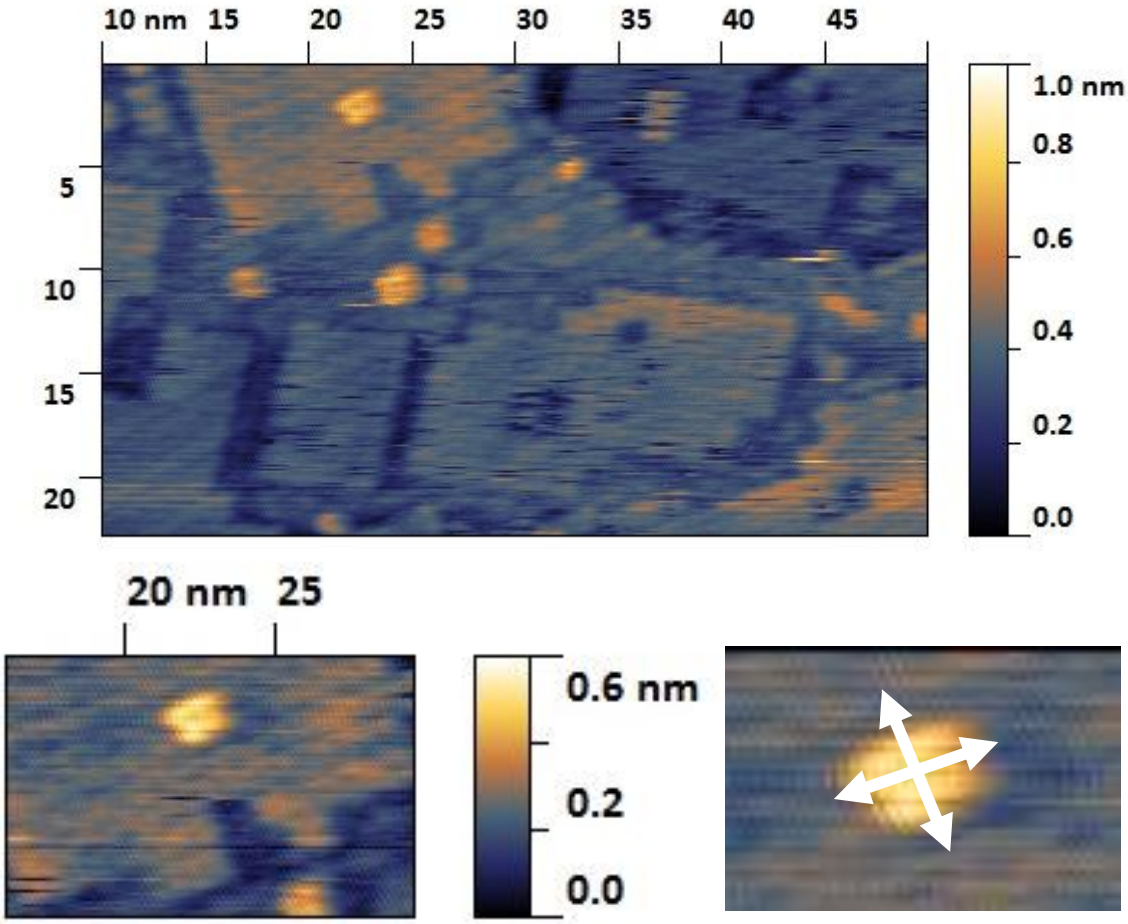

Figure 3.7 – STM of VOPc/Au (111) at approximately 0.9ML, V_s = -1V, I = 100 pA

A similar situation is shown in Fig 3.8 where a row of molecules (separated by longer distances than those in the monolayer) are shown on top of a monolayer island. Where these features are observed they are molecularly resolved rather than as appearing as stripes or 'spikes' in the tunnelling current. This leads to the assumption that they are weakly chemisorbed in metastable geometries rather than diffusing freely around the surface.

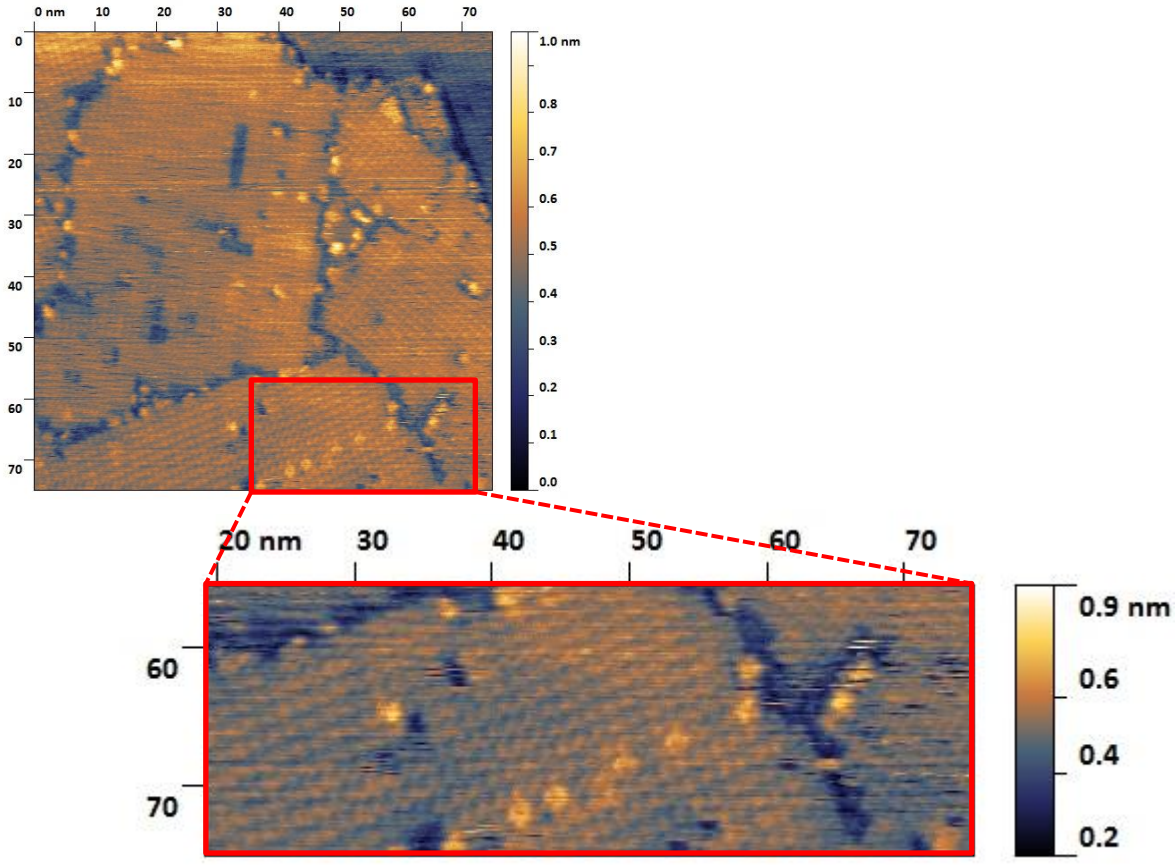

Figure 3.8 – STM of VOPc/Au (111) at approximately 0.9ML, V_s = -0.9 V, I = 100 pA

While high resolution imaging was possible, the surface appeared to be metastable at room temperature, shown by the mobility of surface features during imaging. The images presented in Fig 3.9 were recorded one minute apart and show changes in molecular vacancies and ad-molecules as the surface is scanned repeatedly. A threefold molecular vacancy (white circle **1**) evolves into a single molecule vacancy, a double vacancy (white circle **2**) to a triple vacancy and a single vacancy (white circle **3**) is filled. The red circle shows a molecule adsorbed onto the top of the molecular island and between images it is seen to move laterally across the long axis of the molecular rows. These observations suggest that either the surface is spontaneously undergoing local structural changes or imaging the sample is causing the observed differences. As a small tunnelling current (100 pA) is being used at a moderate sample bias (-0.9 V), the interaction between the tip and the surface should not be large enough to remove molecules from their adsorption sites. However, the

nature and magnitude of the interaction between the VOPc and the Au surface has not been fully characterised so a small perturbation may be enough to change the surface structure.

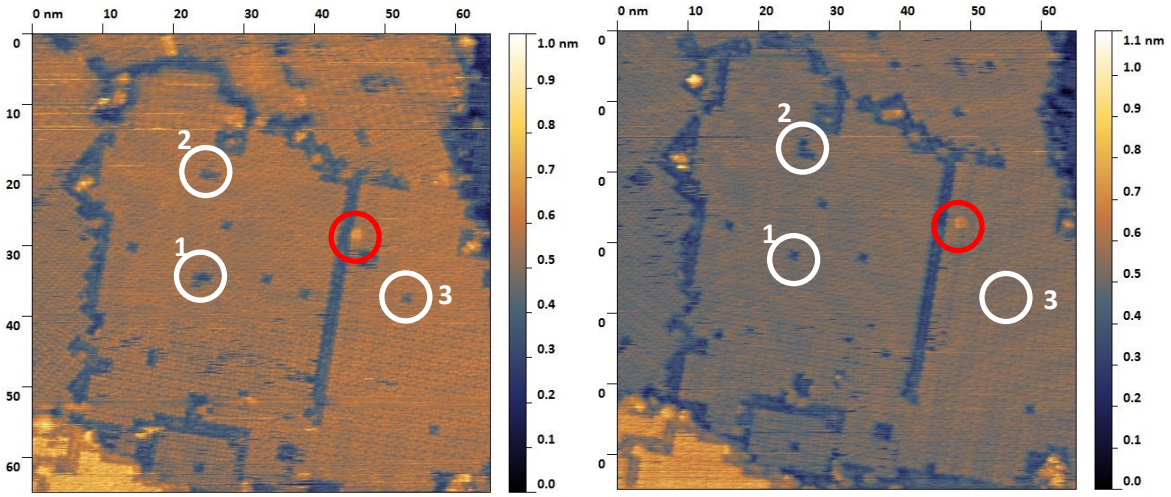

Figure 3.9 – STM of VOPc/Au (111) at approximately 0.9ML, V_s = -0.9 V, I = 85 pA. The right hand panel was obtained 1 min after the left hand panel, white circles mark vacancies and red circles mark ad-molecules

Changes in the azimuthal rotation between molecules are also obvious at multiple points on the surface. As the molecules pack with the electron dense lobes of one molecular 'cross' nesting into the gaps between lobes on each neighbour, this affects a dislocation within the domain (Fig 3.10). Where rotationally different domains meet, a difference in stacking angle of close to 30° is evident. While the molecule is not planar, and as such does not belong to the D_{4h} point group of planar phthalocyanines, the symmetry of the Pc ligand is almost unchanged. If the oxovanadium moiety is projected out of the surface plane, the Pc ligand system will be the dominant interaction with the surface and therefore the largest driving force for self-assembly.

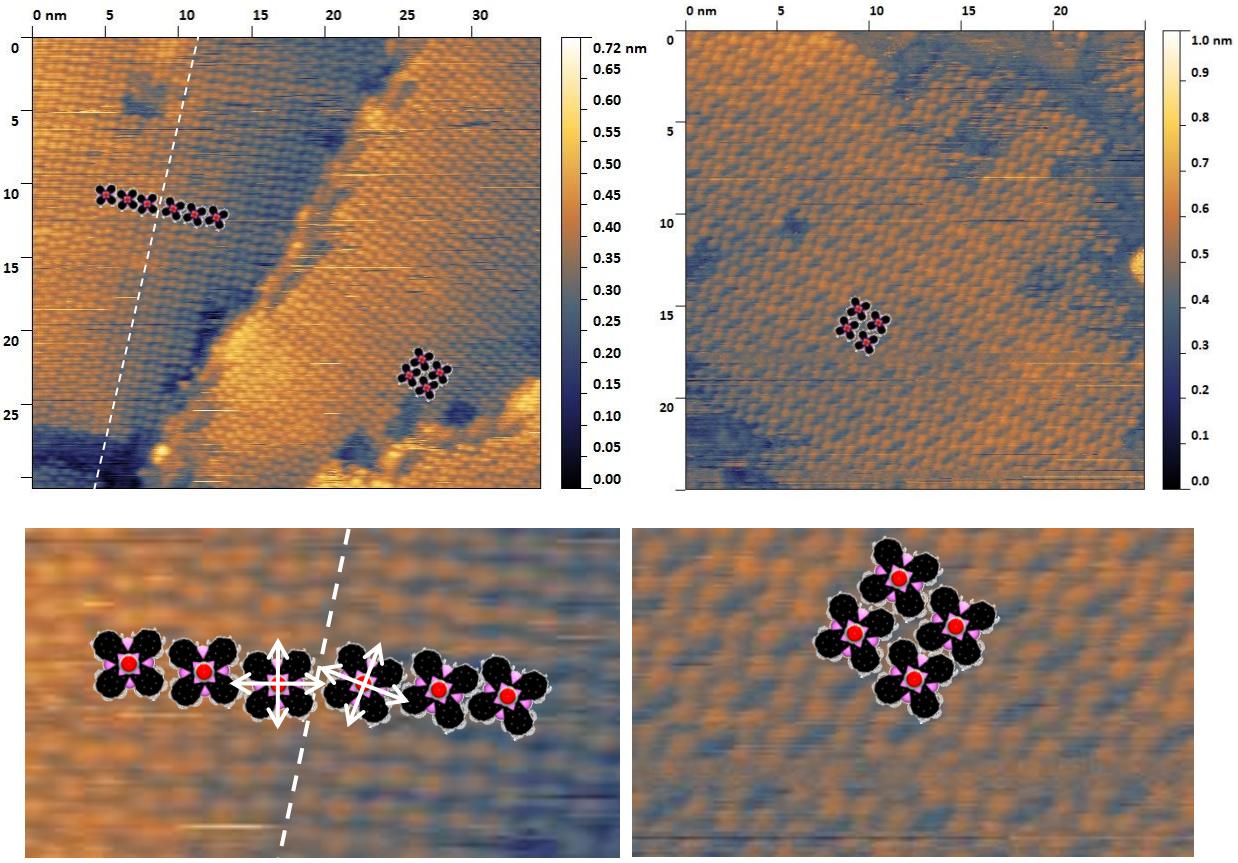

Figure 3.10 – STM of VOPc/Au (111) at approximately 0.9ML, V_s = -1 V, I = 85 pA

A large scale (75 x 75 nm^2) image demonstrating sub-molecular resolution is shown in Fig 3.11 together with the corresponding LEED pattern. The LEED pattern contains three concentric rings: the outermost is defined by collections of three spots, the middle barely visible in the CCD capture (although visible to the naked eye) and the innermost made up of single spots. These patterns appear initially unrepresentative of the square unit cell common to many MPc molecules (due to the D_{4h} symmetry of the Pc ligand). However, as previously discussed in the literature, the pattern can be understood as a superposition of multiple patterns with the same dimensions (and therefore arising from the same d-spacings on the surface). As LEED is sensitive to symmetry over the spot size of the primary electron beam (which is much larger than the image presented in Fig. 3.11 of 75 x 75 nm^2) the diffraction features cannot be related to single island domains of the VOPc

layer. Rather, there must be a number of symmetrically in-equivalent orientations with respect to the substrate that all molecules on the surface adopt.

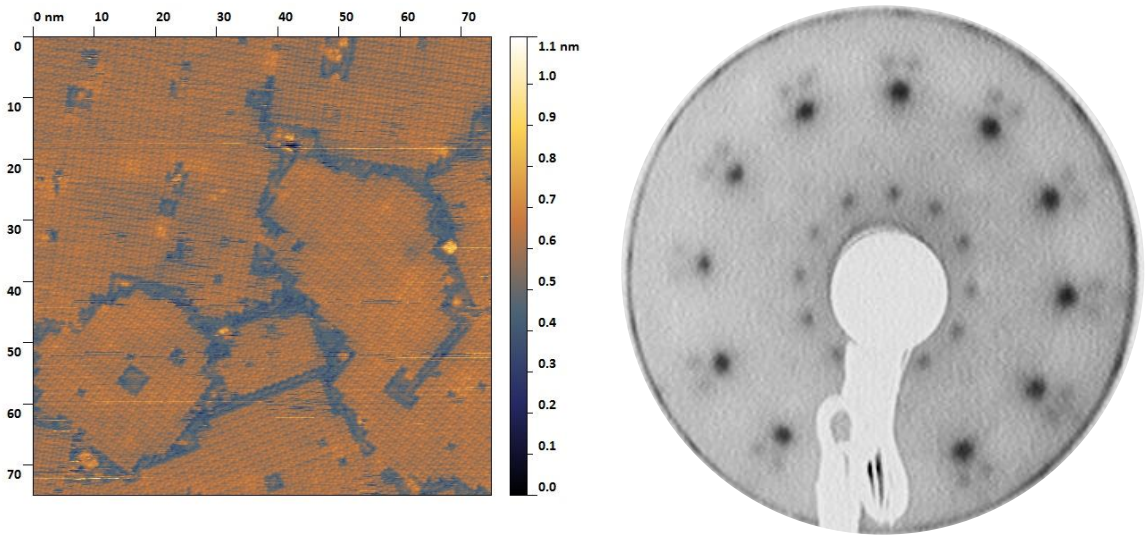

Figure 3.11 – STM of VOPc/Au (111) at approximately 0.9ML, V_s = -0.8 V, I = 85 pA and corresponding LEED pattern at 12 eV (inverted for clarity)

With this in mind the two dimensional fast Fourier transform (2D-FFT) was taken of the image presented in Figure 3.11. This produces a good approximation of the real space structure mapped in reciprocal space[7] and as such can be directly compared to LEED. It is immediately obvious from Figure 3.12 that the 2D-FFT of the image produces a good match for all of the features observed in the LEED pattern.

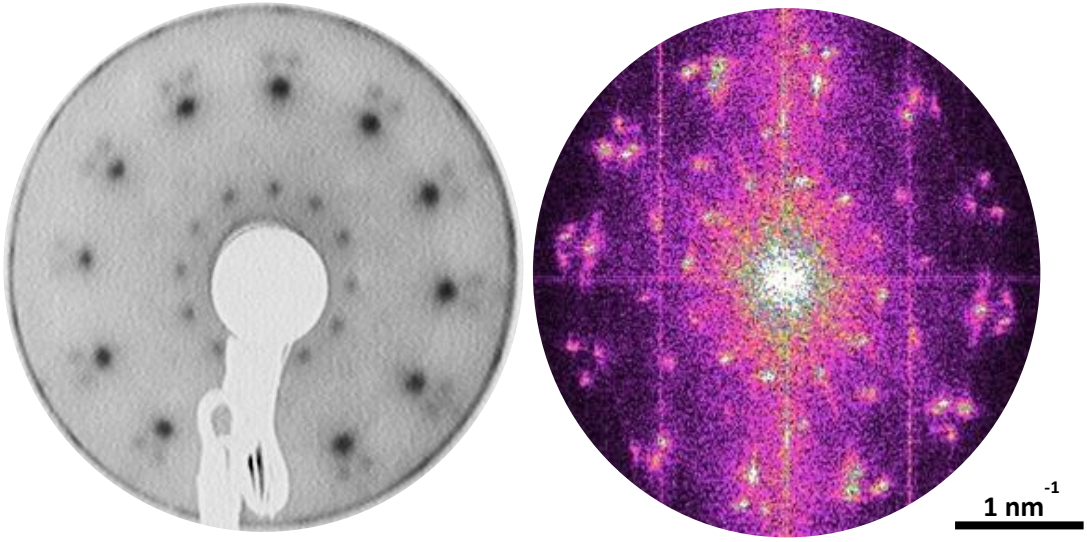

Figure 3.12– LEED pattern at 12 eV (inverted for clarity) and 2D FFT of the image in 6.12 (arbitrarily scaled to match LEED pattern)

In order to ascertain which features are producing the component patterns of the overall pattern sections of the large scale molecular resolution image were taken and separate 2D-FFT patterns were produced (Fig. 3.13). As the large scale image was sufficiently resolved two principle packing axes could be assigned to the VOPc molecules in each domain.

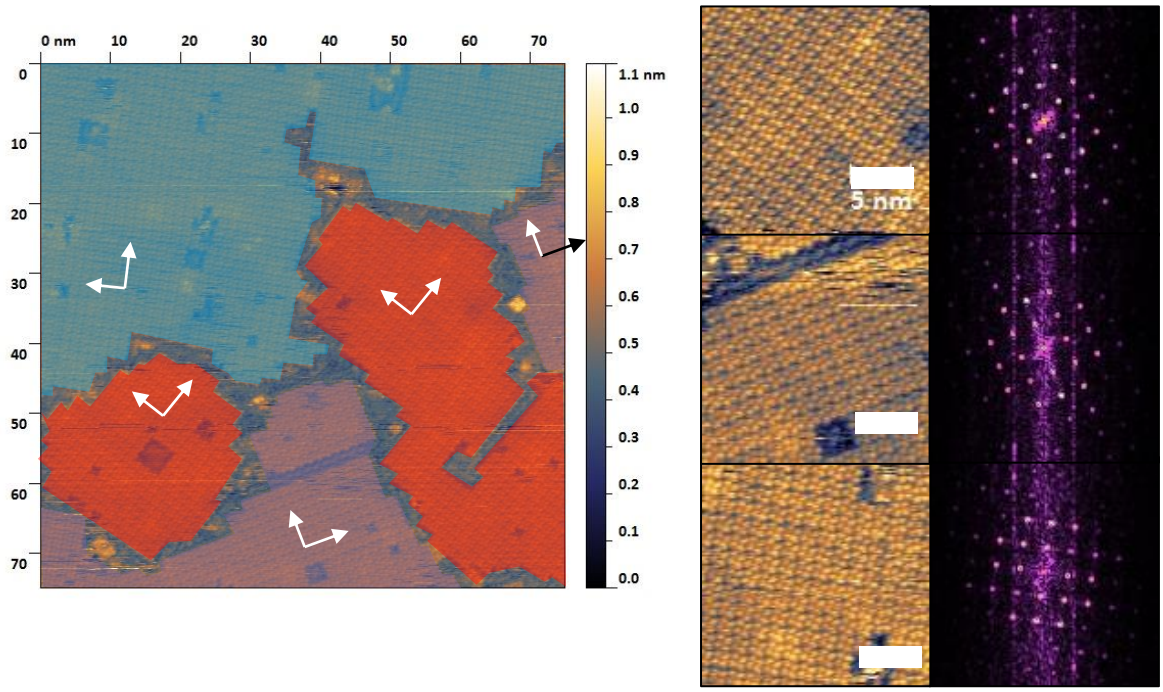

Figure 3.13 – STM of VOPc/Au (111) at approximately 0.9 ML (from Fig. 6.12) with coloured overlays to mark domains. Right hand panel shows sections from each orientation in the larger image and their 2D-FFT power spectra (scale bars are 5 nm)

This allowed the surface to be split into three symmetrically unique domains with respect to the crystallographic axes of the single crystal surface. These are shown and colour coded in Figure 3.13 with the two arbitrary axes used for this assignment marked. One section from each of these was taken and used for the 2D-FFT analysis discussed above.

Each region produces a similar pattern with square symmetry, showing multiple repetitions of the reciprocal space representation of the irreducible symmetry of the surface. If the first order pattern on each is considered, the rotation of each pattern with respect to the others (and therefore the surface) is obvious.

The pattern is a combination of three square patterns which match the unit cell shape of planar phthalocyanines previously analysed using LEED. The relative intensities of each spot appear to be the same in both the inner and outer patterns, suggesting that averaged over the LEED primary beam spot each of the relative orientations has the same population on the surface.

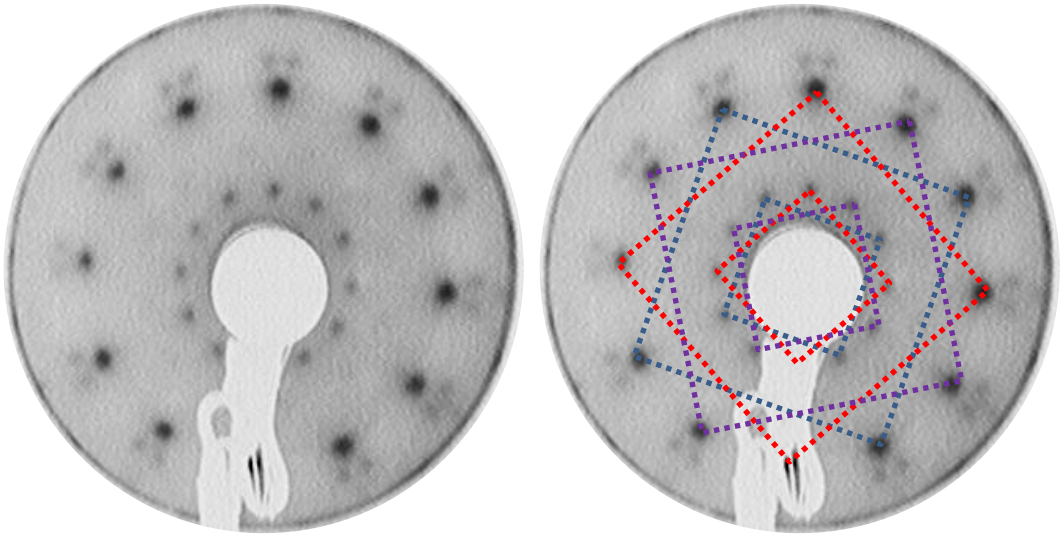

Figure 3.14 – LEED pattern at 12 eV (inverted for clarity) and LEED pattern with over layed domain assignment

As twelve spots are present in both the inner and outer patterns, alignment of all spots with a substrate spot is impossible. The patterns are oriented such that that half of the spots of each

pattern are aligned with principle crystallographic axes of the Au (111) substrate and half are centred between the spots. As the hexagonal Au (111) pattern is made up of six spots they are separated by 60° so the midpoints between them are 30° which matches the previous assignment.

This suggests that the origin of the symmetrical in-equivalence of each unique domain orientation is due to alignment with one of the principle surface axes. The square unit cell must therefore be positioned in three unique orientations with respect to the surface, aligned with one principle axis in each case.

Similar behaviour and LEED patterns have previously been observed with InClPc (a non-planar MPc) on the MoS_2 (0001) surface which also has a hexagonal close packed symmetry. The assignment here agrees with a triple-domain structure presented by the authors although no scanned probe imaging was previously used.

UPS spectra of the sample used for STM and LEED analysis is presented in Fig 3.15, with expanded views of the secondary electron cut-off region (3.15(i)) and low binding energy region (near the Fermi Edge, E_f) (3.15(iii)). The low binding energy region (3.15(iii)) shows the previously observed[8] asymmetric HOMO peak at 0.93eV binding energy. In contrast to previous studies of planar phthalocyanines, a double-peak form is completely formed at one monolayer rather than the multilayers required to produce such a feature[9]. While this feature has been previously assigned to multilayer growth the same feature is observed here with just under a monolayer of molecules[10].

A more likely scenario is described by Toader et al.[11] where hybridisation of an MPc molecule (CoPc) by the surface electronic states is suggested as the reason for this feature. Moreover, the authors suggest a site-dependent charge transfer process to be occurring in a monolayer film, and the effect of the metal can be demonstrated by comparison to other work using organic/organic interfaces with non-planar phthalocyanines where a single peak is observed[12]. Therefore, this peak form is due to the interaction of the metal surface and the monolayer of VOPc present.

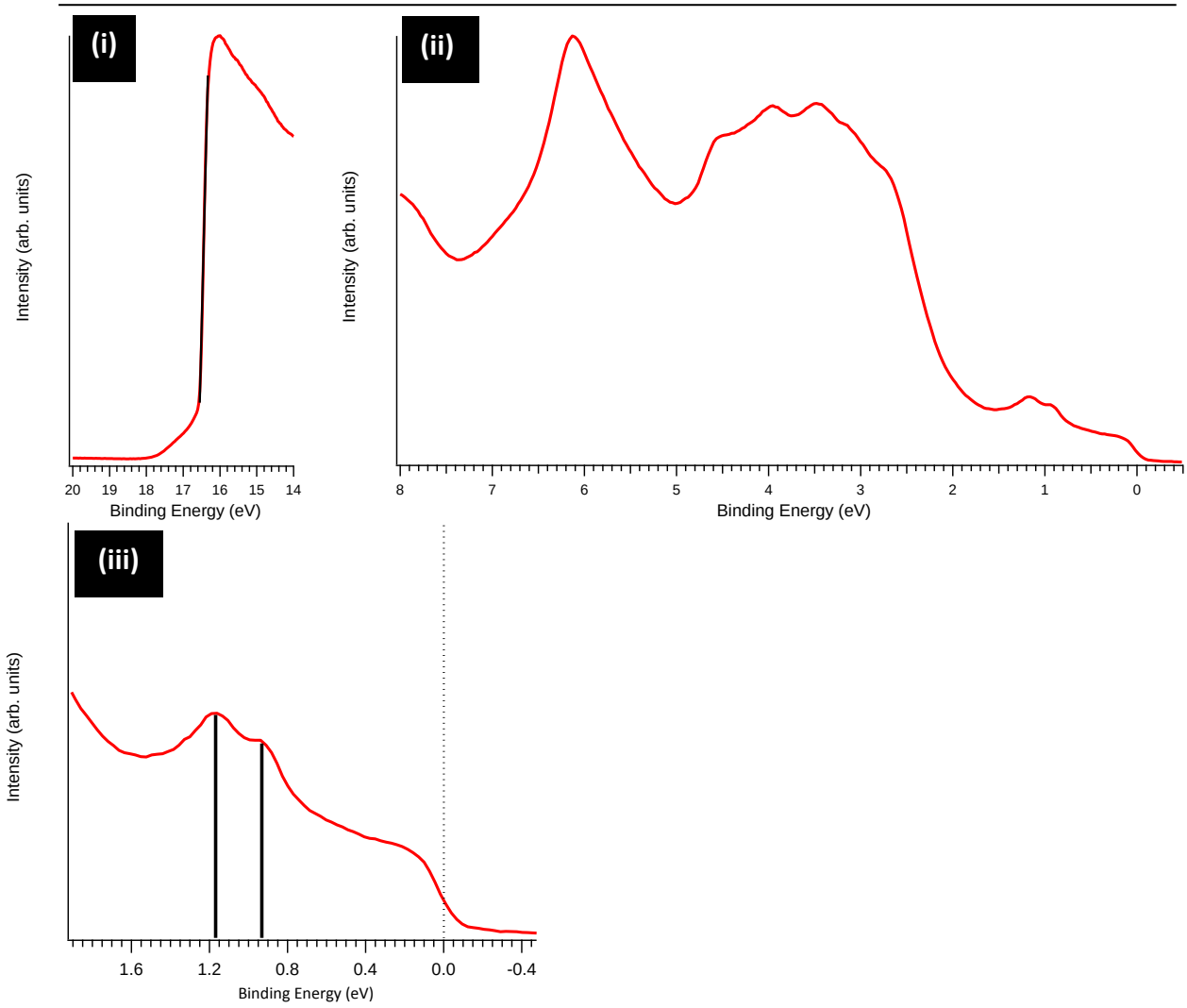

Figure 3.15 – UPS data for approximately 0.9ML VOPc/Au(111); the lower panel (iii) is an expanded view of the low binding energy region of the valence band (ii)

The VOPc molecules are weakly physisorbed on to the surface as had been previously suggested by the observation of the herringbone reconstruction underneath the molecular layer. The lack of states over the Fermi edge strongly suggest that the VOPc molecular states are pinned to the local vacuum level not the Fermi level and as such are not pseudo-metallic. Analysis of the position of the secondary electron cut-off allows the work-function of the interface to be assigned at 4.62 eV, a drop of 0.58eV compared to pristine Au(111). This drop in work function can be explained by the pushing back of charge into the metal surface or passivation of the surface state charge of the gold surface. As such the presence of each molecule, while not adding or removing electrons through charge transfer, lowers the local work function. At close to one monolayer almost all adsorption sites are filled resulting in a global work function reduction due to the summation of all local shifts.

This situation should also result in the molecular states of the VOPc molecule being shifted with respect to the Fermi edge with increasing coverage (molecules added to the layer reduce the overall pinning to the local vacuum level of the system due to molecule-molecule screening). Films were therefore grown for UPS analysis from 0.25ML up to 0.9ML and the results are presented in Figure 3.16.

In the thinnest (0.25ML) film no feature relating to the HOMO of VOPc can be discerned although a state close to E_f is observed, assigned as the supressed surface state of the Au (111) (Fig 3.16(iii)). Even with only 0.25ML coverage the work function shifts by 0.3eV indicative of the 'push-back' effect involved in the physisorption of the VOPc molecules. STM images presented earlier suggest that molecules are spread evenly over the surface at very low coverage presumably to minimise repulsive lateral interactions between them.

Low binding energy HOMO peaks are observed close to the Fermi edge in 0.5ML films and move to higher binding energies in 0.75ML and 1ML films (Fig. 3.16(iii)). The work function drops to

4.62eV at 0.75ML and remains unchanged in thicker films due to the saturation of surface adsorption sites causing no further push-back of charge (Fig. 3.16(i)).

The HOMO peak moves further from the Fermi edge as the thickness of the film is increased and evolves into a split peak above 0.75ML (Fig. 3.16(iii)). These observations confirm the assumption that the VOPc/Au (111) interaction is relatively weak involving physisorption and long-range interactions. Although the work function of the Au (111) surface is decreased by the growth of VOPc layers this change is small (0.58 eV) and no charge transfer is inferred in this interaction.

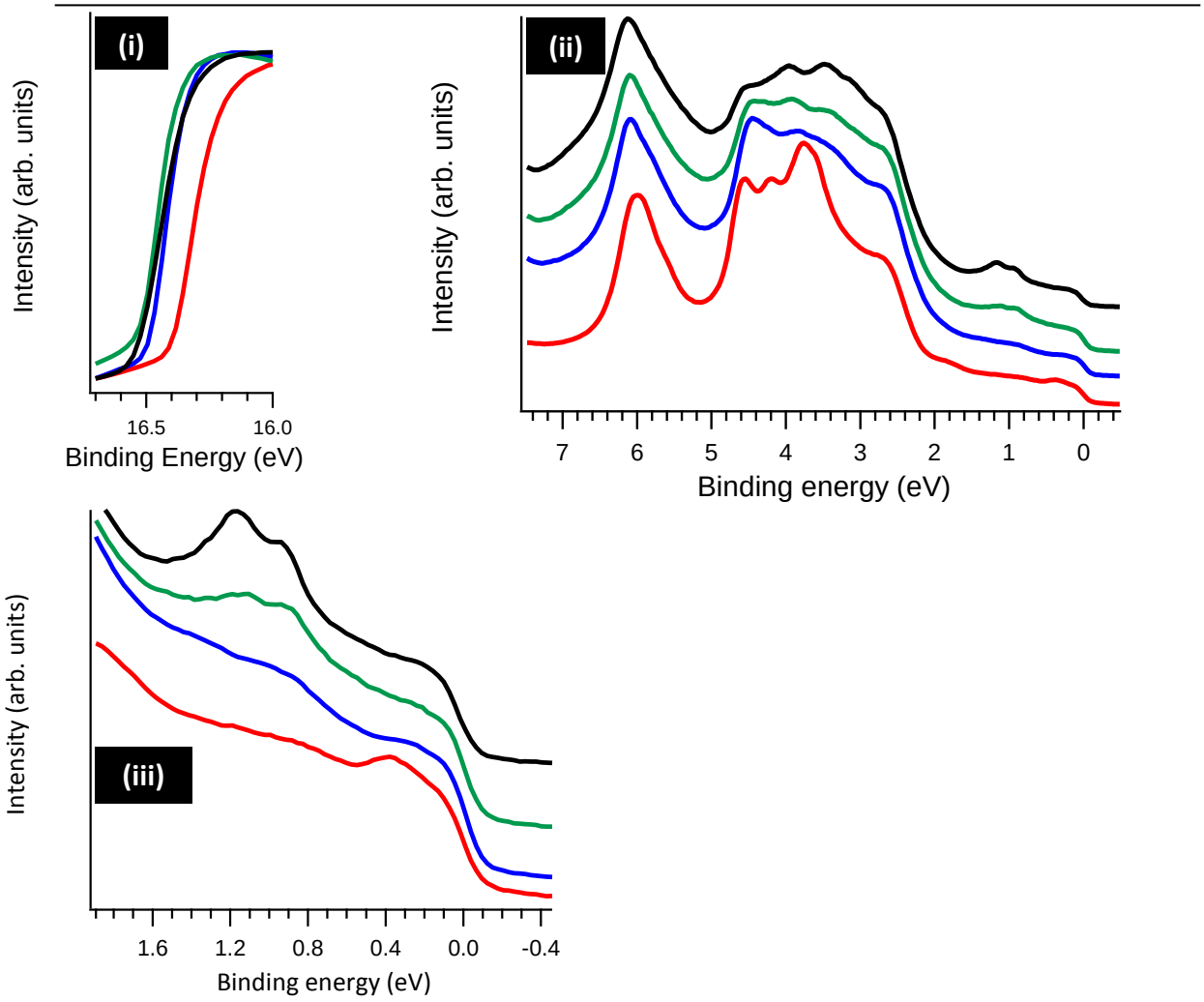

Figure 3.16 – UPS data for 0.25 ML (red) 0.5 ML (blue) 0.75 ML (green) and 0.9 ML (black) VOPc/Au (111)

3.2 – VOPc / Ag (111)

Identical conditions were used to prepare VOPc/Ag (111)/Mica films up to 0.9 ML thick to compare surface and electronic structure with VOPc/Au (111). LEED patterns (Fig. 3.17) are similar to those for the VOPc/Au (111) system and can therefore be explained using ideas presented in the proceeding section.

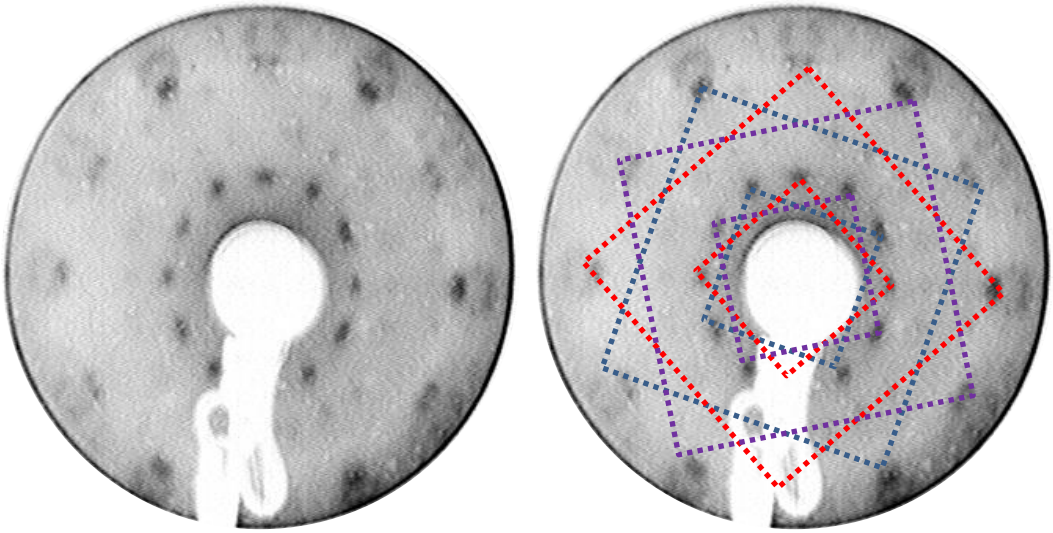

Figure 3.17 –LEED pattern for approximately 0.9ML VOPc / Ag (111) and overlayed domain assignments

STM images indicate that the VOPc islands present on the Ag (111) surface are larger than those on Au (111) (up to 40 x 40nm^2 on Au and 100 x 100nm^2 on Ag) but possess the same molecular vacancy and ad-molecule features. Molecular and sub-molecular resolution images demonstrate the same visualisation of the LDOS of the VOPc molecule and similar slipped-stack features within islands are observed.

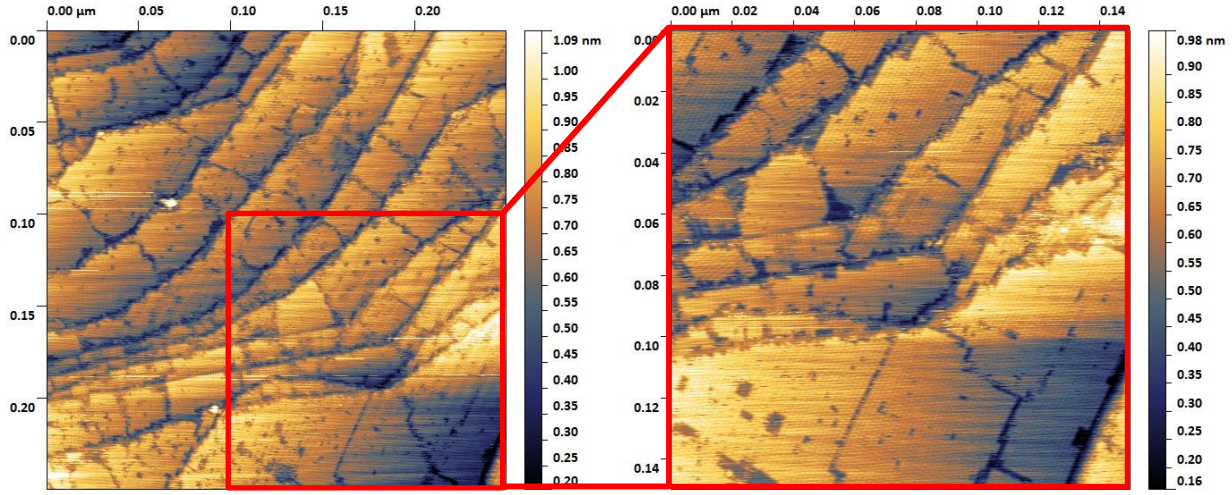

Figure 3.18 – STM of VOPc/Ag (111) at approximately 0.9ML, V_s = -0.6 V, I = 85 pA

The larger domain size may be due to the lack of surface reconstruction on Ag (111) compared with Au (111), providing no low energy nucleation sites (elbow sites and reconstruction lines) and therefore larger single domains. This is difficult to comment upon as STM only probes local structure in the vicinity of the tip, and the transfer width of the low energy electrons used in LEED is larger than the smaller islands on Au (111).

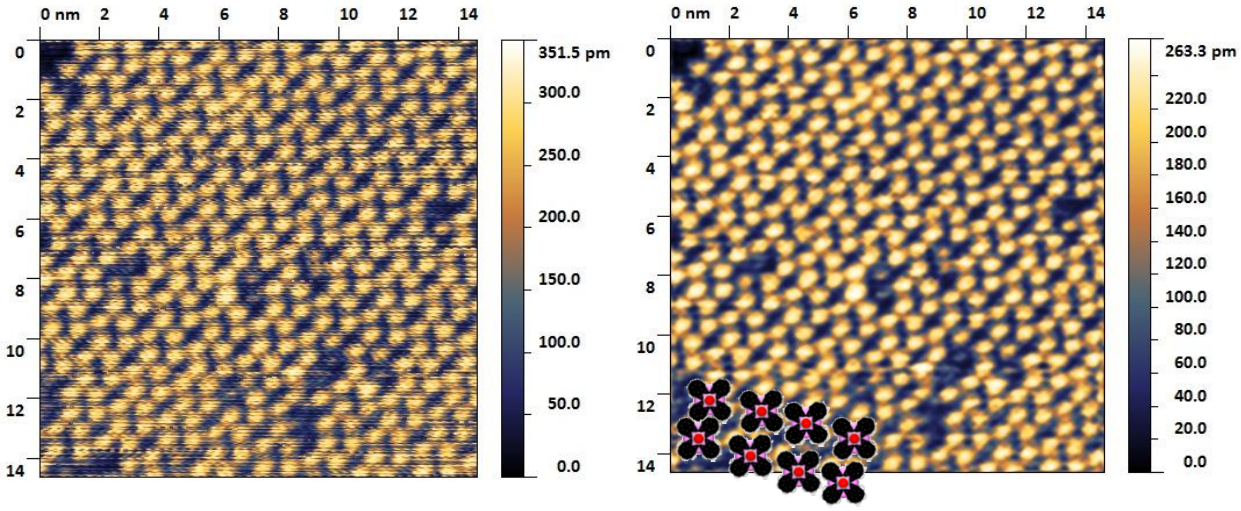

Figure 3.19 – STM of VOPc/Ag (111) at approximately 0.9ML, V_s = -1 V, I = 115 pA. The left panel is raw data and the right has been low pass filtered to remove noise

At 0.9 ML coverage a similar double peak feature to that recorded from Au (111), assigned as the VOPc HOMO, is observed in the low binding energy region of the UP spectrum (Fig. 3.20(iii)). The position of the centre of the two peaks is 0.4 eV further from the Fermi edge on Ag compared to Au. Similar behaviour was previously observed on Ag (111) with CuPc[13] although experiments were conducted at low temperatures rather than room temperature. The shape of the HOMO peak is also subtly different although the lack of scanned probe imaging and the difference in molecular species makes comparison difficult.

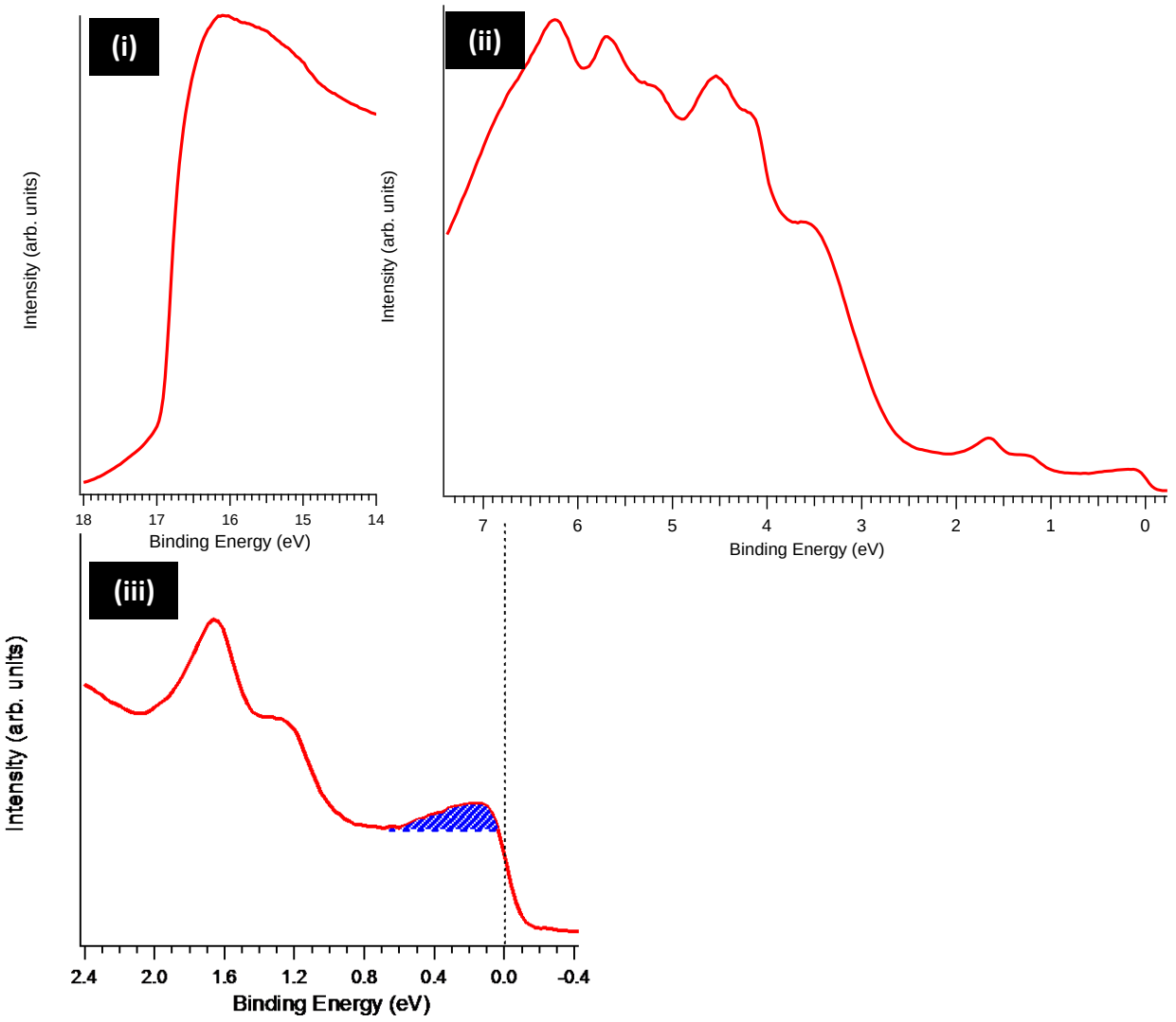

Figure 3.20 – UPS data for approximately 0.9ML VOPc/Ag(111) (i) and (ii); the lower panel (iii) is an expanded view of the low binding energy region of the valence band. The blue shading highlights the charge transfer induced electron density near the Fermi edge

The appearance of a populated state close to the Fermi edge suggests the presence of charge transfer at the VOPc/Ag(111) interface unlike VOPc/Au(111). This extra state may be a former LUMO state which has been populated by electron density from the d-band of the Ag (111) surface, and as such is shifted just under the Fermi level. The most intense of the d-band features also appears split in the VOPc/Ag(111) film compared to the clean Ag(111) surface. Thinner films were grown to observe the appearance of this state and any shifts in position or changes in form of the HOMO features of the VOPc molecule (Fig. 3.22)

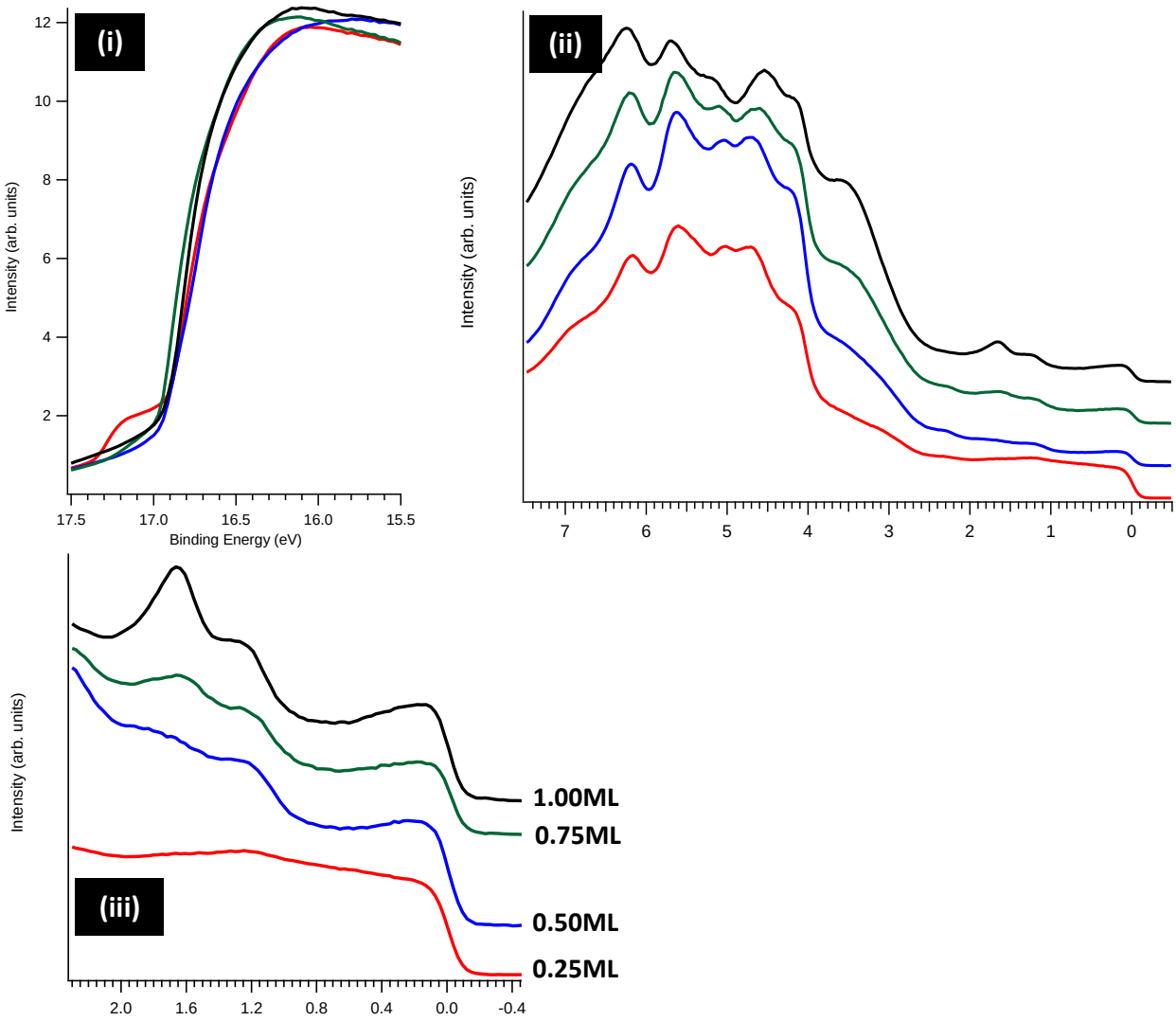

Figure 3.21 – UPS data for 0.25ML (red) 0.5ML (blue) 0.75ML (green) and 0.9ML (black) VOPc/Ag (111)

At 0.25 ML a broad HOMO peak is observed 1.2eV below the Fermi level and no filled LUMO state is obvious at the Fermi edge (Fig. 3.22(iii)). If the coverage is increased to 0.5ML the HOMO position does not move but its peak shape is more defined and the filled LUMO state begins to emerge. At 0.75ML a clear double-peak HOMO, with the lower binding energy portion still centred at 1.2 eV and an additional feature emerging at 1.6 eV, and the former LUMO level still present over the Fermi edge is observed. If the low binding energy regions of the 0.75ML and 0.9ML spectra are compared their similarity is obvious other than the increase in intensity of the higher binding energy portion of the double HOMO peak. They both show the filled LUMO feature characteristic of charge transfer at the metal/organic interface.

The work function of the Ag (111) surface is decreased by the addition of VOPc by a similar amount to Au(111), 0.52 eV compared with 0.58 eV. The difference in these values is within the energy resolution of the analyser used for these measurements. This shows that despite the filling of the LUMO level by the Ag surface the presence of VOPc molecules still lowers the work function of the surface by pushing charge back into the metallic surface.

3.3 – VOPc / Cu (111)

Identical parameters were also used to fabricate monolayer films on the Cu (111) surface. LEED patterns (Fig. 3.22) were significantly different to those observed on Ag (111) and Au (111), containing twice the amount of spots. The first Laue zone is hexagonal rather than circular (some of the spots must therefore be further from the specular beam than others). This shows that the symmetrical relationship of the molecule with the surface is different on Cu (111) compared to Au (111) and Ag (111). This suggests that a single lattice is not responsible for all of the spots present in this pattern although the lattice spacings must be very similar if they are observed in such close proximity at the same beam energy.

The contributions to the pattern can be separated into two parts, hexagonal and rectangular, by careful examination of the spot intensities and positions. The pattern closest to the

specular beam (therefore the largest lattice parameters) consists of twelve spots and can be indexed as a combination of rectangular unit cells rotated by 30° with respect to each other. Although the shape of each pattern (and therefore the unit cell) is different from that observed on Ag (111) or Au (111), the symmetrical relationship of the VOPc unit cell with the surface lattice is similar.

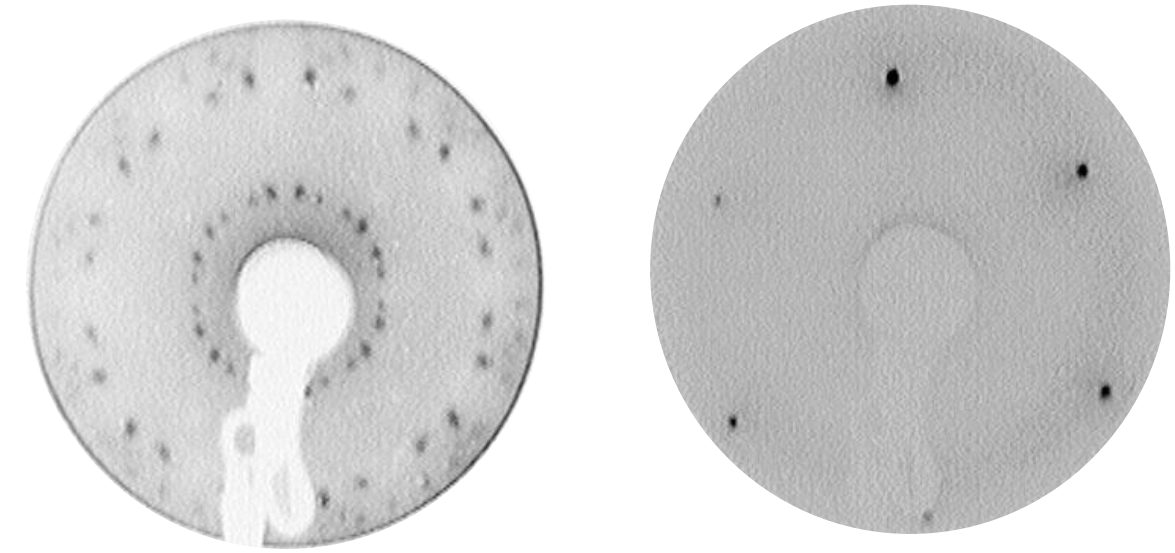

Figure 3.22 – LEED pattern for approximately 0.9ML VOPc / Cu (111) collected at 12 eV and the 1x1 substrate pattern at 120 eV

The remaining twelve spots of the pattern cannot be indexed to the same unit cell due to their radial positions and distance from the specular beam. This separate pattern also consists of twelve spots but each pair of spots is positioned such that an angle of approximately 15° is defined between them and the specular beam. One possible assignment of this is two superimposed hexagonal patterns rotated about the specular beam (Fig 3.23). This indicates a deviation from both the square unit cell observed on Ag(111) and Au(111) and the rectangular cell in the other pattern on Cu(111). The complexity of the LEED pattern suggests that multiple assembly modes, and possibly adsorption geometries, are present on the surface.

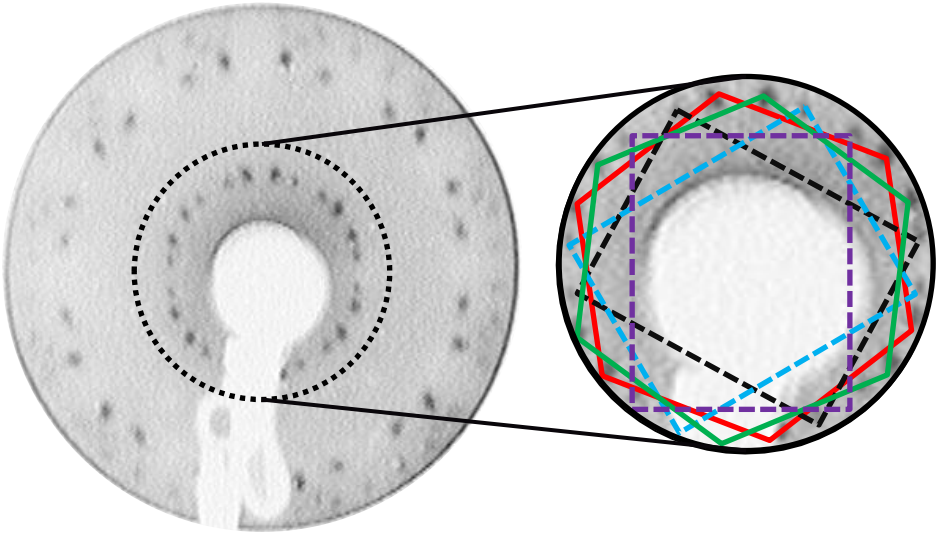

Figure 3.23 – LEED pattern for approximately 0.9 ML VOPc / Cu (111) at 12 eV and overlaid domain assignments

STM topographs of the same surface revealed two distinct molecular appearances and packing modes; cross-like molecules in square symmetry lattices and more rounded or spherical features (Fig. 3.24).

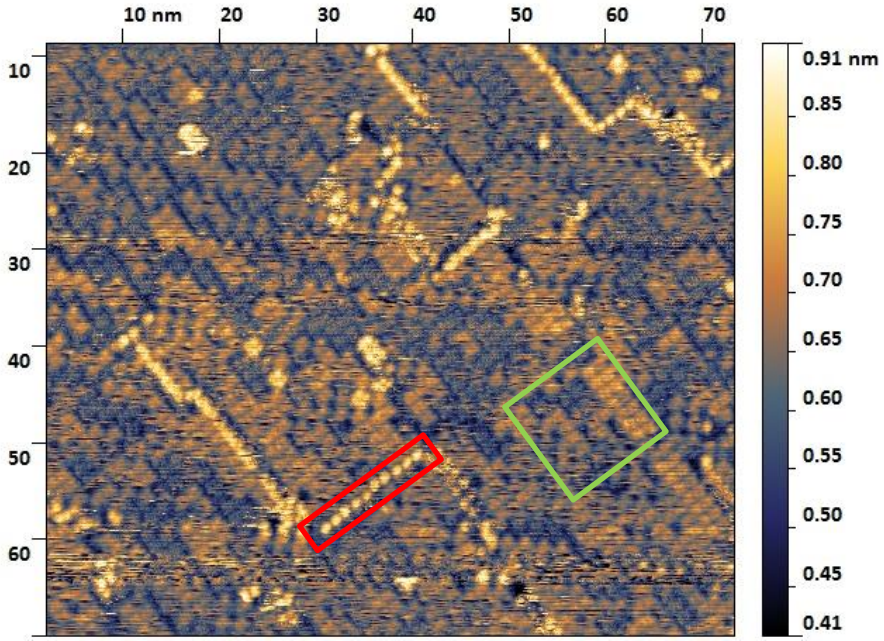

Figure 3.24 – STM of VOPc/Cu (111) at approximately 0.9ML, V_s = -1.6 V, I = 85 pA . The green square marks 'square' assembly and the red rectangle shows a line of the rounded visualisation

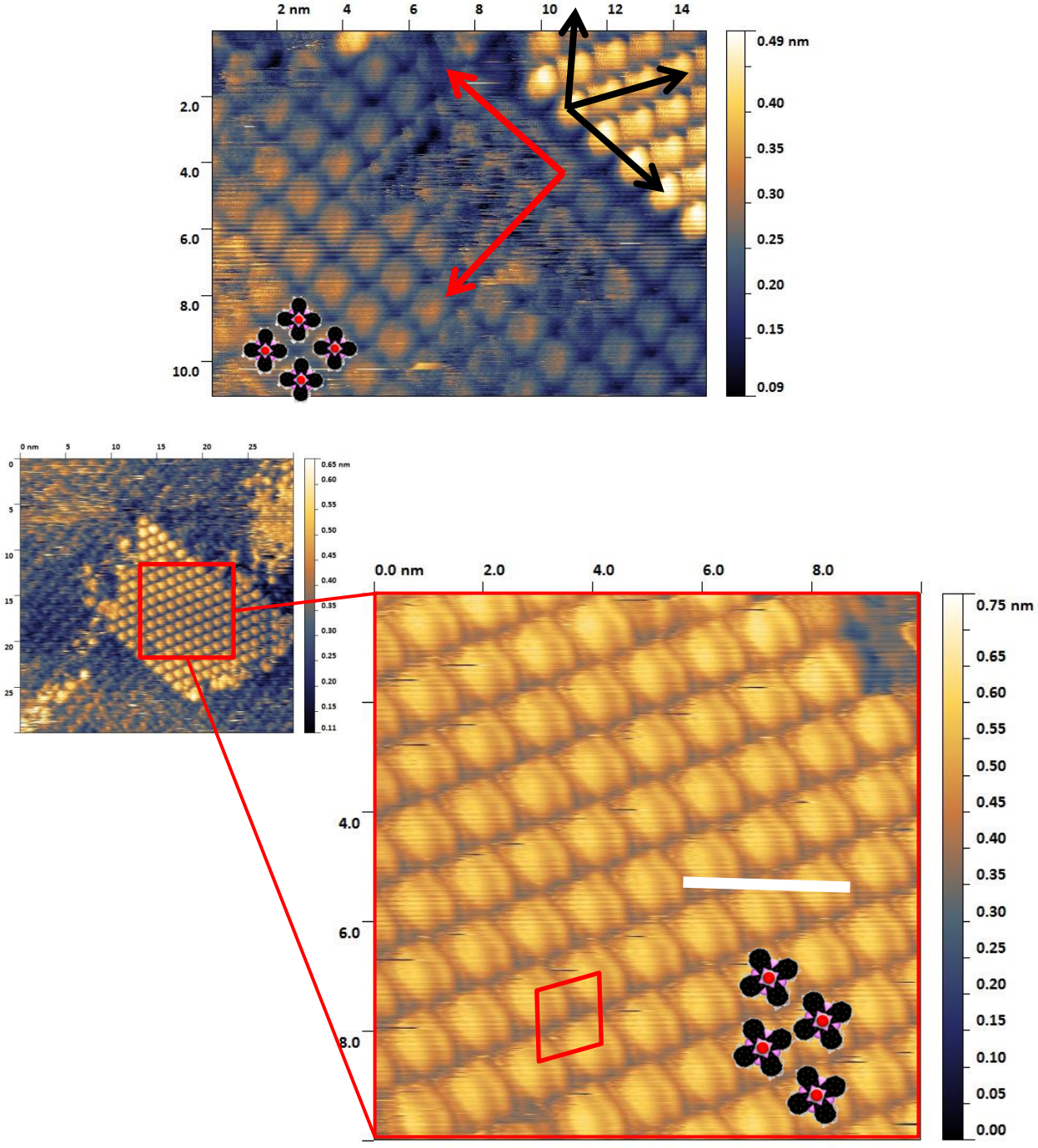

Figure 3.25 – STM of VOPc/Cu (111) at approximately 0.9 ML, V_s = -1.5 V, I = 65 pA . The red and black lines show the lattice vectors for the square and hexagonal structures, respectively

Some areas of the surface contain high densities of the second visualisation assembled into hexagonally packed domains (Fig 3.25). These species appear highly mobile and with repeated scanning of the same area islands grow and shrink along close-packed axes while larger islands seem

unstable at the edges (Fig 3.26). In other areas of the surface molecular vacancies within islands are observed and are highly mobile. The underlying (or coexisting) surface is made up of VOPc molecules packing similarly to the inter-digitated self-assembled structures observed on Au and Ag. Multi-layer growth may be in evidence on the surface although the possibility of different tunnelling pathways producing height differences in the topographs makes this assignment problematic.

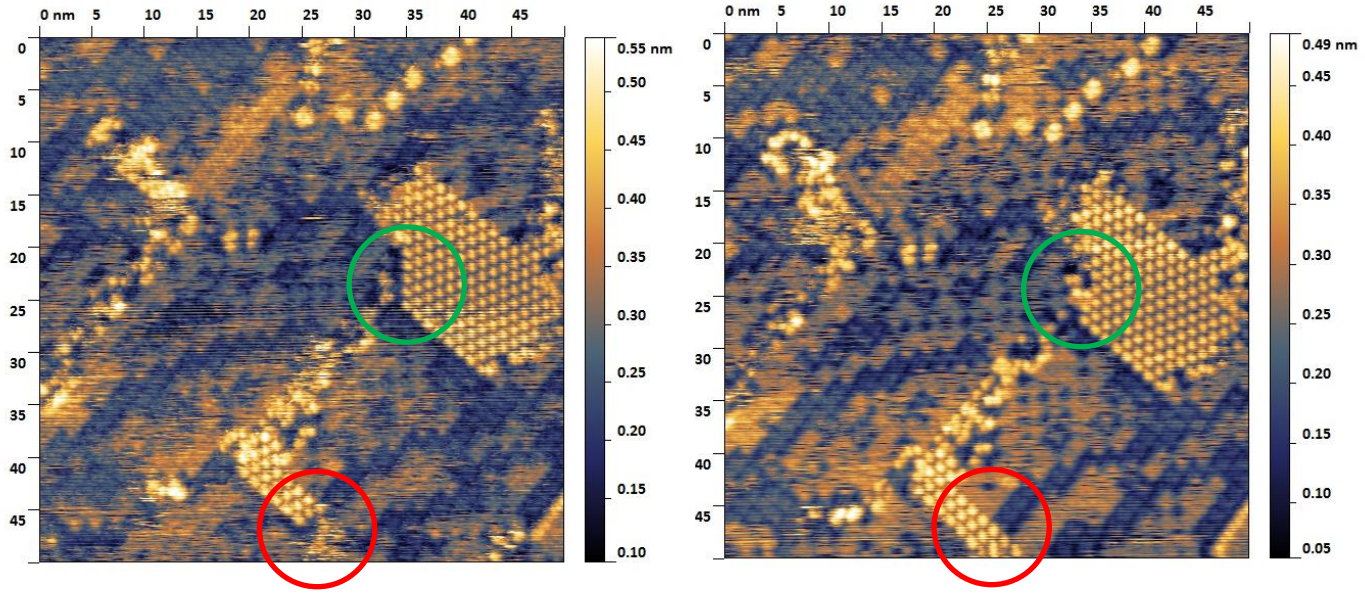

Figure 3.26 – STM of VOPc/Cu (111) at approximately 0.9ML, V_s = -1.64V, I = 85 pA . The right hand pane is taken one minute after the left hand pane. Green and red circles highlight areas of growth between scans

To produce hexagonal packing, the adsorption geometry of the VOPc molecule must deviate from the flat-lying cross-shaped adsorption mode observed on Au (111) and Ag (111). This suggests that either the molecule is tilted off axis with its molecular plane at an angle to the substrate (similar to the case of TiOPc on Ag (111)[14]), or by interacting with the surface the molecular shape has been altered. In Figure 3.28 the visualisation is that of cross-shaped features and in Figure 3.29 cross-like molecules and rounded hexagonally packed molecules appear at very similar height scales. This makes the assignment of the hexagonal VOPc as the topmost layer difficult to confirm.

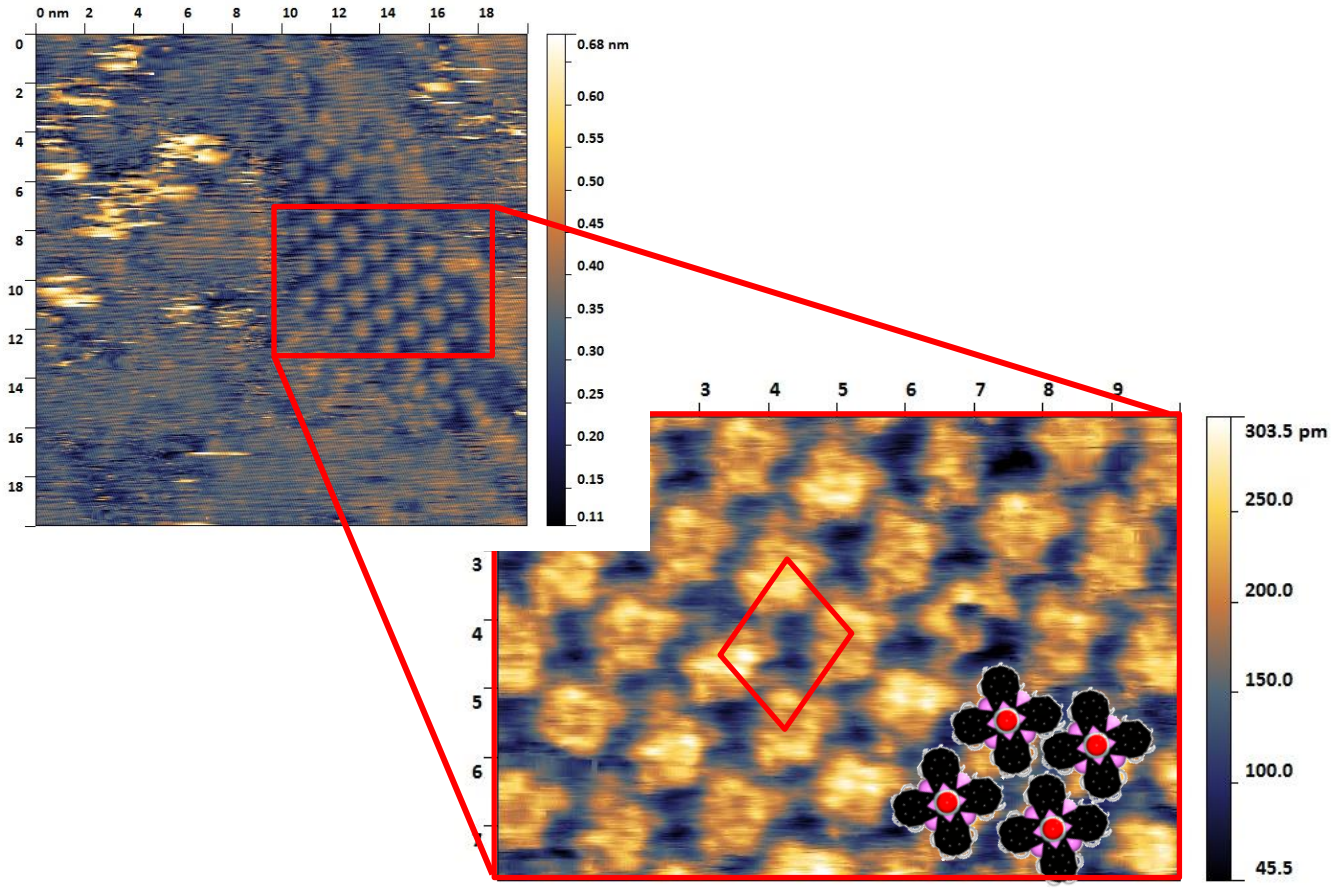

Figure 3.27 – STM of VOPc/Cu (111) at approximately 0.9 ML, V_s = -1.2V, I = 100 pA .

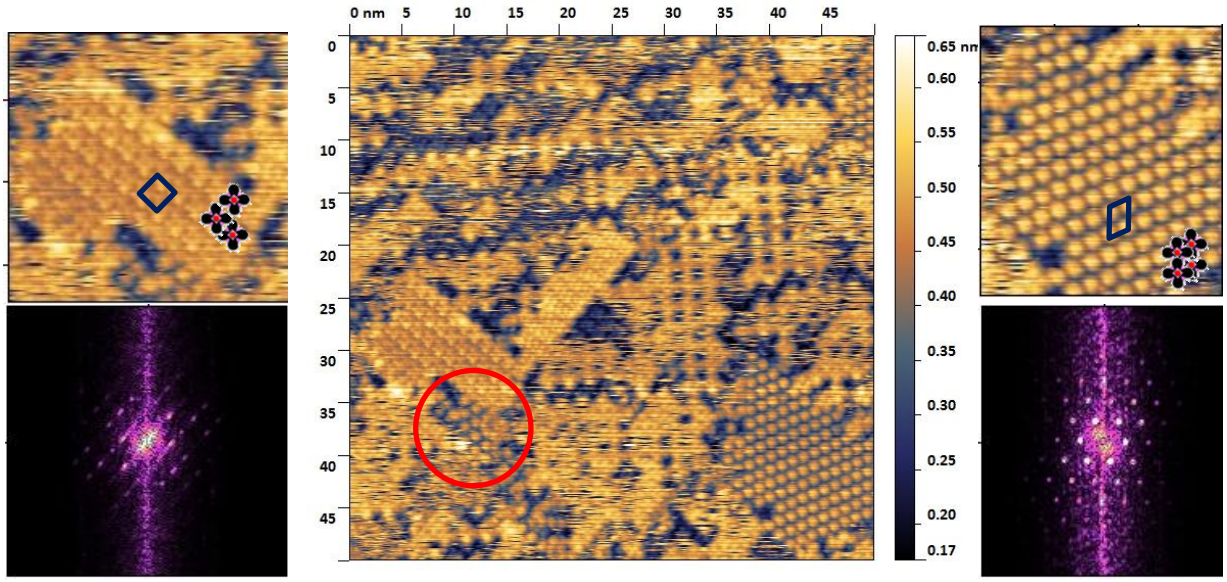

Figure 3.28 – STM of VOPc/Cu (111) at approximately 0.9 ML, V_s = -1.5 V I = 125 pA

Two models can be constructed for hexagonal packing, firstly a layer of molecules with modified symmetry altering the packing of molecules adsorbing on top, and secondly charge transfer directly causing the packing changes.

The self-assembly of symmetrically altered MPcs would produce an electronically non-uniform periodic surface defined by the lobes of the Pc ligand and the central oxygen atom of the VOPc (Fig. 3.29). This is a similar assignment to one suggested in literature for planar phthalocyanines on Cu (111) surfaces. As VOPc is adsorbed on top, a 'tilted' geometry may be adopted to maximise the interaction of the oxovanadium moiety with the electron rich or poor lobes of the underlying VOPc. A smaller separation between molecules in the topmost layer would then be produced due to the tilted molecular plane and a slipped stack hexagonal packing motif observed.

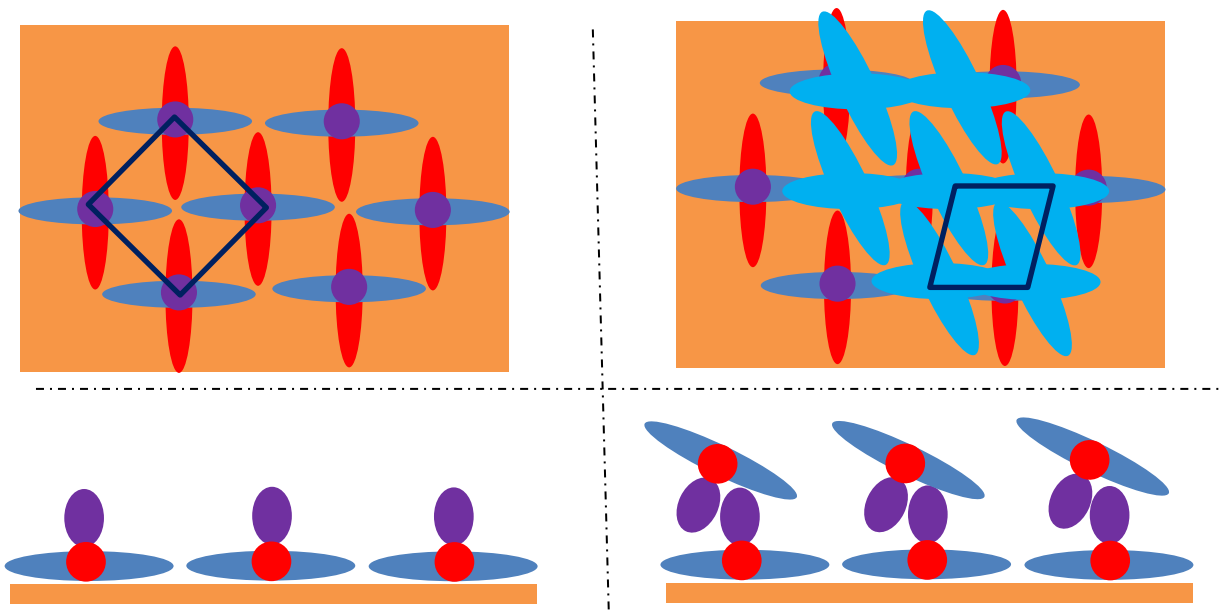

Figure 3.29 – Schematics of molecular packing in (left) square and (right) hexagonal structures.

More VOPc was deposited in an attempt to increase the surface coverage of hexagonally packed molecules for higher resolution imaging. This did not have the desired effect and only square packing was observed when another 0.5 ML equivalent was deposited (Fig 3.30). Some mobile

molecules are evident on top of the square layer but no extended areas with hexagonal packing were observed. This suggests that adding more molecules drives assembly to square packing, and molecules are screened from the effect of the electronically corrugated first layer by lateral neighbours. LEED patterns collected of the surface after adding more VOPc did not, however, suggest any change in structure.

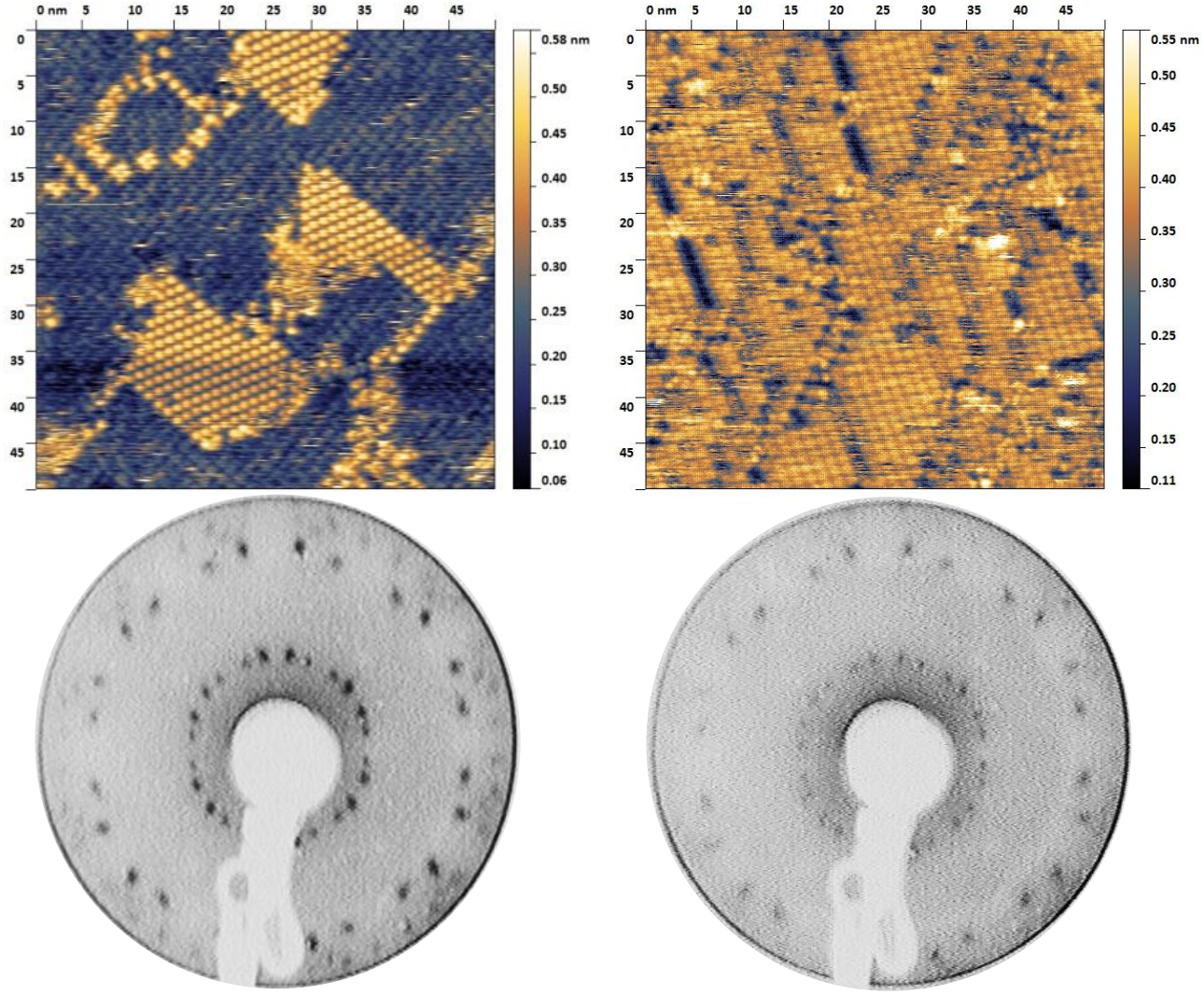

Figure 3.30 – STM of VOPc/Cu (111) at approximately 0.9ML (left) and 1.4ML (right) , V_s = -1.6V, I = 85 pA . The corresponding LEED patterns are shown underneath

If charge transfer was directly causing the change in packing due to modification of the structure of the molecule, annealing should preferentially produce the most stable assembly mode in the thin film. In a situation where charge transfer was present we assume that a charge transfer directed assembly mode would be the most stable and lowest energy conformation possible. The previously observed surface is assumed to be away from equilibrium in terms of occupation of multiple metastable assembly environments.

Annealing experiments were performed to produce larger molecular islands for imaging by STM and to observe the influence of temperature changes on the assembly of the VOPc molecules. A film was grown using the same parameters for 0.9 ML growth on Au and Ag at room temperature and annealed to 175°C in vacuum for 12 hours, after which LEED patterns were collected (Fig. 3.31).

A pattern very similar to that produced by the non-annealed sample was observed although a lower inelastic background was observed and diffuse (1,1) spots were weakly visible. STM images (Fig. 3.31) showed a mixture of isolated molecules, small clusters of close packed molecules and finally large molecular islands (around 100 nm). The packing inside these islands is different to that observed on Ag and Au, with molecules in closest contact on the edges of their ligand pi systems rather than inter-digitated. This produces a larger unit cell which is confirmed by the smaller specular beam-pattern distance observed at 12 eV on Cu compared with Au and Ag.

Further annealing to 200°C was used to attempt to desorb the topmost layer of molecules and test if a second layer was actually present on the sample. Once temperatures above 180°C were reached, no LEED pattern could be observed even after the sample was cooled to room temperature; no useful STM images were produced. This indicates that while the sample may be a collection of single and double layers locally, it is not possible to selectively desorb the second layer. It is possible that films of VOPc on Cu(111) grow in an inherently 3D manner due to the screening energetics of adsorbing multiple layers simultaneously.

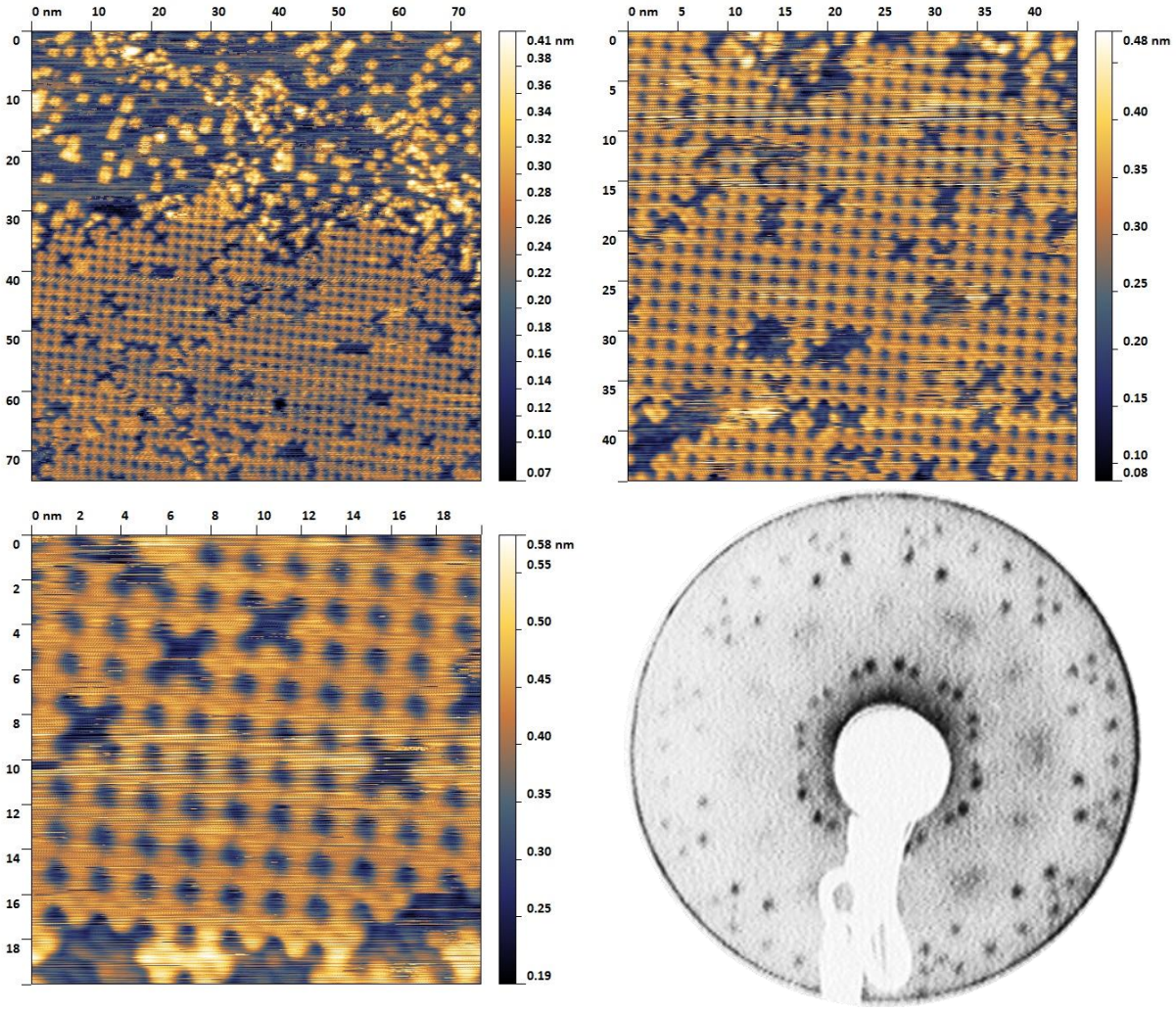

Figure 3.31 – STM of VOPc/Cu (111) at approximately 0.9 ML, V_s = -1.6 V, I = 85 pA at various scan sizes with corresponding LEED at primary beam energy of 12eV

The predominant packing mode is defined by a rectangular unit cell with dimensions of approx. 1.9 nm x 2.1 nm^2 although no calibration has been applied to the images. This is larger than that observed on Ag and Au suggesting that close contact is not energetically favourable within these islands.

In order to explain this change in packing, we can consider the previously reported charge transfer characteristics of phthalocyanines on Cu (111). If charge transfer is inducing a change in symmetry (and therefore shape) in the VOPc molecule at the surface it follows that the VOPc molecule is most probably adsorbed with the oxygen atom of the oxovanadium component close to the substrate. This is based on the STM experiments of Niu et al.[15] which show that only when the

component projected out the molecular plane in non-planar MPcs is in close contact with the surface is symmetry modification observed. Recent studies using DFT and X-ray standing wave (XSW) techniques on the related molecules ClAlPc[16] and ClGaPc[17] reach the same conclusion.

If this geometry leads to molecular distortion due to charge transfer the two lobes of the Pc ligand on opposite sides of the VO centre would both become either electron rich or poor. The molecule-molecule assembly could therefore be driven by the edge to edge repulsion of the electron rich lobes and attraction of the electron poor lobes or interactions between electron rich and poor lobes. In either case the intermolecular interaction would be maximised when the molecules were positioned with the Pc ligands of nearest neighbours touching i.e. edge to edge. This would avoid contact with the other set of arms of the Pc ligand and maximise the screening of the charge or hole accumulation in the molecule.

Molecular symmetry modification at the Cu (111) surface has also been demonstrated[18] to have dependence on the position of the molecule with respect to the crystallographic axes of the substrate. The 'symmetry reduced' molecules can be assumed to be constrained by the surface lattice which would direct assembly along surface lattice directions rather than being lead purely by molecular interactions. If the distortion of the molecule is energetically favourable, movement between similar adsorption sites would be preferred over movement to sites that did not produce this distortion. This seems to be the case for VOPc on Cu (111) as molecular vacancies appear most often connected together diagonally rather than edge to edge.

If significant charge transfer was present into the VOPc molecule, a filled LUMO state similar to that seen on Ag(111) could be expected. UPS was therefore used to probe the electronic structure of the interface, initially at the nominal 0.9 ML thickness which produced hexagonal packing of VOPc.

UPS spectra differ from Au (111) and Ag (111) surfaces in both form and the position of features observed. UPS of 0.9 ML coverage shows a split feature at low binding energy close to the Fermi edge together with a single broad feature closer to the d-band states of the Cu (111)(Fig. 3.32(iii)). The form of the low binding energy region is similar to that recently observed in GaClPc on Cu(111)[17] and as such the feature closest to the d-band states can be assigned as the HOMO peak of the VOPc. The origin of the states closer to the Fermi edge is not clear and in order to improve our understanding thinner films were grown.

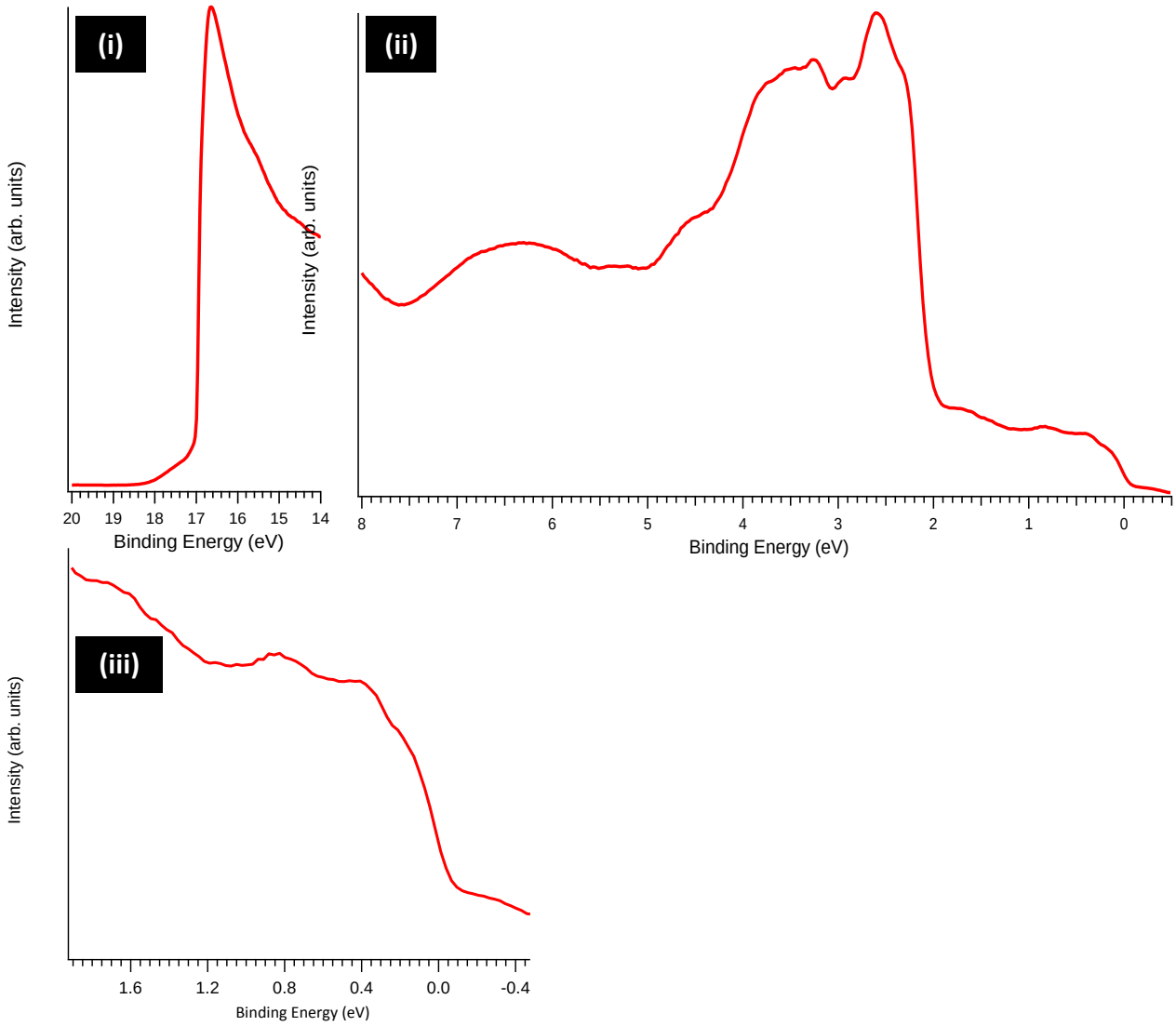

Figure 3.32 – UPS data for 0.9 ML VOPc/Cu (111); the lower panel (iii) is an expanded view of the low binding energy region of the valence band (ii)

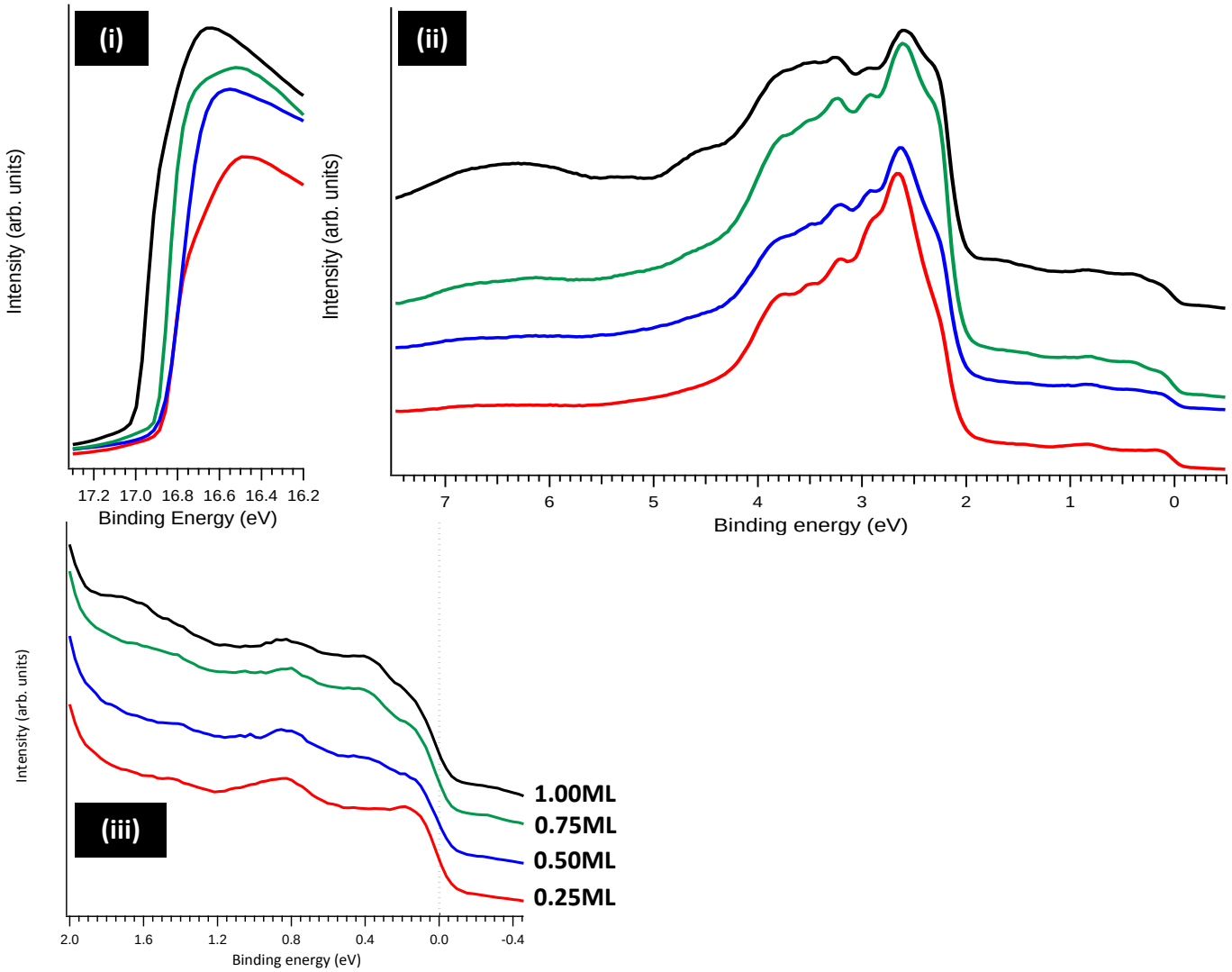

Figure 3.33 – UPS data for 0.25 ML (red) 0.5 ML (blue) 0.75 ML (green) and 0.9 ML (black) VOPc/Cu (111)

For the thinnest films (of 0.25 ML coverage) no feature is observed in the HOMO region but two broad peaks are observed 0.1-0.8 eV below the Fermi edge (Fig. 3.33(iii)). These peaks appear to be remnants of the Shockley surface state (just below the Fermi edge) of the Cu (111) surface and a parasitic Helium emission line d-band satellite. At higher coverage (0.5 ML) the peak closest to the Fermi edge shifts to higher binding energy and appears less well defined. At 0.75 ML a pair of peaks similar to those seen for the split HOMO state on Au and Ag is observed centred 0.6eV under the Fermi edge. At 0.9 ML these peaks are still observed, and a broad feature centred 1.7 eV below the Fermi edge derived from the molecule HOMO state also emerges. Annealing experiments had no

impact on electronic structure as very similar UPS spectra were collected and are not presented here.

The lack of interface states just below the Fermi edge (as in the case of VOPc / Ag(111)) suggests that if charge transfer is occurring, it is not populating a LUMO state in the VOPc. This could either be due to a lack of charge transfer or the re-hybridisation of the molecular orbitals of the VOPc molecule. If, as other authors suggest, MPcs form covalent bonds with Cu (111) and a large geometric distortion occurs, the form and population of the molecular orbitals of the isolated VOPc molecule will be radically altered. Therefore HOMO and LUMO states may be mixed with the energetically most accessible substrate orbitals, the d band and surface state of Cu (111). This would produce a situation where no state over or close to the Fermi edge would be observed due to the modified electronic structure of the molecule-metal interface.

The form of the two low intensity peaks close to the Fermi edge in 0.75 ML and 0.9 ML films are similar to those observed as the HOMO derived state in 0.9 ML films of VOPc / Au (111) and VOPc / Ag (111). This peak shape has been previously discussed in the literature and assigned as being due to vibronic progression of electrons through the Pc ring[13]. If a similarly shaped feature is present close to the Fermi edge, this suggests an energetic separation of density of states contributions from the central oxovanadium portion and the Pc ligand system. Further experiments including synchrotron based studies are planned to provide deeper insight into this complex system.

The work function change induced by adsorption of VOPc molecules clearly proceeds rapidly below 0.25 ML, with a 0.4 eV change observed with respect to clean Cu (111). At 0.9 ML coverage a 0.6 eV change is realised which is unaffected by the annealing step discussed earlier in this chapter. This suggests that the spontaneous adsorption geometry of the VOPc molecule produces the work function change, and the orientation of the dipole moments produces the largest possible change without the need to anneal the substrate. The affinity of Cu surfaces for oxygen is widely known as demonstrated by the spontaneous and rapid oxidation of clean samples on exposure to air. This

allows us to rationalise the difference between the behaviour observed here with VOPc to the behaviour observed by Gerlach et al. with GaClPc[17].

The overall change in work-function is very similar to that observed on Au(111) (0.58 eV) and Ag(111) (0.52 eV). This seems to negate the influence of the adsorption geometry of the VOPc molecule on the work function of the interface, as experimental evidence shows Au (111) and Ag (111) have the same VOPc adsorption behaviour while Cu (111) differs significantly. The situation is complicated by the unclear nature of the interaction between VOPc and Cu (111) indicated by the complex surface structures observed in STM and LEED experiments, and the unusual features present in the low binding energy region of UPS spectra. Charge transfer, changes in molecular shape and electronic structure induced by interaction with the Cu (111) surface may be convoluting the influence of the presence of the VOPc molecule on the work function of the substrate.

3.4 – Conclusions

In conclusion, the non-planar MPc VOPc has been prepared in ultra-thin film morphology at a variety of thicknesses on the Au(111), Ag(111) and Cu(111) surfaces and characterised by STM, LEED and UPS. In the case of Au (111) self-assembled layers composed of molecules lying with their oxygen atoms projecting away from the surface are observed in STM images. LEED patterns reveal multiple azimuthal orientations with respect to the principal crystallographic axes of the surface, and STM is used to observe the thin films' morphology. Electronic structure analysis by UPS suggests no electron transfer is induced at the interface and a thickness-dependant work function change is observed.

On the Ag (111) surface, very similar molecular assembly is observed in STM and LEED patterns are almost identical. UP spectra show that charge transfer is present from the substrate into the LUMO of the molecule, most probably from d band states. This populates the LUMO and produces an occupied state just below the Fermi level of the Ag (111) surface.

The behaviour of VOPc on Cu (111) is in contrast to both of the other surfaces used, producing markedly different LEED patterns and surface structures in STM experiments. A unique rounded topography is present along with more familiar square molecular features. A range of assembly modes are observed including a hexagonally close packed structure which allows a tentative assignment of the complex LEED pattern produced. This behaviour is rationalised by assuming that the shape of the VOPc is altered and its symmetry changed by interacting with the Cu surface and by charge transfer from or into the molecule. UPS spectra are also dissimilar to those produced from Au (111) and Ag (111) surfaces, with no clear molecular HOMO derived state. The nature of the electronic structure shown by the UPS experiments is discussed, but the underlying molecule-surface interaction remains difficult to assign unambiguously.

References:

(1) Heutz, S.; Ferguson, A. .; Rumbles, G.; Jones, T. . Morphology, structure and photophysics of thin films of perylene-3, 4, 9, 10-tetracarboxylic dianhydride. *Organic Electronics* **2002**, *3*, 119–127.

(2) Ishida, N.; Fujita, D. Adsorption of Co-Phthalocyanine on the Rutile TiO 2 (110) Surface: A Scanning Tunneling Microscopy/Spectroscopy Study. *The Journal of Physical Chemistry C* **2012**, *116*, 20300–20305.

(3) Tekiel, A.; Goryl, M.; Szymonski, M. Copper phthalocyanine molecules on an InSb(001) c(8 × 2) surface studied by ultra-high-vacuum STM and non-contact AFM. *Nanotechnology* **2007**, *18*, 475707.

(4) Liu, L.; Yang, K.; Jiang, Y.; Song, B.; Xiao, W.; Li, L.; Zhou, H.; Wang, Y.; Du, S.; Ouyang, M.; Hofer, W. a; Castro Neto, A. H.; Gao, H.-J. Reversible single spin control of individual magnetic molecule by hydrogen atom adsorption. *Scientific Reports* **2013**, *3*, 1210.

(5) Gimzewski, J.; Modesti, S.; Gerber, C.; Schlittler, R. R. Observation of a new Au (111) reconstruction at the interface of an adsorbed C_{60} overlayer. *Chemical Physics Letters* **1993**, *213*, 401–406.

(6) Barlow, D. E.; Hipps, K. W. A Scanning Tunneling Microscopy and Spectroscopy Study of Vanadyl Phthalocyanine on Au(111): the Effect of Oxygen Binding and Orbital Mediated Tunneling on the Apparent Corrugation. *The Journal of Physical Chemistry B* **2000**, *104*, 5993–6000.

(7) Aketagawa, M.; Takada, K. Correction of distorted STM image by using a regular crystalline lattice and 2D FFT. *Nanotechnology* **1995**, *6*, 105–110.

(8) Fukagawa, H.; Yamane, H.; Kera, S.; Okudaira, K. K.; Ueno, N. UPS fine structures of highest occupied band in vanadyl-phthalocyanine ultrathin film. *Journal of Electron Spectroscopy and Related Phenomena* **2005**, *144-147*, 475–477.

(9) Toader, M.; Knupfer, M.; Zahn, D. R. T.; Hietschold, M. Initial growth at the F16CoPc/Ag(111) interface. *Surface Science* **2011**, *605*, 1510–1515.

(10) Ying Mao, H.; Wang, R.; Wang, Y.; Chao Niu, T.; Qiang Zhong, J.; Yang Huang, M.; Chen Qi, D.; Ping Loh, K.; Thye Shen Wee, A.; Chen, W. Chemical vapor deposition graphene as structural template to control interfacial molecular orientation of chloroaluminium phthalocyanine. *Applied Physics Letters* **2011**, *99*, 093301.

(11) Toader, M.; Shukrynau, P.; Knupfer, M.; Zahn, D. R. T.; Hietschold, M. Site-dependent donation/backdonation charge transfer at the CoPc/Ag(111) interface. *Langmuir* **2012**, *28*, 13325–30.

(12) Schlaf, R.; Parkinson, B. a.; Lee, P. a.; Nebesny, K. W.; Armstrong, N. R. HOMO/LUMO Alignment at PTCDA/ZnPc and PTCDA/ClInPc Heterointerfaces Determined by Combined UPS and XPS Measurements. *The Journal of Physical Chemistry B* **1999**, *103*, 2984–2992.

(13) Kröger, I.; Stadtmüller, B.; Stadler, C.; Ziroff, J.; Kochler, M.; Stahl, A.; Pollinger, F.; Lee, T.-L.; Zegenhagen, J.; Reinert, F.; Kumpf, C. Submonolayer growth of copper-phthalocyanine on Ag(111). *New Journal of Physics* **2010**, *12*, 083038.

(14) Wei, Y.; Robey, S. W.; Reutt-Robey, J. E. Flux-Selected Titanyl Phthalocyanine Monolayer Architecture on Ag (111). *Journal of Physical Chemistry C* **2008**, 18537–18542.

(15) Niu, T.; Zhou, M.; Zhang, J.; Feng, Y.; Chen, W. Dipole Orientation Dependent Symmetry Reduction of Chloroaluminum Phthalocyanine on Cu(111). *The Journal of Physical Chemistry C* **2013**, *117*, 1013–1019.

(16) Chang, S.-H.; Kuck, S.; Brede, J.; Lichtenstein, L.; Hoffmann, G.; Wiesendanger, R. Symmetry reduction of metal phthalocyanines on metals. *Physical Review B* **2008**, *78*, 233409.

(17) Gerlach, a.; Hosokai, T.; Duhm, S.; Kera, S.; Hofmann, O. T.; Zojer, E.; Zegenhagen, J.; Schreiber, F. Orientational Ordering of Nonplanar Phthalocyanines on Cu(111): Strength and Orientation of the Electric Dipole Moment. *Physical Review Letters* **2011**, *106*, 156102.

(18) Chang, S.-H.; Kuck, S.; Brede, J.; Lichtenstein, L.; Hoffmann, G.; Wiesendanger, R. Symmetry reduction of metal phthalocyanines on metals. *Physical Review B* **2008**, *78*, 233409.

Chapter 4

High temperature deposition of organic thin films

In this chapter the influence of substrate temperature (T_{sub}) on the morphology and crystal structure of MPc films is investigated. Surface morphology (measured by AFM) is monitored as a function of substrate temperature (T_{sub}) during deposition for MPc films on oxidised silicon (SiO_2) surfaces. Finally a copper iodide (CuI) structural template layer is prepared at elevated temperature on SiO_2 and used to control the growth of OSC layers subsequently deposited. The effect of T_{sub} on the morphology and structure of the CuI layer during deposition and subsequent impact on OSC templating behaviour is examined.

4.1 – FePc and MnPc single layers on oxidised silicon

MPc layers have been employed in a wide variety of OPV and OTFT devices, usually grown at room temperature, on substrates specifically useful for each application. An example of this is using indium tin oxide (ITO) coated glass to provide a transparent back electrode for OPV applications[1]. The weak van der waals (VdW) forces that hold organic crystals together can be easily influenced by changing the chemical nature of the substrate used or by applying heat or other physical stimulus (e.g. magnetic or electric fields) during or after the growth process[2,3,4]. This can produce drastic changes in the structure or properties of the OSC layers and is therefore of scientific and technological interest. The simplest approach to incorporate into a mass production environment is the use of elevated temperatures such as those used in dye sublimation or powder coating processes. Although a variety of work has been carried out exploring the effects of using elevated temperatures during the deposition of MPc layers but few extensive studies have been undertaken[5,6,7]. With this in mind, two MPcs (iron phthalocyanine (FePc) and manganese phthalocyanine

(MnPc)) were used to explore the structural changes observed with elevated temperature deposition.

4.1.1 – FePc thin films

FePc films grown on room temperature substrates with little chemical reactivity (such as glass, quartz, SiO_2 or mica) demonstrate morphology typical of the α phase of planar phthalocyanines. Films are composed of roughly 100 nm crystallites upon which no faceting or crystallographic features can be discerned, so they are commonly referred to as spherical[8]. At 10 nm thickness smooth films with complete surface coverage are obtained and negligible surface morphology changes with thickness are observed **(Fig 4.1(i))**.

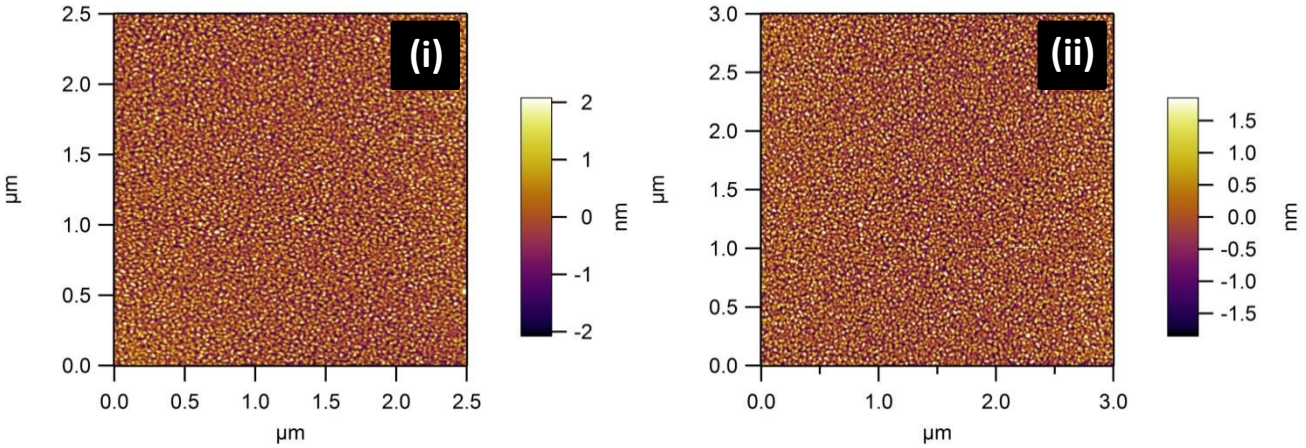

Figure 4.1 – AFM images of (i) 10nm and (ii) 100nm thick FePc films at ambient T_{sub}

With SiO_2 substrates held at room temperature coated with 10nm of FePc no diffraction peaks are observed in XRD traces **(Fig 4.2(i))**. Using sufficiently thick films (in this case 50nm) diffraction patterns consisting of only a single peak can be recorded showing strong preferred orientation in films **(Fig 4.2(ii))**. A number of crystal structures based on single crystal and powder minimisation experiments have been proposed for FePc, and

simulations of XRD patterns from each structure produce either a (100) or (001) reflection between 6° and 7°. In each case this corresponds to a d spacing above 1 nm, which is the inter-stack spacing between molecules rather than the smaller face to face separation distance. The conclusion that molecules are predominantly stacking edge to edge (and are therefore edge rather than face on to the substrate) with respect to the substrate is made. Similar behaviour has been observed for a variety of planar phthalocyanines on chemically inert (weakly interacting) substrates, and used to approximate the relative molecular orientation (with respect to the surface) within crystals[9].

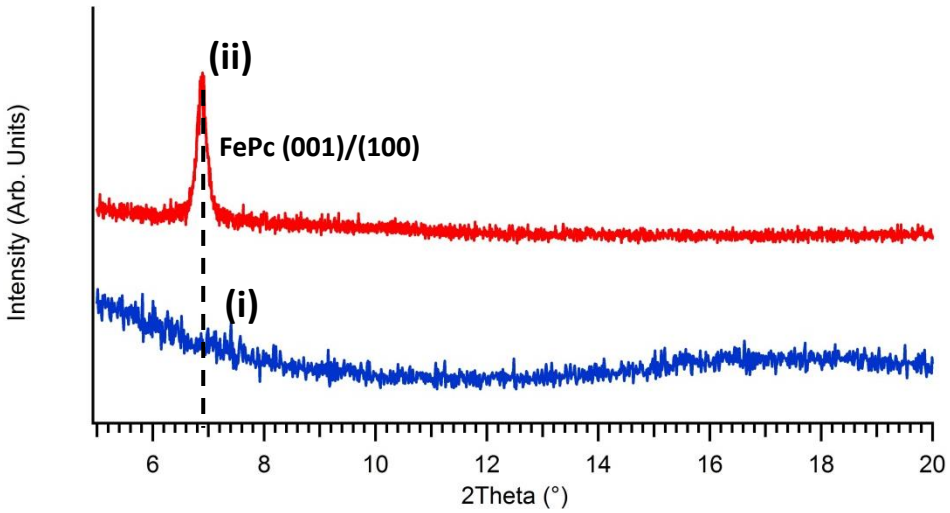

Figure 4.2 – XRD traces of (i) 10 nm and (ii) 50 nm thick FePc films at ambient T_{sub}

Changing T_{sub} during deposition has a huge impact upon the crystal structure, size and morphology of phthalocyanine thin films with a range of molecule-substrate combinations explored. The work of Miller et al. [10] used elevated temperatures on a sapphire (1120) substrate to control the crystal size of evaporated FePc thin films. Some discussion is presented on the nature of the interaction of the single crystal surface with the impinging molecules in the molecular beam, but similar results had been obtained

previously on glass or oxidised silicon substrates[11,12]. While these demonstrate similarly chemically inert characteristics and possess low R_q values (surface roughness of approx. 0.2-0.5nm) no surface structure (e.g. atomic steps) can be observed with scanned probe techniques. The nature of the interaction between amorphous SiO_2 surfaces and FePc molecules is not immediately obvious in this case. We can assume that the intermolecular VdW interaction between FePc molecules absorbing on to the surface as the film is formed are stronger (and therefore have more influence on film morphology) than the molecule/surface interaction.

To test this hypothesis, high T_{sub} deposition was carried out on solvent-cleaned and UV-Ozone treated SiO_2 wafer pieces. These were cleaved from a single crystal Si (100) wafer (IDB technologies) to a size of approximately 10mm x 10mm. They were attached to an Omicron® style sample plate using spot-welded tantalum foil strips. Substrates were pre heated to growth temperatures for 30 mins before deposition and no in-situ cleaning was carried out.

In order to have a reproducible, accurate and representative measurement of the surface temperature of the SiO_2 during growth, both a fixed thermocouple I contact with the sample and optical pyrometry measurements were used. The thermocouple was fixed in the sample holder and an optical pyrometer (IRCON®) was positioned at surface normal to measure the sample temperature concurrently. Measurements suggest a 24°C temperature difference between the surface and the temperature measured by the thermocouple, and a constant offset was assumed as the lowest temperature measurable by the pyrometer was 300°C.

Due to the length of time required to grow and analyse each sample, the temperature range of ambient (approx. 23°C) to 100°C was not investigated. A surface

temperature of 109°C was used as the starting point for elevated T_{sub} experiments. At 109°C changes are observed in the surface morphology of the thin film, with grain size increasing and elongation obvious along the crystallites in the plane of the surface **(Fig 4.3(i))**. The RMS surface roughness increased from 0.730 nm (at room temperature) to 0.866 nm which can be explained by the presence of larger crystallites with more protrusion out of the surface plane due to growth along preferred axes. When T_{sub} is increased to 173°C an obvious change in morphology is clear, the substrate surface is covered with highly anisotropic crystallites **(Fig 4.3(ii))**. These crystallites demonstrate a large degree of preferred orientation with their longer axis in the plane of the surface. Faceting is clear along the plane parallel to the surface, but reliable step heights are difficult to obtain as the features are non-uniform and not completely flat. The clear presence of areas of bare SiO_2 substrate suggests non uniform nucleation across the surface, with a tendency for growth along certain axes of existing crystallites rather than creation of new crystals. A large increase in surface roughness is observed, with a roughness of 5 nm at 173°C compared to 0.957 nm at 109°C.

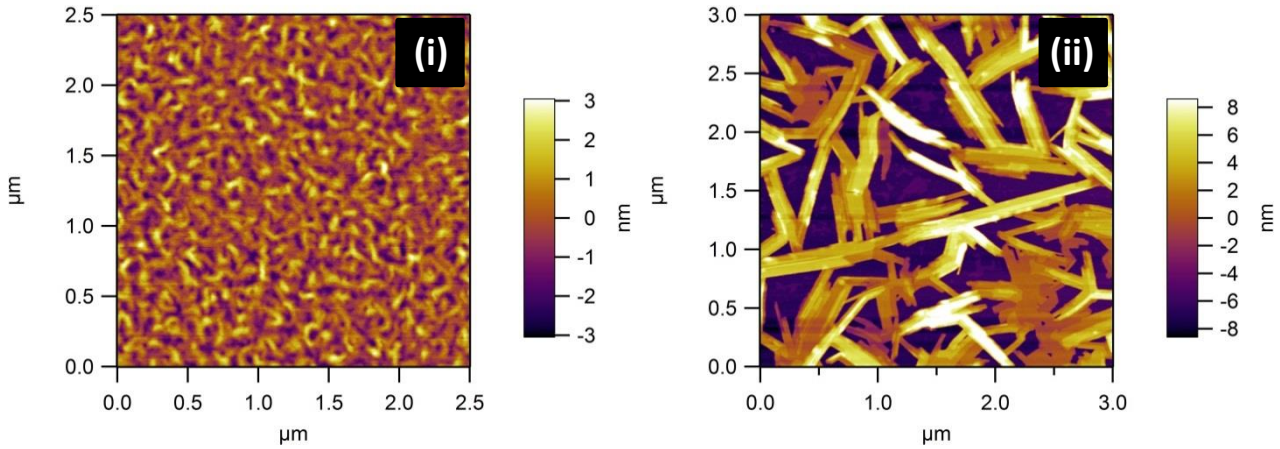

Figure 4.3 – AFM images of 10 nm FePc films at T_{sub} of (i) 109°C and (ii) 173°C

The largest single features were observed for T_{sub} = 193°C with what appear to be single crystals of up to several micrometres in length formed on the surface **(Fig 4.4)**. Step heights of 1.3-1.4 nm are observed on top of the crystallites, and long protrusions on the highest features suggesting anisotropic growth along the surface plane, rather than out of it, are present. One explanation for this is that each layer of 1.3-1.4 nm in height is a single molecular layer with the FePc molecule standing upright. XRD measurements presented later in this chapter will provide further evidence for this assignment. The growth mechanism is difficult to comment on, as incomplete coverage is obvious due to 'holes' down to the substrate layer separating film features.

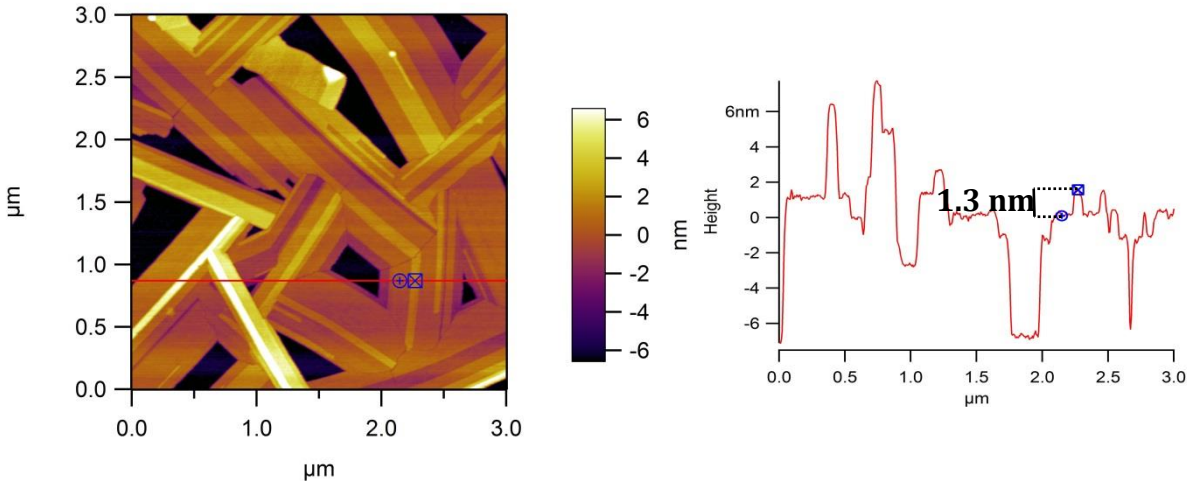

Figure 4.4 – AFM image and corresponding height profile for 10 nm FePc/SiO_2 film at T_{sub} = 193°C

Layers also appear incomplete with missing rows and the extrusions along the surface plane appear at multiple points on the surface and height scale. This may suggest preferential growth along the face-to-face packing direction of the FePc molecules (high anisotropy in domains and step heights provide more evidence). Molecular resolution imaging, which was not possible with the equipment available, would be necessary to comment on orientation and packing further.

At T_{sub} of 203°C surface morphology undergoes another change; smaller features are present with the same molecular scale height as at T_{sub} = 193°C **(Fig 4.5(i))**. The roughness also decreased from 2.755 nm to 1.125 nm, but imaging was difficult due to the presence of high protrusions spread randomly across the surface. The height of these features cannot be commented on as the AFM could not track them reliably. Presumably these are due to out-of-plane nucleation of nanocrystallites as previously observed in literature[13].

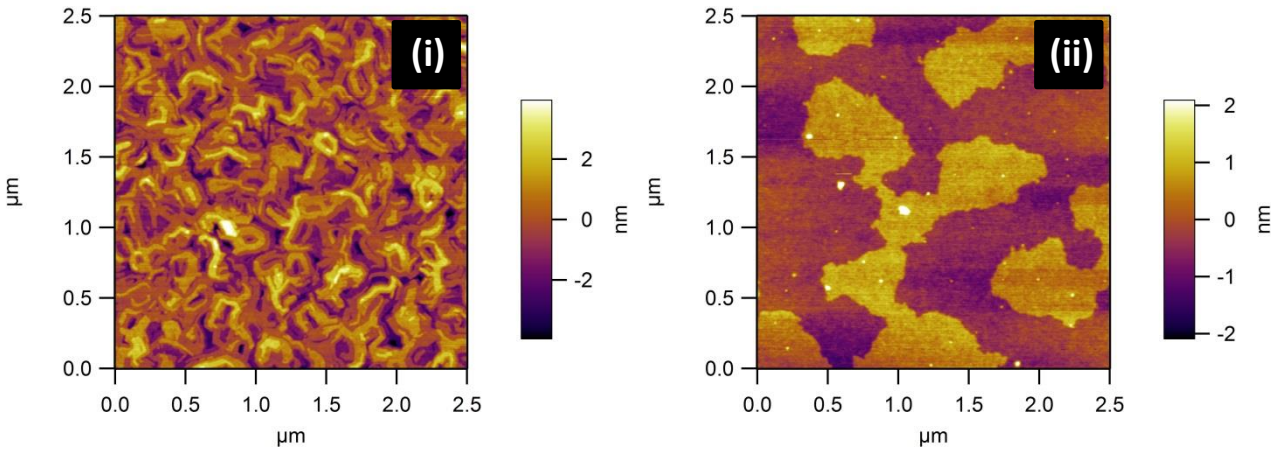

Figure 4.5 – AFM images of 10 nm FePc films at T_{sub} of (i) 203°C and (ii) 213°C

Another 10°C increase in T_{sub} to 213°C produced a low surface coverage of FePc with a randomly shaped island morphology **(Fig 4.5(ii))**. The height of these islands is uniformly 1.4 nm suggesting that the first monolayer layer is composed of upright molecules. At this temperature the sticking coefficient is clearly greatly reduced which in turn reduces the effective growth rate to around one tenth of that in lower temperature films. Higher temperatures were not investigated and longer growths at this temperature were not used in order to maintain a uniform measured growth rate between samples.

In order to confirm the assignment of the film's structure inferred from AFM, XRD measurements were used to probe the crystal structure out of the plane of the substrate.

XRD patterns were not produced by films with a thickness of 10nm due to the very limited number of planes present to diffract X-rays and the weak scattering properties of all atoms except the Fe at the centre of the molecule. This is in direct contrast to the work of Miller et al.[10] where 10 nm films produce not only diffraction peaks but associated interference fringes indicative of high quality thin film growth. In order to analyse the crystal structure of the films 50 nm samples were necessary to provide sufficient diffraction intensities. As T_{sub} = 193°C produced the largest domains in 10nm films this temperature was used for thicker growth for XRD analysis.

Substrate temperature and growth rate were kept constant for all film thicknesses, and while AFM analysis showed a modified morphology, step heights matched the height of an on-edge molecule and molecular orientation was judged to be identical to that observed in thinner samples **(Fig 4.6)**. Diffraction patterns were recorded for this film with only a single strong feature observed at 6.95°, corresponding to an inter-planar distance of 1.27 nm **(Fig 4.6)**. A very weak second order reflection of this peak at 14° is observed at low intensity with no further reflections. A diffraction pattern from a film grown at room temperature and one grown at 193°C are presented in **(Fig 4.7)**.

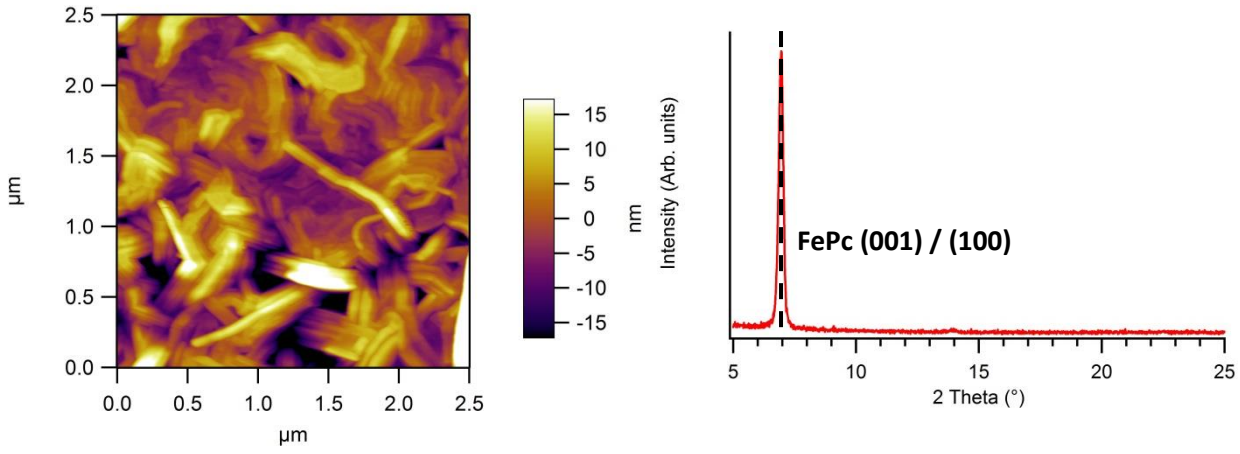

Figure 4.6 – AFM image and XRD trace for a 50 nm FePc film at T_{sub} = 193°C

While a small shift in the (001) peak is observed with an increase of T_{sub} to 193°C (indicative of an α to β phase transition[14]), the alignment accuracy of the diffractometer make this difficult to quantitatively analyse. This does not affect the assignment of the peak which matches the interplanar distance corresponding to the spacing between stacks of molecules along the (001) direction of the unit cell. This is a common motif in XRD of planar phthalocyanines but due to the lack of other peaks in the pattern no further structural conclusions can be made. Due to the weak nature of the peaks no comment on peak width or correlation with domain size is made, especially as the full width at half maximum (FWHM) of the peak increases from 0.17 to 0.22 while scanned probe studies show that crystal size increases.

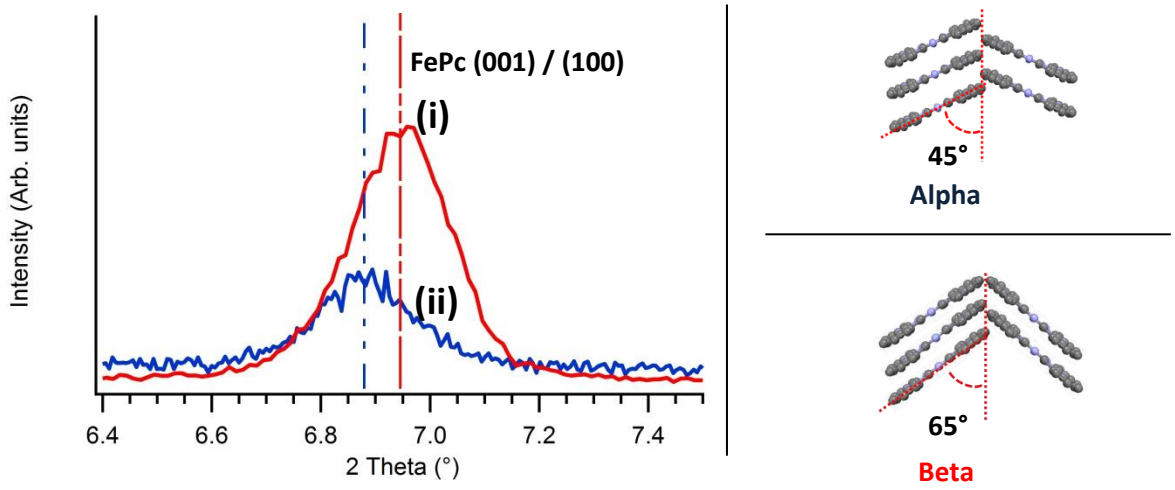

Figure 4.7 – XRD traces of 50 nm FePc films at Tsub of (i) ambient and (ii) 193°C

4.1.2 – MnPc thin films

MnPc films grown at room temperature on SiO_2 substrates also demonstrate morphology typical of the alpha phase of planar phthalocyanines[15].

At T_{sub} = 123°C the film undergoes a change in morphology with larger features that appear to be elongated crystallites or aggregates of crystallites appearing (**Fig 4.8(i)**). This is a similar but less pronounced effect than that observed in FePc, with the introduction of larger crystallites and therefore long range order.

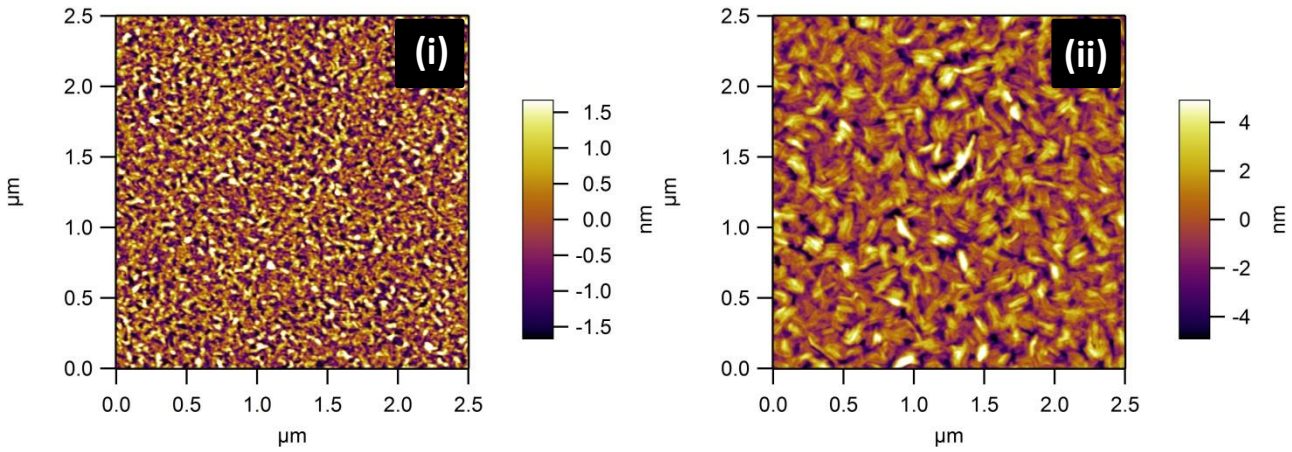

Figure 4.8 – AFM images of 10 nm MnPc films at T_{sub} of (i) 123°C and (ii) 173°C

When T_{sub} is increased to 173°C a more profound change is observed with larger interlocking faceted crystals (**Fig 4.8(ii)**). Crystallites range between 250 and 500 nm in lateral size, but grain boundaries are difficult to discern making this analysis inherently inaccurate. It is difficult to discern if the features are individual crystallites or bundles of axially oriented fibre like crystals. The growth shows 3D character as the surface rapidly roughens in thin films and protrusions are obvious in the topography while the thickness by QCM is identical.

As the temperature is increased by 10°C to 183°C the grain size increases along with surface roughness with larger bare SiO_2 patches separating crystallites (**Fig 4.9**). At T_{sub} = 193°C grain size and surface roughness increase but the surface morphology is very similar to that observed at 183°C.

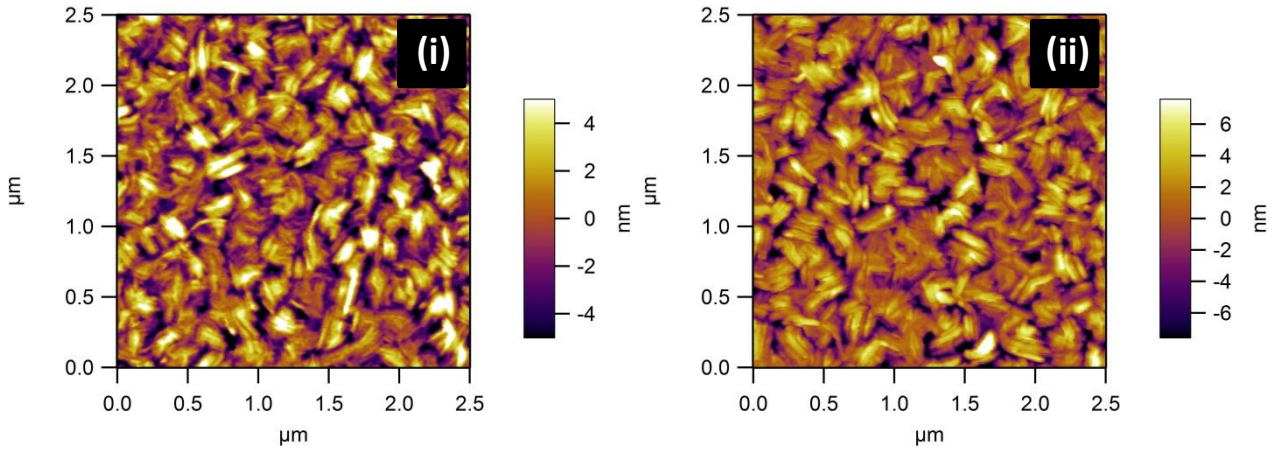

Figure 4.9 – AFM images of 10 nm MnPc films at T_{sub} of (i) 183°C and (ii) 193°C

T_{sub} of 203°C and 213°C produce crystallites with similar morphology but more of the bare substrate is exposed at the higher temperature (**Fig 4.10**).

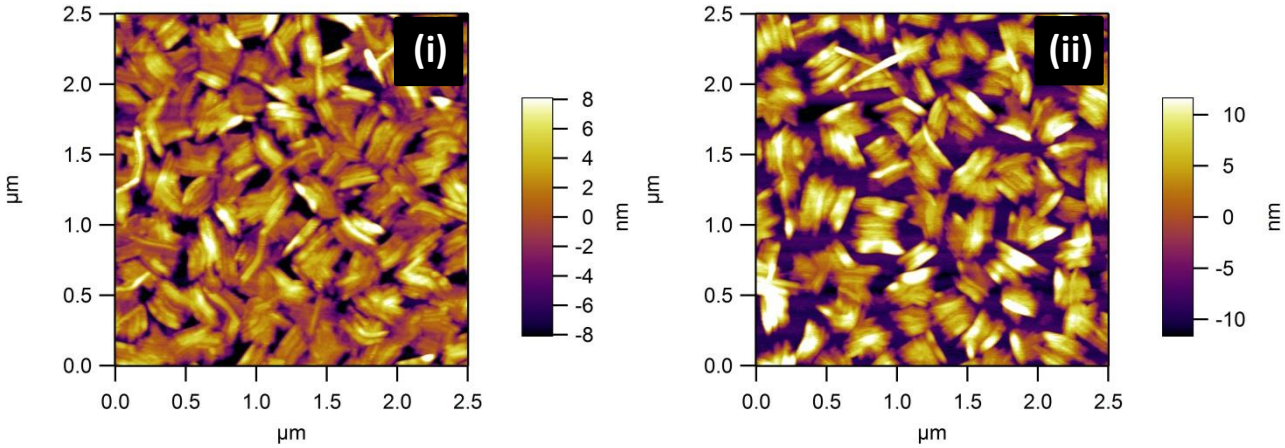

Figure 4.10 – AFM images of 10 nm MnPc films at T_{sub} of (i) 203°C and (ii) 213°C

A temperature of 223°C produces similar morphology to 213°C but features protruding further from the surface increase the RMS roughness. The highest temperature at which growth of MnPc is observed is 233°C at which point elongated crystallites ranging from 200 to 500nm wide and 200 to 1500nm long are present on the surface separate by large (approx. 500nm x 500nm^2) portions of bare substrate (**Fig 4.11**).

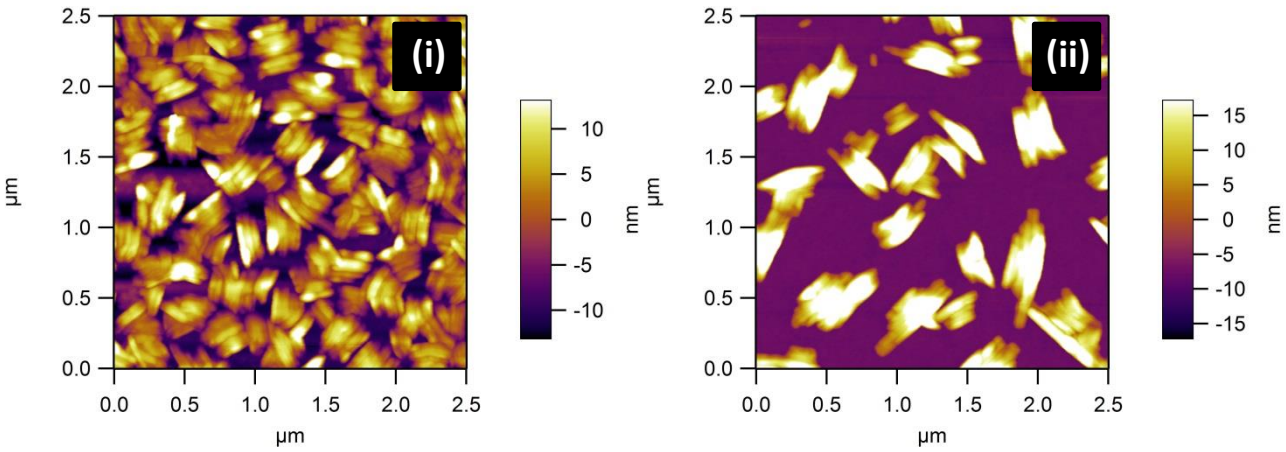

Figure 4.11 – AFM images of 10 nm MnPc films at T_{sub} of (i) 223°C and (ii) 233°C

The crystals appear to be collections of multiple smaller elongated needle-like crystals, or are much more highly faceted that those observed in FePc. If T_{sub} is increased to 243°C no growth is observed on the SiO_2 substrate suggesting that the surface is too hot for molecules to adsorb.

Surface roughness increases non-linearly with temperature (**Fig 4.12**) suggesting sensitivity to surface temperature that varies in different temperature ranges. While a clear change in morphology with temperature was observed, no layer-by-layer growth characteristics were obvious and high protrusions out of the substrate plane were observed.

It is interesting to note that the lateral dimensions of crystals formed on the surface are much smaller than those observed for FePc. While measurements of crystal size are unreliable the largest dimension (width or length) of crystallites found in any MnPc film is 450nm compared to 3500nm in FePc. While lateral dimensions of the crystallites are hard to measure due to their shape and the presence of interlocking crystals the large difference in domain size is apparent. In samples of MnPc prepared by thermal gradient sublimation, the macroscopic crystals recovered are much smaller and finer than those observed with CuPc and FePc (**Fig 4.12**). The reason for this is not known but further experiments are planned to understand this observation.

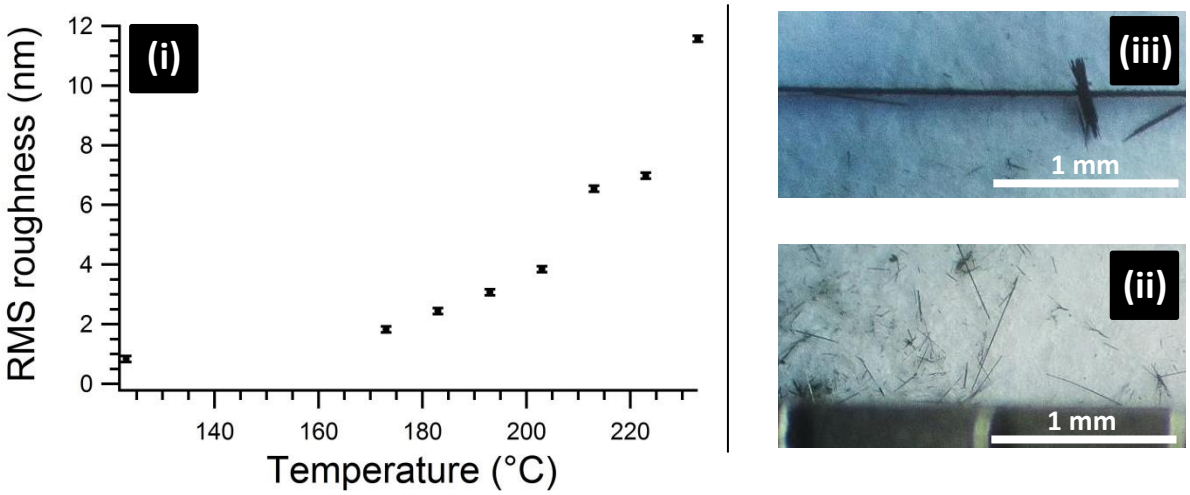

Figure 4.12 – (i) Graph of RMS roughness vs. temperature and optical micrographs of (ii) MnPc and (iii)FePc crystals

With both FePc and MnPc larger crystallites and modified film morphology is observed with increases in substrate temperature. As both are planar MPc molecules we can assume that their surface interactions with SiO_2 are similar, and discuss the changes observed together.

Increasing T_{sub} will increase the ease of lateral diffusion of MPc molecules which adsorb at the SiO_2 surface (assumed to be uniform, flat and inert). The presence of bare

areas of SiO_2 suggests that after nucleation molecules have a preference for adsorption on top of or next to other molecules rather than bare surface. This leads to the creation of three dimensional crystallites rather than growth of a layer by layer film. This in turn suggests that the molecule-molecule interaction is the most important consideration in creating large crystalline domains of MPc molecules. Increasing T_{sub} allows molecules to diffuse to their energetically preferred orientation with respect to each other and crystallographic axes of growing crystallites. As such they no longer 'hit and stick' to the substrate and the substrate plays only a very small part in the formation of the film past the first monolayer.

At a critical T_{sub} (different for each MPc molecule) the temperature reaches an approximation to equilibrium between adsorption and diffusion so that single crystalline domains are grown preferentially and nucleation is greatly reduced. The size of domains is presumably governed by surface imperfections/contamination, local sites that act either as nucleation points or barriers to the highly anisotropic growth of FePc crystals, or contamination in the molecular beam of FePc.

As T_{sub} is increased further the equilibrium is shifted away from adsorption of molecules, or rather the sticking coefficient of the surface with respect to the molecule is reduced. As such sufficient surface energy is present for the molecule to not attach to the surface at all, re-sublime in to vacuum or grow into an ordered structure.

With these assumptions in mind, each molecule-substrate combination should have a T_{sub} at which this balance of interactions is achieved. Factors such as surface reactivity (e.g. the presence of dangling bonds on semiconductors) and the relative strength of the molecule-molecule interaction should also affect this temperature.

4.2 – CuI template layers

4.2.1 – CuI thin films

CuI thin films have been demonstrated as structural templating layers in OPV devices, but little emphasis has been placed on the preparation and characterisation of CuI or the mechanism by which it causes structural changes in MPcs. With this in mind thin films were prepared by molecular beam deposition onto solvent-cleaned SiO_2 wafer pieces. This substrate was chosen to provide a flat and chemically inert platform on which to explore the innate morphology of thin CuI films.

When CuI powder (Sigma-Aldrich, UK) is sublimed on to SiO_2 pieces at ambient T_{sub} flat (R_q of 0.687 nm) film composed of small (approx. 50-150nm in diameter) crystallites is formed (**Fig 4.13**). Films prepared on room temperature substrates by this method have been employed in literature to alter the orientation of phthalocyanine over-layers[16,17] but surface characterisation was not used.

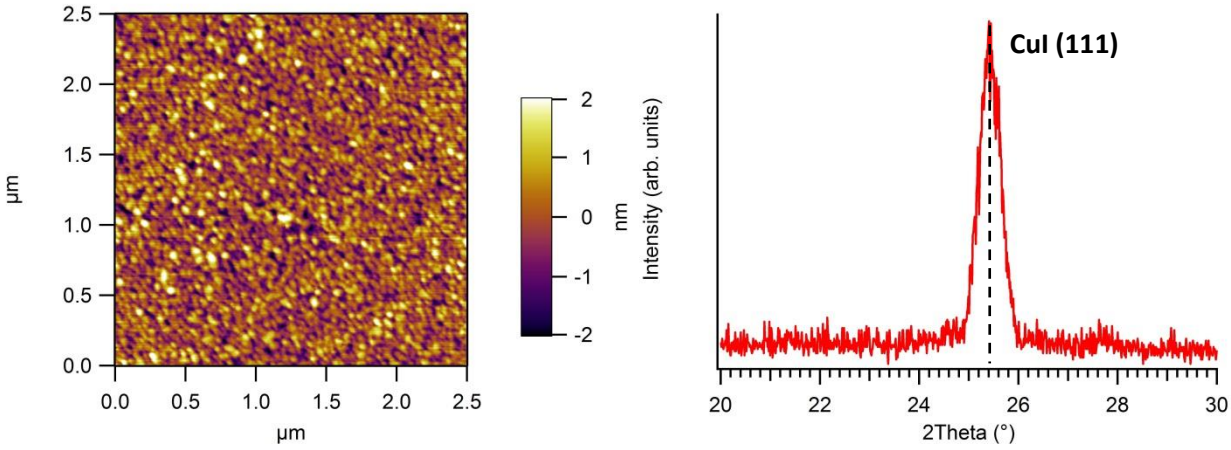

Figure 4.13 – AFM image and XRD trace for 14nm CuI layer at ambient T_{sub}

XRD traces (**Fig 4.13**) show only a single peak at 25.38° when films are grown to a thickness of 14nm (at ambient temperature). The peak is relatively broad with full width at half maximum (FWHM) of 0.53° and corresponds to the (111) spacing of the cubic CuI crystal structure[18]. AFM and XRD therefore suggest that CuI grows as a highly polycrystalline thin film with predominantly (111) preferred orientation (or (111) texture) at room temperature on SiO_2.

To investigate the nature of the CuI-MPc surface interaction (responsible for the templating effect) model layers with large single crystal domains, ideally single crystal surfaces, were desirable. Two approaches were used for this purpose; annealing in vacuum after deposition and deposition at elevated substrate temperature. Films were first annealed at 193°C for one hour and then cooled back to room temperature before ex situ analysis, where a profound change in surface morphology was observed.

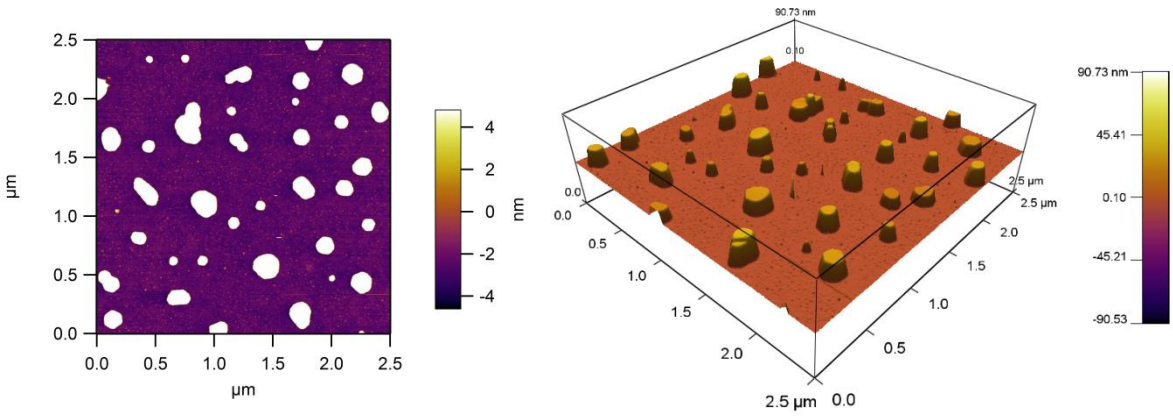

Figure 4.14 – AFM image and 3D representation for 14nm annealed CuI film

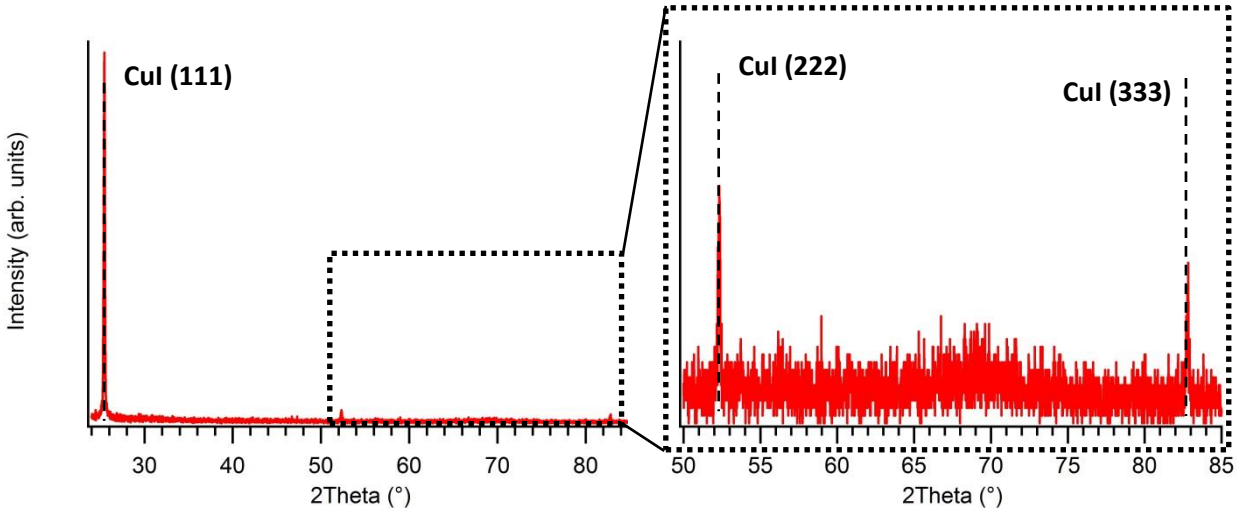

Figure 4.15 – XRD trace for 14nm CuI layer annealed at 193°C and expanded view of higher angles

Rather than a smooth film composed of small interlocked grains much larger (100-500nm) dispersed islands were present in annealed films (**Fig 4.14**). These islands were distributed such that only approximately 10% of the surface was covered by CuI and the rest was assumed to be bare SiO_2.

The islands possess roughly hexagonal symmetry and the top surfaces are flat with some obvious steps. XRD traces (**Fig 4.15**) once again show a strong reflection corresponding to the (111) plane but now the (222) and (333) reflections are also visible.

As (111) surfaces are hexagonally symmetrical in cubic crystal structures (a combination of two three-fold symmetry axes) these islands are assumed to be crystalline domains growing with their (111) surface projected out of the plane of the substrate. The unit cell viewed along the 'a' axis is illustrated **Figure 4.16**, along with a view perpendicular to the (111) plane.

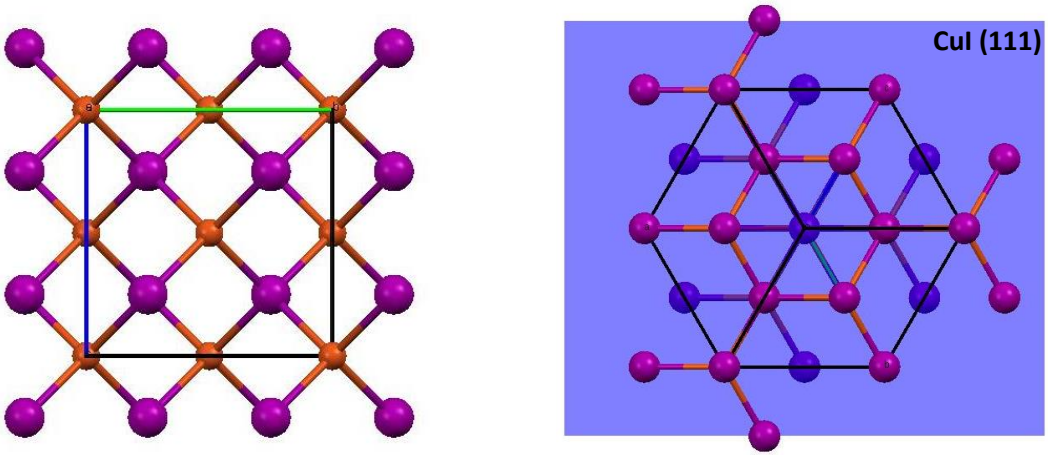

Figure 4.16 – Crystal structure of CuI viewed along the a axis and perpendicular to the (111). The (111) plane is shown in blue, Cu atoms in orange and I in purple

The hexagonal symmetry along the (111) plane is obvious and is in evidence in the growth habit of the isolated crystals. The production of these features from a less crystalline film with smaller grains suggests a sufficiently weak CuI/SiO_2 interaction to allow surface diffusion and recrystallization at 193°C. While it is tempting to assume that these features are single crystals, measurements to prove this are not possible in the current experimental geometry.

When elevated substrate temperatures were used during growth, a similar change in morphology is observed. A T_{sub} of 193°C produced hexagonal structures distributed such that approximately 28% of the surface was covered.

AFM height images show that the crystallites have flat top faces and phase contrast images reveal their faceted nature (**Fig 4.17**). As these samples were produced at elevated temperature this suggests a growth regime where absorption of CuI onto the SiO_2 surface is in equilibrium with surface diffusion. The weak nature of the interaction between the film and the substrate is clear, as the differences between annealed films and high temperature growth are small.

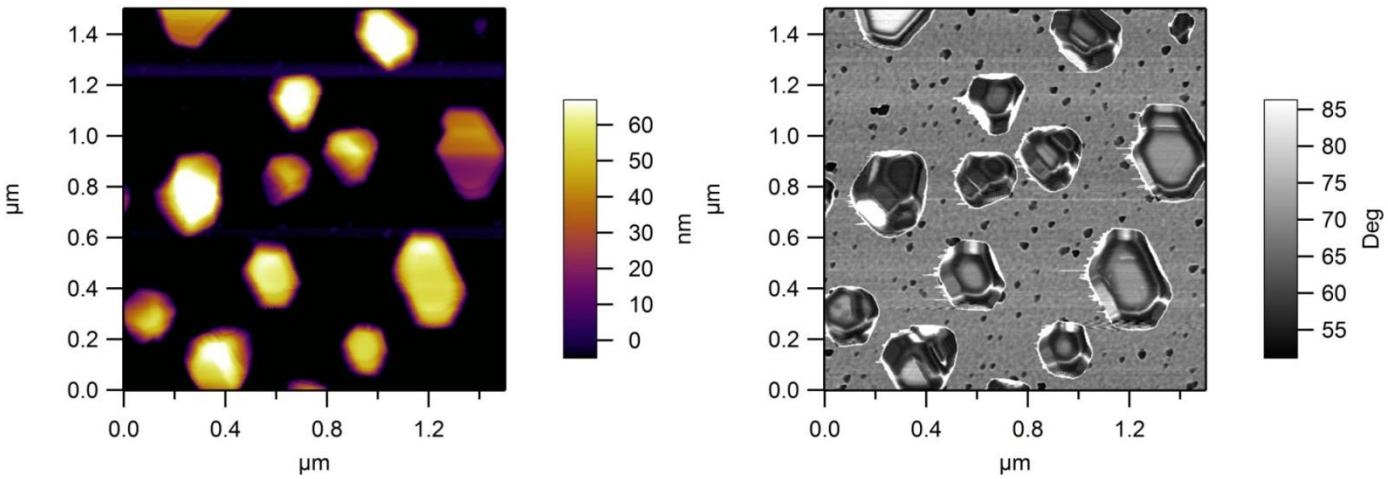

Figure 4.17 – AFM of CuI grown at T_{sub} = 198°C with corresponding phase contrast image

Higher temperatures were also used in an attempt to select larger domain sizes in the CuI film. Increasing the T_{sub} to 203°C produced smaller isolated crystallites than those observed at 193°C. A tendency for elongation along the plane of the surface is also evident which could indicate a change in growth habit (**Fig 4.18**). While this behaviour was interesting, the goal was to increase crystal size so further analysis was not undertaken. At 223°C no growth was observed at the surface suggesting that the sticking coefficient was sufficiently reduced to prevent adsorption from the impinging CuI beam.

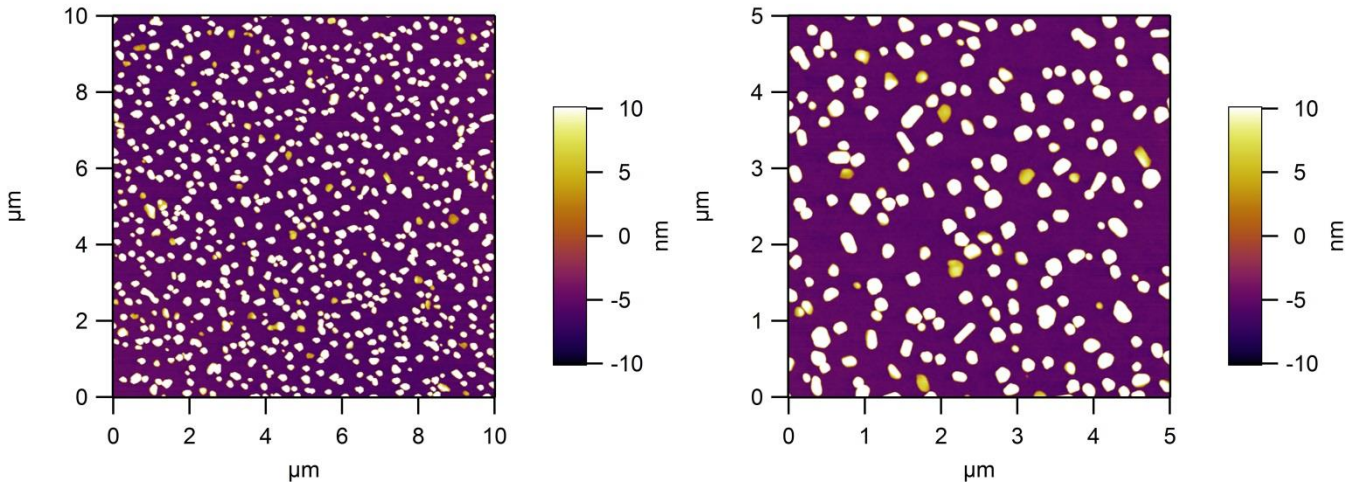

Figure 4.18 – AFM images of a 14nm CuI thin film grown at T_{sub} = 223°C

In each case, some post growth annealing was unavoidable as the sample was not actively cooled to room temperature with the time taken to cool completely around 45 minutes. AFM images suggest that the selected substrate temperature was responsible for the changes in morphology, but to test this hypothesis further annealing experiments were undertaken. A sample grown at a surface temperature of 193°C was maintained at growth temperature for 1 hour and 12 hours to compare the effects of intentional post growth annealing.

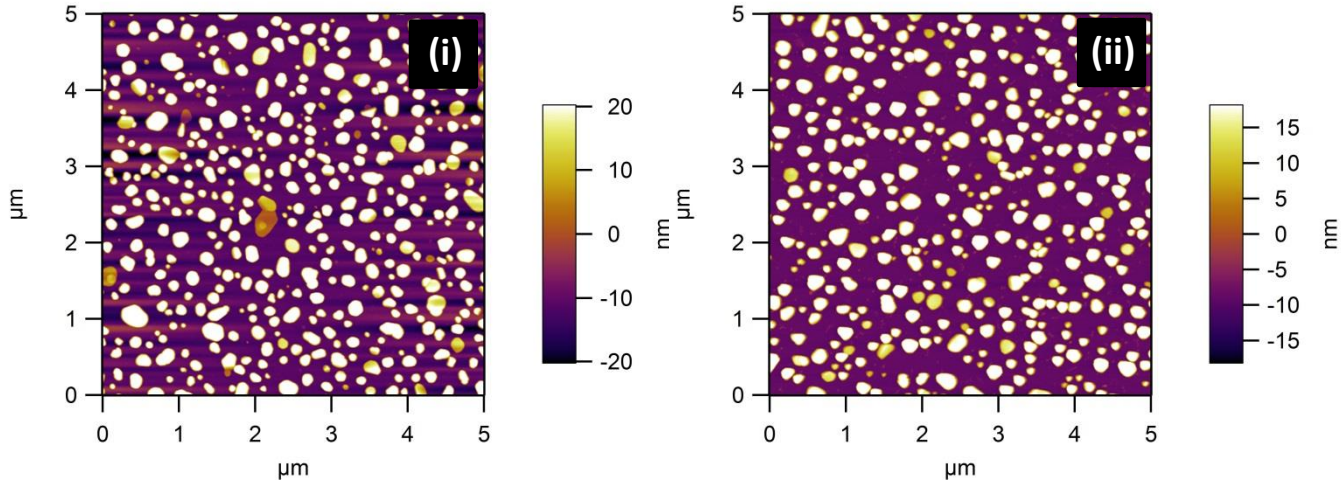

Figure 4.19 – AFM of CuI annealed for (i) 1 hour and (ii) 12 hours at T_{sub} = 193°C

Annealed samples showed little changed in domain size or surface coverage compared with non-annealed samples (**Fig 4.19**). A few areas were identified where clear layer by layer growth of hexagonal islands was apparent. Similar areas were observed in annealed and non-annealed samples so the assumption can be made that these structures are formed during growth rather than annealing. It should be emphasised that while films were composed of mostly hexagonal isolated features they were fairly inhomogeneous with a broad variation in feature height and crystallite lateral size. It is difficult, therefore, to assign any subtle changes in morphology to annealing effects or rates of cooling. However the obvious difference between films grown on room temperature substrates and those produced either by annealing or high T_{sub} during growth demonstrates control of film morphology and feature size.

To produce complete surface coverage of crystallites and provide a smooth crystalline film the target thickness was increased from 14 nm to 42 nm (calibrated QCM thickness reading). This procedure produced continuous hexagonally faceted films and while AFM analysis showed some pits and holes this surface provided a better approximation to a

single crystal than ambient T_{sub} films (**Fig 4.20**). As the final thickness of films was 42 nm a calibrated growth rate of 0.03 angstroms per second could be approximated.

Analysis by XRD confirmed that strong (111) ordering was present in the thicker film and interference fringes were also observed around the (111) reflection suggesting higher quality growth at high T_{sub} (**Fig 4.20(i)**). SEM images confirm the presence of approximately 200-750 nm hexagonal grains with visible grain boundaries (**Fig 4.20(ii)**). These films therefore provide almost purely (111) faces upon which to deposit thin organic films and allowed the effect of grain size upon MPc templating to be investigated.

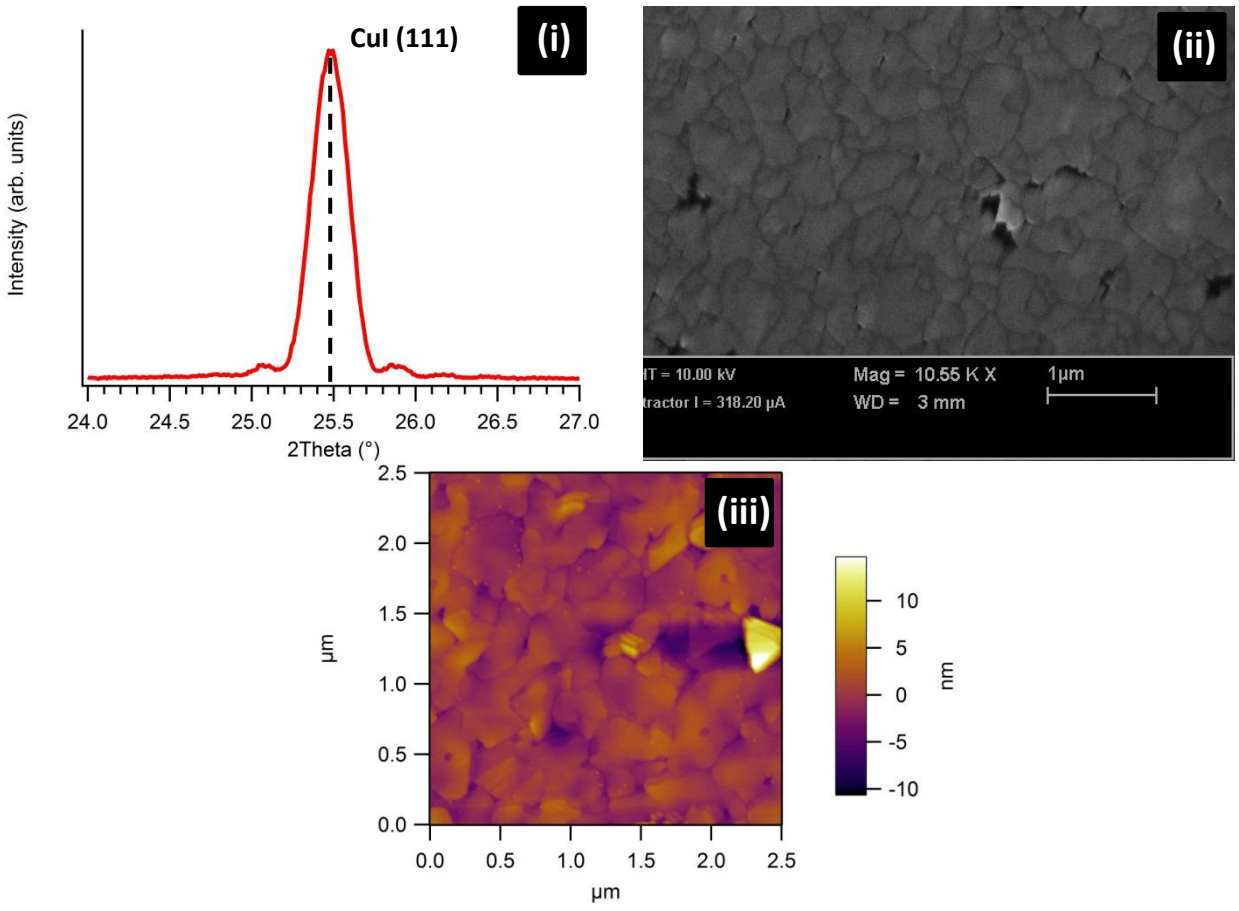

Figure 4.20 – (i) XRD (ii) SEM and (iii) AFM analysis of a 42nm thick CuI film grown with T_{sub} = 193°C

4.3 – Templated films and high temperature templated films

Two different approaches were used to investigate the interaction of FePc molecules with the surface of the high T_{sub} CuI films. Either films were allowed to cool to room temperature before FePc was evaporated or elevated T_{sub} was maintained during the growth of the organic layer. SEM, AFM and XRD were used to compare the films produced by each of these methods.

4.3.1. – Room temperature T_{sub} FePc

Firstly FePc was grown to 10nm thickness on a CuI layer grown at room temperature (21-23°C). In comparison to growth on unmodified SiO_2 the templated film shows larger grains and a much rougher surface, with an RMS roughness of 2.7 nm compared to 0.75nm (**Fig 4.21**). This is in contrast to the observations made by Rand et al.[16], although the ITO substrates used in their work are inherently rougher than SiO_2 and as such changes in roughness may have been difficult to detect.

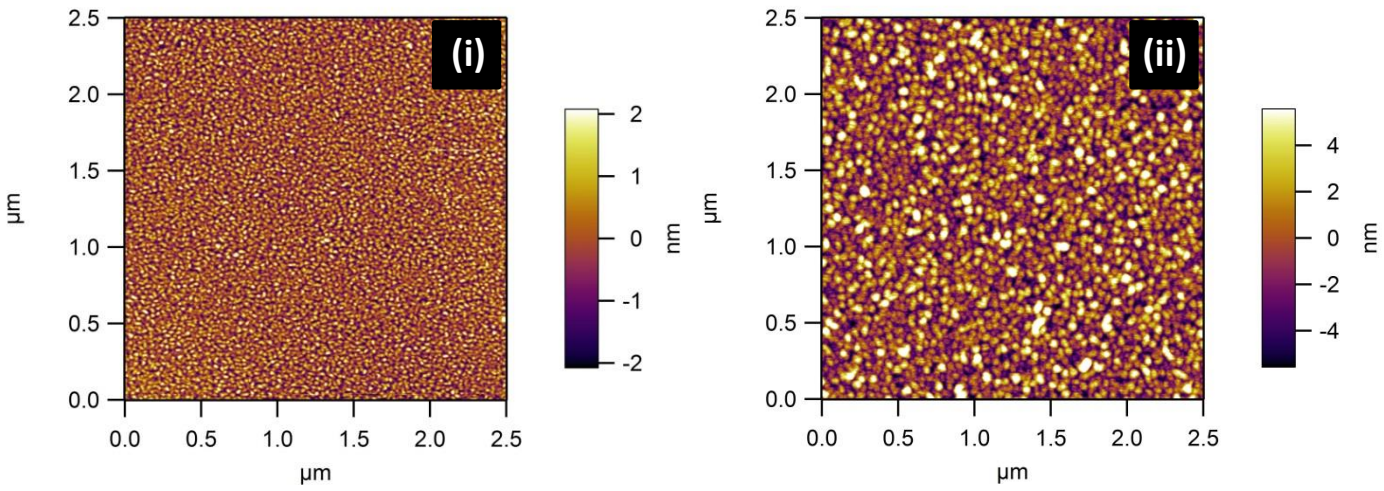

Figure 4.21 – AFM images of (i) untemplated and (ii) CuI templated 10 nm FePc thin films grown at room temperature

High T_{sub} (193°C) CuI thin films were then employed as substrates for FePc growth; SEM images of 5 nm, 10 nm, and 50 nm films of FePc/CuI are presented in (**Fig 4.22**). Images show the non-uniform coverage of the CuI surface by the FePc layer in all films. At a thickness of 5 nm the FePc film is composed of irregularly shaped islands with a wide distribution of lateral sizes. Small regions of growth can be observed at grain boundaries between CuI grains and larger areas with thickness contrast (suggesting multilayer growth) are also present. The brightest portions are bare CuI and the enhanced contrast is due to partial electron beam charging as the films were not conductively coated before imaging. At 10 nm and 50 nm thickness the film still demonstrates inhomogeneous coverage with bare areas of CuI.

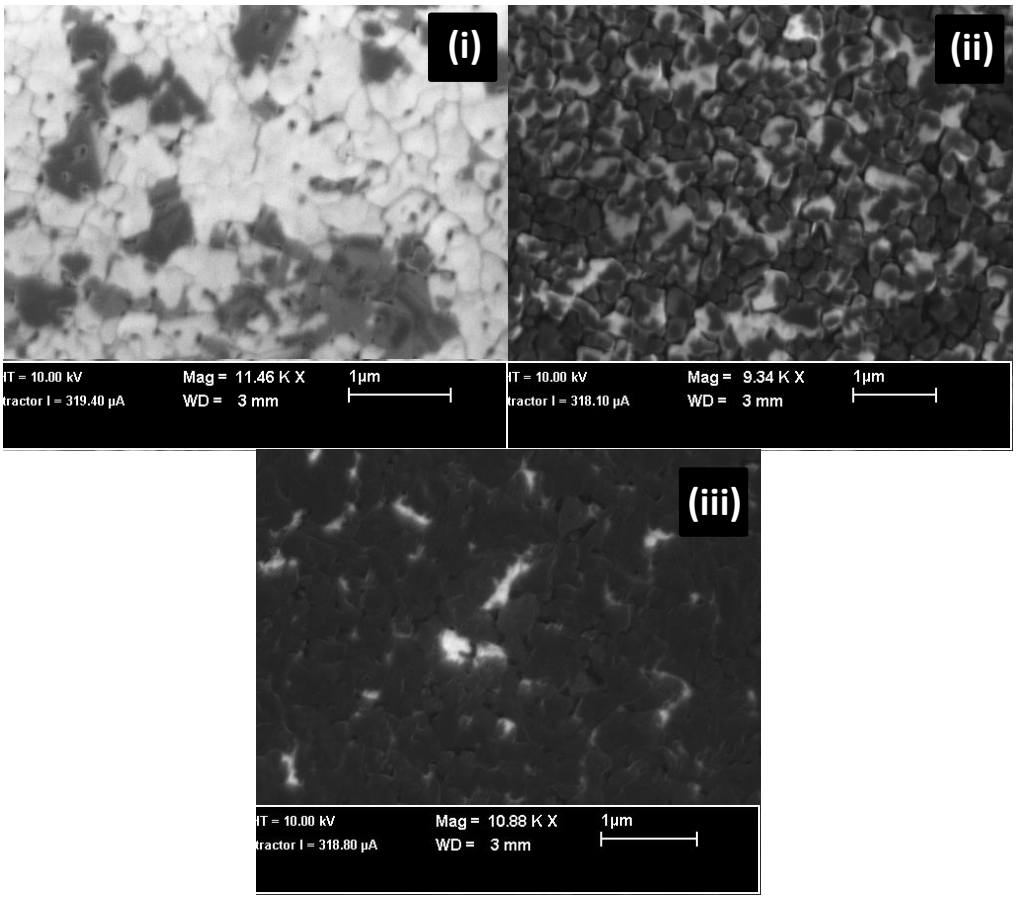

Figure 4.22 – SEM images of (i) 5 nm (ii) 10 nm and (iii) 50 nm FePc/CuI(111) bilayers grown at room temperature

At ambient T_{sub} the structural evolution of the films seems to be directed by the morphology of the underlying CuI surface. AFM images (**Fig 4.23**) show that FePc grains do not grow across grain boundaries and appear to be a mixture of rounded and faceted crystallites. At 50 nm thickness large grains (up to 1 µm) are observed with 20-30 nm deep boundaries running between them. The crystallites in the final film are of comparable size to the grains in the CuI(111) film, so it seems that the grain boundaries act as both nucleation sites and energetic barriers to the propagation of crystal growth and coalescence of crystals. While the assignment of these features as single crystals cannot be made, their size is much greater (up to 10 times) that those observed without the CuI(111) layer.

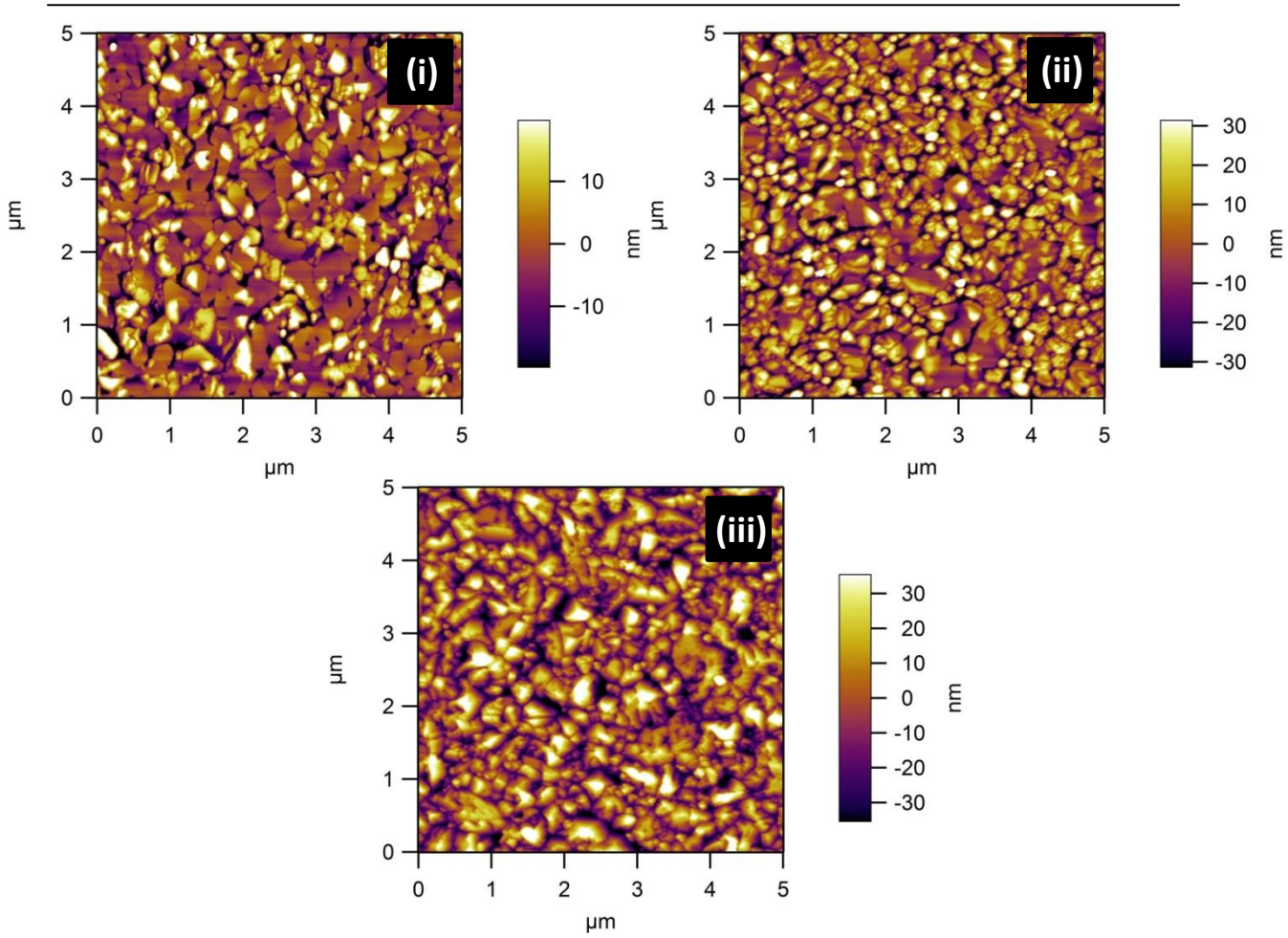

Figure 4.23 – AFM images of (i) 5 nm (ii) 10 nm and (iii) 50 nm FePc/CuI(111) bilayers grown at room temperature

XRD traces (**Fig 4.24**) of 50 nm films do not exhibit the low angle peaks usually observed in MPc thin films deposited at ambient temperature. Only a single extra peak is observed (compared to XRD traces of CuI(111)/SiO_2 bilayers) at 28.02° with a d spacing of 0.32 nm. Peaks at similar angle have previously been indexed to the inter-molecular spacing of the face-to-face packing direction of molecules in MPc layers[19]. This suggests that the majority of the out-of-substrate plane structure is due to the molecules stacking face-to face with respect to the substrate. This situation has been previously observed and indexed in literature and is in agreement with similar experimental work with ZnPc molecules on CuI layers[16]. The difference in assignment here and in the previous work on ZnPc can be understood because of the lack of a solved single crystal structure for the ZnPc molecule. This has presumably caused the (313) spacing (to which the 28° peak is indexed by Rand et al.) to be assigned purely from comparison to simulated powder patterns. This plane does not pass through any electron dense regions of the ZnPc molecule and as such is not expected to be highly scattering.

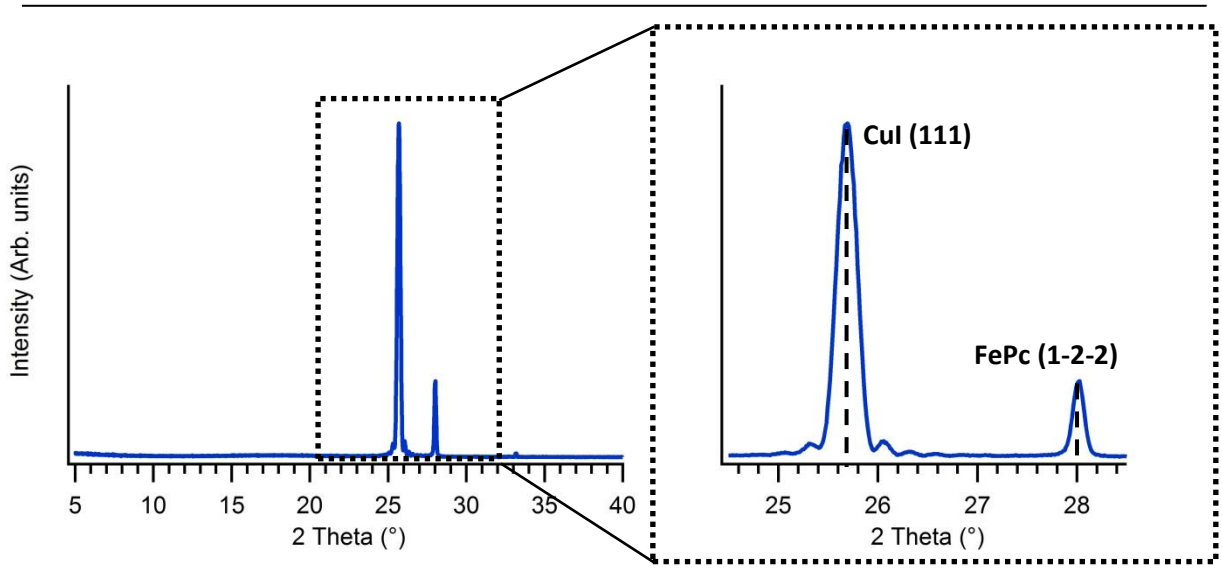

Figure 4.24 – XRD trace for a 50 nm FePc/CuI(111)/SiO_2 bilayer grown at room temperature (right hand pane shows an enlargement of the area of interest)

4.3.2 – High T_{sub} FePc

Due to the sensitivity of the CuI layer to annealing, high T_{sub} deposition of FePc on to room temperature CuI is not representative of either room temperature or high temperature growth regimes. However, an experiment was undertaken in which a 14 nm layer of CuI was deposited, then annealed at 193°C for 30 minutes and held at this temperature while FePc was deposited. Another marked change in morphology was observed, with the production of nanowire protrusions from 10 nm of growth. AFM was attempted (**Fig 4.25(i)**) but was difficult due to the height of the features, so SEM imaging was used. Images (**Fig 4.25(ii)+(iii)**) showed an incomplete coverage of needle like crystallites 200-1000 nm in length and 25nm in width (all approximated from SEM images).

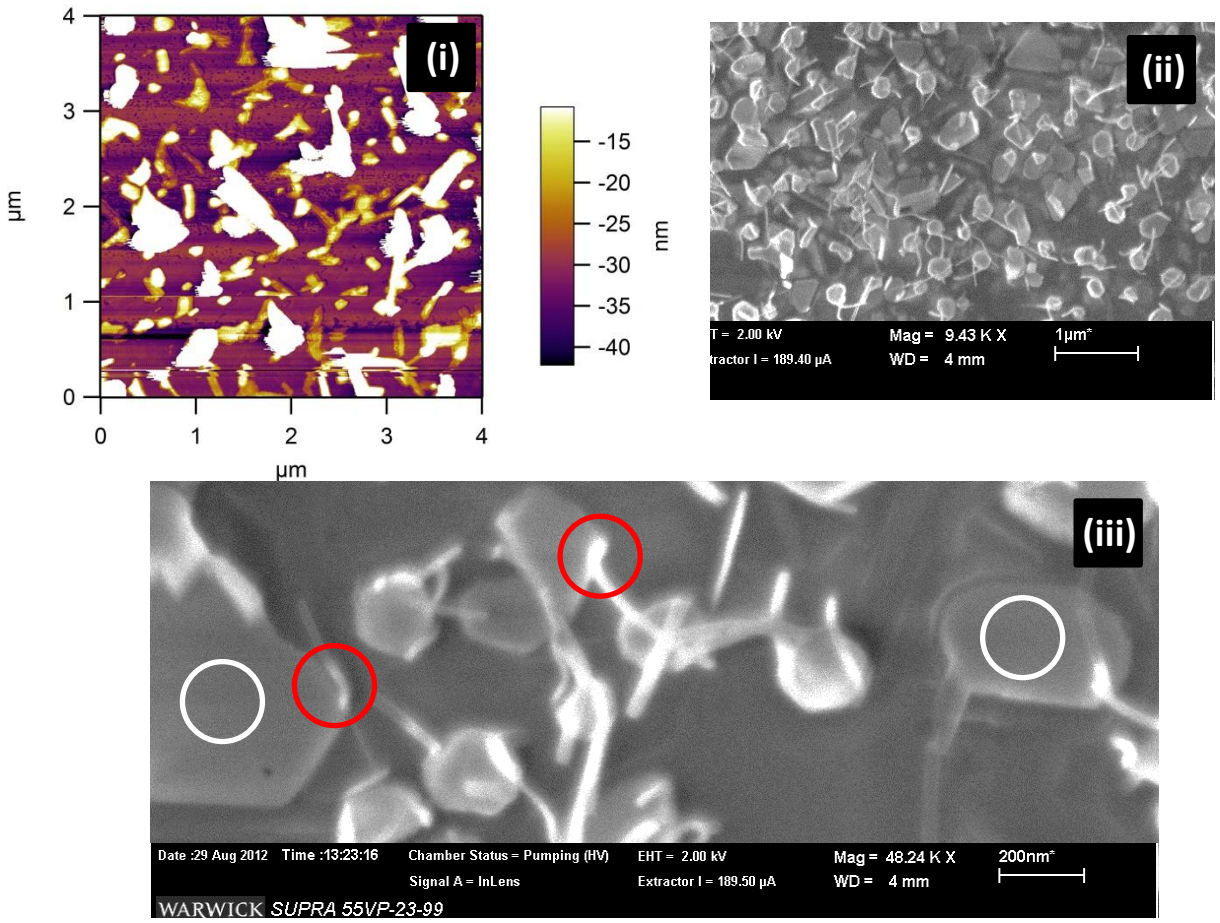

Figure 4.25 – AFM image (i) of 10 nm FePc film deposited at Tsub = 193°C onto Sio_2 partially covered with CuI (111). SEM images (ii) and (iii) of the same sample

Crystals appear to be nucleating from the edges of the CuI islands (which are visible in the higher resolution image marked with red circles) rather than from the (111) faces (white circles). When the thickness of the FePc layer was increased to 50 nm, a higher coverage of nano-crystallites was produced separated by hundreds of nanometres at their ends (**Fig 4.26**). The surface is also partially visible through the forest-like collection of nanocrystallites.

The needles were found to be sensitive to beam damage in the SEM, so cryo temperatures were employed to produce more stable high resolution images. Images produced at approximately 77 K (with liquid nitrogen cooling) were more stable and allowed easier imaging due to the protective layer of ice that encases the samples when they are prepared at cryo temperatures.

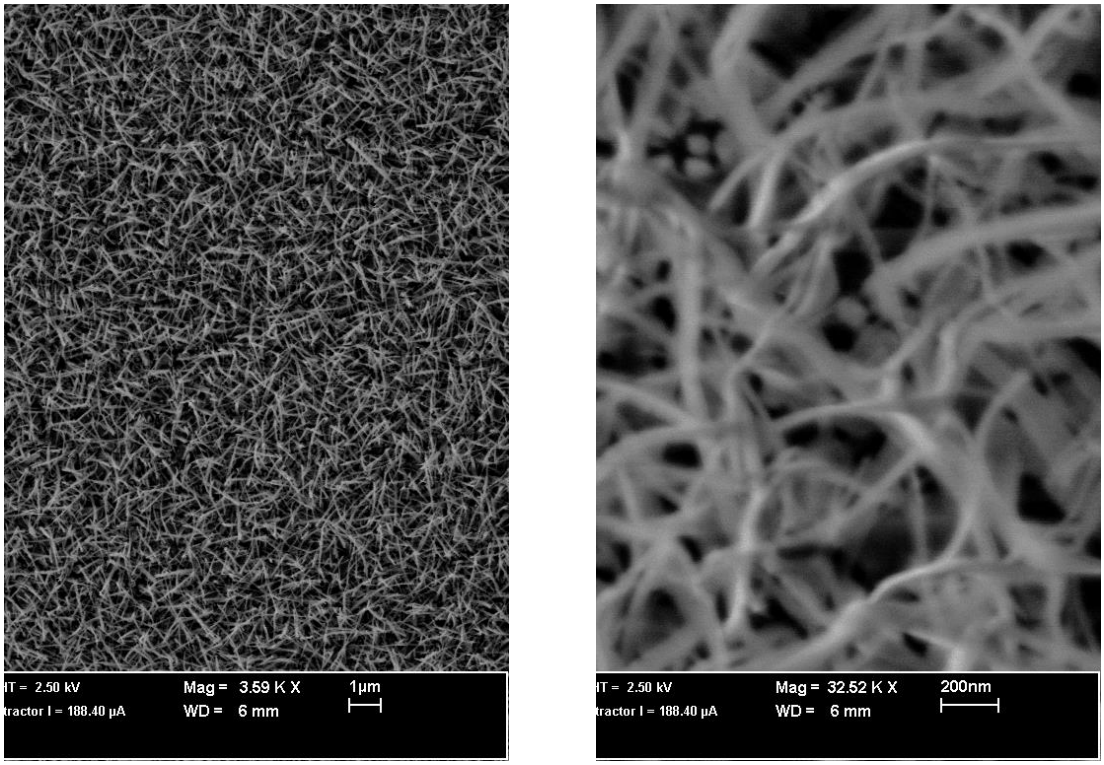

Figure 4.26 – SEM images of 50 nm thickness FePc films grown at Tsub = 193°C on partial coverage of CuI(111)

Areas of the surface appear similar to 50 nm films grown on unmodified SiO_2 at high T_{sub}, which are presumably the areas of bare substrate not covered by CuI (**Fig 4.27**). Bunches of crystals have nucleated from points on the surface which are assumed to be CuI(111) islands which are not visible due to nano-crystallite growth. The crystals are not growing orthogonally out of the surface plane as would be expected if the (111) facets of the CuI islands were nucleating this kind of growth. Some areas (marked by red circles) appear similar to those observed without the CuI layer suggesting these are FePc layers grown on the bare SiO_2 between CuI(111) islands.

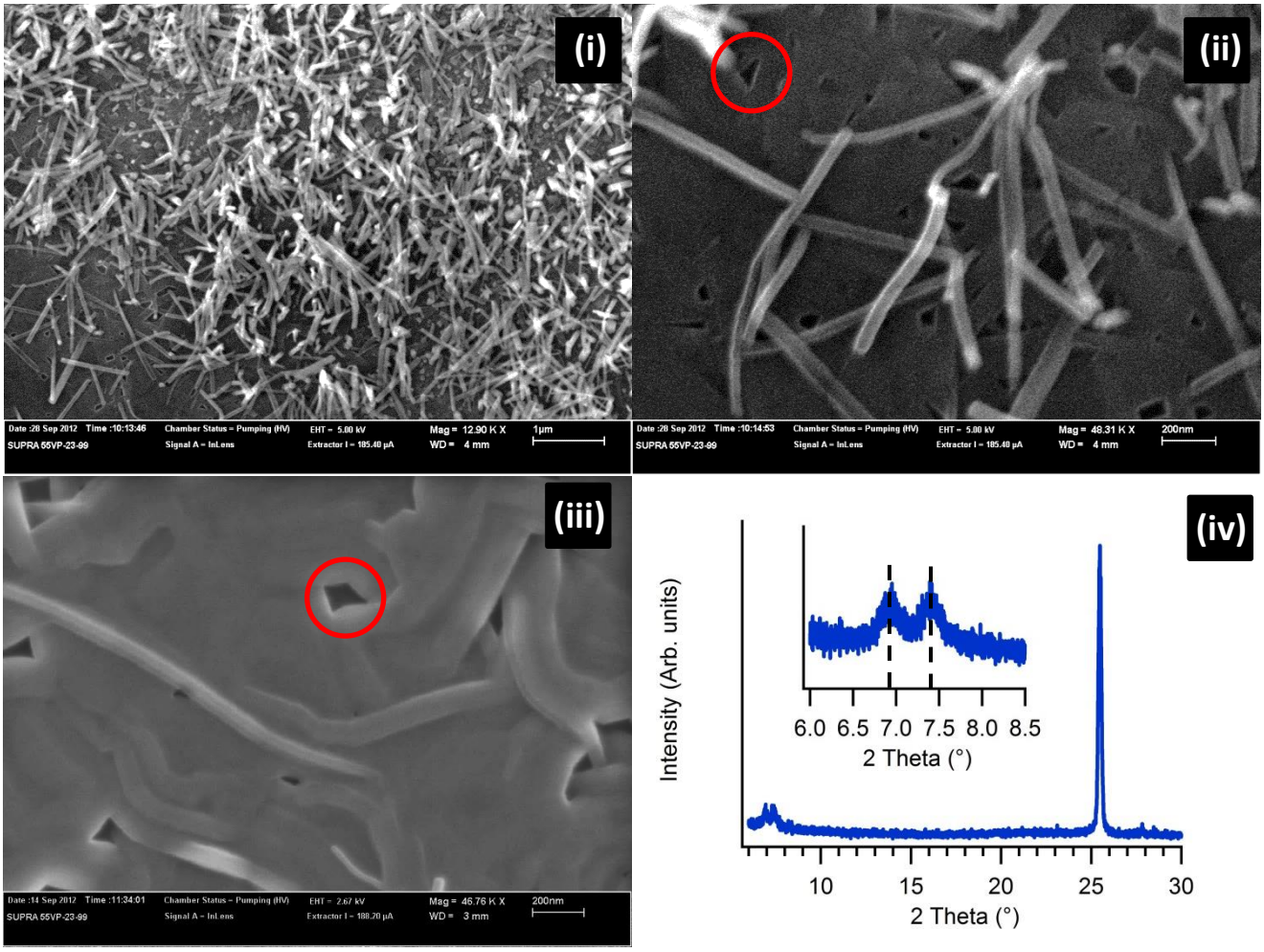

Figure 4.27 – SEM images of 50 nm FePc grown at T_{sub}=193°C on (i),(ii) partial coverage of CuI(111) and (iii) SiO_2. (iv) shows the XRD trace for the sample shown in (i) and (ii) with an inset enlargement of the low angle region

It is also interesting to note the transparent nature of the crystallites, as features of the surface can be observed through them. This suggests that their thickness is less than the transmission path length of the electron beam in the SEM of approximately a few tens of nanometres.

XRD of the 50nm film (Fig. 4.27) showed a pair of peaks at 6.9° and 7.4° corresponding to d-spacings of 1.27 nm and 1.20 nm respectively. While it is difficult to comment on the absolute crystal structure of MPcs due to the variety of polymorphs observed[20], it is clear that each type of growth (nanowire and layer-by-layer film) is producing one of the diffraction peaks. As a large d-spacing is indicated by the low angle of the peak this suggests that the edge to edge spacing is different in the two forms of FePc present on the surface.

High T_{sub} grown films were then used as FePc templates, with T_{sub} held at the growth temperature of the CuI film. The surface roughness of the FePc film rapidly increases making AFM analysis impractical (reliable imaging of 50 nm films was not possible for this reason) in this regime. SEM imaging (**Fig 4.28**) of a 10 nm thick film shows a subtle change when compared to the ambient temperature growth, slightly more of the CuI substrate seems to be uncovered and thickness contrast in the FePc crystals can be discerned. This suggests preferential growth directed out of the plane of the surface which produces the high aspect ratio features which makes AFM imaging difficult. AFM images of thinner (5nm and 10nm) films show tall features which may be the initial stages of this form of growth mixed with flatter more rounded crystallites (**Fig 4.29**).

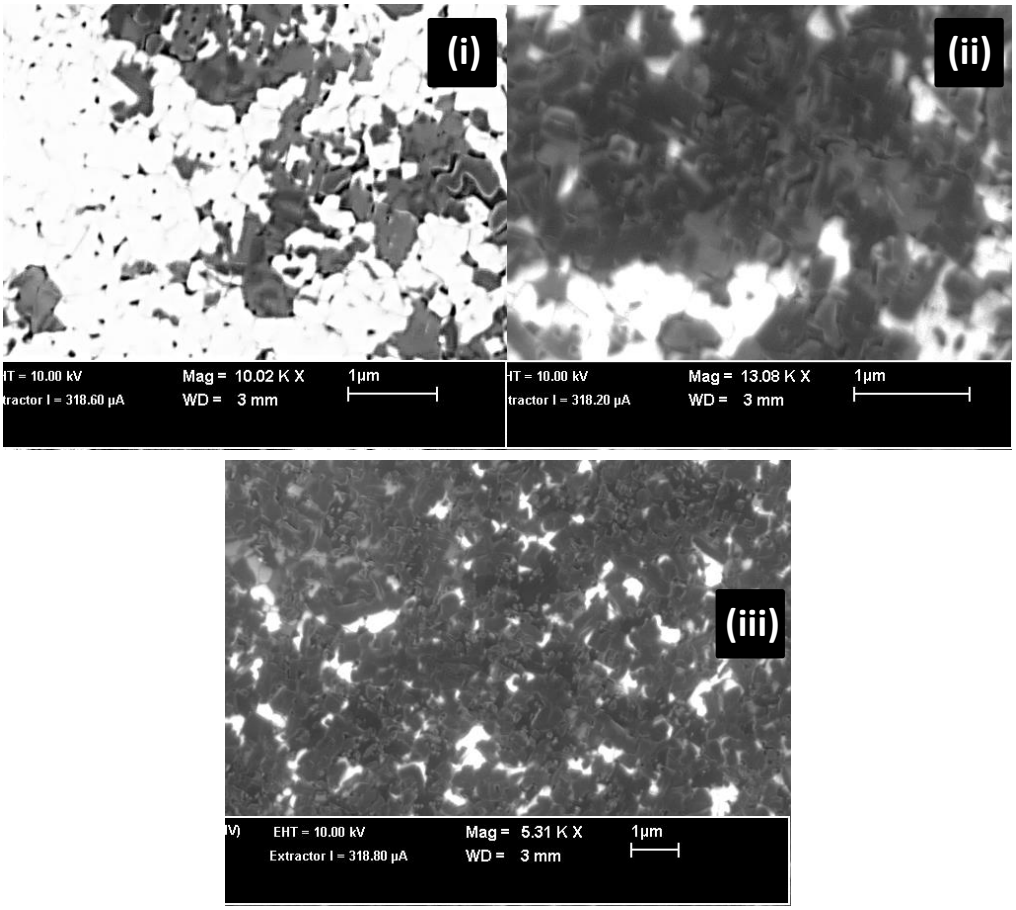

Figure 4.28 – SEM images of (i) 5 nm (ii) 10 nm and (iii) 50 nm FePc/CuI(111) bilayers grown at T_{sub} = 193°C on complete Cu(111) layers

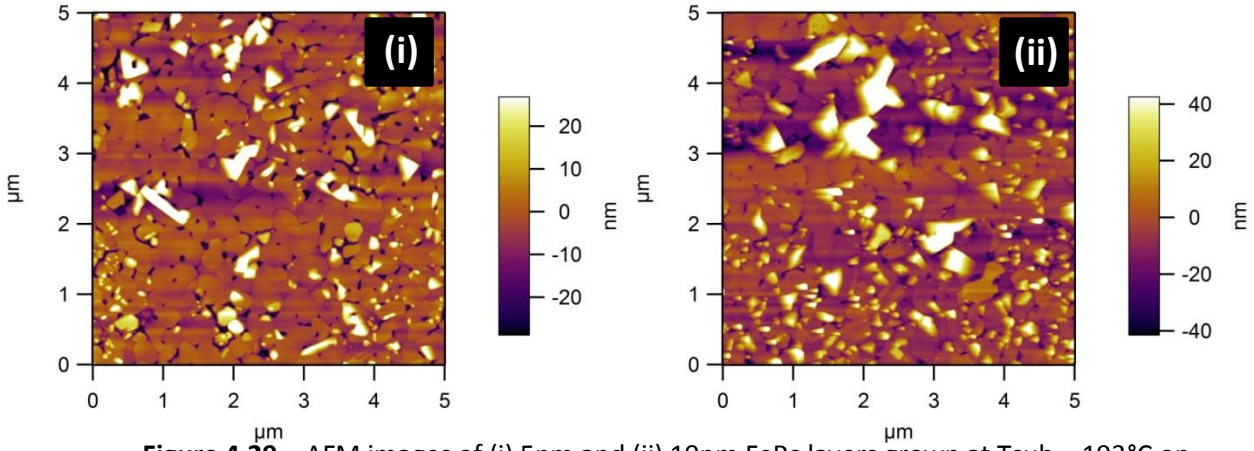

Figure 4.29 – AFM images of (i) 5nm and (ii) 10nm FePc layers grown at Tsub = 193°C on complete CuI (111) layers

Structural analysis by XRD was performed on the 50 nm film and showed a similar reflection at 28° (spacing of 0.32nm), but also included a pair of low angle peaks at 6.9° and 7.4°, similar to those observed in the partial coverage FePc/CuI(111) layers (**Fig 4.30**).

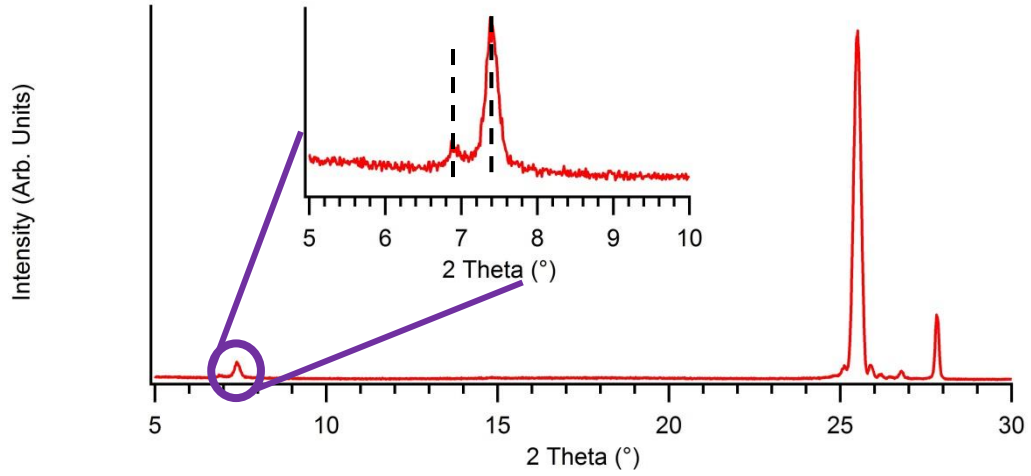

Figure 4.30 – XRD trace for a 50 nm FePc/CuI(111) bilayer grown at Tsub = 193°C. Inset is an enlargement of the low angle peaks

This suggests that in the high T_{sub} film three distinct d spacings are present; face-to-face stacking (28°) and two different edge-to-edge spacings previously observed in templated FePc. The relative intensities of peaks are also different to those observed with incomplete CuI template layers; at higher coverage, the higher angle peak is more than eight times more intense. While only a qualitative analysis of this can be made, this suggests that more of the crystallites producing the higher angle peak are present, or more are oriented out of the plane of the surface with complete CuI coverage.

While the relative orientation of the molecules is altered by the presence of the CuI layer growing at elevated temperatures still produces peaks corresponding to the edge-to-edge packing of the FePc molecules. This suggests that the FePc crystal structure is unaltered by the CuI layer as both orientations can be grown on the CuI layer (both peaks

can be indexed to the same crystal structure) and application of heat is simply driving the growing system to the thermodynamically more stable orientation, which minimises the surface energy. The lack of full surface coverage of FePc on top of the CuI(111) layer agrees qualitatively with this assumption, as the surface-molecule interaction is minimised by 3D growth of islands rather than multiple nucleation sites.

4.4 – Conclusions

The effect of changing the temperature of an amorphous and inert substrate during the deposition of two planar phthalocyanines, FePc and MePc, has been investigated. In both cases larger crystalline domains were observed with increasing temperature up to a critical point at which the sticking coefficient was sufficiently reduced to prevent molecular adsorption. While both molecules produced larger crystals at high temperatures those observed with FePc were always larger, a characteristic also observed in macroscopic crystals.

The effect of adding a CuI structural template layer which was prepared both at ambient and elevated substrate temperature was also investigated. Higher temperatures produced larger crystalline domains in the (111) oriented CuI layer and these in turn produced large grains of FePc which was grown on top at room temperature. The orientation of the FePc layer was changed such that the molecules switched from a face-on orientation with respect to the substrate to edge-on.

When FePc was deposited on to elevated temperature substrates on to the large-grained CuI(111), a mixture of edge-on and face-on orientations were observed, suggesting that the templating effect does not produce the most thermodynamically stable crystalline form of FePc. The surface morphology rapidly roughened with growth on heated CuI(111)

suggesting that increasing the thermal energy of the system and therefore ease of molecular diffusion allowed a minimisation of the contact between the FePc crystallites and the CuI(111) surface.

References:

(1) Hancox, I.; Sullivan, P.; Chauhan, K. V.; Beaumont, N.; Rochford, L. A.; Hatton, R. A.; Jones, T. S. The effect of a MoOx hole-extracting layer on the performance of organic photovoltaic cells based on small molecule planar heterojunctions. *Organic Electronics* **2010**, *11*, 2019–2025.

(2) Schünemann, C.; Elschner, C.; Levin, A. A.; Levichkova, M.; Leo, K.; Riede, M. Zinc phthalocyanine — Influence of substrate temperature, film thickness, and kind of substrate on the morphology. *Thin Solid Films* **2011**, *519*, 3939–3945.

(3) Kolotovska, V.; Friedrich, M.; Zahn, D. R. T.; Salvan, G. Magnetic field influence on the molecular alignment of vanadyl phthalocyanine thin films. *Journal of Crystal Growth* **2006**, *291*, 166–174.

(4) Dittmer, J. .; Lazzaroni, R.; Leclère, P.; Moretti, P.; Granström, M.; Petritsch, K.; Marseglia, E. ; Friend, R. ; Brédas, J. ; Rost, H.; Holmes, A. . Crystal network formation in organic solar cells. *Solar Energy Materials and Solar Cells* **2000**, *61*, 53–61.

(5) Senthilarasu, S.; Baek, S.-J.; Chavhan, S. D.; Lee, J.; Lee, S.-H. Effect of Temperature on Stacking Orientations of Zinc Phthalocyanine Thin Films. *Journal of Nanoscience and Nanotechnology* **2008**, *8*, 5414–5417.

(6) Karan, S.; Mallik, B. Templating Effects and Optical Characterization of Copper (II) Phthalocyanine Nanocrystallites Thin Film: Nanoparticles, Nanoflowers, Nanocabbages, and Nanoribbons. *Journal of Physical Chemistry C* **2007**, *111*, 7352–7365.

(7) Laudise, R. .; Kloc, C.; Simpkins, P. .; Siegrist, T. Physical vapor growth of organic semiconductors. *Journal of Crystal Growth* **1998**, *187*, 449–454.

(8) Yang, J. L.; Schumann, S.; Jones, T. S. Nanowire-array films of copper hexadecafluorophthalocyanine (F_{16}CuPc) fabricated by templated growth. *Journal of Materials Chemistry* **2011**, *21*, 5812.

(9) Bayliss, S. M.; Heutz, S.; Rumbles, G.; Jones, T. S. Thin film properties and surface morphology of metal free phthalocyanine films grown by organic molecular beam deposition. *Physical Chemistry Chemical Physics* **1999**, *1*, 3673–3676.

(10) Miller, C.; Sharoni, A.; Liu, G.; Colesniuc, C.; Fruhberger, B.; Schuller, I. Quantitative structural analysis of organic thin films: An X-ray diffraction study. *Physical Review B* **2005**, *72*, 104113.

(11) Xiao, K.; Liu, Y.; Yu, G.; Zhu, D. Influence of the substrate temperature during deposition on film characteristics of copper phthalocyanine and field-effect transistor properties. *Applied Physics A: Materials Science & Processing* **2003**, *77*, 367–370.

(12) E, J.; Kim, S.; Lim, E.; Lee, K.; Cha, D.; Friedman, B. Effects of substrate temperature on copper(II) phthalocyanine thin films. *Applied Surface Science* **2003**, *205*, 274–279.

(13) Tong, W. Y.; Djurisić, a B.; Xie, M. H.; Ng, a C. M.; Cheung, K. Y.; Chan, W. K.; Leung, Y. H.; Lin, H. W.; Gwo, S. Metal phthalocyanine nanoribbons and nanowires. *The Journal of Physical Chemistry. B* **2006**, *110*, 17406–13.

(14) Yim, S.; Heutz, S.; Jones, T. S. Model for the α→β[sub 1] phase transition in phthalocyanine thin films. *Journal of Applied Physics* **2002**, *91*, 3632.

(15) Hashimoto, T.; Kaito, T.; Yanagiya, S.; Mori, a.; Goto, N. Birefringence measurements of MnPc thin film by polarization microscopy. *Applied Surface Science* **2008**, *254*, 7947–7949.

(16) Rand, B. P.; Cheyns, D.; Vasseur, K.; Giebink, N. C.; Mothy, S.; Yi, Y.; Coropceanu, V.; Beljonne, D.; Cornil, J.; Brédas, J.-L.; Genoe, J. The Impact of Molecular Orientation on the Photovoltaic Properties of a Phthalocyanine/Fullerene Heterojunction. *Advanced Functional Materials* **2012**, *22*, 2987–2995.

(17) Cheng, C. H.; Wang, J.; Du, G. T.; Shi, S. H.; Du, Z. J.; Fan, Z. Q.; Bian, J. M.; Wang, M. S. Organic solar cells with remarkable enhanced efficiency by using a CuI buffer to control the molecular orientation and modify the anode. *Applied Physics Letters* **2010**, *97*, 083305.

(18) Yashima, M.; Xu, Q.; Yoshiasa, A.; Wada, S. Crystal structure, electron density and diffusion path of the fast-ion conductor copper iodide CuI. *Journal of Materials Chemistry* **2006**, *16*, 4393.

(19) Heutz, S.; Cloots, R.; Jones, T. S. Structural templating effects in molecular heterostructures grown by organic molecular-beam deposition. *Applied Physics Letters* **2000**, *77*, 3938.

(20) Leznoff, C.C. Lever, A. B. P. *Phthalocyanines : Properties and Applications*; VCH (New York), 1989.

Chapter 5

5.1 - Morphology and crystal structure of F_{16}CuPc thin films

While F_{16}CuPc has been employed as a semiconducting material in OPVs and OTFTs only a few studies have concentrated on structural and morphological analysis of thin films with thicknesses equal to those used in devices[1]. Evidence for thickness-dependant structural transitions and polymorphic behaviour also make it an interesting molecule from a crystal structure perspective[2].

In this section the single crystal structure is firstly re determined by synchrotron X-ray diffraction and compared to literature. This structure differs significantly from the structures already reported in literature due the lack of the common herringbone packing motif present in phthalocyanines. Thin evaporated films supported on solution-processed graphene oxide layers are then analysed by AFM, XRD and TEM. Thickness dependant structural changes where investigated by varying the thickness of the F_{16}CuPc films, and characterisation of the crystalline starting material is also undertaken.

5.1.1 – Structural analysis of single crystals

In order to obtain a complete single crystal structure, F_{16}CuPc crystals were grown using controlled recrystallization from vapour in high vacuum. F_{16}CuPc powder (Sigma-Aldrich UK) was firstly triply purified by thermal gradient sublimation to remove volatile contaminants present in the powder. For each purification experiment only the purest band closest to the hot zone of the furnace was collected for further use. After this the sample consisted of small (smaller than 0.05mm in length) blue-purple needles that were too small to easily handle individually. This made their use in X-ray measurements impossible, so larger single crystals were required. In order to prepare larger crystals the same purification

apparatus was used but with only a small amount of material (approx. 500mg) and a modified ramping and cooling procedure. Temperature was ramped at 1°C per minute up to a temperature 50°C lower than the evaporation temperature of F_{16}CuPc (370°C). After this the temperature was ramped in 0.1°C increments every minute and the final temperature was maintained for twelve hours. In addition to this solvent cleaned pieces of a single crystal Si (100) (20 x 15mm with a thermally grown oxide layer) were placed at various points along the purification tube to provide a variety of substrate temperatures. These acted as ultra-flat recrystallization platforms for the molecules and produced larger needle like crystals. After cooling the substrates were inspected by eye and the largest single crystals were selected for further analysis.

XRD measurements were carried out at beam line I19 at Diamond light source at Harwell Science and Innovation campus (UK). Diffraction measurements had been previously attempted using a laboratory single crystal diffractometer, but the intensities were too low for full data collection. Integration was performed using Rigaku CrystalClear-SM Expert 2.0 r5 while refinement was carried out using SHELXL-97 and the structure was solved in SHELXS-97. This allowed unit cell parameters and atomic positions within the lattice to be resolved, producing the structure which is summarised in **Fig 5.1**. Unlike other recent reports the unit cell is found to be triclinic and contain only a single molecule. This effectively halves the unit cell volume and negates the possibility of the herringbone packing arrangement found in some phthalocyanine polymorphs.

(i)

Crystal Data	$CuC_{32}N_8F_{18}$
Formula Weight	863.93
Z	1
Temperature / K	120
Crystal System	Triclinic
Space Group	$P\bar{1}$
a / Å	4.89(2)
b / Å	10.29(4)
c / Å	14.91(7)
α / °	74.24(12)
β / °	87.22(10)
γ / °	80.80(13)
Crystal Description	Purple Needle
Crystal Dimensions / mm	0.12 x 0.02 x 0.015
Data Collection	
Radiation	Synchrotron, λ = 0.68890 Å, Diamond Light Source Station I19
Data Collection Software	CrystalClear-SM Expert 2.0 r5
Total Reflections	4298
Independent reflections	2306 952 with $I > 4\sigma(I)$
Refinement Software	SHELXL-97

(ii)

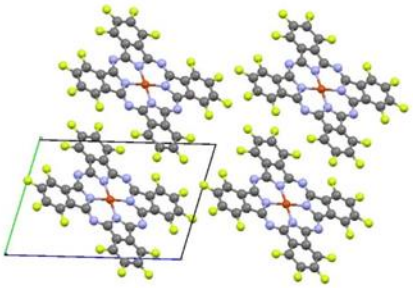

(iii)

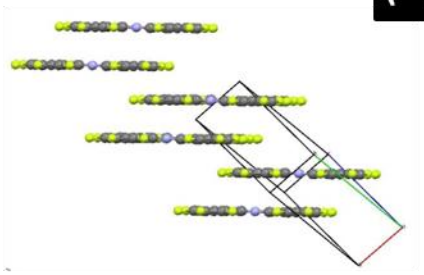

Figure 5.1 – (i) Crystal structure table for $F_{16}CuPc$ and views along the (ii) 'a' axis of the unit cell and (iii) the (1-2-2) plane along which the molecular axis lies

5.1.2 – Structural analysis of bulk purified $F_{16}CuPc$

TEM was used to confirm that the single crystal structure (from synchrotron measurements) was representative of the material used for growth of thin films. SAED patterns were recorded by sprinkling a small number of the single crystals obtained by triple purification onto a lacy carbon TEM support (**Fig 5.2**). A liquid nitrogen cooled single tilt specimen holder was used to avoid damage to the sample during diffraction measurements. Patterns could readily be obtained from the crystals and the most commonly observed orientation at zero specimen tilt corresponded to a view along the (01-1) axis. These patterns could be indexed to the structure refined from synchrotron measurements and

good agreement between the two datasets was found. Full structural characterisation from TEM for comparison was attempted but limitations of sample morphology and the single tilt axis available on the sample holder prevented views down appropriate zone axes. Twinning of crystals was observed in multiple patterns, doubled spots suggesting the twin axis was the (100) plane. This agrees qualitatively with other reports of electron diffraction experiments on single crystals of planar phthalocyanines[3].

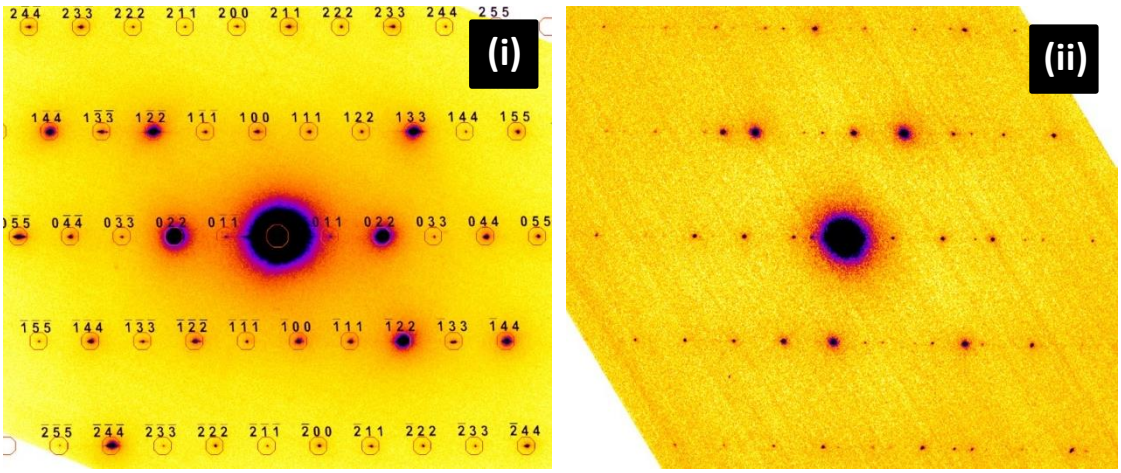

Figure 5.2 – SAED patterns from F16CuPc single crystals. Patterns are both taken down the (01-1) plane with predicted spot positions in red (i); (ii) shows doubling of spots consistent with twinning along the (100) axis.

X-ray diffraction measurements were also performed on the purified F_{16}CuPc powders using a Panalytical X'Pert Pro MRD (Cu Kα) for further confirmation of structure (**Fig 5.3**). Due to the large lattice spacings present in the material, data was only collected between 5° and 40° for comparison to the new structure (from synchrotron measurements).

Diffractograms show a strong reflection at 28.5° which corresponds to the (1-2-2) plane from the refined crystal structure presented here. Herringbone stacked structures (such as the structure present by Yoon et al.) do not predict this peak when powder patterns are simulated. This can be rationalised by considering the nature of the intermolecular

spacings and the differences between them in planar slipped stack structures and herringbone packing. With parallel stacks, the spacing separating molecules (d_{int}) must always correspond to an inter-planar spacing between Miller planes as only one molecule defines the unit cell. In herringbone-stacked structures d_{int} does not necessarily correspond to a unit cell lattice plane. Reflections from planes close to the plane of the flat molecule will also be increased in intensity due to the high concentration of electron density along the plane passing through the plane of the molecule (therefore an increased structure factor in this plane).

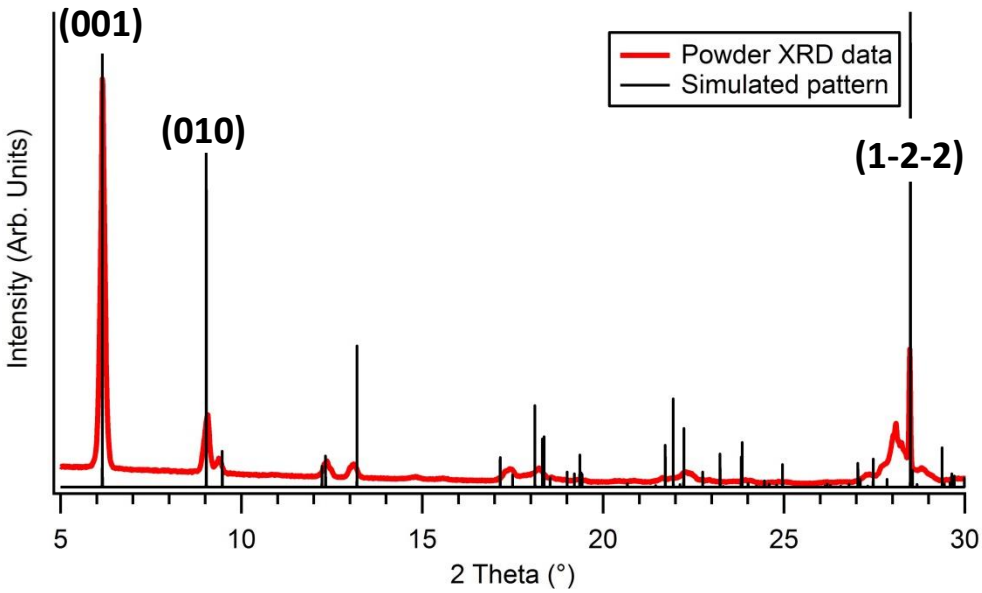

Figure 5.3 – Powder XRD of purified F16CuPc with over-layed single crystal structure

By comparing the simulated pattern from the Yoon et al. structure, the simulated pattern from our proposed structure and experimental powder XRD we can confirm that only a single reflection is observed at 28.5° in both the experimental data and our simulated pattern. The presence of this and the absence of multiple reflections around this angle

confirm that a parallel stack rather than herringbone packing is present in F_{16}CuPc powders and single crystals.

5.1.3 – TEM imaging and AFM of GO supported F_{16}CuPc thin films

Graphene oxide was used as a low contrast support for the deposition of F_{16}CuPc to allow high resolution imaging and diffraction experiments without obscuring the features and diffraction spots of the organic film. Previous research has demonstrated the use of GO as a support for TEM and describes the methodology used to produce it in solution in detail[4,5]. Briefly, GO solutions were produced by oxidation of graphite powders using a modified Hummers' method. These were spin coated from hydrazine onto single crystal Si(100) wafers with a thermally grown oxide layer and drop cast onto lacy carbon TEM grids.

A custom sample holder based on an Omicron sample plate was fabricated to hold both the GO coated wafers and TEM grids and allow simultaneous deposition of F_{16}CuPc onto both (**Fig 5.4**).

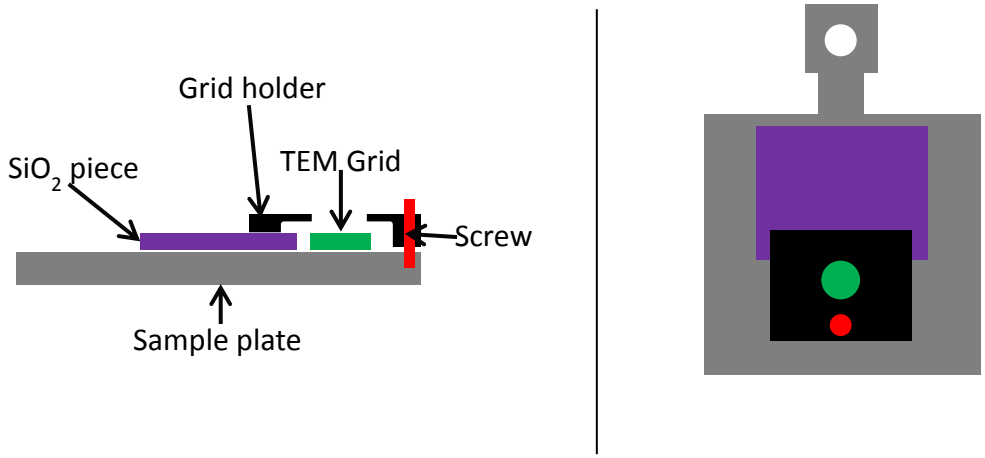

Figure 5.4 – Side and front view of the custom sample holder used in this work

Film thickness was monitored by a QCM, with only the total mass of the film deposited was recorded rather than the actual thickness of the film. While external AFM measurements were used to calibrate the QCM, thick (50-100 nm) films were used for these

measurements and the morphology of the films was not considered. Three thicknesses were deposited; 1 nm, 5 nm and 80 nm to observe any thickness dependant structural changes, with each film grown at the same rate of 0.03Ås^{-1}. At 1 nm a film approaching a monolayer was expected as the height of a phthalocyanine molecule is around 1.3 nm (previous measurements suggest that planar phthalocyanines stand with their pi systems parallel to non-interacting substrates). Thicker films (5 nm) should begin to reflect the bulk structural properties of F_{16}CuPc; 80 nm films are assumed to reflect completely bulk crystal structure with little influence from the substrate.

AFM images of 1 nm and 5 nm films are shown in (**Fig 5.5**) and while imaging was attempted for 80 nm films the surface was found to be too rough. Images show that the film is highly polycrystalline even at 5 nm suggesting that a vast number of crystals nucleate and grow on nanometre length scales simultaneously. This behaviour is common in the growth of planar MPcs on non-interacting surfaces at room temperature. Even in the thinnest films a island formation is obvious, three dimensional features forming even after a very small amount of material has been deposited (1 nm total thickness). In 5 nm films island features reach heights of 9 nm which emphasises the extent of the individual crystallisation of small crystals rather than layer formation.

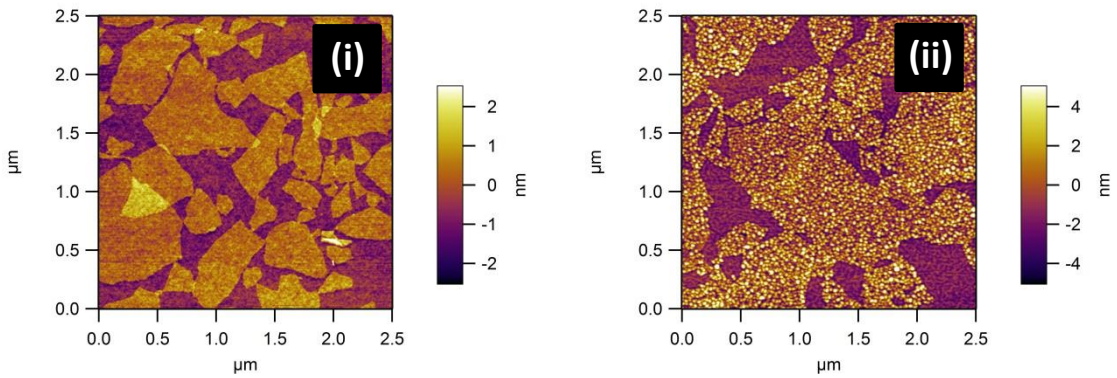

Figure 5.5 – AFM images of (i) 1nm and (ii) 5nm thickness F_{16}CuPc/graphene oxide/SiO_x layers

As 80 nm films were too rough to image by AFM, SEM was used to image the surface of 1 nm, 5 nm and 80 nm samples (**Fig 5.6**). A 30 nm thick film was also fabricated to allow further analysis of the change in morphology. Films of 1 nm thickness show few features large enough to discern with the SEM, but the graphene oxide sheets are clearly visible on the surface of the silicon oxide layer. As the thickness is increased to 5 nm, crystallites are visible on the surface of the GO flakes and the SiO_2 surface but are too small to resolve in detail with the limited resolution of the SEM. Previous SEM and AFM studies have made similar observations describing the crystals as 'spherical' and assigning them as α-phase in structure[6]. The film is composed of interlocking crystallites which seem to have a tendency to elongate preferentially along one axis (similar to large needle like single crystals of the same material). At a thickness of 80 nm multiple crystallites can be seen protruding from the film surface which explains the difficulties encountered with AFM imaging. A transition (with increasing thickness) to growth out of the surface plane as high aspect ratio needles has previously been observed in literature.

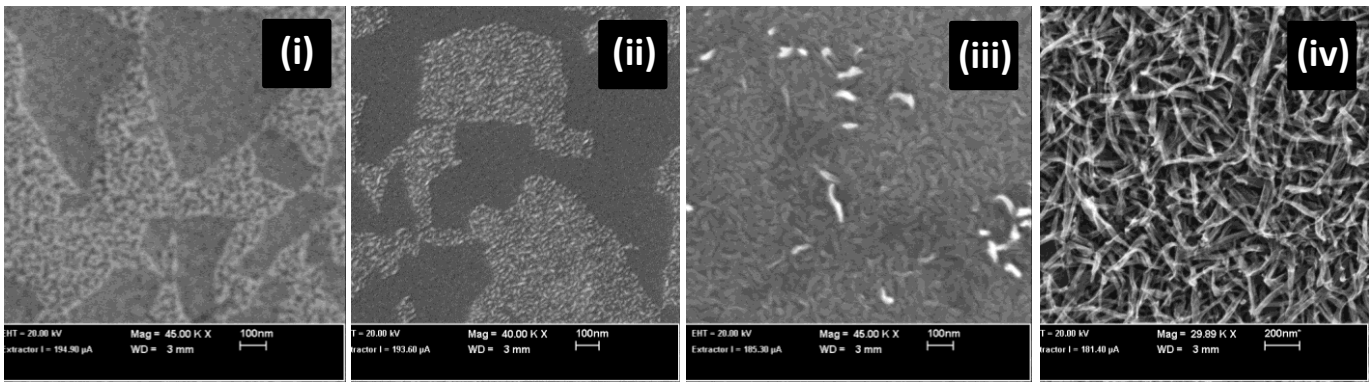

Figure 5.6 – SEM images of (i) 1nm (ii) 5nm (iii) 30 nm and (iv) 80 nm thick F16CuPc/graphene oxide/SiO_2 films

Films evaporated onto drop cast GO films on lacy carbon TEM grids were also imaged by bright field TEM. Sufficient contrast could not be achieved with 1 nm films; this could be due to lack of material or instantaneous damage to the structure by the electron beam. TEM images were captured of the 5 nm and 80 nm thick films and are presented in Figure 5.7. TEM images confirm that small (10-50nm diameter) crystallites form on the graphene oxide sheets and are also observed along the lacy carbon support. In 80 nm thick films a similar morphology is observed to that inferred from SEM images, larger crystallites covering the whole surface with darker regions indicating crystal growth out of the plane of the substrate. The overall picture of the growth of $F_{16}CuPc$ on oxidised silicon and GO is that of a largely polycrystalline thin film composed of nanometre-scale crystallites with a tendency to form elongated preferentially oriented networks as thickness increases.

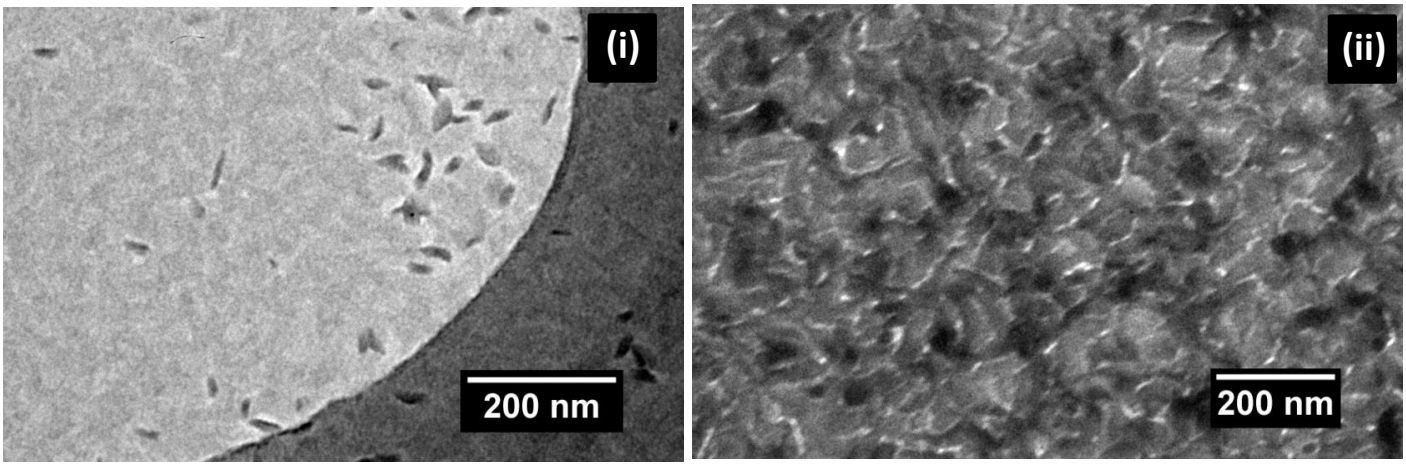

Figure 5.7 – Bright field TEM of (i) 5nm (ii) 80nm $F_{16}CuPc$/GO/Lacy carbon

5.1.4 – Structure of GO supported F_{16}CuPc thin films by SAED

SAED was used to probe the crystal structure of the same 1,5 and 80 nm films imaged by bright field TEM. The presence of the GO lattice provided an in-situ calibration as the lattice parameters are well known and can be used to calibrate the hexagonal diffraction pattern produced. This in turn allows the spacings responsible for other simultaneously recorded diffraction patterns to be accurately ascertained.

Even in the thinnest (1 nm) films diffraction features corresponding to the F_{16}CuPc film can be observed together with the GO pattern (**Fig 5.8**). Due to the polycrystalline nature of the film, rings are observed rather than the spots observed for highly crystalline samples. Two weak rings are present between the transmitted beam and the diffraction spots from the GO support film, the reciprocal length of which corresponds most closely with the (100) (inner) and (1-2-2) (outer) planes of the F_{16}CuPc crystal structure.

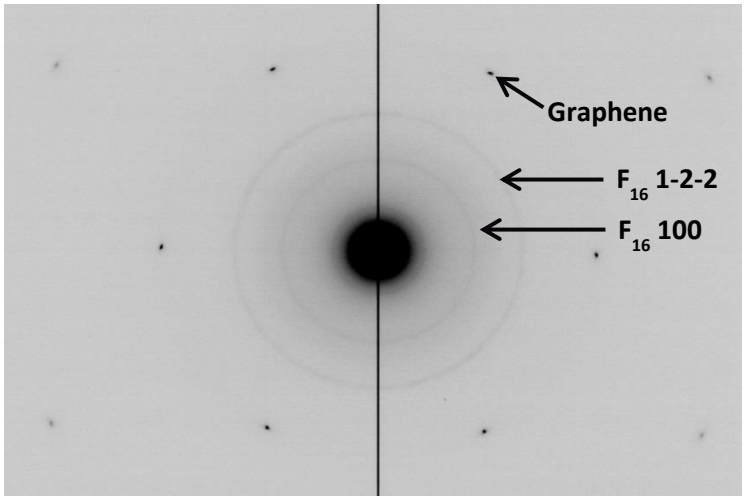

Figure 5.8 – SAED pattern from 1 nm film

When thickness is increased to 5 nm (**Fig 5.9**), the ring corresponding to the (1-2-2) plane increases in intensity, providing further evidence of parallel stacks of molecules rather than herringbone packing (the (1-2-2) reflection would be absent or very low in intensity in a herringbone packed structure). As the diffraction pattern was collected with the transmitted beam perpendicular to the substrate, the (1-2-2) plane of the polycrystalline film is also roughly perpendicular to the substrate plane. The intensity is radially even around the ring, suggesting that no epitaxial alignment with the underlying GO lattice is present. If this were the case intensity fluctuations in the same regions as the GO spots are observed would be expected.

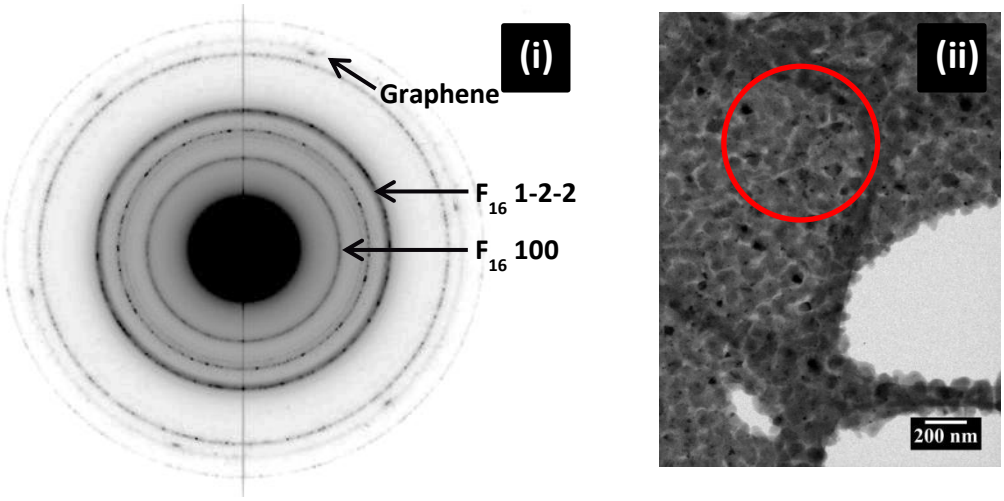

Figure 5.9 – (i) SAED pattern from 5 nm film and (ii)corresponding bright field region (marked with red circle)

At a film thickness of 80 nm patterns (**Fig 5.10**) still contain the same features as the other two thicknesses, diffraction spots from the GO support and rings corresponding to the (001) and (1-2-2) planes. Bright field imaging and SEM images suggest that the morphology of the film evolves into a collection of fibre like nano-crystals at this point. The similarity between the diffraction patterns at 80 nm, 5 nm and 1 nm suggest that the fibre-like

crystals have the same crystal structure as the rest of the film. While this observation is limited to the out-of-substrate plane structure due to the experimental geometry, the highly polycrystalline nature of the sample leads to some averaging in other spatial orientations.

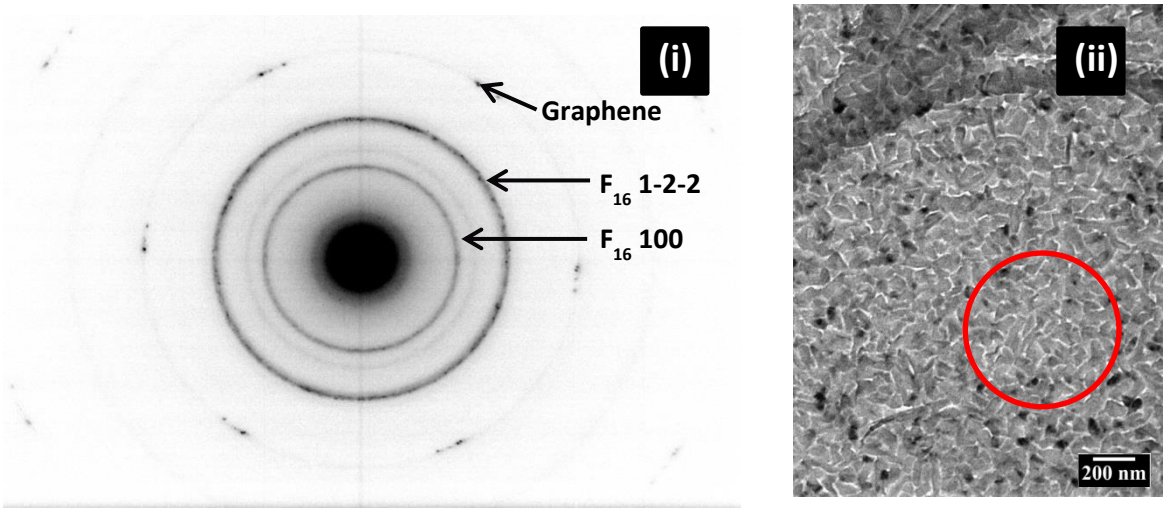

Figure 5.10 – (i) SAED pattern from 80 nm film and (ii)corresponding bright field region (marked with red circle)

In order to assess the overall out-of-plane morphology of the films radial averages were taken through the diffraction rings and compared to patterns simulated from the proposed single crystal data (**Fig 5.11**). Intensity differences between the observed and simulated patterns are clear in the (100) reflection and both the (001) and (0-11) reflections are absent. This suggests some degree of preferred orientation which has removed the (001) and (0-11) from a geometry preferable for scattering in SAED.

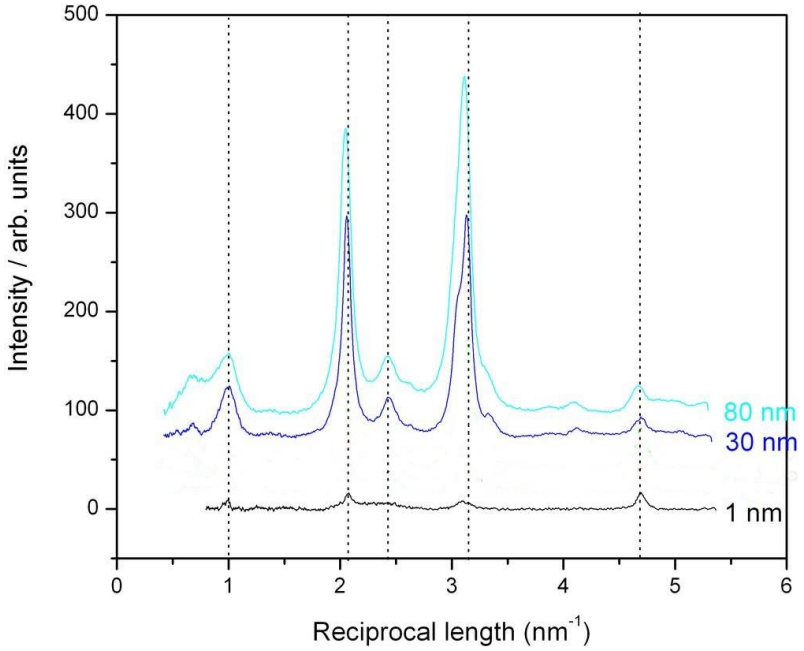

Figure 5.11 – Intensity averages for 1 nm 30 nm and 80 nm films

As the (1-2-2) peak shows a surprisingly high intensity, we may assume preferred orientation relating to the (1-2-2) plane. This hypothesis was tested by altering the angle of incidence between the transmitted beam and the film by tilting the sample holder by 45° (**Fig 5.12**).

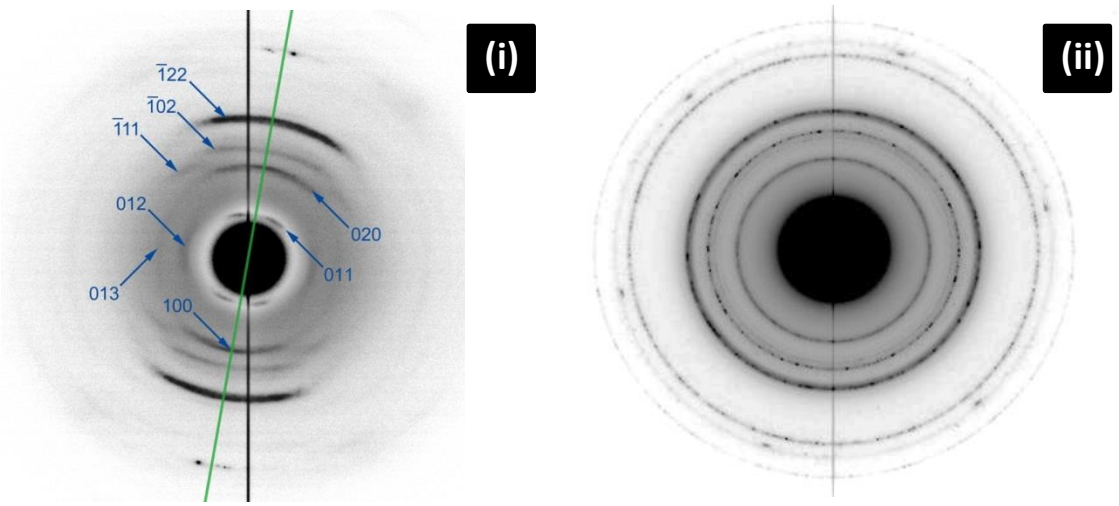

Figure 5.12 – (i) Tilted SAED pattern for 80 nm film and (ii) the corresponding un tilted pattern

Two distinct effects are obvious when the patterns taken at 0° and 45° are compared; the splitting of rings into arcs and the appearance of rings not previously observed. In the 0° pattern rings corresponding to (011) and (1-2-2) appear radially equivalent in terms of intensity, but at 45° both split into pairs of arcs. As the original patterns were taken at 0° we can assume that the axis along which the film is strongly morphologically oriented is perpendicular to both the (011) and (-122) axes. The appearance of the arcs at 45° that are not present at 0° can be rationalised by the introduction of planes that are not normally incident with the transmitted electron beam into its path by tilting the sample. Further structural conclusions from cannot made due to the weakness of the reflections and the limitations of a single tilt axis on the holder used for these experiments.

5.2 - Magnetic properties of F_{16}CuPc

While MPc molecules are widely studied as semiconducting materials, they also exhibit interesting magnetic characteristics[7]. Understanding and controlling these characteristics is of huge interest for applications such as information storage and magnetic sensors[8]. With these results in mind the reliance of magnetic properties of F_{16}CuPc films on crystal structure and morphology were investigated. Kapton® polyimide films were used as a support film due to their chemically inert nature and non-magnetic properties.

5.2.1 – Film morphology and structure

Films were grown from powders of F_{16}CuPc and PTCDA (Sigma-Aldrich, UK) which were further (triply) purified by thermal gradient sublimation. Films were evaporated onto pieces of Kapton® polyimide film (Katco) cleaned with isopropyl alcohol before growth and held at room temperature. Growth rate and film thickness was monitored by a QCM positioned close to the substrate.

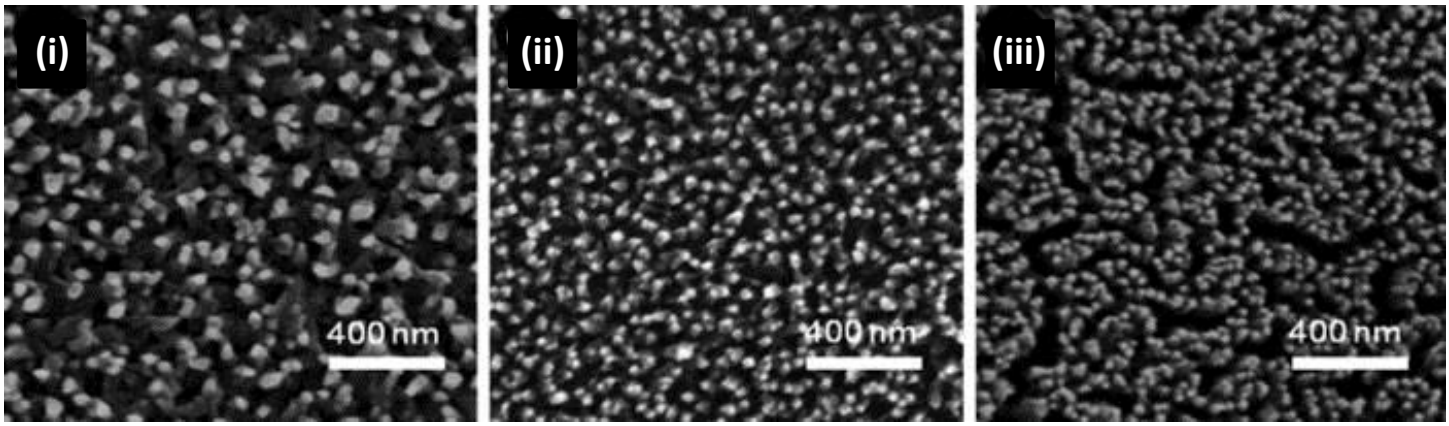

Figure 5.13 – SEM images of (i) 100 nm F_{16}CuPc/Kapton (ii) 160 nm F_{16}CuPc/Kapton and (iii) F_{16}CuPc/PTCDA/Kapton

When F_{16}CuPc was directly grown onto the Kapton substrate to a thickness of 100nm (necessary for good signal to noise for magnetic measurements) multiple crystallite morphologies and height profiles are obvious in SEM images (**Fig 5.13**).

As the thickness was increased to 160 nm similar features were observed but their density increased with respect to the surface suggesting more nucleation of out-of-surface plane crystallites. When a PTCDA template layer was grown on the Kapton before the F_{16}CuPc even higher density features are observed with a slight decrease in their lateral size. Similar growth behaviour has been observed on SiO_2 and indium tin oxide (ITO) coated glass suggesting that the Kapton film is similarly non-interacting with respect to the F_{16}CuPc layer.

XRD patterns from these samples are presented in (**Fig 5.14**) along with powder XRD data for the purified F_{16}CuPc film and a simulated pattern based on the crystal structure solved above.

In F_{16}CuPc films grown directly on Kapton, an apparent change in morphology and structure is observed with the increase in thickness. At 100 nm, a single diffraction peak at 6.2° corresponding to the (001) spacing of the F_{16}CuPc crystal structure is observed. With an increase of thickness to 160 nm an additional broad feature centred at 28.4° is also in evidence. This suggests one of two things; that thickness dependant structure or preferred orientation is observed and secondly that the texture is identical in both films but too few diffracting planes responsible for the second peak are present in the thinner film. With the similarity in morphology from SEM imaging in mind the second of these situations seems most likely. The thicker film appears to have a higher density of the high aspect ratio protrusions out of the substrate plane which may be producing higher scattering intensity at the 28.4° peak. Electron diffraction data presented earlier in this work does not show any evidence for thickness dependant crystal structure changes or texture. Preferential growth

of high aspect ratio ribbons or needles of F_{16}CuPc past a critical thickness has been observed in literature, so assuming that differences in XRD traces is purely due to thickness rather than texture seems logical.

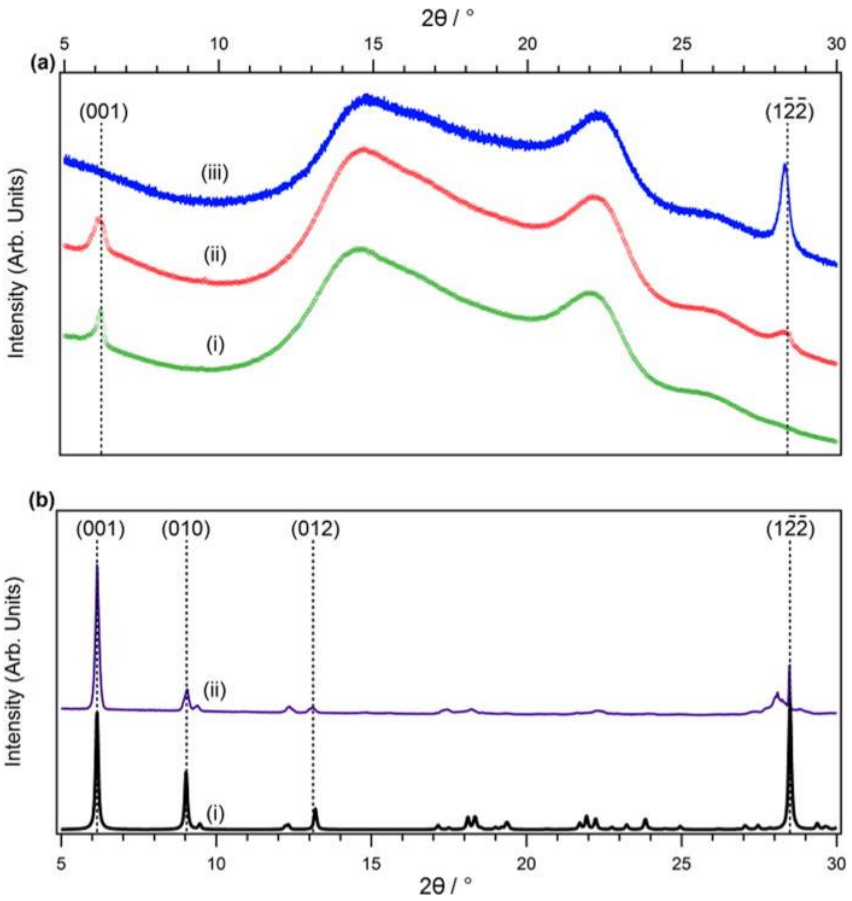

Figure 5.14 – (bottom panel) XRD of (ii) F_{16}CuPc powder and (ii) corresponding single crystal data. (top panel) XRD of (i) 100 nm F_{16}CuPc (ii) 160 nm F_{16}CuPc and (iii) F_{16}CuPc/PTCDA

When a structural template layer of PTCDA (5 nm thickness) is evaporated onto the Kapton before the F_{16}CuPc a marked change in the XRD trace is observed. The low angle feature at 6.2 is no longer observed and the higher angle peak at 28.4° increases in intensity and appears sharper. As this templated film thick enough to expect the low angle (001) peak from α-phase phthalocyanines its absence can be associated with a change in orientation or structure.

A similar templating effect was previously observed with CuPc on PTCDA layers and the angles of peaks present (and therefore their assignments) are comparable. This suggests that the unit cell of the F_{16}CuPc molecule is 'rotated' with respect to the substrate when the templating layer is introduced. This produces a situation in which the plane defining the π system of the phthalocyanine ligand is laying orthogonal to the surface plane rather than along it in non-templated films. In this situation the (1-2-2) plane defining the intermolecular face-to-face packing direction is oriented out of the substrate plane and therefore detected by the diffractometer in θ-2θ scans in the grazing incidence geometry employed.

A schematic of the packing directions and relative orientation of F_{16}CuPc in templated and non-templated films are presented in (**Fig 5.15**).

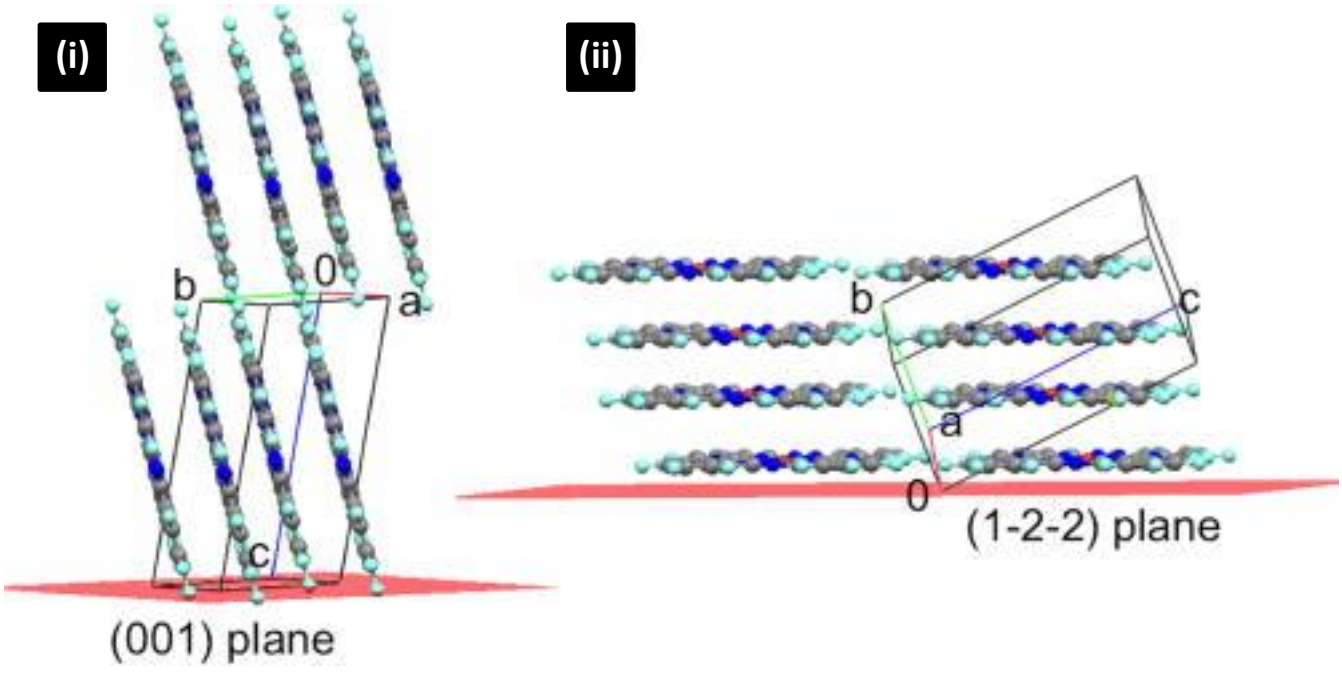

Figure 5.15 – Orientation of molecules within single crystals with respect to the substrate before (i) and after (ii) PTCDA interlayers are introduced

While scattering from other planes (particularly those close to the (001) and (1-2-2)) will also be detected by the diffractometer, the properties and of MPc thin films reduces the likelihood of this. The strong preferred orientation within crystalline grains of the inherently polycrystalline films masks other local order within crystallites; and only the planes which contain the Cu atom at the centre of the molecule are usually observed due to the weak scattering ability of the lighter carbon and nitrogen atoms of the Pc heterocycle. These features combine to reduce the number of peaks observed in thin films, even when compared to powder XRD collected from bulk samples of F_{16}CuPc.

5.2.2 – Magnetisation measurements of F_{16}CuPc samples

SQuID magnetometry was used to measure the magnetic characteristics of purified F_{16}CuPc powders and thin films (both templated and non-templated). Magnetisation (M) versus magnetic field (H) curves (M-H) are presented for all samples measured in (**Fig 5.16**). The Brillouin function for a 1/2 spin paramagnet appropriate for F_{16}CuPc is also plotted on the same axes.

The data wer corrected for the number of Cu atoms based on the density of the material from single crystal XRD measurements and calibrated thickness measurements in film samples. Almost identical characteristics are observed in F_{16}CuPc prepared as powders, thin films on Kapton and templated films grown on PTCDA layers. Due to the high aspect ratio of the features present in the thin films the number of spins present is inherently overestimated for these samples, but this manifests as a constant scale factor which can be corrected.

For comparison purposes the curves are independently scaled such that the magnetisation at a field strength of 7 Tesla (at which point all of the curves are assumed to

be saturated) each experimental curve matches the Brillouin function. The difference in the factor of this scaling can be explained by the different molecular orientation presented to the sensing coils of the magnetometer (as well as film density differences). The expected isotropy of the field response of the d^9 Cu centre of each F_{16}CuPc molecule is consistent with this observation.

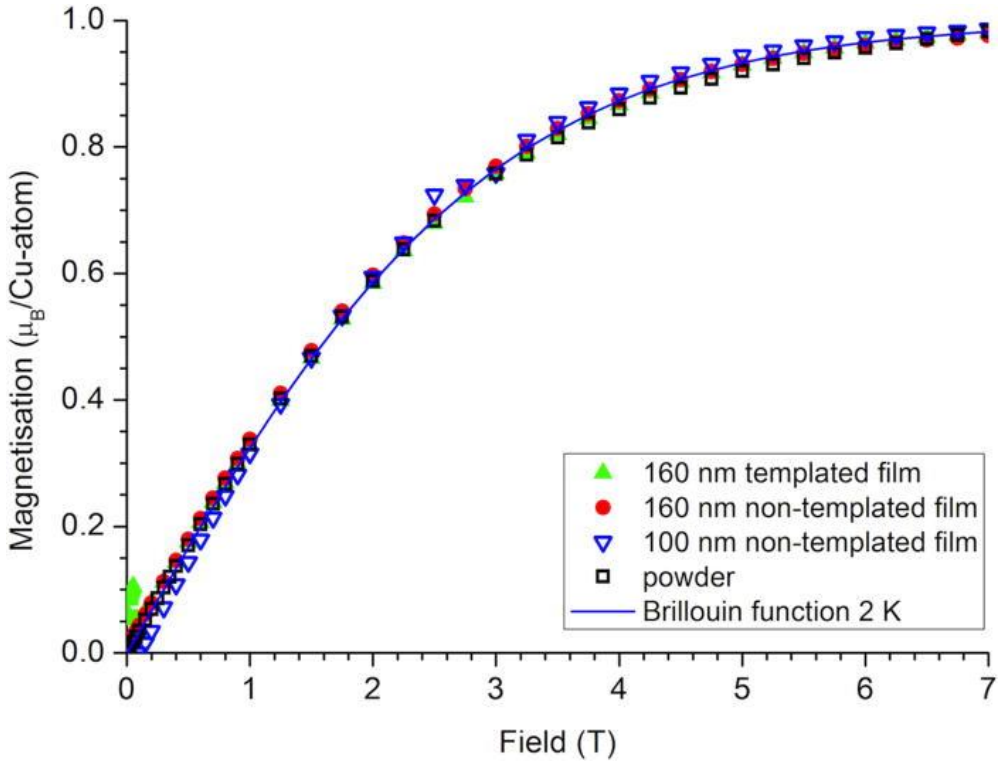

Figure 5.16 – Collected magnetism data for F_{16}CuPc powders and thin films

The Brillouin function provides a good fit to experimental data across the range of applied fields confirming the expected paramagnetic nature of all samples. This result is also consistent with DFT calculations (presented in the next section) which predict an interaction temperature of 0.02K which is experimentally indistinguishable from 0. As such, all samples are assumed to have the same crystal structure (their intermolecular interactions and

therefore spacings are identical) but possess different morphology and preferred orientation due to templating.

It should be emphasised that despite a fair understanding of the magnetic properties of F_{16}CuPc the data collected were not perfect. Small amounts of ferromagnetic contamination were present in the 160 nm thick templated film and were in evidence at all temperatures up to 150 K. This contribution was removed by subtracting the experimental magnetisation data at high field and temperature. This produces an artificial peak at low field (less than 0.05 T) as the contamination is not saturated at this point, but as this only affects the lowest field portion of the data and a good fit to the data can still be produced.

5.2.3 – Simulation of magnetic properties of F_{16}CuPc

Kohn-Sham single electron orbitals were first simulated for isolated F_{16}CuPc and CuPc molecules in the region close to the Fermi level for comparison and are presented in **Fig 5.17**. The b_{1g} state (one of the components of the HOMO) is one irreducible representation of the D_{4h} symmetry group occupied by the molecule. Simulations suggest that the b_{1g} state is derived mostly from the Cu d_{x2-y2} orbital and is singly occupied in contrast to the doubly occupied a_{1u} (HOMO) and empty e_g (LUMO) states which have mostly Pc ligand character. If we compare the computed values for states these to those of CuPc[9], we notice a 1 eV shift in both eigenvalues due to the electronegativity of the fluorine atoms present in the Pc heterocycle. This matches experimental observations and while the absolute eigenvalues are shifted the form of the orbitals is not perturbed by fluorination. The b_{1g} state is almost identical which is unsurprising as the spin polarisation of the central Cu atom is spatially far from the peripheral fluorine atoms of the Pc rings. All of these observations match previous observations made in literature, and suggest that the magnetic

intermolecular interaction is identical to CuPc (namely indirect exchange by spin polarization of the Pc ligand by the Cu centre followed by through space intermolecular propagation).

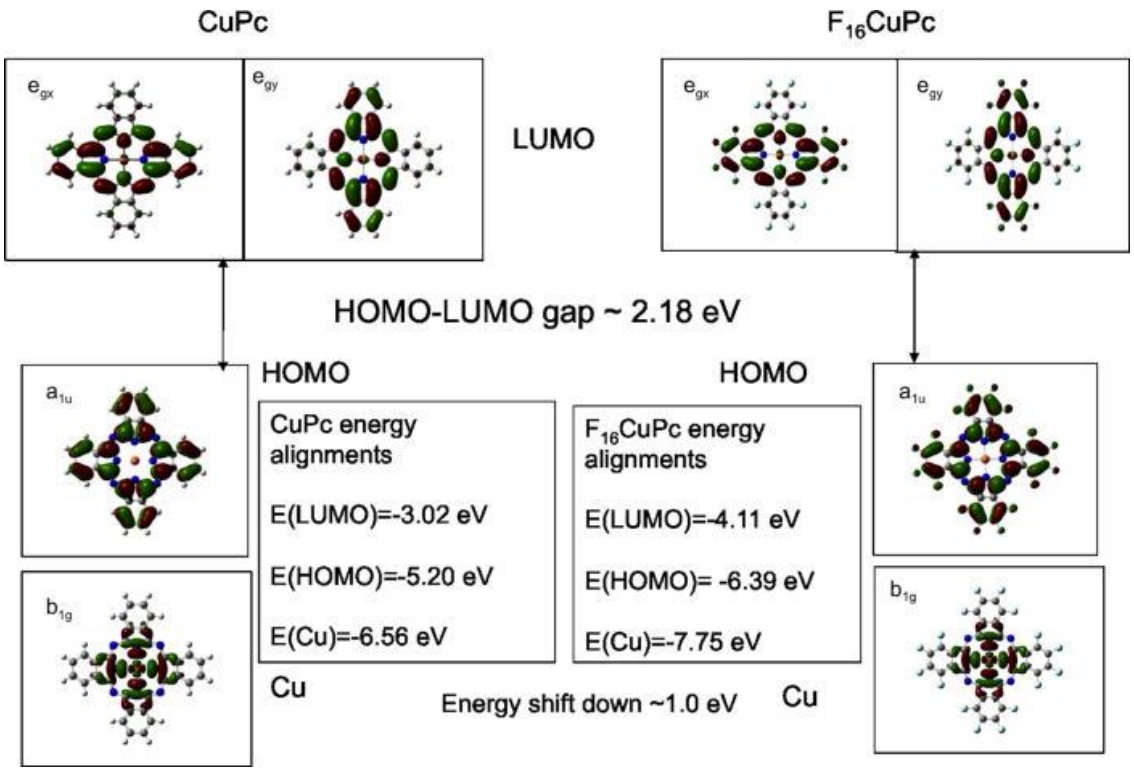

Figure 5.17 – Forms and energetic positions for CuPc and F16CuPc molecules

Once the isolated molecules had been simulated and understood, the simulation was extended to a 1-D molecular chain to understand the electronic structure and exchange interaction in the solid state (**Fig 5.18**). This model has been demonstrated as a good model for MPc systems due to anisotropic through-space interactions in the solid state due to the large difference in spacings within and between stacks of MPc molecules.

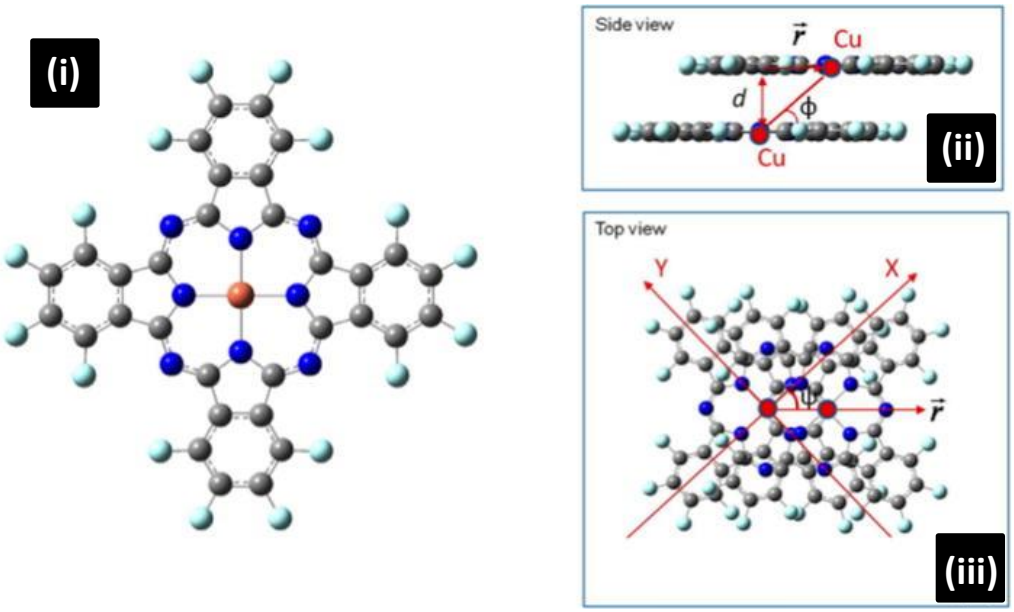

Figure 5.18 – The F_{16}CuPc molecule (i) and the stacking (ii) and sliding (iii) angles

The exchange interaction was computed with the sliding (φ) and stacking (ϕ) angles as variables to understand the influence of each parameter. The result is presented in **Fig 5.19** and demonstrates strong dependence upon the intermolecular stacking angle but only weakly on the sliding angle within the molecular plane.

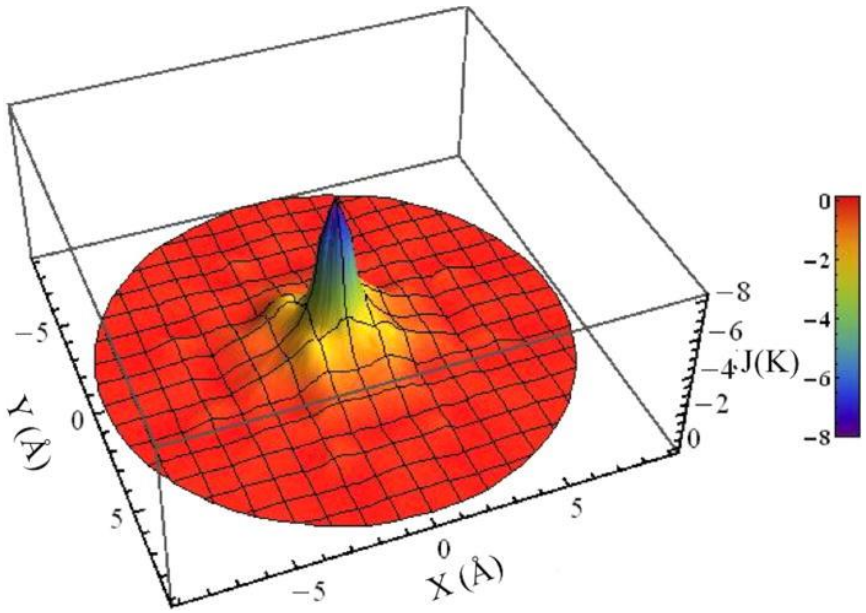

Figure 5.19 – Dependence of exchange interaction on stacking and sliding from DFT calculations

The exchange interaction reaches its maximum at 90° (ϕ), which is when the molecules are face to face in orientation. This value is twice that observed for CuPc[9] and represents the maximum possible exchange in the ideal geometry. When parameters are fixed to those observed in the single crystal structure of F_{16}CuPc, a good agreement is found between the simulation and the experimentally observed paramagnetic behaviour.

In order to approximate the band structure and density of states of the molecular chain anti-ferromagnetic (a-FM) and ferromagnetic (FM) exchange are considered. The computed band gap is 2.0 eV which closely approximates the electronic structure of the isolated molecule and matches the Q-band optical adsorption previously reported for F_{16}CuPc[10] (wavelength of 650nm, approx. 1.9 eV).

The magnetic super cell considers the interaction between two molecules and as such is double the length of the crystallographic unit cell (‘a’ axis of 0.978 nm). By comparison of a-FM and FM partial density of states (PDOS) the singly occupied Cu d-orbitals can be identified and lie 1.5 eV below the valence band consistent with isolated molecular electronic structure calculations.

The form of the computed bands is similar to those computed for CuPc emphasising the small influence of fluorination on the spin states of the molecule. These bands are not dispersed among the other DOS of the molecule, suggesting that adjacent copper spins cannot readily interact through direct super-exchange. This band is close to the Pc ligand DOS, so ligand spin polarisation should be a much simpler process, confirming the assignment of the through-space interactions of the molecules.

Other possible geometries (from other variants of the crystal structure) vary significantly in terms of band width, highlighting the strong dependence of π-π interactions between Pc ligands on inter-molecular geometry. These interactions mediate the spin

polarisation transfer between molecules and hence between Cu centres; geometry dependant bandwidth should produce geometry dependant exchange interactions.

This was tested using Green's Functional Perturbation Theory (GFPT) using the same approach as earlier (varying the X (φ) and Y (ϕ) positions with exchange interactions (hopping integrals produced from the DFT calculations) as input (**Fig 5.20**). A strong dependence on stacking angle but a weak dependence on sliding angle is demonstrated agreeing qualitatively with the DFT calculations.

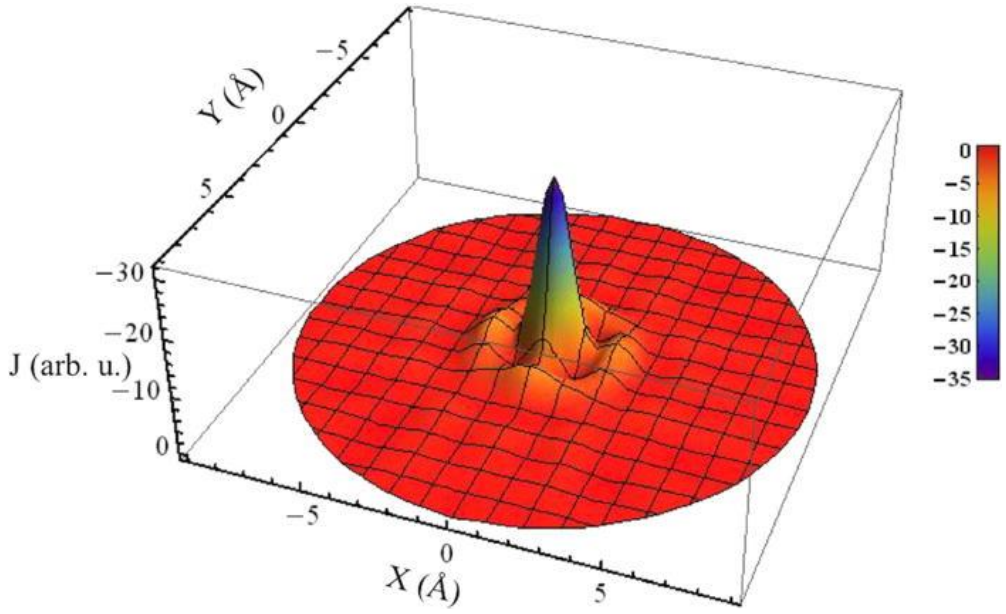

Figure 5.20 – Dependence of interaction on stacking and sliding from GFPT calculations

The maximum exchange interaction suggested by GFPT for F_{16}cupc is double that previously calculated for CuPc. This may be a reflection of the larger hopping integrals between ligand π systems due to the slightly smaller inter-plane spacing of F_{16}CuPc compared with CuPc.

5.3 – Conclusions

F_{16}CuPc has been studied as powder and prepared as thin films by SEM, XRD and SQuID magnetometry with theoretical modelling to support observations. The crystal structure of 100 nm and 160 nm thick films is consistent with the single crystal structure solved in this chapter. A comparable templating interaction in the F_{16}CuPc/PTCDA system to that in CuPc/PTCDA is observed and is shown to cause a change in texture and relative molecular orientation rather than crystal structure.

Magnetic measurements show that all films and powders are paramagnetic and the behaviour of each sample can be modelled using the same Brilloun function. Simulations of exchange interactions match the paramagnetic character of all samples well. In contrast to CuPc (with antiferromagnetic character in the α-phase and paramagnetic character in the β phase), the magnetic character of F_{16}CuPc does not change depending on preparation conditions suggesting that no change in crystal structure is present.

References:

(1) Hancox, I.; Rochford, L.; Clare, D. Optimization of a High Work Function Solution Processed Vanadium Oxide Hole-Extracting Layer for Small Molecule and Polymer Organic Photovoltaic Cells. *The Journal of Physical Chemistry C* **2012**, *117*, 49–57.

(2) De Oteyza, D. G.; Barrena, E.; Ossó, J. O.; Sellner, S.; Dosch, H. Thickness-dependent structural transitions in fluorinated copper-phthalocyanine (F_{16}CuPc) films. *Journal of the American Chemical Society* **2006**, *128*, 15052–3.

(3) Wu, J. S.; Spence, J. C. H. Structure and bonding in alpha-copper phthalocyanine by electron diffraction. *Acta crystallographica. Section A, Foundations of Crystallography* **2003**, *59*, 495–505.

(4) Wilson, N. R.; Pandey, P. A; Beanland, R.; Rourke, J. P.; Lupo, U.; Rowlands, G.; Römer, R. a On the structure and topography of free-standing chemically modified graphene. *New Journal of Physics* **2010**, *12*, 125010.

(5) Sloan, J.; Liu, Z.; Suenaga, K.; Wilson, N. R.; Pandey, P. A; Perkins, L. M.; Rourke, J. P.; Shannon, I. J. Imaging the structure, symmetry, and surface-inhibited rotation of polyoxometalate ions on graphene oxide. *Nano Letters* **2010**, *10*, 4600–6.

(6) Yang, J. L.; Schumann, S.; Jones, T. S. Nanowire-array films of copper hexadecafluorophthalocyanine (F_{16}CuPc) fabricated by templated growth. *Journal of Materials Chemistry* **2011**, *21*, 5812.

(7) Ishikawa, N. *Functional Phthalocyanine Molecular Materials*; Jiang, J., Ed.; Springer Berlin Heidelberg: Berlin, Heidelberg, 2010; Vol. 135, pp. 211–228.

(8) Heutz, S.; Mitra, C.; Wu, W.; Fisher, A. J.; Kerridge, A.; Stoneham, M.; Harker, a. H.; Gardener, J.; Tseng, H.-H.; Jones, T. S.; Renner, C.; Aeppli, G. Molecular Thin Films: A New Type of Magnetic Switch. *Advanced Materials* **2007**, *19*, 3618–3622.

(9) Wu, W.; Kerridge, A.; Harker, A.; Fisher, A. Structure-dependent exchange in the organic magnets Cu(II)Pc and Mn(II)Pc. *Physical Review B* **2008**, *77*, 184403.

(10) Alonso, M. I.; Garriga, M.; Ossó, J. O.; Schreiber, F.; Barrena, E.; Dosch, H. Strong optical anisotropies of F[sub 16]CuPc thin films studied by spectroscopic ellipsometry. *The Journal of Chemical Physics* **2003**, *119*, 6335.

Chapter 6

Conclusions and further work

6.1 - Surface and electronic structure of VOPc

Thin films of VOPc on Au (111) Ag (111) and Cu (111) surfaces were prepared and characterised using STM, LEED and UPS. On Au (111) molecules assemble with their oxygen atoms projecting away from the surface and LEED patterns show multiple orientations with respect to the principle crystallographic axes. Electronic structure analysis suggests no electron transfer at the interface and a thickness-dependant work function change is observed. On Ag (111) similar behaviour is observed with STM and LEED while UP spectra show that charge transfer is present from the substrate into the LUMO of the molecule.

Growth behaviour on Cu (111) is markedly different; LEED patterns and surface structure in STM images differ significantly from Au (111) and Ag (111). Multiple assembly modes are explained using the postulate that the molecule's shape is altered by interacting with the copper surface and charge transfer into the molecule. UP spectra are also dissimilar to those produced from Au (111) and Ag (111) surfaces, with no clear molecular HOMO derived state. The nature of the electronic structure shown by the UPS experiments is discussed but the underlying molecule-surface interaction remains ambiguous.

6.2 – High temperature deposition of organic thin films

The effect of changing the temperature of SiO_2 substrates during the deposition of two planar phthalocyanines, FePc and MnPc, was investigated. With both molecules larger crystalline domains were observed with increasing T_{sub} up to a temperature at which the sticking coefficient

was reduced, preventing adsorption of molecules. Larger crystals were produced from both molecules at high temperatures, but FePc crystals were always larger. This characteristic also observed in macroscopic crystals of the molecules studied.

Copper iodide structural template layers prepared both at ambient and elevated substrate temperature were investigated. Higher temperatures produced larger crystalline domains in the (111) oriented CuI layers and these in turn produced larger grains of FePc grown sequentially on top at ambient temperature. The orientation of the FePc layer was changed such that the molecules switched from a face-on orientation (100) (with respect to the substrate) to edge-on (1-2-2).

FePc deposited at elevated substrate temperature on to the CuI (111) showed a mixture of edge-on and face-on orientations with respect to the substrate. This suggests that the templating effect does not produce the most thermodynamically stable form of FePc. The surface morphology rapidly roughens as the thickness is increased suggesting minimisation of the contact between the FePc crystallites and the CuI(111) surface.

6.3 – Structural and magnetic properties of F_{16}CuPc

As a starting point for structural analysis of F_{16}CuPc, its single crystal structure is solved and shown to be different to previously published structures. Thin F_{16}CuPc films were grown and a combination of AFM, TEM imaging and electron diffraction experiments were used to characterise them. This revealed the strong preferred orientation in the films and allowed proposed changes in structure and morphology as a function of thickness to be analysed.

F_{16}CuPc was then prepared as purified powders and thin films on non-magnetic substrates before SEM, XRD and SQuID magnetometry were used for analysis. XRD patterns showed that films of 100 nm and 160 nm thickness are consistent with the single crystal structure presented here.

PTCDA was also used as a structural template to control the orientation of crystallites in F_{16}CuPc thin films. A templating interaction in the F_{16}CuPc/PTCDA system comparable to that in CuPc/PTCDA is observed and is shown to cause a change in preferred orientation and relative molecular orientation rather than crystal structure.

Magnetic measurements show that all F_{16}CuPc films and powders are paramagnetic and the behaviour of each sample can be modelled using the same Brilloun function. Simulations of exchange interactions match the paramagnetic character of all samples well. In contrast to CuPc (with antiferromagnetic character in the α-phase and paramagnetic character in the β-phase) the magnetic character of the material does not change depending on preparation conditions suggesting that no change in structure is present.

6.4 – Further work

The surface studies of VOPc presented here have provided an insight into the behaviour of a non-planar phthalocyanine within the first monolayer of growth. Further work is clearly necessary to fully understand the underlying processes responsible for the surface morpholgies and electronic properties observed. Synchrotron-based surface measurements would provide a great deal of information about VOPc, both structurally and electronically. Fine structure techniques such as X-ray standing wave (XSW) or photoelectron diffraction (PhD) would allow the molecule and the topmost layers on the supporting substrate to be probed without damaging the sample. X-ray absorption spectroscopies such as extended X-ray photoelectron fine structure (EXAFS) or near edge X-ray fine structure (NEXAFS) would also provide a wealth of information useful in understanding the structure of the interface. The presence of an adsorbate induced surface reconstruction could also be probed

with all of these techniques. Planning is currently underway to construct an experimental proposal for this work.

Low temperature STM, UPS and LEED experiments would facilitate the observation of structures at lower coverages than those possible at room temperature. The earliest stages of film formation may be important in the assembly and electronic structure observed and understanding this would provide a more complete picture of the surface interactions which occur at MPc /metal interfaces. While this equipment is not available in our own labs discussions with collaborators are ongoing.

The growth of phthalocyanines and inorganic templating layers at high temperatures has shown promise in controlling and understanding the structure of MPcs in thin films. If highly crystalline CuI (111) layers can also be prepared on conductive substrates the possibility of atomic resolution imaging via STM can be realised. This would also allow imaging of the formation of the phthalocyanine over-layer as it could be evaporated in situ without exposure to air. LEED experiments could also be used to probe the crystal structure of the interface and UPS would allow the electronic structure to be analysed. Preliminary experiments for this work are currently underway with further work planned.

Magnetic characterisation of phthalocyanines remains a neglected field of study and systematic studies are uncommon. Development of a high throughput method of screening MPc molecules for interesting or useful properties would be hugely important if the field is to progress. As such, single crystal, powder and thin film samples could be created in exactly the same way using optimised experimental parameters and used for magnetic measurements. Combining this with the ability to tune the structure and magnetic properties through structural or chemical modification would allow rapid accumulation of a catalogue of interesting and technologically relevant molecules for magnetic applications.

Concomitant with this the single crystal structures of each of the planar metal phthalocyanines could be checked or analysed for the first time. This would allow a much more complete understanding of the through space interactions responsible for the physical and electronic structure of MPc systems. The use of sublimation techniques developed in our labs allows the reproducible fabrication of high quality single crystal samples. This negates problems associated with the production of single crystals from solutions of highly insoluble materials. Preliminary experiments on this topic are currently underway and a wide variety of MPc molecules are planned for use in crystal structure determination experiments.